DANMARKS OG GRØNLANDS GEOLOGISKE UNDERSØGELSE RAPPORT 2011/114

Controls of hydrothermal quartz vein mineralisation and wall rock alteration in the Paamiut and Tartoq areas, South-West Greenland

Jochen Kolb (editor)

(1 DVD included)

GEOLOGICAL SURVEY OF DENMARK AND GREENLAND
MINISTRY OF CLIMATE AND ENERGY

GEUS

DANMARKS OG GRØNLANDS GEOLOGISKE UNDERSØGELSE RAPPORT 2011/114

Controls of hydrothermal quartz vein mineralisation and wall rock alteration in the Paamiut and Tartoq areas, South-West Greenland

Jochen Kolb (editor)

(1 DVD included)

GEOLOGICAL SURVEY OF DENMARK AND GREENLAND
MINISTRY OF CLIMATE AND ENERGY

GEUS

Contents

Abstract **5**

Introduction **8**

Regional geological setting **10**

The Sioraq block 10
The Paamiut block 11
The Neria block 11
The Sermiligaarsuk block 11

Geology of the Paamiut area **13**

Lithology 13
Structural geology 14
References 15

Results from 2010 field work in the Paamiut area (Kolb and Weatherley) **17**

Geology of the Akuliaq peninsular 17
Geology between Nigerlikasik and Akulleq 25
Geology between Nigerlikasik and Akulleq glaciers 32
Geology of the Mellembygden area 39
Regional structural model 45
Model for hydrothermal gold mineralisation 46
Conclusions 48
References 48

Mapping and structural analysis of the Akuliaq Peninsula, near Paamiut, SW Greenland (Hastie) **49**

Abstract 49
Introduction 49
Materials and methods 51
Results 52
Foliations and lineations 53
Folds 57
Shears/faults 61
Kinematic indicators 61
Gold mineralisation 63
Discussion 63
Conclusions 66
References 66
Appendix A 67
Appendix B 72

Mapping and petrographic analysis of the lithology of Akuliaq Peninsula, Paamiut region, Southwest Greenland (Glendenning) 79

Abstract ... 79
Introduction ... 79
Objectives ... 80
Methods ... 80
Results ... 82
Discussion ... 94
Conclusions ... 99
Appendix – C: Stratigraphy ... 100
Appendix – D: Cross section ... 101
Appendix – E: Cross section ... 102
References ... 115

Structural geology and emplacement of the Tartoq Group, SW Greenland (Kisters et al.) 116

Introduction ... 116
Synopsis of the regional structural inventory ... 117
Geology of individual supracrustal belts of the Tartoq Group ... 120
Discussion: models for the emplacement of the Tartoq Group ... 139
Summary ... 146
Acknowledgements ... 147
References ... 147

Summary of 2010 field work in the Tartoq Group, Paamiut region, SW Greenland (Polat & Dziggel) 148

Introduction ... 148
Camp 1 (Iterlak) ... 149
Camp 2 (Midternæs N) ... 152
Camp 3 (Sioralik) ... 155
References ... 158

Gold occurrences of the Tartoq area (Kolb) 159

Nuuluk gold prospect ... 160
Iterlak gold prospect ... 163
Amitsuarsua gold occurrence ... 166
Naalagaaffik and Akuliarusaq gold occurrences ... 169
Bikuben gold occurrence ... 172
References ... 173

Summary and conclusions 175

Abstract

This report comprises an introduction to the regional geology and six field reports, reviewing different field areas and geological aspects. The study area reaches from the Frederikshåb Isblink in the north to south of Sermiligaarsuk Fjord and is made up of grey gneiss, supracrustal belts and syn- to late-tectonic granitoid intrusions of the North Atlantic craton. It is divided into four blocks, namely the ca. 2870-2840 Ma Sioraq block, the ca. 2880-2850 Ma Paamiut block, the ca. 2980-2870 Ma Neria block and the ca. 3000-2840 Ma Sermiligaarsuk block. Field work was focused on the gold endowed Paamiut and Sermiligaarsuk blocks.

Kolb & Weatherley focus on the regional structural grain and related gold mineralisation in the Paamiut block, the Paamiut gold province. The area is represented by an east-vergent fold-and-thrust belt that forms a lateral and frontal ramp geometry. Supracrustal belts and grey gneiss are involved in progressive shearing from the ductile to the brittle regime. Leuco-granite intruded syn- to late-tectonically into the shear zones. Hydrothermal gold mineralisation and alteration is controlled by these structures, forming gold mineralisation in quartz veins in structurally complex zones and at lithological contacts. The characteristic hydrothermal alteration assemblage is quartz, amphibole, biotite, tourmaline, pyrrhotite, arsenopyrite and, locally, garnet, carbonate and muscovite. The eastern area was probably involved in subduction, showing prograde metamorphism in the granulite facies, and exhumation along back thrusts in the compressional orogen characterised by the fold-and-thrust belt.

Hastie concentrates in his BSc thesis on structural interpretations and mapping from the Akuliaq peninsula in the Paamiut gold province, where active gold exploration is done by NunaMinerals A/S. Three deformation stages are distinguished. D_1 formed isoclinal folds and an S_1 foliation, which is refolded during D_2 resulting in m-scale N-NW plunging folds and a penetrative S_2 foliation. This S_2 foliation is defined by the peak metamorphic assemblage in the amphibolite facies. The D_2 stage is characterised by early E-W compression (regional D_1 by Kolb & Weatherley) and late E-W extension (regional D_2 by Kolb & Weatherley). During D_3, F_2 folds and the S_2 foliation are refolded into m-scale open folds (interpreted as D_1 sheath folds by Kolb & Weatherley). The auriferous quartz veins formed during the D_2 stage of deformation.

Glendenning mapped together with Hastie the southern tip of the Akuliaq peninsula on a 1: 2,500 scale and focused in his BSc thesis on the petrology of wall rocks and quartz veins. The study area consists of lenticular ultramafic rocks (hornblendite, serpentinite), meta-gabbro, amphibolite, aplitic dykes, grey gneiss and pegmatite dykes. The mineral assemblages are characteristic of metamorphism in the amphibolite or epidote-amphibolite facies. The lithology is interpreted to represent a part of Archaean oceanic crust that is intruded by TTG magmas during the subduction process and progressively exhumed and intruded by pegmatite. The latter process is related to gold mineralisation in quartz veins, which are grouped into quartz-sulphide veins, milky quartz veins and blue quartz veins. Quartz-sulphide veins are boudinaged on a m-scale and contain pyrite, pyrrhotite, arsenopyrite, chalcopyrite and hematite. Milky quartz veins are generally barren and form folded

rods and sheets on a m-scale. Larger, up to 10 m wide veins, often have a rim of blue quartz. Blue quartz veins are, however, also found as cm-scale veins associated with the quartz-sulphide veins.

Kisters et al. worked on the regional structural grain of the Sermiligaarsuk area and the possible control of mineralisation in the Tartoq gold province. Supracrustal rocks of the Tartoq Group occur in six belts, forming allochtonous, infolded inliers in the TTG-dominated terrane. Two main stages of deformation, D_1 and D_2, are distinguished only followed by late-stage brittle faulting (D_3) with only minor influence on the present-day configuration of the belts. The D_1 deformation results in the imbrication of supracrustal packages of possibly different origin or crustal level. D_{1a} deformation along the shear zones point to dominantly top-to-the-SE thrust kinematics. The thrust zones are connected by steep strike-slip zones, resulting in an overall lateral and frontal ramp geometry in a fold-and-thrust belt. Subsequent deformation (D_{1b}) is characterised by extensional fabrics in chlorite schist and cataclasites, showing top-to-the W kinematics. The D_2 stage forms regional-scale fold structures during broadly SE-NW compression, which is responsible for the preservation of Tartoq Group belts in F_2 synclinoria. The structures are interpreted to having formed in a Neoarchaean subduction zone channel. The structural and metamorphic record is consistent with burial and exhumation of oceanic crust during NW-directed subduction, followed and overlapped by SE-directed return flow and accretion of the Tartoq Group rocks to the base of an overriding TTG terrane located to the west. Exhumation of the slivers to shallow-crustal levels is associated with pervasive fluid infiltration, pervasive to localised retrogression of the rocks and, in places, economic-grade gold mineralisation.

Polat & Dziggel describe the field relationships and petrology of ultramafic to felsic rocks of the Tartoq Group in the Iterlak, Amitsuarsua and Bikuben belts as a basis for later geochemical interpretation. The Iterlak belt is characterised by greenschists that are intercalated with up to 50 m thick meta-gabbro in which the primary magmatic textures are generally well-preserved. The typical greenschist facies mineral assemblages in the mafic rocks comprise chlorite, quartz, plagioclase, calcite, opaques, and minor epidote. The Amitsuarsua belt comprises variably deformed and hydrothermally altered pillow basalts and basaltic lava flows and minor ultramafic rocks. The pillow cores consist of quartz, chlorite, plagioclase, muscovite, calcite and epidote. Plagioclase is replaced by muscovite and/or epidote and zoisite. The 1-5 cm wide pillow rims are composed of chlorite and epidote. Mineral assemblages are interpreted to represent seafloor alteration and regional metamorphic overprint in the greenschist facies. In the Bikuben belt, peak metamorphic conditions reached the amphibolite facies with peak metamorphic mineral assemblages in the mafic rocks of hornblende, plagioclase, quartz and minor clinopyroxene and garnet. The rock types are banded amphibolites, ultramafic rocks, altered mica schists, pegmatite and orthogneiss.

Kolb & Olsen summarise field work and data compilation on hydrothermal mineralisation in the Tartoq gold province. Hydrothermal orogenic gold mineralisation occurs in all six belts of Tartoq Group rocks. With the exception of the amphibolite facies Bikuben area, the mafic rocks have a regional hydrothermal alteration assemblage comprising carbonate, chlorite and pyrite. Gold enrichment is recognised in the foot wall of thrust zones and fold hinges in spatial association with strike-slip zones. Furthermore, gold mineralisation is lithologically controlled by favourable wall rock composition, such as graphite- or magnetite-rich green-

schist and banded iron formation. The proximal hydrothermal alteration zone comprises ankerite, muscovite, quartz, pyrite, arsenopyrite, pyrrhotite, chalcopyrite, tennantite and gold. Magnetite in banded iron formation is mainly replaced by pyrite. Quartz and quartz-ankerite veins formed at various scales, ranging in width from mm- to m-scale. The hydrothermal alteration is characterised by a regional carbonate alteration and proximal enrichment in K, Si, base metals, Au and, locally, As. In the Bikuben area, the gold mineralisation is not fully understood and formation of foliation-parallel laminated quartz veins and hydrothermal alteration in the amphibolite facies or retrograde in the greenschist facies are possible.

Both gold provinces are characterised by the most important geological features that would be necessary to form large orogenic gold deposits. The areas are endowed with gold, represent compressional orogens, mainly formed in the greenschist and lower amphibolite facies and show syn- to late-tectonic intrusions. Based on this, the Paamiut and Tartoq gold provinces are considered to be highly prospective gold exploration areas in southern West and South-West Greenland.

Introduction

This is a field report covering localities studied in June–July 2010 in SW-Greenland. The field expedition and the follow up research work is co-financed by GEUS and the Bureau of Minerals and Petroleum (BMP), Nuuk, Greenland under the project entitled “Strukturelt kontrolleret hydrotermal omdannelse og mineralisering på regional skala og detaljestudie af udvalgte grønstensbælter i Sydvestgrønland 61°30’ – 64°00’”. The focus was two areas of known gold mineralisation, the Paamiut area in the north and the Tartoq area in the south. Additionally, available and public data from earlier investigations (both GEUS and various mineral exploration companies) in the Tartoq area were compiled and the results are described here. The aim of this report is to document the field investigations and the data collected during fieldwork and compilation, and combining and discussing this new data together with previous investigations and published accounts. A special focus is drawn on the potential for hydrothermal mineralisation and the documentation of the studied occurrences.

Four teams of two geologists and one additional geologist worked in different areas supported by helicopter: (1) J. Kolb (GEUS, project leader) and S. Weatherley (Oxford University) started fieldwork on Akuliaq in the Paamiut area and covered several locations in order to evaluate the regional gold potential. (2) M. Glendenning and E. Hastie (Windsor University) mapped the known gold occurrence on the Akuliaq peninsular at a 1: 2500 scale as part of their bachelor project. (3) D.M. Schlatter (GEUS) and K. Reynolds (Imperial College) worked on detailed sections on known gold occurrences in the Tartoq area. This work is part of K. Reynolds’ MSci thesis. (4) A. Dziggel (Aachen University) and A. Polat (Windsor University) studied the stratigraphy and regional metamorphic conditions in the Tartoq area and on the Akuliaq peninsula. (5) A.F.M. Kisters (University of Stellenbosch) studied the regional structural grain of the Tartoq area. As a basis, the 1:100 000 geological map sheets and the detailed field maps, field reports of the geologists that worked in the area before and open file company reports were taken into account and were found to be very useful (Anonymous 1985; Edsen & Halkjær 1992; Geisler 1972, 1973, 1974, 1975; Gowen 1992, 1993; Higgins 1990; Kalsbeek *et al.* 1990; King 1983, 1985; Petersen 1991, 1992). The field maps, especially those from the various exploration campaigns in the Tartoq area turned out to be very detailed and no major discrepancy between the maps and our investigations were found. However, some of the 1:100 000 geological map sheets are not very accurate, details are lost and the distinction between the different supracrustal rocks is not always correct. This is explained by the fact that mapping of the region was completed at a time when Archaean quartzofeldspatic gneisses were interpreted to be of sedimentary or volcanic origin (Andrews 1973; Berthelsen 1960; Kalsbeek 1970; Ramberg 1949). This was re-interpreted later, but the entire area between Frederikshåbs Isblink in the north and Sermiligaarsuk in the south is presented as one continuous region of undivided TTG gneiss, narrow belts of amphibolite and gabbro-anorthosite and the Tartoq Group (Higgins 1990; Kalsbeek *et al.* 1990). Inconsistencies in the maps are addressed in discussions with the colleagues from the mapping project with the BMP, and will be subject to amendments on the digital geological map.

Additional detailed information was compiled by J.Kolb and S.D. Olsen and is stored on the accompanying DVD. The DVD contains data from exploration companies and GEUS, geo-

logical maps of Neria, Midternæs and Ivigtut all at 1:100 000 scale, plus additional geological maps of Nuuluk, Iterlak, Amitsuarsua and Naalagaaffik in between 1:1000 to 1:5000 scales. Furthermore, the field data, figures and geochemical data from the Paamiut area are stored in a separate folder. The user is expected to be familiar with computers and software. The ArcGIS file is made in version 9.3.1, and the sample spread sheets in MS Office® 2003, hence the latter files have .xls extensions. The DVD contains three folders in the GIS Tartoq folder, ArcGIS931, Documentation and Geochemistry. ArcGIS931 contains the main file Taartoq_Gold_Province.mxd, when opened, it lists in hierarchical order rock-, sediment samples, contours and the geological maps. The detailed maps are displayed on top of the 1:100 000 scale maps. Subfolders under ArcGIS931 are Geology, Samples and Topography. The Documentation folder contains all the open file company reports, plus field reports by D.M. Schlatter. The Geochemistry folder contains Excel® spread sheets of the samples, arranged according to sampling method. If any of the data is used, the companies and GEUS/KMS hold the copyrights and the relevant references have to be made.

Disclaimer: GEUS is not liable or in any way guaranteeing for the data presented in the company reports.

Regional geological setting

The study area is situated in the southern part of the North Atlantic craton in western Greenland to the south of the Tasiusarsuaq terrane, which was the focus of field work in 2008 and 2009. Based on differences in metamorphic grade, the area is divided into four different blocks (Friend & Nutman 2001; McGregor & Friend 1997), from north to south: (1) the largely granulite facies Sioraq block; (2) the amphibolite facies Paamiut block; (3) the Neria block that was largely retrogressed from the granulite facies; and (4) the low metamorphic Sermiligaarsuk block comprising the volcano-sedimentary Tartoq Group. The Sioraq and Neria blocks both overly the Paamiut block with sharp contacts interpreted representing tectonic and/or thrust contacts (McGregor & Friend 1997). The Sioraq block underlies the Tasiusarsuaq terrane in the north, and the Neria block overlies the Sermiligaarsuk block (Friend & Nutman 2001). The Neria block was re-interpreted as representing a nappe of rocks that were retrogressed from the granulite facies to the amphibolite facies during thrusting and, therefore, re-named Neria nappe (Windley & Garde 2009). This nappe is interpreted to overly a continuous block of rocks of similar age, the ca. 2850 Ma Kvanefjord block, including Sioraq, Paamiut and Sermiligaarsuk blocks (Windley & Garde 2009).

The Sioraq block

The Sioraq block is characterised by TTG and, locally, dioritic gneiss. Supracrustal rocks form belts in the gneiss and comprise layered and homogeneous amphibolite, meta-ultramafic rocks and biotite-garnet-sillimanite gneiss (Fig. 1). In places, layered meta-gabbro and meta-leucogabbro units occur. The granodioritic gneiss shows evidence of partial melting, and orthopyroxene is present in the TTG gneiss where not retrogressed from granulite facies peak (Friend & Nutman 2001; McGregor & Friend 1997). Garnet is widespread in TTG gneiss that is retrogressed to the amphibolites facies (Friend & Nutman 2001; McGregor & Friend 1997). Garnet at the expense of orthopyroxen in the retrogressed gneiss possibly indicates an isobaric cooling path for the Sioraq block (cf., Harley 1989).

The large-scale structure is characterised by map-scale fold interference pattern. Early folds show NW-SE trending axial traces, whereas the axial planes of the later folds are close to orthogonal and trend NE-SW (Fig. 1).

U-Pb zircon age data of TTG gneiss yield 2863 ± 7 Ma, 2839 ± 9 Ma and 2837 ± 8 Ma as magmatic protolith ages (Friend & Nutman 2001). Zircons dated at 2812 ± 9 Ma, 2797 ± 10 Ma and 2786 ± 19 Ma are interpreted as representing the granulite facies metamorphic event (Friend & Nutman 2001). Retrogression to amphibolites facies possibly occurred at ca. 2760 Ma. A zircon age of 2717 ± 34 Ma may be interpreted as the age of further amphibolite facies retrogression and juxtaposition with the Tasiusarsuaq terrane (Friend & Nutman 2001).

The Paamiut block

The Paamiut block (Fig. 1) is made up of TTG gneiss that is dominated by biotite as the mafic mineral. Pegmatites poor in mafic minerals are common as concordant sills in the TTG gneiss (McGregor & Friend 1997). Up to 1.5 km thick supracrustal belts are dominated by amphibolites with local meta-ultramafic rocks and biotite schist interpreted as representing a meta-sedimentary rock (Friend & Nutman 2001). The mineral assemblages and locally preserved igneous textures in the TTG gneiss are used to suggest that metamorphism of rocks in the Paamiut block not exceeded amphibolite facies grades (Escher 1971; McGregor & Friend 1997).

The map pattern of foliation trends and supracrustal belts shows a fold interference pattern with early NE-SW trending and younger NW-SE trending axial traces (Fig. 1).

Intrusion ages of the magmatic protoliths of TTG gneisses are dated by U-Pb zircon data at 2852 ± 7 Ma, 2874 ± 10 Ma and 2872 ± 16 Ma, respectively (Friend & Nutman 2001).

The Neria block

The Neria block (Fig. 1) is dominated by nebulitic tonalitic and dioritic gneiss that show evidence for retrogression in the amphibolites facies after granulite facies peak metamorphism (McGregor & Friend 1997). The TTG gneiss shows abundant layer-parallel pegmatite sills and, locally, intrusions of trondhjemitic gneiss (Friend & Nutman 2001; McGregor & Friend 1997). Enclaves and rafts of metamorphosed mafic rocks and leucogabbro-melanogabbro-anorthosite rocks are common. The entire block forms a tight synform with NE-SW trending axial trace (McGregor & Friend 1997).

U-Pb zircon ages for the intrusion of the magmatic precursors of the TTG gneiss vary considerably between 2978 – 2872 Ma (n=6, Friend & Nutman 2001; Nutman & Kalsbeek 1994), possibly indicating multiple episodes of magmatism and a complex history of the Neria block gneisses. Data derived from zircon overgrowth point to a major metamorphic event at around 2830 Ma (2827 ± 11 Ma Nutman & Kalsbeek 1994) (2816 ± 12 Ma Friend & Nutman 2001). Detrital zircons from a meta-sedimentary rock yield 2857 ± 12 Ma as a possible age of sedimentation (Nutman *et al.* 2004). Metamorphic overgrowths suggest metamorphism of the sedimentary rock at ca. 2830 Ma, 2750 Ma and 2650 Ma (Nutman *et al.* 2004).

The Sermiligaarsuk block

This block is characterised by the volcano-sedimentary rocks of the Tartoq Group that overly TTG gneiss in synformal structures (Fig.1 , Higgins 1990; Higgins & Bondesen 1966) (Berthelsen & Henriksen 1975). The Tartoq group consists of amphibolite, hornblende-chlorite schist, chlorite schist and minor meta-conglomerate, quartzite, meta-pelite, quartz-muscovite gneiss, BIF, serpentinite and talc-schist (Appel & Secher 1984; Ayrton 1963; Higgins 1968; Higgins & Bondesen 1966; Weidmann 1964). The characteristic metamor-

phic grade of the lithologies lies in the greenschist to lower amphibolite facies (Higgins 1968, 1990; Higgins & Bondesen 1966) (Berthelsen & Henriksen 1975).

The TTG gneiss comprises biotite and hornblende gneiss (Higgins 1968; Higgins & Bondesen 1966). The contacts to the Tartoq Group are generally tectonic, however, interfingering and layer-parallel gneiss sheets in greenstone belts suggest an intrusive relationship (Higgins & Bondesen 1966; Windley *et al.* 1966). Syn- to late-tectonic pegmatites are common along the contact between TTG gneiss and the Tartoq Group rocks (Higgins 1968).

Two deformation stages are distinguished (Higgins 1968): (1) The penetrative foliation is formed and the rocks are folded into large-scale nappe structures; and (2) open, upright folds form the synclines, in which the Tartoq Group greenstone belts are preserved.

The TTG gneiss to the south of the Sermiligaarsuk fjord record ages up to 3.0 Ga (unpubl. data mentioned in Nutman *et al.* 2004). Tonalitic gneiss that intruded into rocks of the Tartoq Group has a U-Pb zircon age of 2944 ± 7 Ma, providing a minimum age for the volcano-sedimentary unit (Nutman & Kalsbeek 1994). However, detrital zircons from quartz-muscovite gneiss from the Tartoq Group yield a minimum age of 2842 ± 6 Ma for their deposition (Nutman *et al.* 2004). This possibly suggests that the rocks summarised under the Tartoq Group from north and south of Sermiligaarsuk fjord are unrelated (Nutman *et al.* 2004).

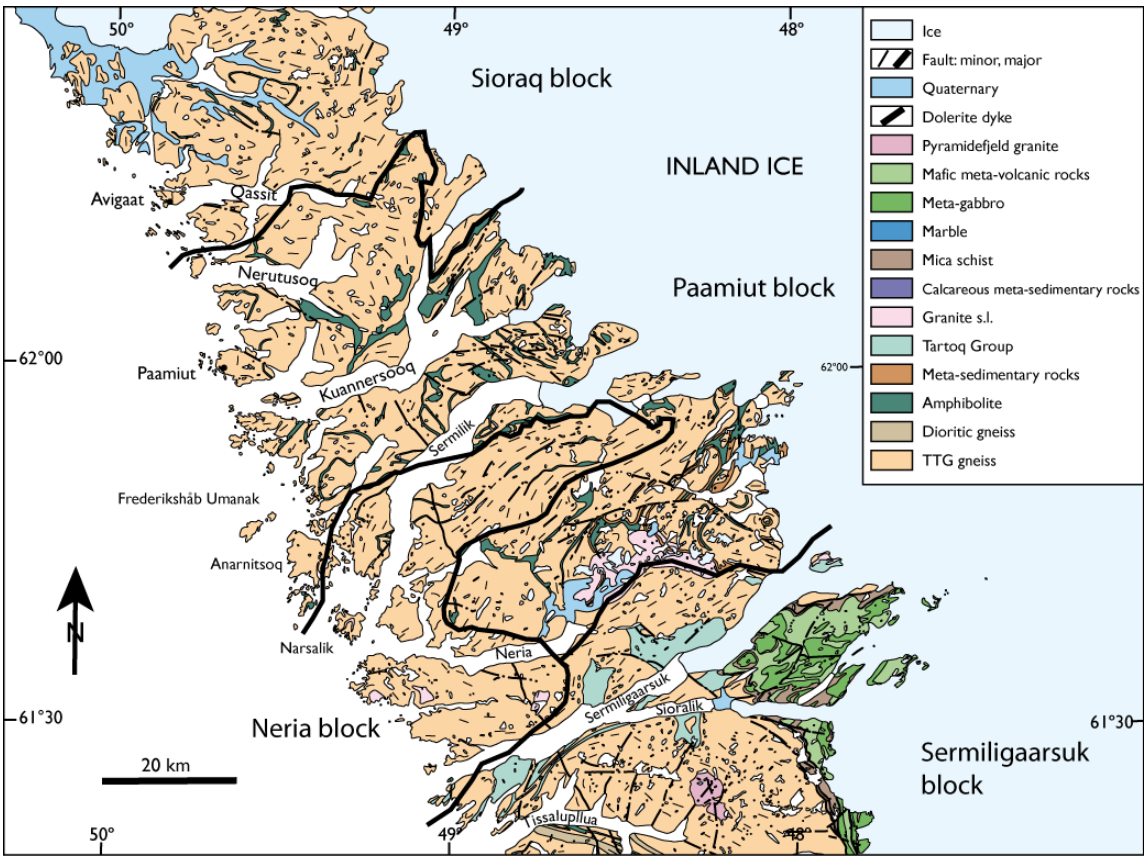

Figure 1. *Geological map of Southwest Greenland and location of the study area covered by field work in 2010 (modified after, Escher & Pulvertaft 1995).*

Geology of the Paamiut area

The Paamiut area was studied in greater detail in a PhD study by J.C.Escher (Escher 1971). In this work some lithologies are described in greater detail. It is clear from the descriptions that the lenses of amphibolite and meta-ultramafic rocks in the gneiss are similar to those from the so called Kvanefjord amphibolites in the larger supracrustal belts (Escher 1971). The distinction into two groups of rocks with different ages was based on the old idea that the supracrustal rocks (i.e. Kvanefjord amphibolite) formed in synclines on top of a gneiss basement and, thus, must be younger than the gneiss and the enclaves in the gneiss. Our view from field impressions is, however, the opposite that the precursor rocks of the gneisses intruded into the Kvanefjord amphibolite and the amphibolite and meta-ultramafic enclaves in the gneiss represent remnants of the Kvanefjord amphibolite.

Lithology

TTG gneiss is the dominant lithology and four types are distinguished (Escher 1971): (1) banded biotite-gneiss; (2) homogeneous nebulitic biotite-gneiss; (3) banded hornblende-biotite gneiss; and (4) agmatitic gneiss containing amphibolite fragments of variable size. The banded gneiss has an about 1 cm leucosome-melanosome banding parallel to the penetrative foliation in the region. The rocks are fine- to medium-grained, granoblastic granite, granodiorite and quartz-diorite with the granodiorite being the dominant lithology. The banded biotite-gneiss is composed of plagioclase, quartz, K-feldspar, biotite and minor apatite, sphene, allanite, zircon and ore. The plagioclase is An_{24} and is devoid of internal zoning. It, locally, forms myrmekitic intergrowth textures with quartz. The K-feldspar is perthitic in places. The hornblende-biotite gneiss is distinguished by the additional presence of hornblende in the mineral assemblage and the agmatitic gneiss as well as the homogeneous nebulitic biotite-gneiss by their fabric. Contacts between the different gneiss types are generally gradational. Epidote, muscovite, chlorite and calcite form a retrograde mineral assemblage in all gneisses. The various gneiss types are mapped as one single group. Field work in 2010 has shown, that the banded and nebulitic gneiss types with evidence for partial melting are most dominant in the eastern parts close to the Inland Ice. Granoblastic to porphyritic TTG gneiss dominates the area from Akuliaq to the coastal areas.

Foliation-parallel lenses of amphibolite and meta-ultramafic rock occur in the gneiss (Escher 1971). The amphibolite is fine- to medium-grained and in places coarse-grained. It is granoblastic comprising hornblende, plagioclase ± garnet, quartz and minor sphene, magnetite, ilmenite and apatite. An-content in plagioclase ranges between An_{30-40}. Amphibolites also show local retrogression by a epidote, biotite, chlorite and carbonate assemblage. During 2010 field work, we were able to distinguish between different types of amphibolites that probably represent different precursor rock types.

The term “Kvanefjord amphibolites” is used to summarise the different supracrustal and ultramafic lithologies of the greenstone belts in the Kvanefjord area (Escher 1971). Five rock types are distinguished (Escher 1971): (1) amphibolite; (2) hornblendite; (3) meta-pyroxenite; (4) meta-peridotite and (5) meta-sedimentary rocks.

The amphibolite is fine- to medium-grained comprising a hornblende, plagioclase and quartz assemblage with minor actinolite, epidote, garnet, biotite, sphene, apatite, magnetite and ilmenite. An-content in plagioclase ranges between An_{30-40}. Amphibolites also show local retrogression by a chlorite and carbonate assemblage. The fabric varies from banded to more massive with locally preserved pillow structures, suggesting that at least some of the amphibolites represent metamorphosed volcanic rocks.

The meta-ultramafic rocks are medium- to coarse-grained and comprise (1) hornblendite with a hornblende, actinolite and tremolite assemblage, with minor magnetite, ilmenite, sphene and plagioclase; (2) meta-pyroxenite with a hornblende and diopside assemblage; and (3) meta-peridotite comprising olivine, serpentine, talc, carbonate, tremolite, actinolite, magnetite and ilmenite. The rocks contain locally retrograde epidote, biotite, chlorite and carbonate. In the meta-peridotite, a replacement paragenesis of olivine to serpentine to talc to magnesite and ore to tremolite and actinolite to talc to chlorite is observed. Meta-sediments are very rare and are sillimanite-bearing gneiss. Pegmatites form concordant and discordant dykes of variable extent.

The contact to the gneiss is either gradational with a zone of increased veining in the Kvanefjord amphibolite or tectonic by shear zones or faults.

The mineral assemblages of all lithologies are characteristic of a peak metamorphic over-print in the amphibolite facies. This peak is followed by two retrograde stages in the epi-dote-amphibolite facies and in the greenschist facies.

Structural geology

Escher (1971) distinguishes five stages of deformation. His interpretation is biased by the idea that the Kvanefjord amphibolites are emplaced on a previously deformed gneiss basement. This is based on discordant planar fabrics at the contact between gneiss and Kvanefjord amphibolite in two places. Therefore, the first two deformation stages are re-stricted to gneiss and after D_2 followed the deposition of the supracrustal rocks. The struc-tural interpretations based on this assumption make a correlation with our data difficult or nearly impossible. Escher's (1971) structural interpretations are summarised briefly below.
The first deformation stage is characterised by intrafolial folds (F_1) that, locally refold an even earlier fold generation, and a penetrative S_1 foliation. During F_2, folds at all scales were developed. They have near-vertical axial planes and N-S to NE-SW trending axial traces. The smaller folds are tight to isoclinal. The third stage is defined by F_3 folds that have variable NW-SE to NE-SW trending axial traces in the Kvanefjord amphibolite. The banding and migmatisation is parallel to the axial planar S_2 foliation and formed in the am-phibolite facies. Smaller F_3 folds are closed to isoclinal. Locally, intrafolial folds were re-folded. F_4 folds have NE-SW trending axial traces, formed in the amphibolite facies and are generally upright. An axial planar S_3 foliation is developed, which located dextral shear in places. Open F_5 folds having NW-SE trending axial traces are locally developed in the gneiss only. Several generations of dykes and faults follow the fivefold stages.

References

Andrews, J.R. 1973: Stratigraphic, structural and metamorphic features of Archaean (pre-Ketilidian) rocks in the Frederikshåb district. In: Park, R.G. & Tarney, J. (eds): The early Precambrian of Scotland and related rocks of Greenland, 179-187. Keele: University of Keele.Anonymous 1985: Efterforskningskoncession til Greenex A/S Uummannaq i området mellem Ivigtut og Frederikshåb. Koncession nr. 61. 1985, 24, Greenex A/S. Internal report.

Appel, P.W.U. & Secher, K. 1984: On a gold mineralization in the Precambrian Tartoq Group, SW Greenland. Journal of the Geological Society London **141**, 273–278.

Ayrton, S.N. 1963: A contribution to geological investigations in the region of Ivigtut, S.W. Greenland., Copenhagen: Geological Survey of Greenland Bulletin.

Berthelsen, A. 1960: Structural studies in the pre-Cambrian of western Greenland. II. Geology of Tovqussap nunâ. Meddelelser om Grønland **123**, 223.

Berthelsen, A. & Henriksen, N. 1975: Geological map of Greenland, 1:100,000 Ivittuut 61 V.1 Syd (with description), 169. Copenhagen: Geological Survey of Greenland.

Edsen, N.A. & Halkjær, M. 1992: Kujataa 1992. Results of geophysical fieldwork, 9, Nunaoil A/S. Internal report.

Escher, J.C. 1971: The geology of Akuliaq with particular bearing on the origin and evolution of the supracrustal Kvanefjord belt, Frederikshåb area, South-West Greenland, 108. Unpublished thesis, University of Lausanne.

Escher, J.C. & Pulvertaft, T.C.R. 1995: Geological map of Greenland, 1:2 500 000, Copenhagen: Geological Survey of Greenland.

Friend, C.R.L. & Nutman, A.P. 2001: U-Pb zircon study of tectonically bounded blocks of 2940-2840 Ma crust with different metamorphic histories, Paamiut region, South-West Greenland: implications for the tectonic assembly of the North Atlantic craton. Precambrian Research **105**, 143-164.

Geisler, R.A. 1972: Investigations on the Renzy Mines Limited Frederikshåb concession, Greenland, to June 15, 1972, 6, Renzy Mines Ltd. Internal report.

Geisler, R.A. 1973: Investigations on the Renzy Mines Limited Frederikshåb concession, Greenland, during the year ended June 18, 1973, 3, Renzy Mines Ltd. Internal report.

Geisler, R.A. 1974: Investigations on the Renzy Mines Limited Frederikshåb concession, Greenland, for the year ending June 15, 1974. , 8, Renzy Mines Ltd. Internal report.

Geisler, R.A. 1975: Investigations on the Frederikshåb exploration concession of Renzy Mines Ltd. During the year ended June 15, 1975, 19, Renzy Mines Ltd. Internal report.

Gowen, J. 1992: Kujata 1992. Re-analysis of Nuuluk drill core, Taartoq greenstone belt, Sermiligaarsuk, SW Greenland, May 1992, 18, NunaOil A/S. Internal Report.

Gowen, J. 1993: 05/92-drilling and prospecting at the Taartoq Archaean greenstone belt, SW Greenland July-August 1993, 16, NunaOil A/S. Internal Report.

Harley, S.L. 1989: The origins of granulites: a metamorphic perspective. Geological Magazine **126**, 215-247.

Higgins, A.K. 1968: The Tartoq Group on Nuna qaqortoq and in the Iterdlak area, South-West Greenland. Rapport Grønlands Geologiske Undersøgelse **17**, 17.

Higgins, A.K. 1990: Descriptive text to 1:100 000 sheets Neria 61 V.1 N and Midternæs 61 V.2 N, 23. Copenhagen: Geological Survey of Greenland.

Higgins, A.K. & Bondesen, E. 1966: Supracrustals of pre-Ketilidian age (the Tartoq Group) and their relationships with Ketilidian supracrustals in the Ivigtut region, South-West Greenland. Rapport Grønlands Geologiske Undersøgelse **8**, 21.

Kalsbeek, F. 1970: The petrography and origin of gneisses, amphibolites and migmatites in the Qasigialik area, South-West Greenland. Meddelelser om Grønland **189**, 70.

Kalsbeek, F., Larsen, L.M. & Bondam, J. 1990: Descriptive text to 1:500 000 sheet 1, Sydgrønland., 36. Copenhagen: Geological Survey of Greenland.

King, A.R. 1983: Report on sampling and prospecting in Sermiligarssuk Fjord area, South-West Greenland, 16, Greenex A/S. Internal Report.

King, A.R. 1985: Sermiligarssuk exploration concession. Report on geological field work carried out in the Sermiligarssuk Fjord, South West Greenland, 18, Greenex A/S. Internal report.

McGregor, V.R. & Friend, C.R.L. 1997: Field recognition of rocks totally retrogressed from granulite facies: an example from Archaean rocks in the Paamiut region, South-West Greenland. Precambrian Research **86**, 59-70.

Nutman, A.P. & Kalsbeek, F. 1994: A minimum age of 2944 ± 7 Ma for the Tartoq Group, South-West Greenland. Rapport Grønlands Geologiske Undersøgelse **161**, 35–38.

Nutman, A.P., Friend, C.R.L., Barker, S.L.L. & McGregor, V.R. 2004: Inventory and assessment of Palaeoarchaean gneiss terrains and detrital zircons in southern West Greenland. Precambrian Research **135**, 281-314.

Petersen, J.S. 1991: Kujataa project 1991. Gold mineralization in the Taartoq group greenstones, SW Greenland, results of structural, geochemical and geophysical studies, 44, NunaOil A/S. Internal Report.

Petersen, J.S. 1992: Kujataa: field report - 1992. Nuuluk-Iterlak gold and massive sulfide project, Taartoq Archaean greenstone belt, SW Greenland, 55, NunaOil A/S. Internal Report.

Ramberg, H. 1949: On the petrogenesis of the gneiss complexes between Sukkertoppen and Christianshaab, West-Greenland Preliminary report. Meddelelser fra Dansk Geologisk Forening **11**, 312–327.

Weidmann, M. 1964: Géologie de la région située entre Tigssaluk fjord et Sermiligârssuk fjord (partie médiane), SW-Groenland, 146. Copenhagen: Geological Survey of Greenland Report.

Windley, B.F. & Garde, A.A. 2009: Arc-generated blocks with crustal sections in the North Atlantic craton of West Greenland: crustal growth in the Archaean with modern analogues. Earth-Science Reviews **93**, 1-30.

Windley, B.F., Henriksen, N., Higgins, A.K., Bondesen, E. & Jensens, B. 1966: Some border relations between supracrustal and infracrustal rocks in South-West Greenland., 43. Copenhagen: Geological Survey of Greenland Report.

Results from 2010 field work in the Paamiut area (Kolb and Weatherley)

Jochen Kolb[1] & Samuel Weatherley[2]

[1] Geological Survey of Denmark and Greenland – GEUS, Øster Voldgade 10, DK-1350, København, Denmark

[2] Department of Earth Sciences, University of Oxford, South Parks Road, Oxford OX1 3AN, United Kingdom

Four sites in the Paamiut area were visited and studied in detail. The first site was chosen on the Akuliaq peninsular in order to prepare M. Glendenning and E. Hastie for their mapping project and to re-evaluate the hydrothermal gold occurrences found by NunaMinerals A/S. We give a brief summary here, but most of the data on Akuliaq will be presented below.

Geology of the Akuliaq peninsular

The dominating lithology on the southern tip of the peninsular is amphibolite (Figs. 1 and 2). In detail, several types of amphibolite that probably represent different precursor rocks are distinguished (Fig. 3): (1) fine-grained massive amphibolite comprising hornblende, plagioclase and quartz; (2) fine- to medium-grained banded amphibolite with variable amounts of hornblende and plagioclase defining the banding; and (3) medium-grained amphibolite containing 2 – 4 mm grains of hornblende and plagioclase. The latter, medium-grained amphibolite forms 20 – 40 cm wide and 2 – 4 m long lenses, whereas the other two types form thick stratigraphic units. In the amphibolites, up to 2 m wide and 10 m long lenses of quartz-biotite schist occur, which is interpreted as metamorphosed aplite (Fig. 3). The quartz-biotite schist is fine-grained, white to light grey and comprises plagioclase, K-feldspar, quartz, biotite and, locally, tourmaline. The feldspars form porphyroclasts in places. Ultramafic lithologies occur mainly in the southeast of Akuliaq. These are mainly black, medium-grained hornblendite with only minor amounts of plagioclase.

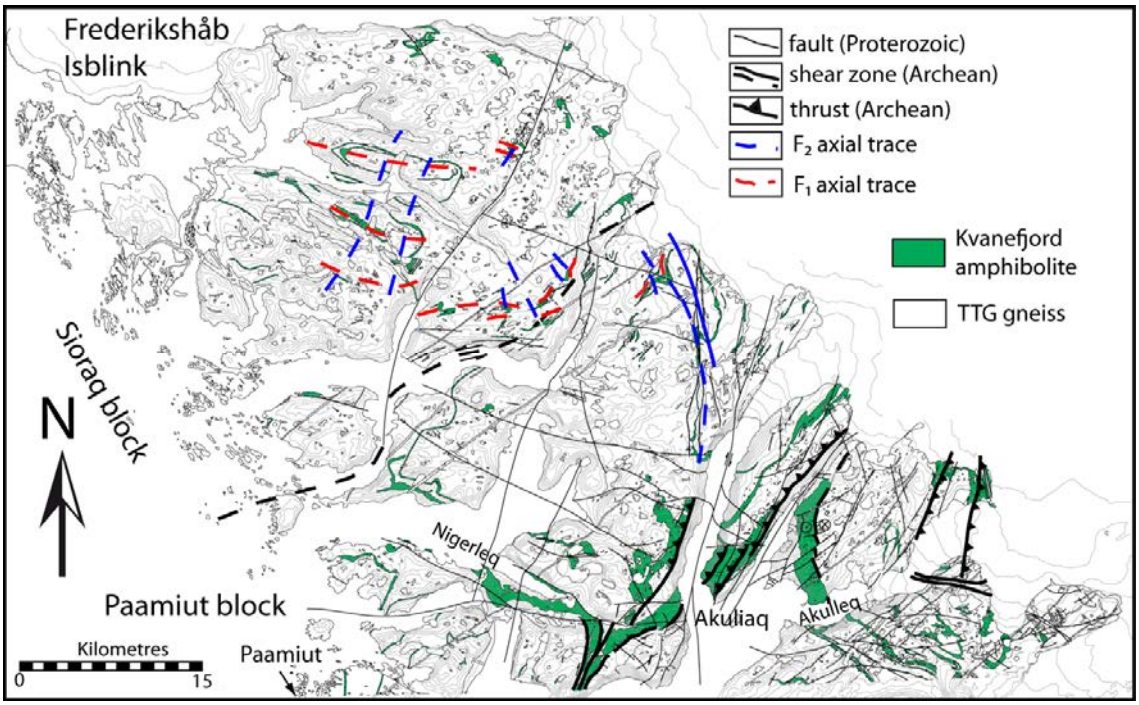

Figure 2. *Schematic geological map of the Sioraq and Paamiut blocks (modified after Escher & Jensen 1976; Jensen 1976). The Sioraq block is characterised by fold interference pattern showing an anti-clockwise rotation to the southern contact with the Paamiut block. The Paamiut block comprises the Kvanefjord amphibolite and a dextral strike-slip – thrust zone system.*

These supracrustal lithologies are intruded by tonalitic gneiss in the north (Fig. 4a). The medium-grained gneiss is composed of plagioclase, quartz, biotite and minor hornblende (Fig. 4b). About 5 m wide and 30 – 70 m long lenses of amphibolite occur foliation-parallel in the tonalitic gneiss. All three types of amphibolite can be found.

All rocks are intruded by a prominent, 5 m wide and > 200 m long pegmatite in the south-east (Fig. 4c). The pegmatite is medium- to coarse-grained, comprising K-feldspar, plagio-clase, quartz, muscovite and, locally biotite, and tourmaline. Tourmaline is mainly found in places where the pegmatite intruded quartz-biotite schist (Fig. 4d).

Figure 3. *Photographs of the major supracrustal rocks on Akuliaq: (a) The contact of massive amphibolite at the base with quartz-biotite schist and medium-grained amphibolite at the top. Note the small quartz vein at the contact between quartz-biotite schist and massive amphibolite; (b) Banded amphibolite that is folded into F_1 folds. (c) Intrusive relationship between quartz-biotite schist and amphibolite. The quartz-biotite schist is interpreted as representing metamorphosed aplite dykes and sills. (d) Dyke-like structure of quartz-biotite schist showing F_1 folds in amphibolite.*

Structure

The structural grain is dominated by a NE-SW trending pervasive foliation that is closely spaced in several up to 100 m wide high strain zones. Compositional banding and hornblende define the S_1 foliation in the amphibolite. The L_1 mineral stretching lineation is defined by hornblende needles and plagioclase rods, and is generally down-dip (Figs. 5a and b). Locally, oblique mineral stretching lineation is observed, which is also defined by hornblende. Shear sense indicators are rare, but σ- and δ-clasts of plagioclase suggest reverse and oblique-reverse sense of movement to the southeast/east (Fig. 6a; D_1). Locally, cm-scale folds are observed (Fig. 3b). These folds are close to isoclinal asymmetric and their fold axes plunge to the north/northwest (Fig. 5b). The fold axes are in places parallel to the mineral stretching lineation or are curved, forming sheath folds with their long axis parallel to mineral stretching (Fig. 6b).

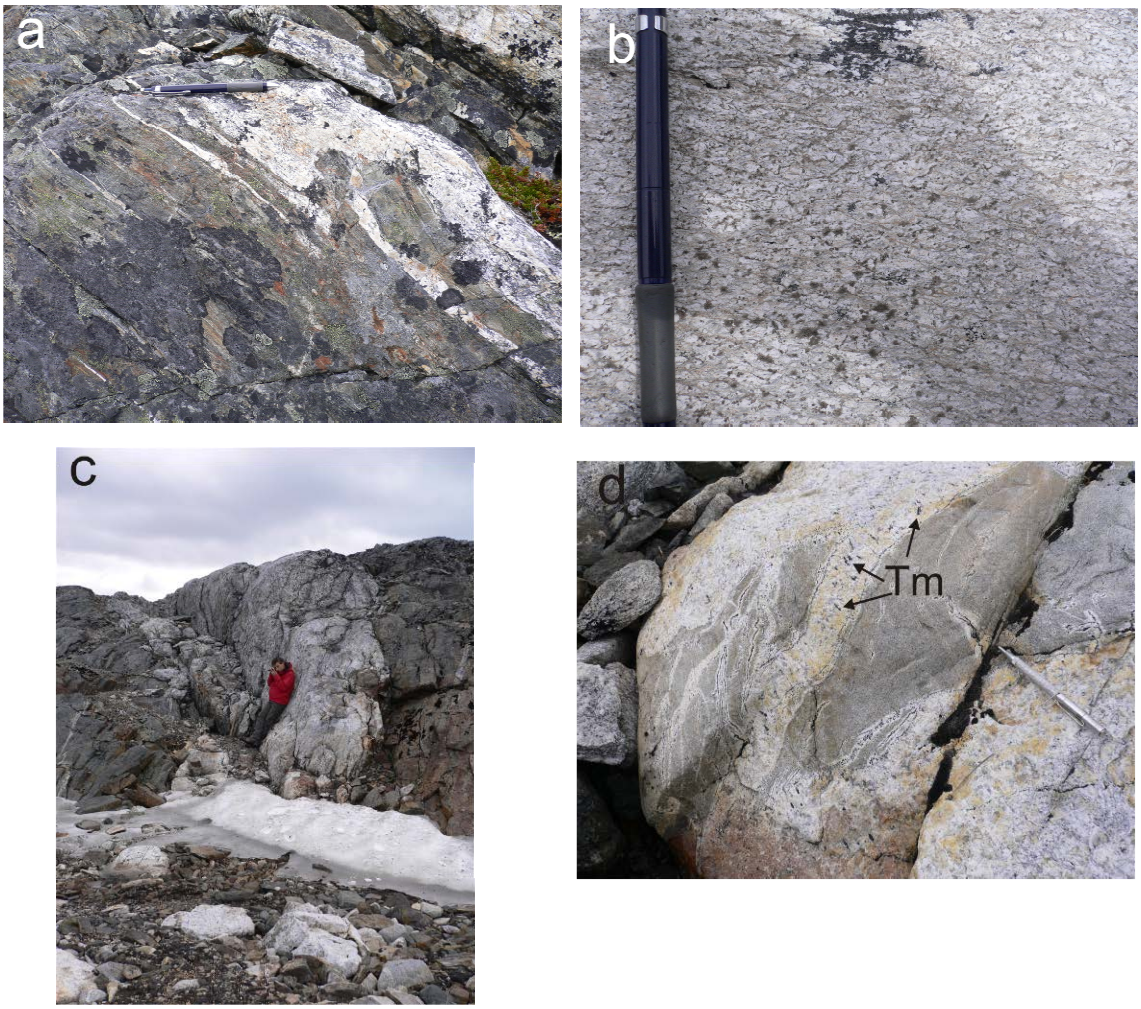

Figure 4. *(a) TTG gneiss-amphibolite contact indicating that the TTG precursor rock intruded into the amphibolite. (b) Characteristic medium-grained porphyritic texture of TTG gneiss on Akuliaq. (c) Pegmatite dyke in amphibolite and hornblendite wall-rock. (d) Tourmaline (Tm) developed in the pegmatite that intruded a meta-aplite dyke.*

A crosscutting foliation has a cm-scale spacing and forms ecc-fabrics together with the S_1 foliation (Fig. 6a). These ecc-fabrics are also defined by hornblende-plagioclase-quartz assemblages. The asymmetry of these fabrics indicates extensional shearing to the northwest. A conjugate set of quartz-calcite-ankerite veins crosscut all foliations. One set dips at 20 – 30° to the northeast, whereas the other set dips at 50 – 60° to the southeast (Figs. 5c and 6c). The intersection probably marks the orientation of the intermediate palaeostress and is plunging shallow at about 25° to the northeast. The acute angle of the conjugate set of fractures together with dragging of the foliation suggests a near vertical orientation of compression and northwest-southeast extension (Fig. 5c). The asymmetry of the conjugate set is consistent with extension to the northwest as recorded by the extensional-crenulation-cleavage, ecc-fabrics (Figs. 6a and c). Both fabrics could therefore mark different steps in progressive extension (D_2). Brittle faults of various orientations crosscut all structures and lithologies.

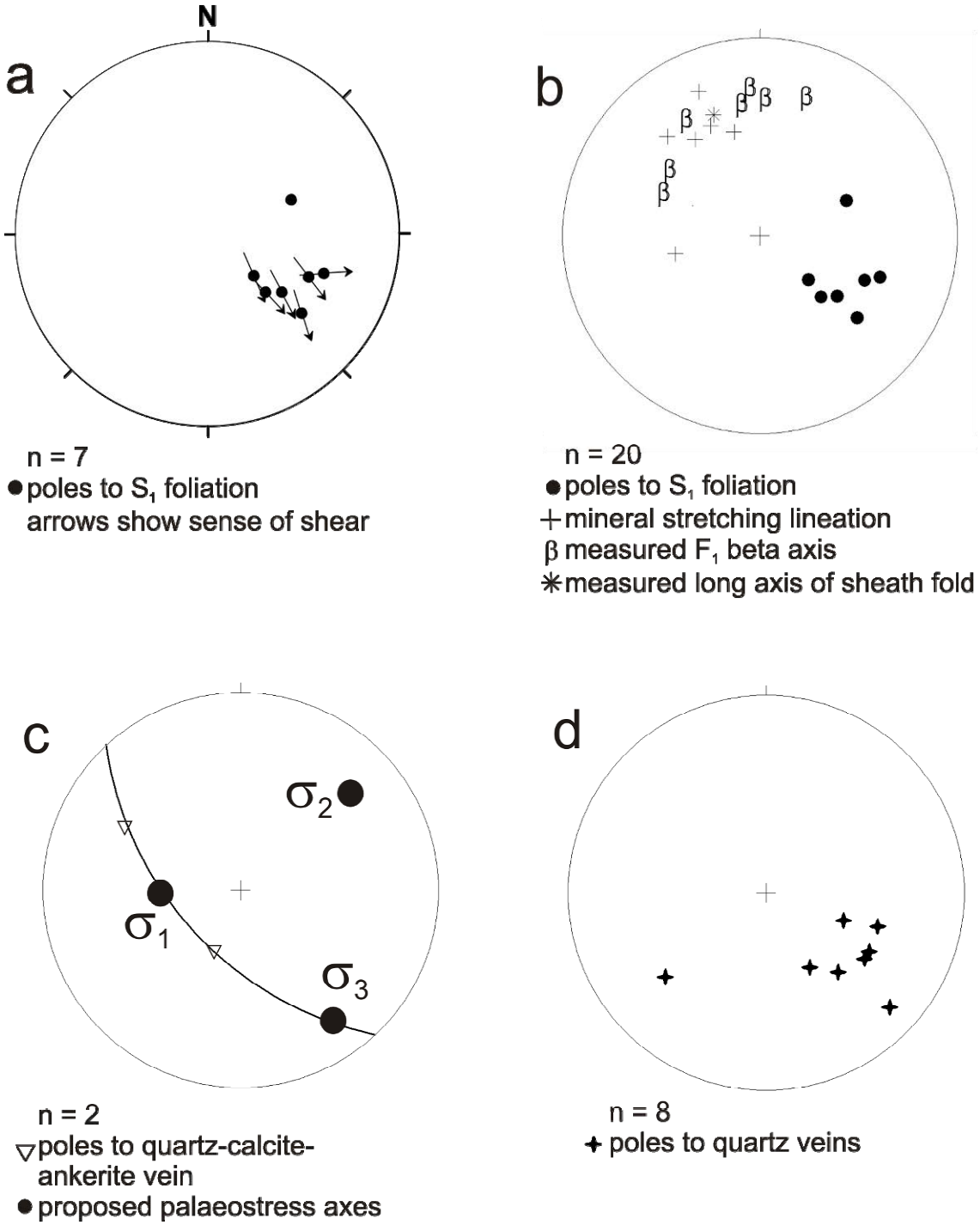

Figure 5. *(a) Poles of S_1 foliation with stretching lineation. Arrows indicate direction of transport (lower hemisphere, equal area projection). (b) Summary of structural data showing poles of S_1, mineral stretching lineation and fold axes. Note that mineral stretching lineation and the long axis of the sheath fold are parallel (lower hemisphere, equal area projection). (c) Poles to the late conjugate fracture system (D_2) and the orientation of the proposed related palaeostress field (lower hemisphere, equal area projection). (d) Poles to hydrothermal quartz veins. Most of the veins are parallel to the S_1 foliation, suggesting that they represent shear veins (lower hemisphere, equal area projection).*

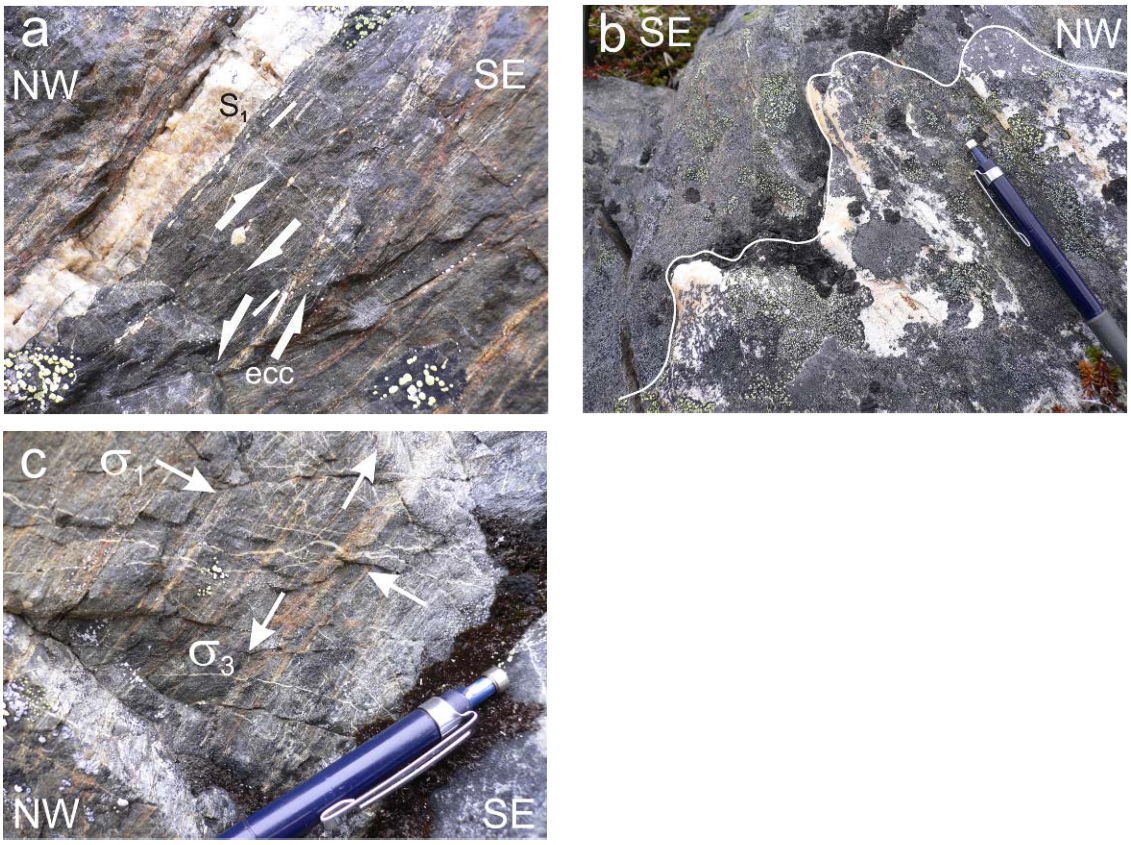

Figure 6. *(a) Various fabrics in amphibolite. The penetrative foliation is the S_1 foliation. σ- and δ-clasts indicate reverse sense of shear to the southeast. A slightly oblique foliation forms ecc-fabrics, pointing to normal shearing to the northwest during D_2. Note the S_1-parallel laminated quartz vein and the rusty sulphide weathering showing the hydrothermal alteration zone. (b) Sheath fold in a felsic layer in banded amphibolite. Note the curvature of the fold axis, which is also represented by the regional structural readings (compare Fig. 5b). The pen marks the orientation of the mineral stretching lineation. (c) Conjugate set of veinlets and proposed palaeo-stress field during their formation. The stress field and the sense of deformation are consistent with the ecc-fabrics (Fig. 6a) and, thus, both fabrics formed contemporaneously during D_2.*

Structure of hydrothermal quartz ± gold veins

Gold mineralisation in the Paamiut area was explored in more detail since 2005 by NunaMinerals A/S on the Akuliaq peninsula. The prospect was, however, not a primary target and not fully explored. Two mineralised zones are distinguished: (1) Quartz-carbonate alteration zones containing pyrite, chalcopyrite and arsenopyrite have up to 12 g/t gold; and (2) quartz veins with carbonate-pyrite-arsenopyrite alteration halos contain up to 4 g/t gold. The gold mineralisation is hosted in quartz and quartz-carbonate veins. Milky quartz veins are generally barren (Fig. 7a).

The quartz veins are generally 2 – 20 cm wide, only very few are wider and reach up to 20 m width. Milky quartz veins crosscut the blue-grey quartz veins that host the bulk of the gold mineralisation. Three different sets of quartz veins are distinguished (Fig. 7): (1) S_1 foliation parallel shear veins; (2) folded veins where the S_1 foliation is axial planar and (3) veins crosscutting the S_1 foliation at an angle typical of extensional shear veins. Due to

progressive deformation, it is not clear whether the folded veins formed before the S_1 foliation or during the development of the same foliation and progressive shortening. The latter explanation is, however, favoured by the authors because all three vein types have the same mineralogy and alteration halos, and the geometry of the folded veins suggests that they probably originated as extensional shear veins and extension veins that are observed to be present in low-strain zones. A model for the development of the different quartz veins is that veins formed initially during D_1 reverse shearing as a set of veins in shear vein, extensional shear vein and extension vein orientation (Fig. 8). Progressive compression deformation and shortening perpendicular to the shear zone boundary resulted in boudinage of shear veins parallel to the S_1 foliation and folding of veins that initially formed oblique to the shear zone boundary, i.e. extensional shear veins and extension veins.

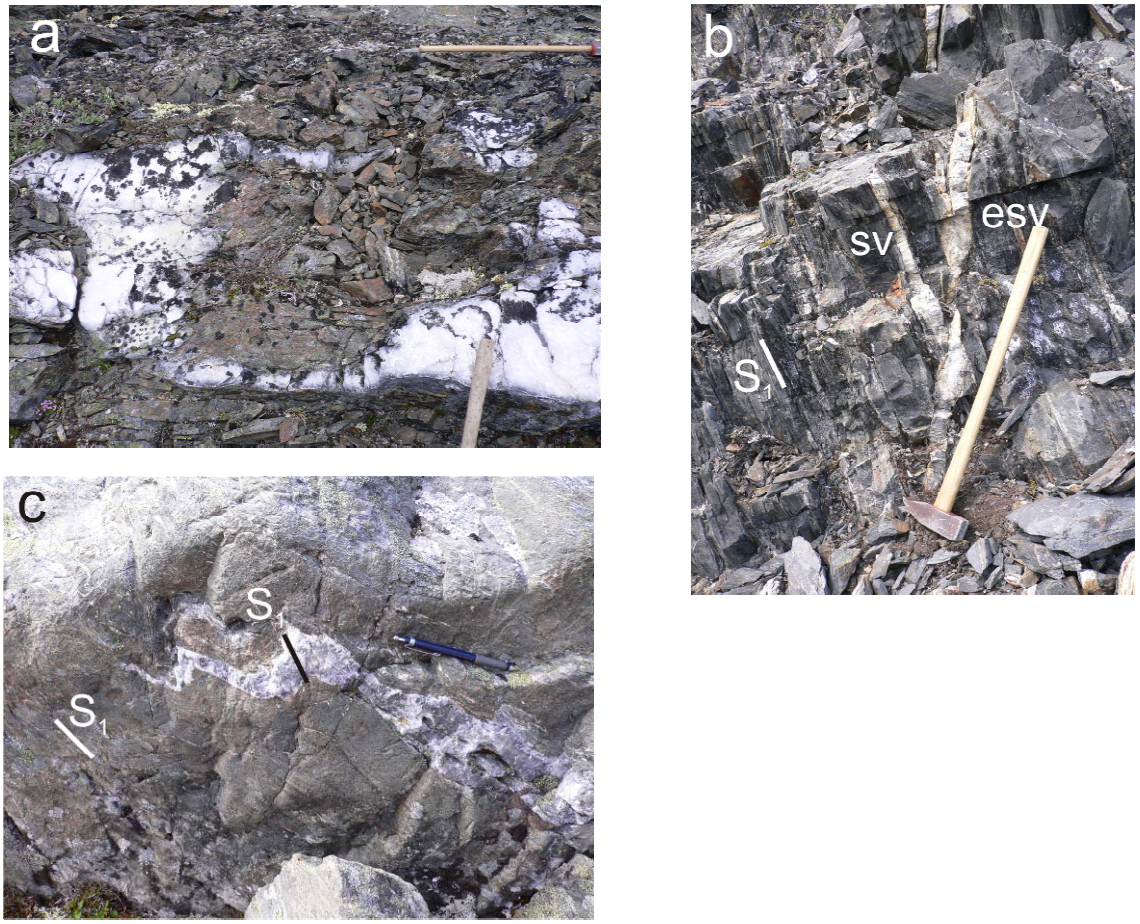

Figure 7. *(a) Large m-scale milky quartz vein. These veins are generally barren. (b) About 3 cm wide veins, one parallel to the S_1 foliation representing a shear vein (sv), and the second vein cross cutting foliation at an angle characteristic of extensional shear veins (esv). (c) Folded extensional shear vein with S_1 as axial planar foliation. The folding is interpreted to be related to progressive D_1 shearing and compression of the shear zone.*

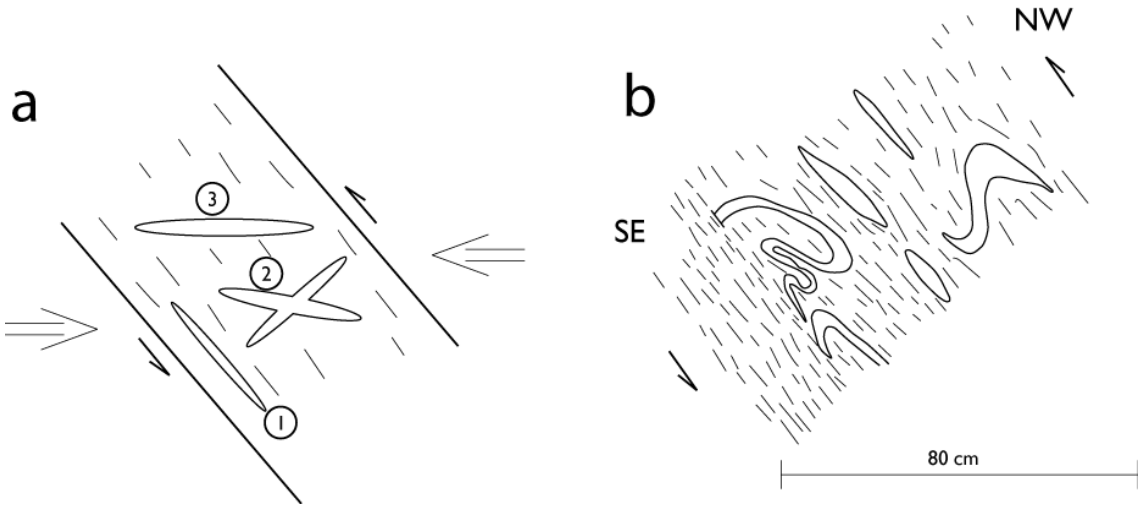

Figure 8. *Model for the evolution of quartz veins during D_1 deformation. (a) Schematic sketch of the initial stage of D_1 reverse shearing. Quartz veins develop as: (1) shear veins parallel to the foliation; (2) conjugate set of extensional shear veins; and (3) extension veins. (b) Schematic sketch of an outcrop at 10SWE003, where shear veins parallel to S_1 remain unaffected by progressive deformation or are boudinaged and the two other vein sets are intensely folded during progressive deformation in the same palaeostress field.*

Hydrothermal alteration and gold mineralisation

Hydrothermal alteration zones of variable width are developed surrounding the quartz veins (Fig. 9). In addition to quartz, the quartz veins locally contain arsenopyrite and up to 380 ppb Au. It should be noted that the samples were not taken in order to define gold grades, but only to show gold enrichment. In amphibolite, the quartz veins have a 1 – 4 cm wide amphibole halo. The distal alteration is characterised by quartz, hornblende or orthoamphibole, biotite, tourmaline, pyrrhotite, arsenopyrite and, locally, garnet and muscovite (Figs. 9a and b). Generally Si, As and Au are enriched. In the quartz-biotite schist, the hydrothermal alteration assemblage comprises quartz, muscovite and hornblende (Fig. 9c). Si, W, As, Mo and Au are enriched.

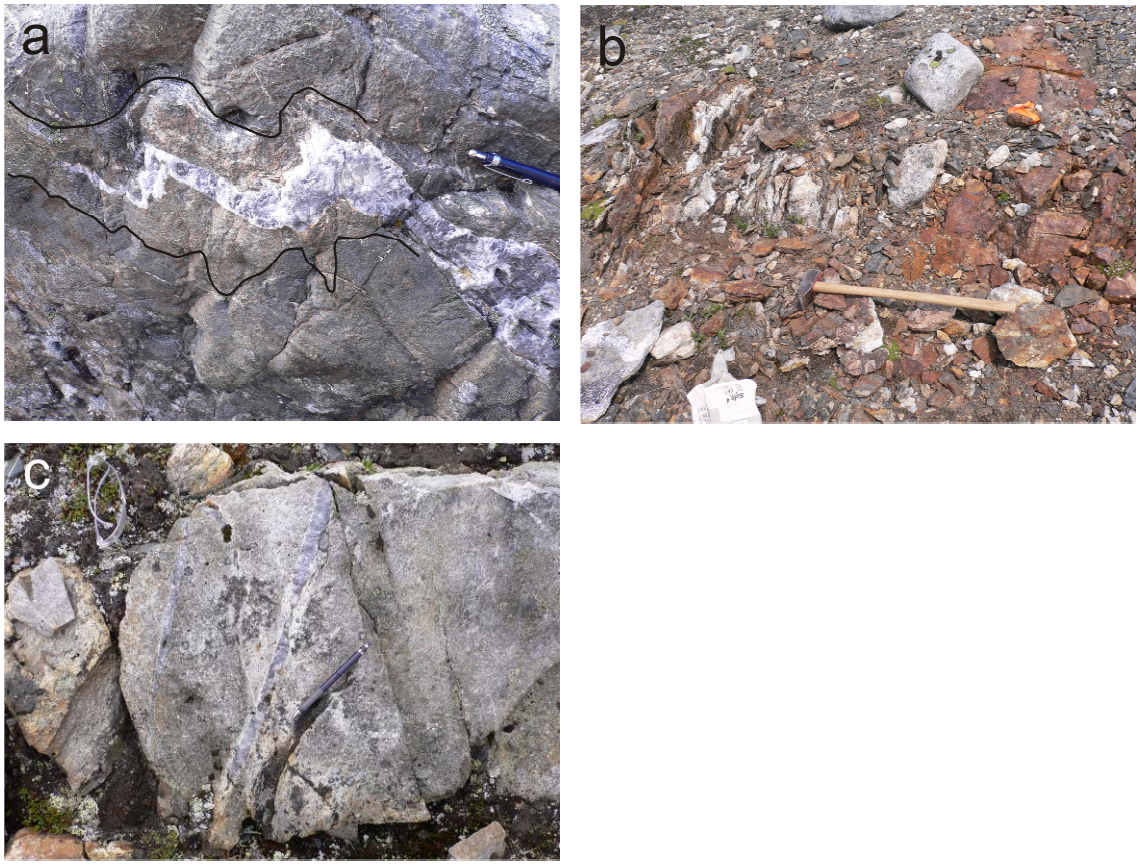

Figure 9. *(a) About 10 cm wide hydrothermal alteration halo around a folded extensional shear vein (approximate outline marked). (b) Outcrop of a hydrothermal quartz vein surrounded by a weathered sulphide-bearing hydrothermal alteration zone. (c) Small alteration halo around hydrothermal quartz veins in quartz-biotite schist. Hydrothermal alteration is easy recognised by the white coloured muscovite alteration of the feldspar.*

Geology between Nigerlikasik and Akulleq

A 1.5 – 2 km wide belt of supracrustal rocks trending north-south is surrounded by TTG gneiss to the east and the west (Figs. 1 and 2). At the lithological contact, several about 2 – 4 m wide sheets of TTG gneiss intruded lit-par-lit into the supracrustal rocks. The TTG gneiss to the east of the belt is medium-grained, well-foliated and comprises quartz, plagioclase, hornblende and, in places, biotite (Fig. 10a). Locally, plagioclase grains form cm-scale porphyroclasts, resulting in an augen fabric of the gneiss. The TTG gneiss is intruded by up to 10 cm wide felsic dykes parallel and oblique to the penetrative foliation (Fig. 10a). The dykes are weakly foliated and contain quartz, K-feldspar, plagioclase and hornblende.
Despite the supracrustal rocks are only mapped and described earlier as amphibolite and meta-ultramafic rocks, they comprise a succession of different rock units that can be distinguished in the field. From east to west, there is an about 1.5 km wide belt of rocks:

- About 7-10 m wide lenses of actinolite-biotite schist;
- Several 100 m of amphibolite and banded amphibolite;
- Several 100 m of meta-andesite and meta-dacite;
- Several 100 m of amphibolite and banded amphibolite;
- About 5 m wide lenses of meta-peridotite.

The actinolite-biotite schist is dark greenish to black, medium-grained and contains biotite, actinolite and plagioclase (Fig. 10b). This rock forms lenses at the eastern contact between the supracrustal rocks and the TTG gneiss. The surrounding rocks are amphibolite and banded amphibolite. They are fine- to medium-grained, greenish rocks, comprising variable amounts of hornblende, plagioclase, quartz, sphene and, locally, garnet and orthoamphibole (Figs. 10c and d). The banding is due to variable amount of amphiboles and plagioclase-quartz in the rocks. Primary textures are in places preserved. The fine-grained amphibolite shows cm-scale rounded fragments that can be interpreted as representing agglutinate fragments deposited during effusive volcanism. The banded amphibolite is characterised by graded bedding showing younging direction towards west and probably represents a metamorphosed crystal tuff (Fig. 10e). The meta-andesite is a buff-coloured fine-grained rock composed of plagioclase, quartz, hornblende, biotite and epidote. It locally preserved primary fiamme textures, indicating an effusive volcanic nature of the rock (Fig. 10e). The meta-peridotite is olivine-rich and has orange-brown colours (Fig. 10f). The olivine is retrogressed to talc and serpentine.

Structure

The supracrustal rocks have a penetrative, near-vertical, north-south trending S_1 foliation (Figs. 11 and 12a, b). The mineral stretching lineation is defined by hornblende needles and plunges moderately to steeply towards northerly directions (Fig. 12b). Sense of shear markers such as σ-clasts, S-C fabrics and S-C' fabrics indicate sinistral oblique reverse movement (Figs. 12 a and b). Minor cm-scale folds were observed locally, characterised by steeply plunging fold axes (Fig. 12b). Locally, close to horizontal fold axes are also observed. The folds form cm-scale, tight to isoclinal intrafolial folds (Fig. 11b). The S_1 foliation forms kink bands in places (Fig. 13). These kink bands indicate vertical compression and horizontal extension, which is interpreted as the D_2 extension. The late, conjugate set of quartz-calcite-ankerite veins is also observed and consistent with D_2 extension as recorded by the kink bands (Fig. 11c).

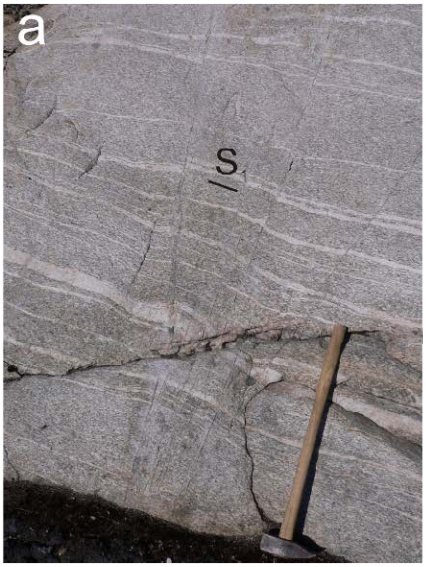
a
S1


b


c
Grt
S1


d
fining


e


f

Figure 10 (previous page). *Photographs of the wall rocks. (a) Porphyritic TTG gneiss with cm-scale felsic dykes parallel and oblique to the S_1 foliation. (b) Typical dark green actinolite-biotite schist showing roundish fabrics, which could be interpreted as primary magmatic. (c) Banded amphibolite showing white to black banding parallel the S_1 foliation due to variable plagioclase and hornblende contents. Note the cm-scale garnet mainly in the black, hornblende-rich layers. (d) Cyclic layering in banded amphibolite, starting with a black, hornblende-rich layer followed by a medium-grained plagioclase-hornblende layer and continuous fining upward. This fabric is interpreted as representing a fining-upward sequence of metamorphosed volcaniclastic rocks and used to define direction of stratigraphic younging. (e) Fiamme-textures in an intermediate rock type, the meta-andesite, indicating a volcaniclastic origin of this rock type. (f) Typical orange-brown surface weathering colour of meta-peridotite. The black minerals are magnetite.*

Figure 11. *(a) Penetrative S_1 foliation showing S-C fabrics that indicate sinistral sense of shear. (b) Tight isoclinal intrafolial fold. The fold formed during regional NW-SE directed progressive shortening and subsequent oblique reverse shearing on S_1 planes. (c) Late, conjugate vein set that formed during D_2 E-W oriented extension.*

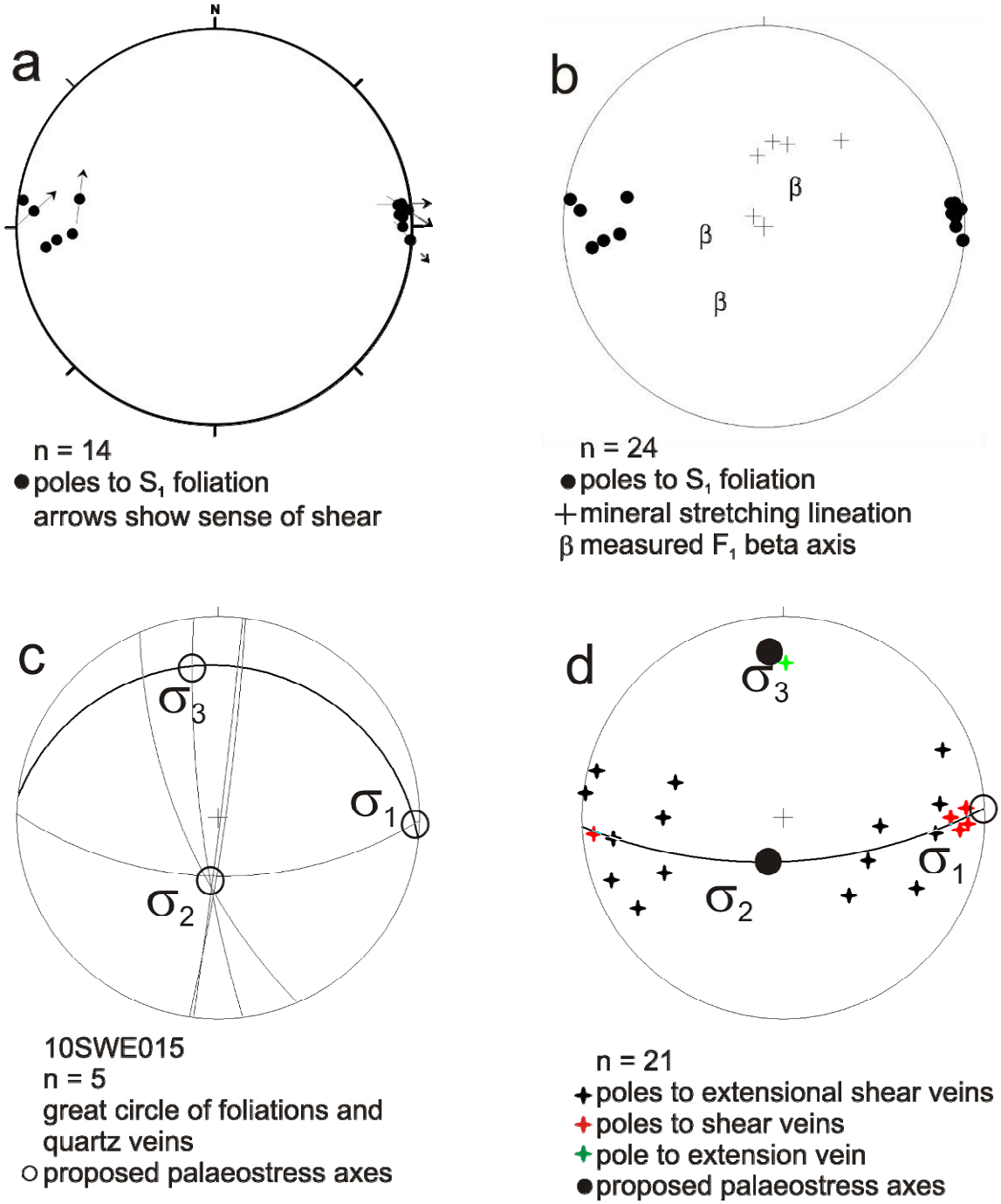

Figure 12. *(a) Poles of S_1 foliation with stretching lineation. Arrows indicate direction of transport (lower hemisphere, equal area projection). (b) Summary of structural data showing poles of S_1, mineral stretching lineation and fold axes (lower hemisphere, equal area projection). (c) Great circles of a conjugate set of hydrothermal quartz veins from one outcrop (10SWE015). The intersections of foliations, shear veins, extensional shear veins and extension veins are used to estimate the palaeostress field during the formation of the hydrothermal gold-bearing veins (lower hemisphere, equal area projection). (d) Poles to hydrothermal quartz veins and proposed palaeostress field (cf.; Fig. 12c). The orientation of various hydrothermal quartz veins of the Nigerlikasik-Akulleq area is consistent with their formation during progressive D_1 E-W directed shortening (lower hemisphere, equal area projection).*

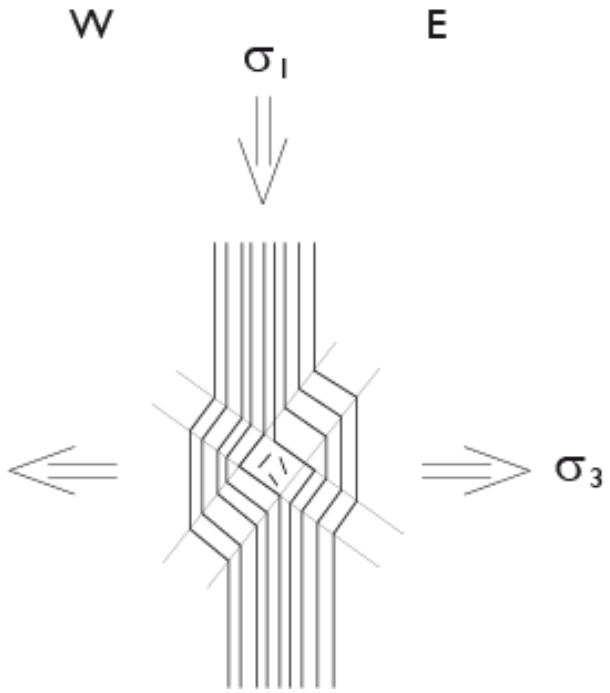

Figure 13. *Schematic sketch of a kink band as commonly observed in the Nigerlikasik-Akulleq area. The kink bands formed during D_2 E-W oriented extension (cf.; Fig. 11c).*

Structure of hydrothermal quartz ± gold veins

Quartz veins occur at the eastern contact of supracrustal rocks and TTG gneiss and at lithological contacts within the supracrustal succession. The blue-grey veins range from mm-scale to up to 3 m wide veins that can be followed over 30 m along strike. Most of the quartz veins are about 10 cm wide and 4 – 6 m along strike. Again, three different sets of quartz veins are distinguished (Figs. 12c, d and 14): (1) S_1 foliation parallel shear veins; (2) veins perpendicular to the foliation, representing extension veins (3) veins crosscutting the S_1 foliation at an angle typical of extensional shear veins. The shear veins occur in vein arrays as laminated veins or with a regular spacing of about 1 m (Fig. 14b). The extension veins and extensional shear veins form conjugate sets and are, locally, aligned en echelon (Figs. 13c, d and 14). In places, these veins form protrusions parallel to the S_1 foliation. The veins oblique to the foliation are commonly folded to a variable degree similar to those on Akuliaq described above.

Some of the vein systems remained intact and can be used to estimate the orientation of the palaeostress field. At 10SWE015 extensional shear veins and extension veins are developed (Figs. 12c and 14a). The extension vein dips at 66° to the south, which, in agreement with the acute angle of the extensional shear veins, indicates east-west oriented compression during the formation of the veins. The intersection of S_1 and all veins is common and plunges at 65° to the south. This probably marks the orientation of the medium principle stress σ_2. Using all the quartz vein data from the area, it is obvious that the extensional shear veins vary in orientation, probably due to progressive deformation (Fig. 13d). The overall picture of the orientation of the palaeostress axes is not different from the detailed observations from one outcrop. All quartz veins, therefore, most probably formed during east-west compression, which is correlated with D_1 deformation in the region.

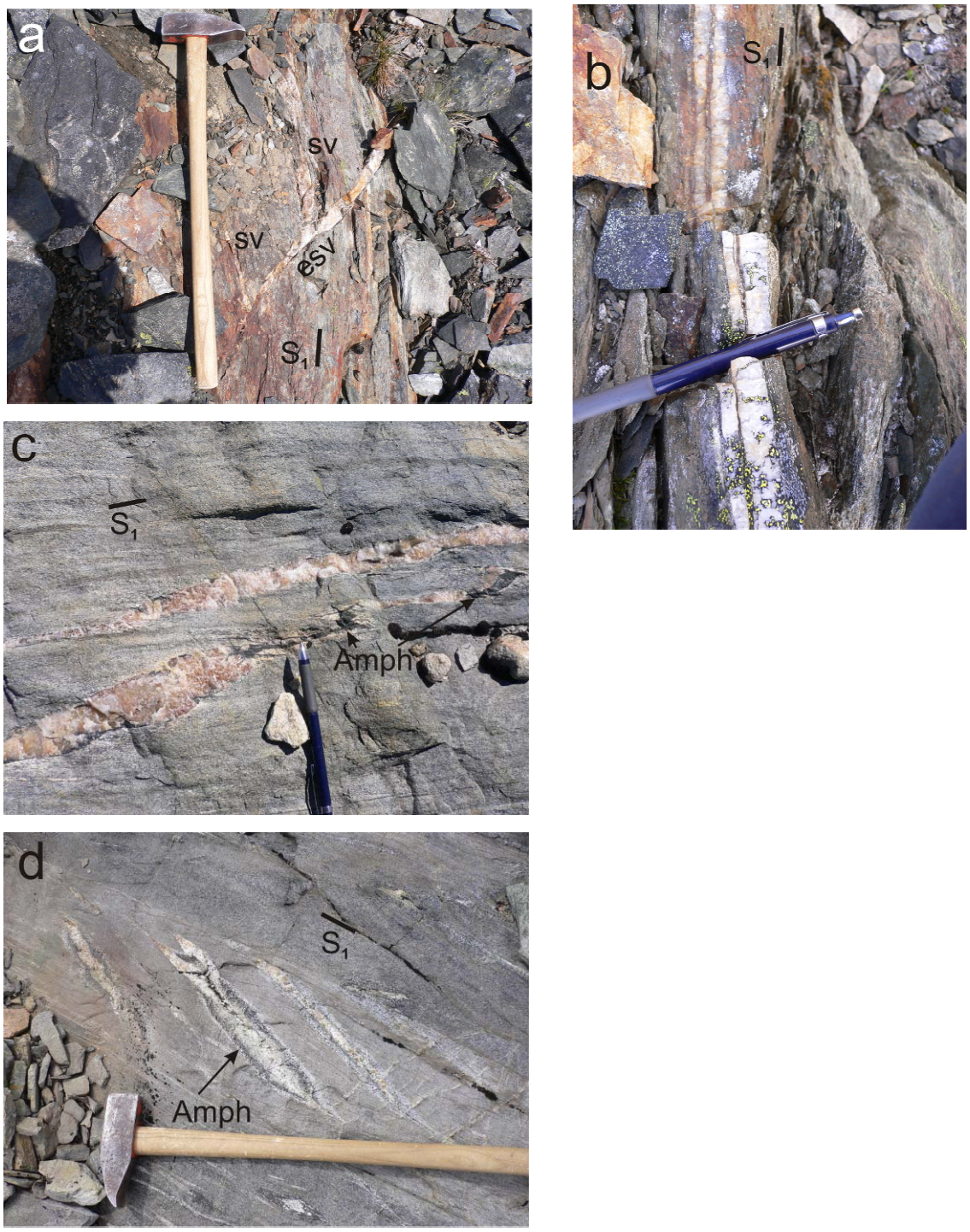

Figure 14. *Photographs of hydrothermal quartz veins and alteration zones. Rusty brown colours are related to the weathering of sulphides in the vein and hydrothermal alteration halo. (a) Conjugate set of shear veins (sv) parallel to S_1 and oblique extensional shear veins (esv) from outcrop 10SWE015 (cf.; Fig. 13c). (b) Laminated quartz veins developed parallel to S_1. (c and d) En echelon extensional shear veins in metamorphosed basaltic (c) and andesitic (d) wall rocks. Note the amphibole (Amph) halo and coarsening of the minerals around the veins due to hydrothermal alteration.*

Hydrothermal alteration and gold mineralisation

Gold was previously not reported from this area, however, the quartz veins and hydrothermal alteration halos are very similar to those from Akuliaq. The veins are composed of quartz and minor pyrrhotite and arsenopyrite. Gold is enriched to up to 40 ppb Au. Hydrothermal alteration halos are variable in size depending on the width and strike extent of the quartz veins. The veins commonly have an amphibole halo (Figs. 14c and d). Generally, the hydrothermal alteration assemblage in amphibolite comprises hornblende, quartz, biotite, arsenopyrite, pyrrhotite and locally orthoamphibole, epidote and calcite. In amphibolite, orthoamphibole or calcite form mm-scale selvages of quartz veins, and a hornblende-biotite-quartz assemblage is characteristic of the broader hydrothermal alteration halo. The meta-andesite shows a saussuritisation of feldspars as the main effect of hydrothermal alteration. Locally, hornblende and biotite are formed (Fig. 14d). The TTG gneiss is characterised by a hornblende-biotite-tourmaline alteration assemblage around the quartz veins. Generally Si, As, Ag, Au and Br are enriched in the alteration zones.

Geology between Nigerlikasik and Akulleq glaciers

An approximately 1 km wide, horseshoe shaped supracrustal belt is situated within TTG gneiss as shown on the geological map. Meta-ultramafic lithologies form lenses in the supracrustal belt, and pegmatites intruded the different lithologies. In the field, the picture is more complicated than shown on the map. The extent of supracrustal rocks is much less than the map suggests. The general picture is that lenses of supracrustal rocks and meta-ultramafic rocks, that are 10 – 50 m wide and several hundred metres along strike, are surrounded by shear zones and syn-tectonic felsic intrusions (Fig. 15a). These coarse-grained felsic intrusive rocks dominate the area and are, therefore termed leuco-granite (instead of pegmatite).

Meta-gabbros are medium-grained black-white-coloured rocks, comprising hornblende, plagioclase and quartz. Locally, compositional, probably primary magmatic layering is observed. The rocks contain cm-scale, coarse-grained leucocratic pockets and dykelets that are composed of plagioclase, quartz and clinopyroxene that are interpreted as *in situ* melt pockets (Figs. 16a and b). Locally, hornblende is observed instead of clinopyroxene.
Metamorphosed ultramafic rocks are medium-grained and greenish or brownish in colour (Fig. 15b). They consist of different amounts of orthopyroxene, clinopyroxene, olivine, magnetite, biotite and minor plagioclase. They are commonly retrogressed and have a talc-serpentine-biotite assemblage. Locally, primary layering is suggested by colour and compositional variations.

The supracrustal rocks are very similar to those described for the other regions but, locally, contain orthopyroxene and *in situ* melt pockets and dykelets (Figs. 15c and 16c). The amphibolites/mafic granulites are fine-to-medium-grained and preserved the banded fabric in places. The rocks are mainly composed of hornblende, plagioclase and minor quartz and garnet. Garnet has commonly a plagioclase rim. The melt pockets are medium-grained and comprise clinopyroxene, plagioclase, garnet and quartz (Fig. 16c). The meta-dacite is fine-grained containing coarse-grained melt pockets. Both comprise quartz, plagioclase and hornblende in different amounts (Fig. 16d).

Figure 15. *Photographs of the different lithologies between the Nigerlikasik and Akulleq glaciers. (a) Lenses of brownish and dark greenish meta-ultramafic rocks and supracrustal rocks surrounded by leuco-granite, forming duplex structures. (b) TTG gneiss (TTG) showing migmatitic banding at a cm-scale parallel to the foliation. The contact to the medium-grained, dark greenish meta-ultramafic rocks (UM) is intrusive. (c) Banded amphibolite/granulite with cm-scale, foliation parallel banding of mafic and intermediate layers. The white, coarse-grained pockets are sites of in situ partial melting. (d) Leuco-granite dyke (LG) intruded into meta-ultramafic rocks (UM).*

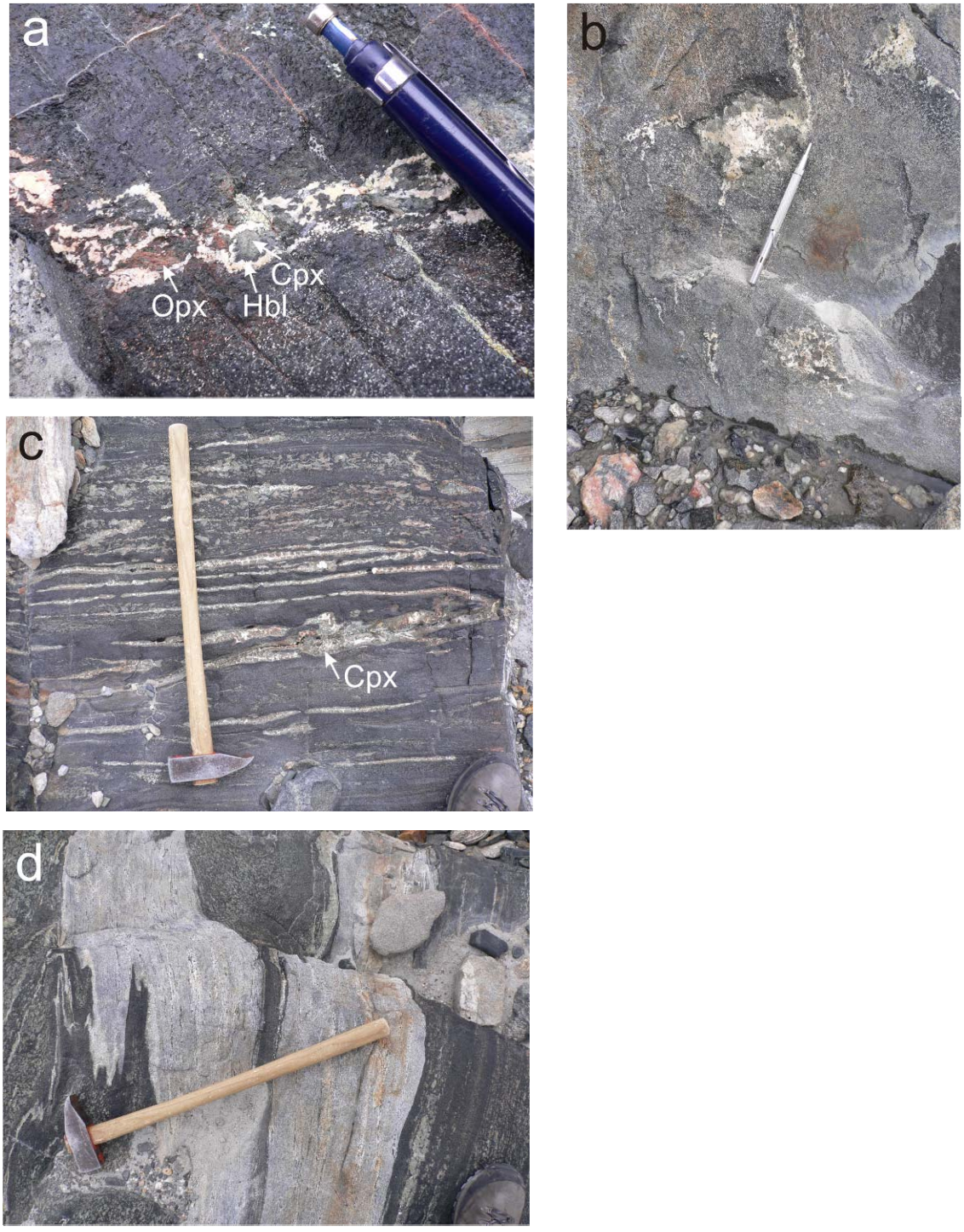

Figure 16. *Photographs of different in situ partial melt fabrics. (a) Partial melt pocket in a meta-gabbro, comprising orthopyroxene (Opx), clinopyroxene (Cpx), plagioclase and quartz. Hornblende (Hbl) forms retrograde rims around clinopyroxene and orthopyroxene. (b) Melt pockets in meta-gabbro. The pockets have an irregular shape with some leucocratic dykelets in their periphery, characteristic of in situ partial melt fabrics. (c) Clinopyroxene, plagioclase and quartz dykelets in amphibolite/mafic granulite forming a set of parallel in situ partial melt pockets. (d) The meta-dacite shows coarser-grained pockets composed of quartz, plagioclase and hornblende indicating in situ partial melting.*

The TTG gneiss is medium-grained and comprises quartz, plagioclase, biotite and, locally, hornblende and magnetite. It is characterised by migmatitic banding at a cm-scale Fig. 15b). The TTG gneiss forms sheets at a 10 – 100s m-scale.

All lithologies are intruded by leuco-granite sheets, which are coarse-grained and contain quartz, K-feldspar, plagioclase, biotite and, locally, hornblende and garnet (Fig. 15d).

Structure

The structure of the area is characterised by broadly north-south trending D_2 thrust zones that dip moderately to the east (Figs. 17a and 18a). These thrust zones have a spacing of several hundred metres. Between the thrust zones earlier D_1 fabrics are preserved being variably reactivated during the later D_2, resulting in a complex interference pattern (Figs. 17b,c and 18b). The early S_1 foliation is mainly preserved in meta-gabbro, meta-ultramafic rocks and TTG gneiss. The TTG gneiss sheets are parallel to this S_1 foliation. This foliation is folded into cm-scale open to close folds with their axial planes parallel to the S_2 foliation in the thrust zones. Locally, an earlier fold generation is observed in TTG gneiss, where the axial planes are near-horizontal (Fig. 17d). The fold axes are parallel and plunge at shallow angles to the north-northwest, indicating coaxial deformation. Especially along the competent meta-gabbro and meta-ultramafic rock lenses, the S_1 foliation is reactivated during D_2, forming large-scale duplex structures (Figs. 17a-c). In the thrust zones, the S_2 foliation is the penetrative foliation and has a down-dip mineral stretching lineation. Shear sense indicators, such as σ-clasts, δ-clasts, S-C fabrics and the duplex structures, point to reverse transport along the thrusts to westerly directions (Figs. 17a-c and 18a). Locally, the S_2 foliation is steepened to near-vertical orientation. Shear sense indicators and mineral stretching lineation indicate a dextral strike-slip deformation in some of the steep zones.

Commonly, the D_2 thrust and steep zones are intruded by leuco-granite (Figs. 17a-c and 18c). These rocks have very different structures ranging from coarse-grained undeformed to mylonitic and cataclasitic, indicating syn-tectonic intrusion (Fig. 17e). Ductile and brittle fabrics are parallel and show consistent sense of movement to the west. If the cataclastic structures are related to the D_2 deformation, a progressive deformation stage from the ductile into the brittle regime or late brittle reactivation remains unclear.

The overall structural picture resembles a melange zone, where different rock types with potentially different metamorphic history are tectonically interleaved.

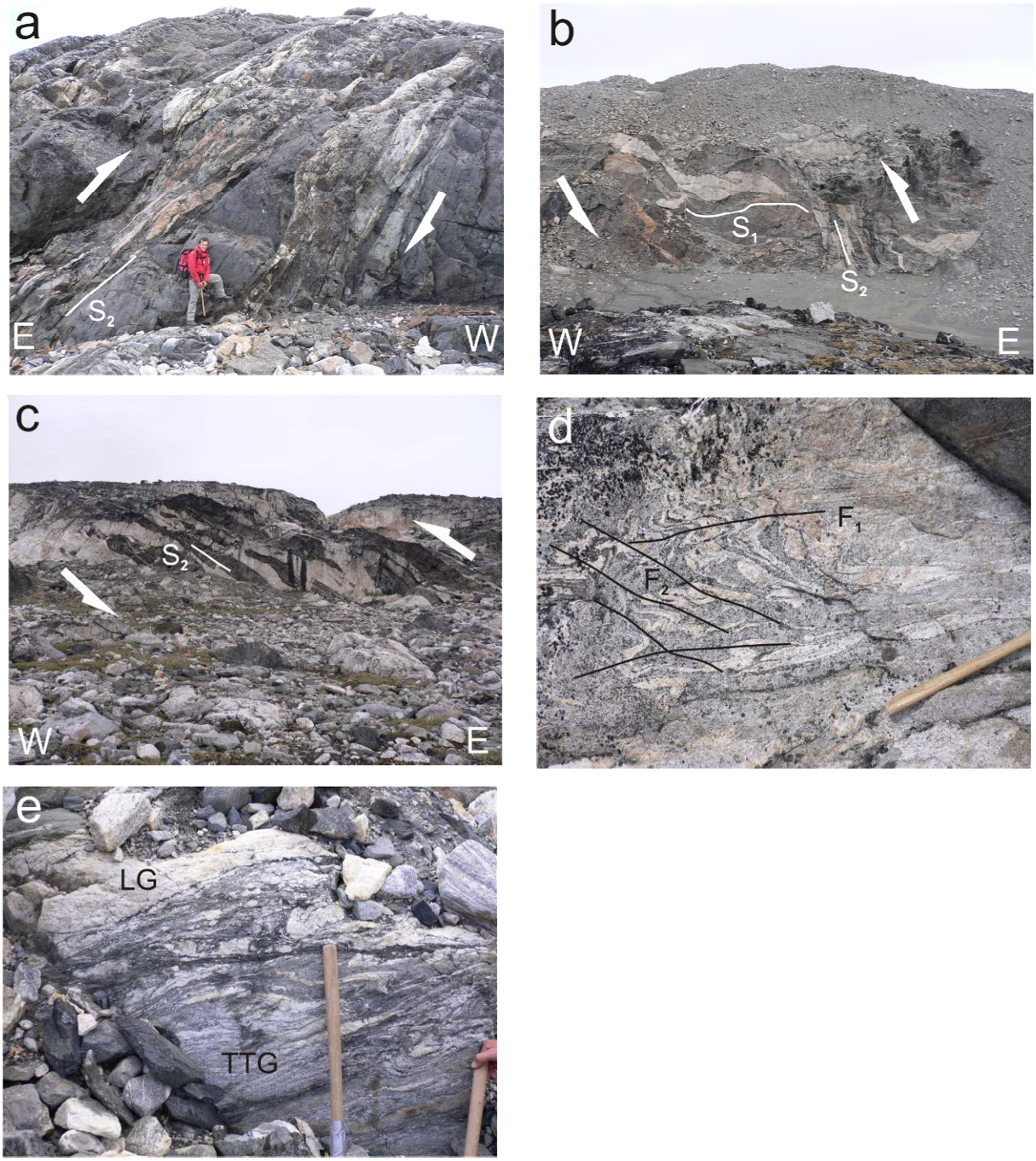

Figure 17. *(a) Lenses of meta-ultramafic rocks form horses in duplex structures of the west-vergent thrust. Leuco-granite intruded syn-tectonically parallel to the S_2 foliation. (b) In the foot wall of a D_2 thrust, sigmoidal S_1 dominates and indicates reverse sense of movement. Note that the leuco-granite intruded parallel to S_2, but also parallel to reactivated S_1. (c) Fragments of amphibolite/mafic granulite that are intruded by leuco-granite in a D_2 thrust system. The leuco-granite has generally a magmatic fabric, suggesting that D_2 deformation occurred during the melt stage. (d) F_1 and F_2 fold interference pattern in TTG gneiss showing migmatitic banding. (e) Leuco-granite – TTG gneiss contact. The contact is defined by a cataclasite indicating brittle deformation. The kinematics are similar to the D_2 stage of deformation, which may suggest a progressive D_2 deformation stage from the ductile into the brittle regime*.

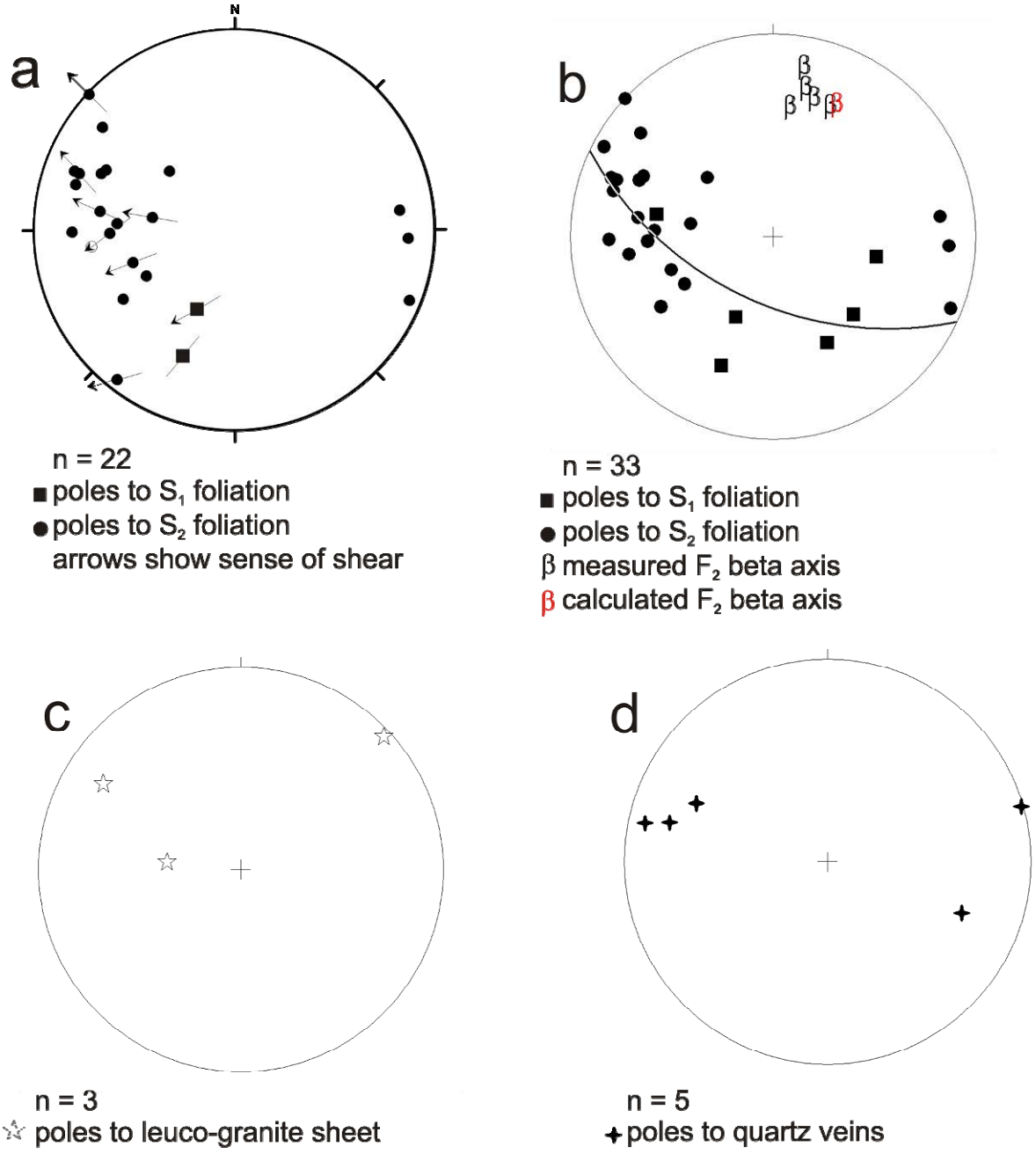

Figure 18. *(a) Poles of S_1 and S_2 foliation with stretching lineation. Arrows indicate direction of transport (lower hemisphere, equal area projection). (b) Summary of structural data of the area. S_1 and S_2 define a great circle which axis is parallel to F_2 fold axes (lower hemisphere, equal area projection). This folding is related to the sigmoidal foliation fabrics in the lithons between the thrust planes (cf.; Fig. 17b). (c) Leuco-granite sheets are generally parallel to the S_2 foliation (poles, lower hemisphere, equal area projection). (d) Hydrothermal quartz veins are developed as shear veins parallel to the foliation (lower hemisphere, equal area projection).*

Structure of hydrothermal quartz ± gold veins

Quartz veins occur in the lenses of meta-gabbro, meta-ultramafic rock and supracrustal rocks and at their contacts with TTG gneiss. Most of the veins are up to 10 cm wide and 4 – 6 m along strike (Fig. 19a). They are mainly parallel to the S_1 foliation, but are also slightly

oblique, thus, representing shear and extensional shear veins, respectively (Fig. 17d). They probably formed during D_1 deformation, but formation during D_2 reactivation of D_1 structures cannot completely be excluded.

Hydrothermal alteration and gold mineralisation

The supracrustal rocks that host some of the hydrothermal quartz veins are very similar to those found on the Akuliaq peninsular hosting gold mineralisation. They are enriched to up to 30 ppb Au. Here, however, orthopyroxene and *in situ* partial melt fabrics in felsic and mafic rocks indicate higher metamorphic conditions in the granulite facies (Fig. 16). Moreover, coarser-grained leucocratic material comprising quartz, plagioclase, clinopyroxene, garnet, chalcopyrite, arsenopyrite and pyrrhotite is spatially associated with quartz veins and can form cm-scale seams around the veins (Fig. 19). These leucocratic seams contain between 100 and 400 ppb Au and, locally, semi-massive sulphides. A possible explanation is that hydrothermal gold-quartz mineralisation occurred relatively early in the tectono-metamorphic history of the area and the rocks were overprinted by prograde granulite facies metamorphism afterwards. Such an interpretation is supported by the observation that: (1) hydrothermal quartz veins are parallel to the early S_1 foliation and (2) in situ partial melting is spatially associated with the quartz veins, where hydrothermal alteration would be expected (Fig. 19). The hydrothermal alteration zones would be enriched in volatiles, which would facilitate preferential partial melting of alteration zones over the unaltered host rock. However, detailed petrological studies are required to confirm this hypothesis.

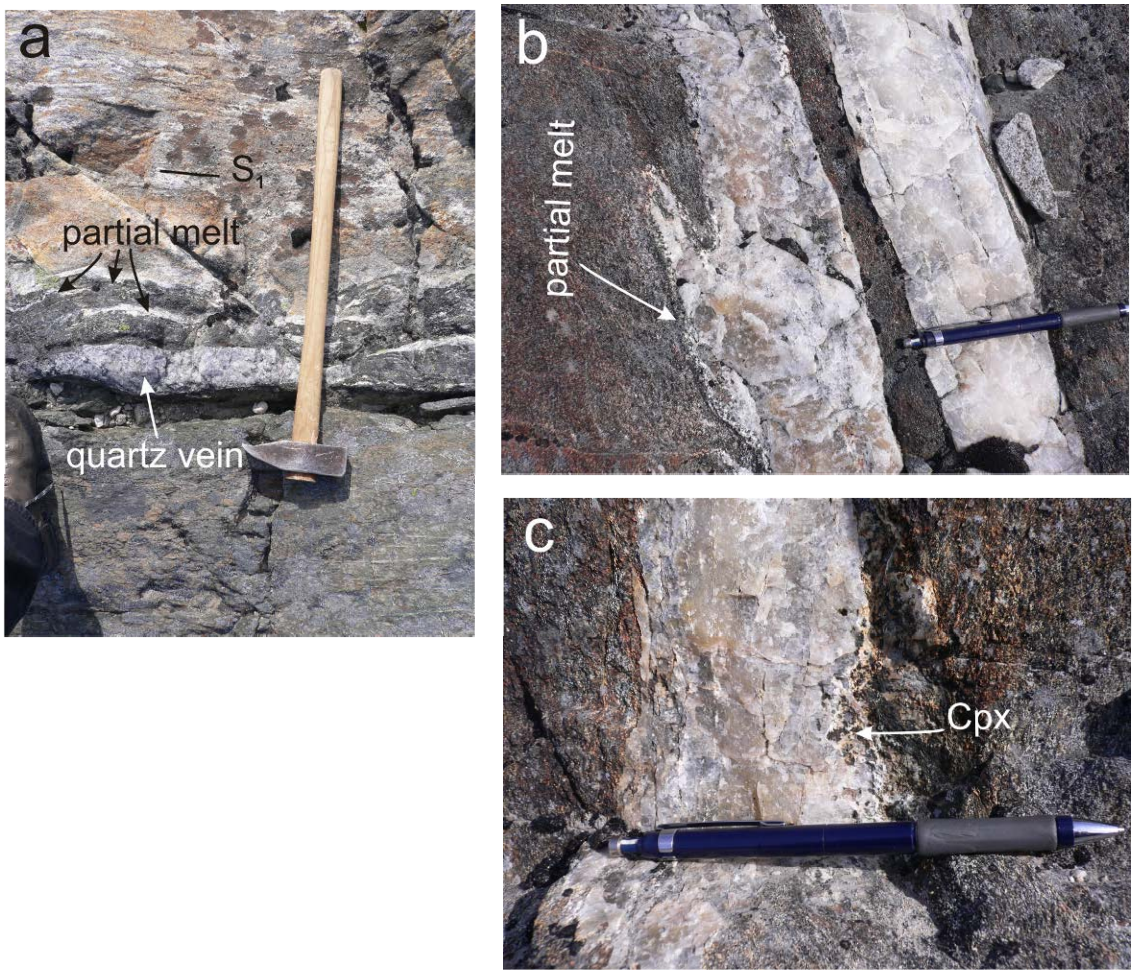

Figure 19. *(a) Hydrothermal quartz vein at lithological contact parallel to S1. Note the white, cm-scale pockets around the quartz veins that potentially represent in situ partial melt of a former hydrothermal alteration assemblage. (b, c) Hydrothermal quartz vein with white partial melt halo composed of quartz, plagioclase and clinopyroxene. The rusty brown colour stems from weathered sulphide minerals that occur in the partial melt zones.*

Geology of the Mellembygden area

This area is characterised by an approximately 1 km wide greenstone belt, striking north-east-southwest for about 14 km (Fig. 20a). The greenstone belt is surrounded by TTG gneiss. Mainly at the lithological contact, several 10s of metres wide leuco-granite sheets intruded into the gneiss and the greenstones. The greenstone belt is dominated by green to grey amphibolite and banded amphibolite (Fig. 20b). The banding is characterised by variation in grain size and modal proportion of hornblende and plagioclase-quartz (Fig. 20c). In places, the grain-size variation is interpreted as graded bedding in a crystal tuff, indicating stratigraphic younging to the northwest. Such a stratigraphy would also suggest an evolution from more mafic to more felsic compositions. The amphibolites are fine- to medium-grained, comprising hornblende, plagioclase, quartz and clinopyroxene in places. A porphyric variety forms small m-scale lenses and has about 2 mm-sized hornblende. At the south-eastern contact to TTG gneiss, several 10s of metres-scale lenses of green meta-ultramafic rocks occur. They are medium-grained and consist of clinopyroxene, hornblende and mag-

netite. In the southwest, komatiite horizons form 1 – 5 m thick and 15 – 25 m long lenses in the banded amphibolite. The komatiite consists of olivine, magnetite and biotite and has a spinifex texture with 5 – 10 cm long blades (Fig. 20d). Up to three 5 – 40 cm thick layers enriched in magnetite are observed in some of the komatiite lenses. Locally, a buff-coloured fine-grained rock composed of plagioclase, quartz, hornblende, biotite and epidote occurs, which is interpreted to be similar to the meta-dacite in the other locations described (Fig. 20e).

The TTG gneiss is medium-grained, comprising plagioclase, quartz and biotite (Fig. 20f). The appearance and fabric is very similar to the gneisses on Akuliaq and between Niger-likasik und Akulleq. The leuco-granite is medium- to coarse-grained and composed of plagioclase, quartz and locally minor K-feldspar (Fig. 20f). Both static and dynamic fabrics indicate syn- to late-tectonic intrusion.

Structure

The structural grain is characterised by a penetrative northeast-southwest trending foliation that dips moderately to north-westerly directions (Figs. 20 and 21a, b). Two maxima show northwest and north-northwest dips, respectively (Fig. 21b). The mineral stretching lineation is weak and plunges at shallow angles both northeast and southwest. Shear sense indicators indicate dextral deformation (Figs. 21a and 22a, b). Several undulating shear zones transect the greenstone belt and are developed at its contacts. The TTG gneiss at the contacts has ultramylonite to mylonite fabrics over a width of about 300 m. Leuco-granite intruded the dextral shear zone in places syn- to post-tectonically. Locally, cataclastic fabrics are developed showing the same kinematics as the mylonitic fabrics and are, therefore, probably the result of progressive deformation from the ductile into the brittle regime (Fig. 22b). The shear zones undulate around lithons that form horse structures at all scales (Fig. 22c). These duplex structures also indicate dextral deformation. The structure in the southwest, where the greenstone belt appears to split into three branches possibly represents a flower structure in the overall dextral structural regime.

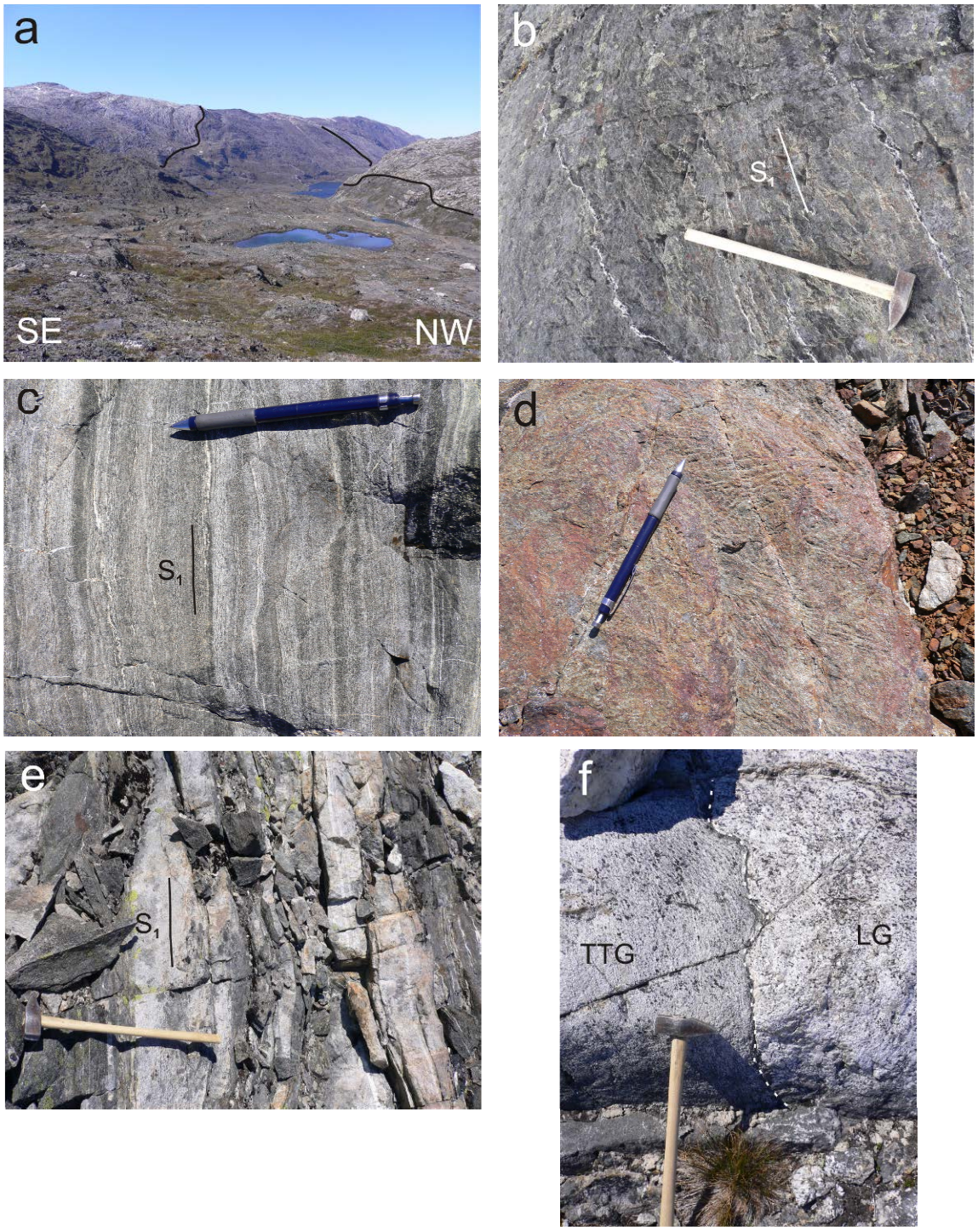

Figure 20. *(a) View along strike of the greenstone belt to the southwest. The irregular contact of greenstones to the surrounding rocks is due to intrusive relationships between the supracrustal rocks, TTG gneiss and late leuco-granite, which is almost indistinguishable from the TTG gneiss on this view. (b) Characteristic dark grey amphibolite with a penetrative S_1 foliation. (c) Banded amphibolite, where the banding is parallel to the S_1 foliation. Note the grain-size and the compositional variation. (d) Komatiite with the characteristic spinifex texture of 5 – 10 cm long blades. (e) Grey felsic layers in amphibolite, resembling meta-dacite from Akuliaq. (f) Intrusive contact between TTG gneiss and leuco-granite. The fabric in the leuco-granite is much weaker than in the TTG gneiss, indicating syn- to late-tectonic intrusion.*

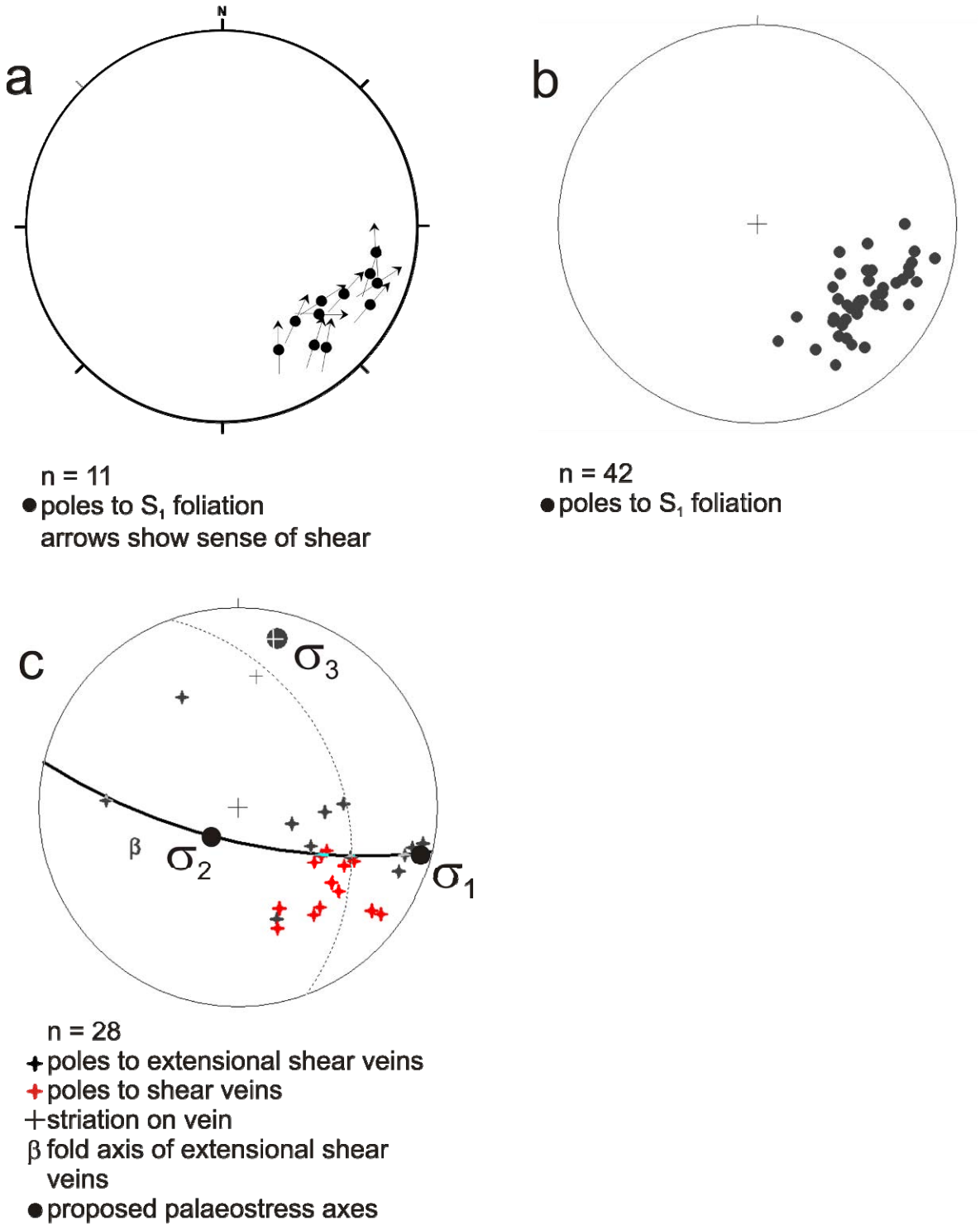

Figure 21. *(a) Poles of S_1 foliation with stretching lineation. Arrows indicate direction of transport (lower hemisphere, equal area projection). (b) Poles of S_1 foliation (lower hemisphere, equal area projection). (c) Structural data of the hydrothermal quartz veins (lower hemisphere, equal area projection). The data is used to estimate the palaeostress field for the formation of the veins.*

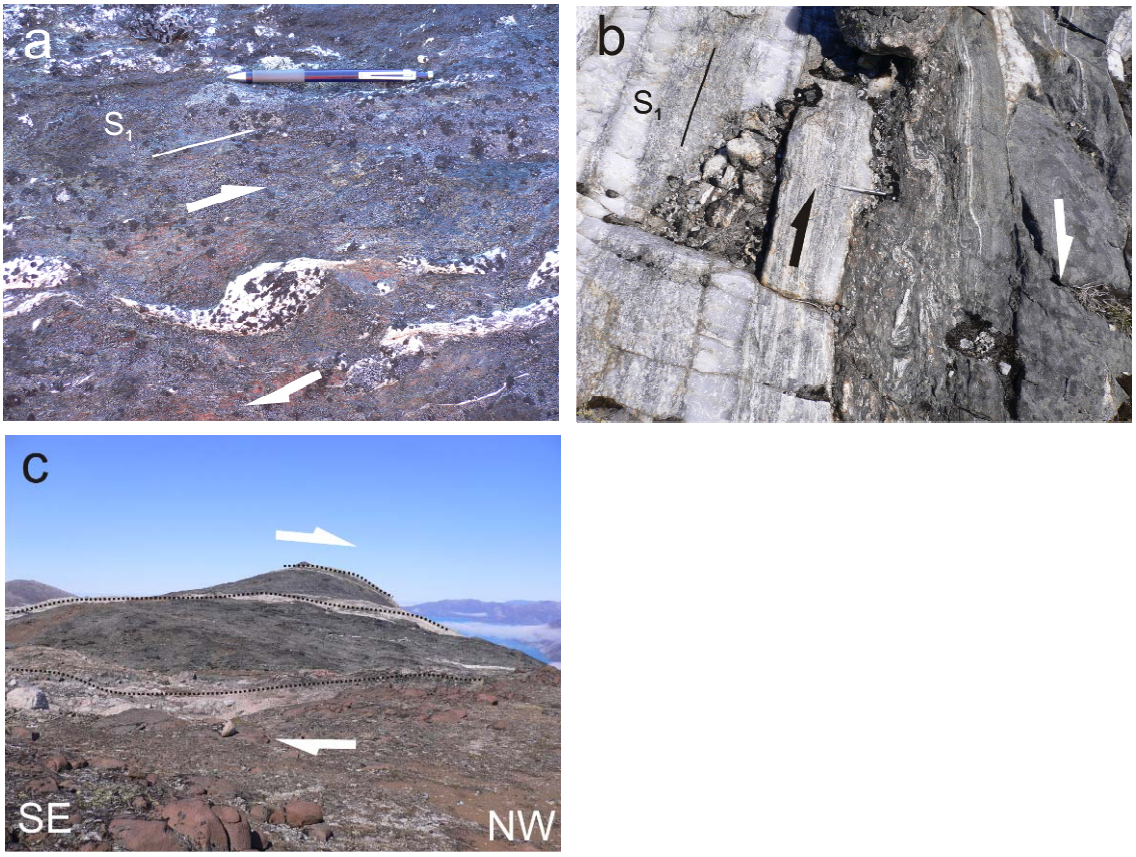

Figure 22. *(a) Deformed pegmatite, indicating ductile dextral strike slip deformation along the S_1 foliation. (b) Leuco-granite – amphibolite contact that is occupied by cataclasite. The cataclasite is parallel to S_1 and also shows dextral shear sense indicators. Note the hydrothermal quartz veins. (c) View to the southwest showing horses of duplex structures surrounded by D_1 dextral strike-slip shear zones (stippled lines).*

Structure of hydrothermal quartz ± gold veins

Quartz veins occur in the greenstones as well as in TTG gneiss. Most of the veins are parallel to the S_1 foliation and represent shear veins (Fig. 21c). They form bluish grey to grey laminated vein sets with 10 – 20 m spacing between the sets (Fig. 23a). Laminated veins that are 30 – 50 cm thick commonly have a milky white centre (Figs. 23a-c). Extension veins and extensional shear veins are rare. They are commonly 10 cm wide milky white quartz veins (Fig. 23d). In places, the extensional shear veins form conjugate sets, where the intersection plunges shallow to the north-northeast (Figs. 21c and 23e). Extension veins and extensional shear veins are often folded into cm-scale upright open to close folds during progressive shortening (Fig. 23e). The fold axis plunges at moderate angles to the southwest (Fig. 21c). The geometry of the veins can be used to estimate the palaeostress field, where the intermediate principle stress is defined by the intersection. The hydrothermal quartz ± gold veins, thus, formed during near horizontal west-northwest – east-southeast compression, whereas the extension direction is broadly north – south (Figs. 21c and 23d, e). The fold geometry of the veins is consistent with progressive deformation in such a stress regime, as is the dextral sense of the shear zones.

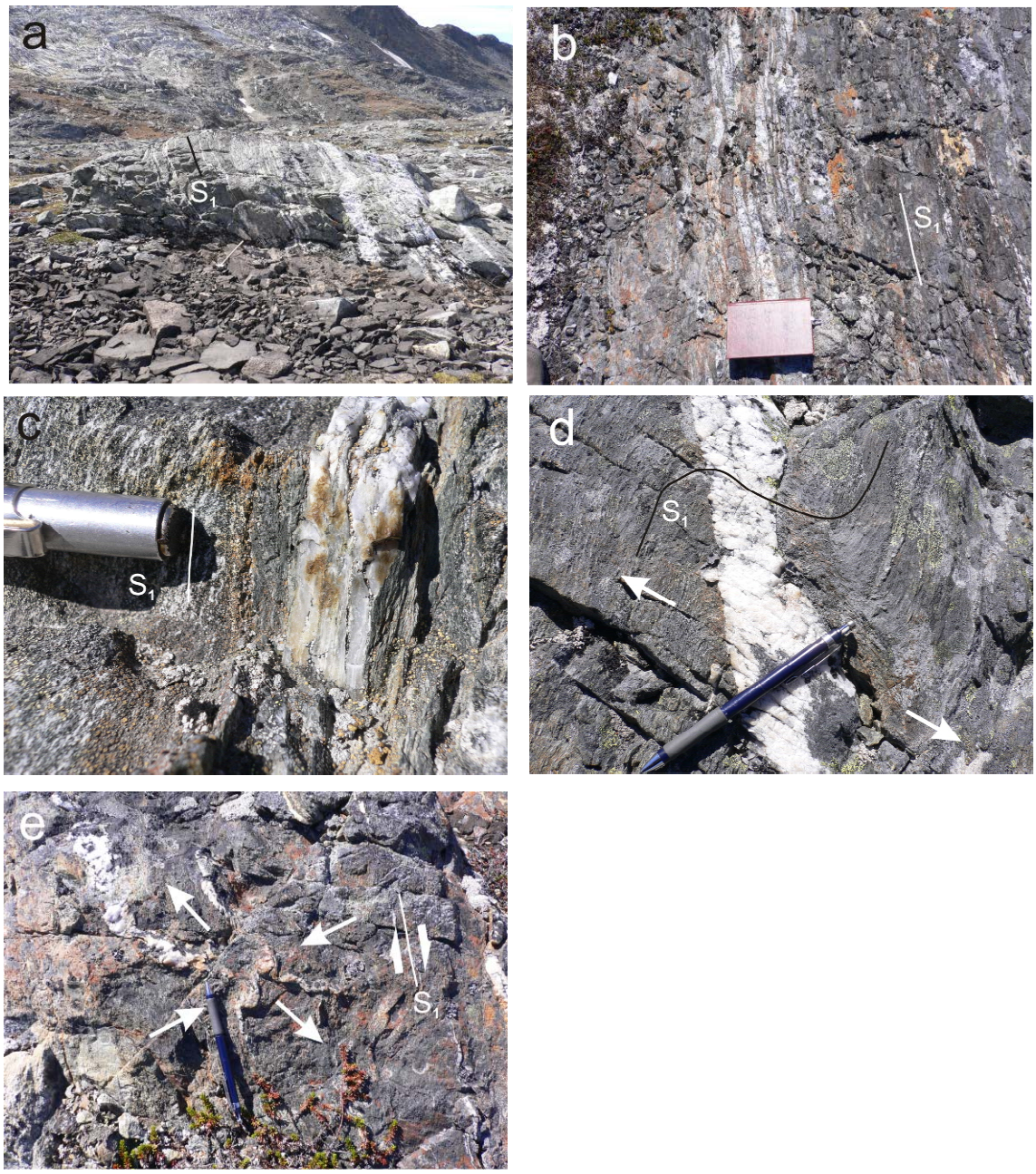

Figure 23. *(a) Outcrop showing a number of S_1 foliation-parallel quartz veins, which form a laminated vein system. (b) Closer view of a laminated quartz vein system that is developed parallel to S_1. (c) Close-up of a laminated quartz vein. Note the internal deformation fabrics in the quartz veins, which indicate deformation of the vein during the progressive regional shearing. (d) Extensional shear vein and transposition of the S_1 foliation during vein formation and deformation. (e) Conjugate set of extensional shear veins, which can be used to estimate the palaeostress field (cf.; Fig. 21c). This stress field is consistent with dextral strike-slip deformation along the S_1 foliation. The extensional shear veins are folded during progressive deformation.*

Hydrothermal alteration and gold mineralisation

Supracrustal rocks and sheared TTG gneiss host hydrothermal quartz veins that contain additional arsenopyrite and up to 16 ppb gold. The quartz veins have a m-scale alteration halo. Its composition varies with host lithology (Fig. 23). Most commonly, hydrothermal alteration is observed in the various amphibolites and contains quartz, epidote, orthoamphibole, biotite, tourmaline, muscovite, carbonate, sphene, arsenopyrite, pyrite, pyrrhotite and chalcopyrite. In the meta-dacite, the hydrothermal alteration assemblage is simpler, comprising hornblende, tourmaline, quartz, arsenopyrite, pyrite, pyrrhotite and chalcopyrite. Hornblende, biotite, muscovite, quartz, arsenopyrite, pyrite, pyrrhotite and chalcopyrite represent the hydrothermal alteration in the TTG gneiss. Elements enriched in all lithologies are Si, K, Cu, W, Mo, As and Au to up to 2.6 ppm.

Regional structural model

In the area between Mellembygden and the Akuliaq peninsula, the penetrative foliation changes its orientation along strike from east-northeast – west-southwest to north-south on Akuliaq and becomes shallower (Fig. 24). The steeper foliation in the Mellembygden area defines dextral strike- to oblique-slip shear zones. On the other hand, on Akuliaq reverse shear zones are developed. This geometry resembles a lateral and frontal ramp system, where the frontal reverse zone is located on Akuliaq and the lateral dextral strike-slip zone is the greenstone-TTG gneiss contact further southwest (Fig. 24). In both areas, hornblende and plagioclase are the minerals defining stretching lineation in amphibolite, indicating deformation at amphibolite facies grades. However, epidote, chlorite, cataclasites and widespread hydrothermal alteration associated with quartz veins suggest that deformation was progressive from amphibolite facies peak conditions to retrograde metamorphic conditions. In the TTG gneiss, plagioclase shows brittle and ductile fabrics in the shear zones, suggesting deformation temperatures of less than 450-500°C.

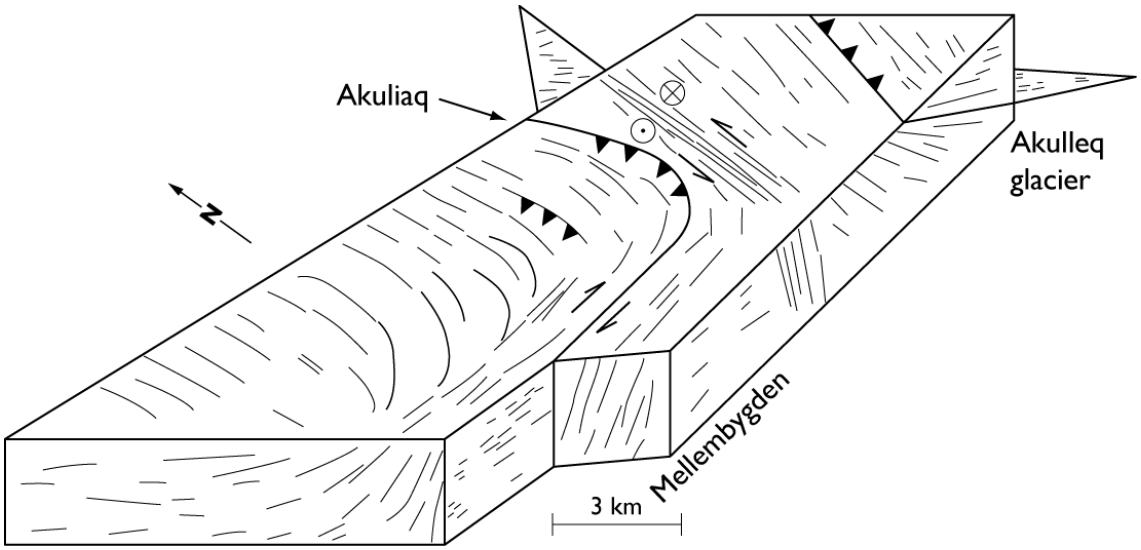

Figure 24. *Schematic 3D sketch summarising the structural elements of the study area. Dextral strike-slip zones in the Mellembygden area and thrust zones on the Akuliaq peninsula form a lateral and frontal ramp system. The steep zone to the southeast of Akuliaq formed due to lateral extrusion between the opposite-facing thrust zones on Akuliaq and in the Akulleq glacier area.*

To the north of the Mellembygden-Akuliaq greenstone belt, upright fold structures are mapped in TTG gneiss and greenstone belts. The axial traces of these folds strike parallel to the reverse shear zones on Akuliaq. They are interpreted to having formed during compressional deformation and reverse shearing in the frontal and lateral ramp system. The folds form during the lock-up of the reverse shear zones in the fold-and-thrust belt (Fig. 25). In the east between the Nigerlikasik and Akulleq glaciers, two foliations form complex fold and duplex structures and the metamorphic peak is higher, probably in the granulite facies. The younger S_2 foliation defines reverse shear zones with transport to the west, which is the opposite direction compared to the Akuliaq area (Fig. 24). The west-vergent shear zones possibly represent back thrusts, along which deeper crustal rocks, including granulite facies rocks and meta-ultramafic rocks, were exhumed. Decompression textures, such as plagioclase rims around garnet, also suggest fast exhumation of the rocks. Large amounts of leuco-granite, likely representing crustal melt, intruded syn-tectonic into and along the D_2 shear zones possibly aided deformation and exhumation tectonics.

The steep zone between Nigerlikasik and Akulleq probably represents a deformation zone, where the east-vergent and the west-vergent transport are accommodated by progressive transposition of the foliation to a near-vertical orientation. The rocks are left-laterally extruded along the near-vertical oblique sinistral shear zones (Fig. 24).

The Paamiut area strongly resembles modern collisional orogens that are characterised by frontal and lateral ramp systems in fold-and-thrust belts and back thrusts as those close to the Inland Ice. Thrusting and folding occurred in an approximately west-east oriented palaeostress field. The crust was probably overthickened, because young extensional structures are common, indicating orogenic collapse in a northwest-southeast extensional regime.

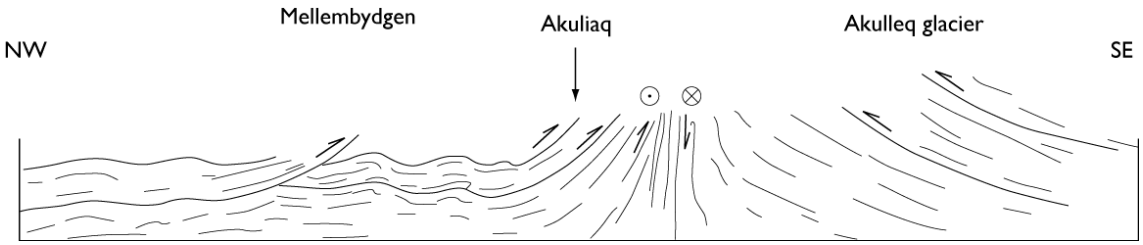

Figure 25. *Schematic structural cross section through the area illustrating the fold-and-thrust geometry.*

Model for hydrothermal gold mineralisation

Hydrothermal gold mineralisation is known from the Akuliaq peninsula, where gold is hosted in quartz veins and surrounding quartz, amphibole, biotite, tourmaline, pyrrhotite, arsenopyrite and, locally, garnet, carbonate and muscovite alteration zones (NunaMinerals A/S; this study). Similar hydrothermal alteration assemblages are found further to the west in the Mellembygden area (this study) and the Nigerleq area (Erfurt & Tukiainen 1997), but also further east in the Nigerlikasik-Akulleq area (this study). The lateral extent of hydrothermal alteration and gold mineralisation in the Kvanefjord amphibolite is estimated at

about 25 km with concentration of alteration features at certain structurally favourable sites (cf.; Figs. 2 and 26). The gold mineralisation is mainly hosted by the Kvanefjord amphibolites or is developed at the contact to the TTG gneiss. In general, lithological contacts between different rock types appear to be favourable sites for gold mineralisation. The lithological contacts represent rheological anisotropies and are commonly deformed, hosting numerous gold-quartz veins. A conjugate set of shear, extensional shear and extension veins is distinguished, although shear veins are the most prominent. The veins formed in a near-horizontal east-west oriented mean principal stress regime with north-south oriented extension (Figs. 9, 13d, 21c, 23d and e). The veins initially developed oblique to the foliation are progressively folded in the same palaeostress field. Since the palaeostress field for the gold-quartz veins and the fold-and-thrust tectonics is similar, the gold mineralising system is most probably triggered by the regional structural evolution. The shear zones of the ramp system and the different thrusts represent fluid conduits for the hydrothermal gold mineralising fluids (Fig. 26). Favourable sites for gold-quartz vein formation are thrusts or reverse shear zones such as on Akuliaq, because they can accommodate the highest fluid overpressure and, therefore, focus large amounts of fluids into fracture zones (i.e. gold-quartz veins). Other potentially favourable sites for gold mineralisation are structurally complex parts of the lateral ramp such as the numerous duplexes and the flower structure south of Mellembygden (cf.; Fig. 2). In these structurally complex areas, shear zones containing gold-quartz veins show a relatively small spacing of numerous branches. Hydrothermal gold mineralisation between Nigerleq and Akulleq, thus, is a characteristic upper mesozonal orogenic gold system. Since hydrothermal gold mineralisation, deformation and metamorphism are broadly contemporaneous, the ca. 2840 Ma amphibolite facies stage in the Paamiut block gives a maximum age for gold mineralisation.

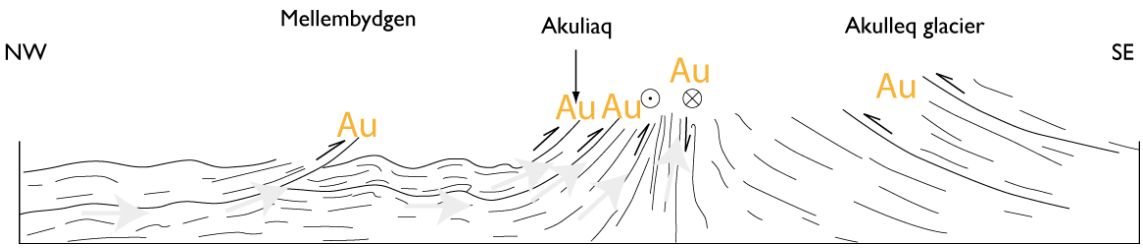

Figure 26. *Schematic cross section of the study area. The grey arrows show the model for structurally controlled hydrothermal fluid migration along structures of the fold-and-thrust-belt. Gold mineralisation is most pronounced in thrust zones.*

In the area of the Nigerlikasik and Akulleq glaciers, hydrothermal quartz veins are also common. However, the regional metamorphic grade is much higher and most probably in the granulite facies, which resulted in partial melting of the rocks. Zones around the hydrothermal quartz veins often are characterised by *in situ* partial melt fabrics, indicating that orogenic hydrothermal mineralisation predated peak metamorphism. The hydrothermal alteration assemblage surrounding the quartz veins was most probably enriched in volatile phases and, therefore, suitable for partial melting during prograde metamorphism. The mineral assemblage is quartz, plagioclase, clinopyroxene, garnet, chalcopyrite, arsenopyrite and pyrrhotite, where the sulphides commonly form semi-massive to massive aggre
gates. The prepeak metamorphic gold mineralisation was remobilised during partial melting of alteration silicates and sulphides and redistributed. Strongest gold enrichment is found in

the sulphide-bearing partial melt pockets and dykelets. Thus, the gold mineralising system is complex with (1) an early hydrothermal orogenic stage, probably contemporaneous with gold mineralisation between Nigerleq and Akulleq, and (2) later remobilisation during partial melting into pockets and dykelets.

Conclusions

Field work in 2010 in the Paamiut block has identified a lateral extent of the known hydrothermal orogenic gold mineralisation on Akuliaq over at least 25 km. Hydrothermal gold mineralisation is hosted in quartz veins and hydrothermal alteration zones that are controlled by the regional structural grain. The regional structure between Nigerleq and Akulleq to the east of Paamiut is characterised by a fold-and-thrust belt in a lateral and frontal ramp geometry. The main structure is an east-northeast – west-southwest trending, dextral strike-slip shear zone extending from Nigerleq to Akulleq that turns into a northeast-southwest trending thrust on Akuliaq. The most favourable sites for gold mineralisation are thrust zones and complex zones in the strike-slip shear zone. The characteristic hydrothermal alteration assemblage is quartz, amphibole, biotite, tourmaline, pyrrhotite, arsenopyrite and, locally, garnet, carbonate and muscovite.

The area of gold mineralisation possibly extends further east to the Inland Ice, where gold is enriched in partial melt pockets characterised by coarse-grained quartz, plagioclase, clinopyroxene, garnet, chalcopyrite, arsenopyrite and pyrrhotite. Gold is probably remobilised into melt pockets by partial melting of the hydrothermal alteration assemblage during prograde metamorphism in the granulite facies.

The area east of Paamiut has strong potential for economic gold mineralisation in structures related to east-west shortening. Similar fold-and-thrust structures and strike-slip shear zones are also developed further to the north and to the south. These areas also could host gold mineralisation, but were not visited under the 2010 GEUS field expedition.

References

Erfurt, P. & Tukiainen, T. 1997: Ujarassiorit 1996 Public minerals hunt programme in Greenland. Danmarks og Grønlands Geologiske Undersøgelse Rapport **1997/88**, 8.

Escher, J.C. & Jensen, S.B. 1976: Geological Map of Greenland, 1:100.000, 62 V.2 Nord, Nigerdlikasik. Copenhagen: Geological Survey of Greenland.

Jensen, S.B. 1976: Geological Map of Greenland, 1:100.000, 62 V.1 Syd, Nerutussoq Copenhagen: Geological Survey of Greenland.

Mapping and structural analysis of the Akuliaq Peninsula, near Paamiut, SW Greenland (Hastie)

Evan Hastie

Department of Earth and Environmental Sciences, University of Windsor, Windsor, Ontario

Abstract

The structural characteristics of the rocks in the Akuliaq Peninsula can be explained in terms of three phases of deformation (D_1, D_2, D_3). In D_1 the earliest foliation (S_1) is only locally preserved in rootless isoclinal folds (F_1). In D_2 the dominant foliation (S_2) is defined by hornblende and was parallel to mm- to cm-scale compositional banding in places. The S_2 foliation strikes to the SW with dips between 25-70^0 NW, and has an associated lineation (L_2) that is generally down dip defined by hornblende and plagioclase crystals. Tight to open cm- to m-scale folds (F_2) are associated with this D_2 stage, and they have fold axes that plunge 30-60^0 N-NW. The shear sense indicators found associated with D_2 suggest an E-W compression that led to a top-to-the-west sense of shearing with an early-ductile to late-brittle progression in this shearing. In the youngest stage of deformation (D_3) a locally developed foliation (S_3) can be seen trending E-W. These S_3 foliations are parallel to the axial planes of open m-scale folds (F_3), which indicates a N-S compression event during D_3. Shear sense indicators and oblique to sub-horizontal lineations (L_3) defined by hornblende and plagioclase crystals suggest dextral shearing in D_3 showing a rotation of L_2 into L_3. This E-W shearing is due to the N-S compression event. This study has produced a new and significantly more detailed map. Possible structural controls on gold include: fluids entering during extensional top-to-the-west shearing and associated ramp structures, or fluid entering dilation zones associated with D_2 shear zones and at shear intersections. The geological setting associated with structural and lithological evidence is an Archaean fold-and-thrust belt that formed as part of a Mesoarchaean oceanic crust.

Introduction

This thesis is part of a combined petrological and structural mapping project in the Akuliaq Peninsula of Greenland, aimed at evaluating the gold potential of the area, and focuses on understanding the structural evolution of the region. In June 2010, accompanying a team of geologists from various parts of the world in cooperation with GEUS (The Geological Survey of Denmark and Greenland) we set out to map in further detail the geology of the Akuliaq Peninsula and expand upon previous work done there. While focusing primarily on the mapping and structural geology of this region, there will also be some brief attention given to the petrology and stratigraphy; making the structural aspects of the area more clear and concise.

The Akuliaq Peninsula is located in SW Greenland in the Paamiut block (62° 05' N, 49° 03' W) approximately 35 km ENE of the town of Paamiut. The area of the Akuliaq Peninsula lies between the Avangnarleq fjord to the west and Akugdleq fjord to the east. The area of study comprised approximately 10 square km and is approximately 1 km from sea level to its highest peak. From 1969 to 1971, a doctoral candidate by the name of Jan Escher conducted the majority of previous work that gives us a basis upon which to begin with the geology of the Akuliaq Peninsula. Escher's thesis was published in 1971 (Escher 1971) and his mapping of the area has been used to this day. Later work was done by Peter Erfurt as part of a public minerals hunt program in 1996. In 2005, the mineral exploration rights to the Akuliaq Peninsula, as well as some of the surrounding region, were procured by NunaMinerals until 2024. From 2005 to 2007 they conducted studies to ascertain the gold potential of this area as a possible mining resource.

The Akuliaq Peninsula is interpreted to be part of the Paamiut tectonic block and is Mesoarchaean in age. This block contains greenstone belts that are located within TTG gneisses, which belong to three adjacent crustal blocks in the southern part of the Archaean craton, and are further bordered to the south by the Palaeoproterozoic Keltilidian Orogen (McGregor & Friend 1997). These blocks have a different metamorphic grade and have been interpreted to be emplaced in their current locations around 2820 Ma. They are then interpreted to have undergone a major tectonothermal event between 2500 and 2700 Ma (Friend & Nutman, 2001). Metamorphism of the rocks in the Paamiut block does not exceed amphibolite facies as indicated by their mineral assemblages and local preservation of igneous textures within the TTG gneisses (Escher 1971; McGregor & Friend 1997).

During early study of the Akuliaq Peninsula, it was thought that the supracrustal rocks, including the greenstones, formed as synclines over a gneissic basement (Escher 1971). GEUS' view, based on field observations over the last 20 years, is that the parent rocks of the gneisses intruded into these amphibolites and that these greenstone belts are the remnants of Archaean oceanic crust. Based upon these observations, changing the former viewpoint on stratigraphy, a more detailed and up to date study of the geology was needed of the Akuliaq Peninsula to improve our understanding of its geological history and how this region fits structurally into SW Greenland as a whole.

Taking previous work into consideration, a more extensive and up-to-date geologic map is required and a complete reworking of the structural history would help illuminate possible structural controls for gold mineralisation in the area. Objectives for this study are as follows:

- Generate a more detailed geologic map of the Akuliaq Peninsula on the scale of 1:10000 and 1:2500 with special attention given to quartz veining.
- Come up with a detailed structural history of the Akuliaq Peninsula based on new evidence and recent theories.
- Provide possible structural controls on gold mineralisation in the Akuliaq Peninsula.

Materials and methods

Upon being dropped off on the Akuliaq Peninsula by helicopter (Fig. 1), a base camp was established at 62° 05’ 44.4” N and 49° 02’ 18.2” W. It was from here that all fieldwork was coordinated for our team on a day to day basis. Five weeks were spent studying the geology of the region and collecting field data. The first week was spent getting a general sense of the local geology of the region and establishing the rock units/stratigraphy to be mapped for our project. Throughout the field season each team utilized a PDA containing ArcPad GIS software (Ganfield 7.0) to record a variety of types of data and GPS coordinates needed for the region, as well as correlative field notes to add further description.

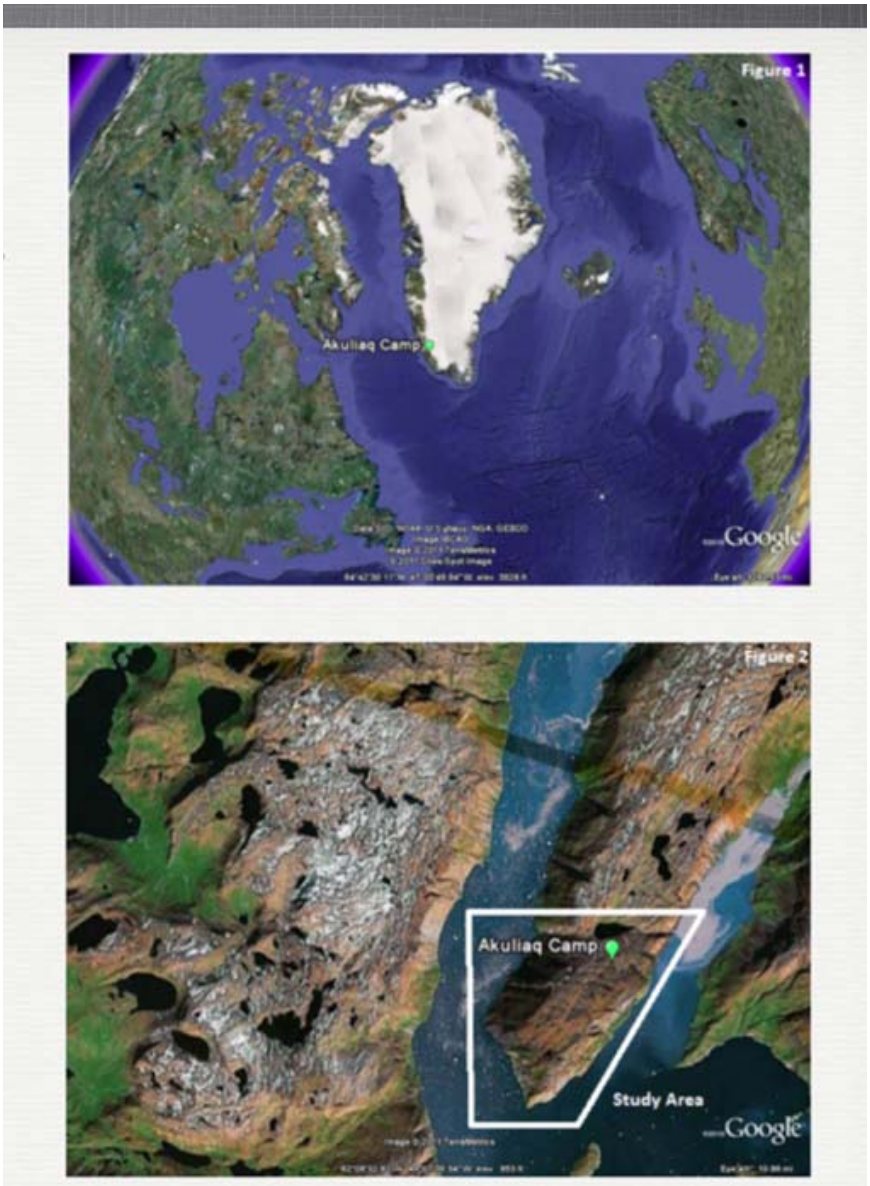

Figure 1. *Location of the Akuliaq Peninsula and base camp.*

After establishing a sense of the local geology we subdivided the region into 37 sections, with two of these sections being mapped on a 1:2500 scale each day. Data from each section map was then transferred to a 1:10000 map of the Akuliaq Peninsula at the end of each day. Special attention was given to the mapping of the quartz veins and alteration

zones in the region to ascertain possible locations for gold mineralisation to be supplied to NunaMinerals at the conclusion of our studies. During the mapping of the area, all relevant petrological and structural data was compiled in the PDA and field notebooks with correlative pictures and samples taken for further study. Rock samples were taken using sledgehammer directly from outcrops. In the field, the Dip-Dip convention was used for all structural measurements, however, measurements were converted to strike and dip following the “Right Hand Rule” convention in North America.

Following mapping of the Akuliaq Peninsula, the final week in the field was spent collecting additional data by helicopter and obtaining a more diverse and sufficient amount of samples. Special focus was paid to structural samples, samples exhibiting possible gold mineralisation, and samples for age dating. Preparation for analyzing the data was supplied in the form of relevant papers as well as Dr. Escher’s PhD thesis and NunaMinerals field reports for the past three seasons.

On returning to Canada, field maps of the region were digitised. ArcPad Ganfeld GIS data was converted for use in ESRI ArcMap 9.3.1 and the maps were converted using an accompanying digitising table. Once geologic units had been added to data from our PDA, structural data was added along with symbology. The result of our digitisation produced a 1:10000 and 1:2500 scaled map of the Akuliaq Peninsula.

Photographs taken in the field were labelled and catalogued on computer, and raw structural data was compiled for use. Stereographic projections were created using this data from foliation, lineation, and fold-axis measurements to help interpret structural geology and create three structural cross-sections of the Akuliaq Peninsula.

Once samples arrived at the University of Windsor, they were unpacked and organised into data tables according to their location, mineralogy and structural context. Representative samples of rock types and structure were prepared for thin section using a diamond-bladed rock saw and sent to Vancouver Petrographics in Vancouver, British Columbia to be made into 30 micron polished thin sections for microscopic study. Twelve quartz samples were also prepared and sent to Actlabs in Ancaster, Ontario to be analysed for gold content to correlate with previous data obtained from NunaMinerals. Thin sections and gold data returned and observations were made to classify petrology and structure.

Results

Based upon field data and sampling, twelve distinct and map able rock units were found in the Akuliaq Peninsula and can be seen on the accompanying 1:10000 map (Appendix C). They are as follows: diabase dyke, pegmatite, rusty quartz, milky quartz, blue quartz, TTG gneiss, aplitic sill, altered amphibolite, silicified amphibolite, banded amphibolite, ultramafics, and metagabbro (Appendix A; Figures 2 and 3). These units were named based upon field observations and are not necessarily petrological. Structures in the study area include: foliations, lineations, folds shears/faults, and kinematic indicators.

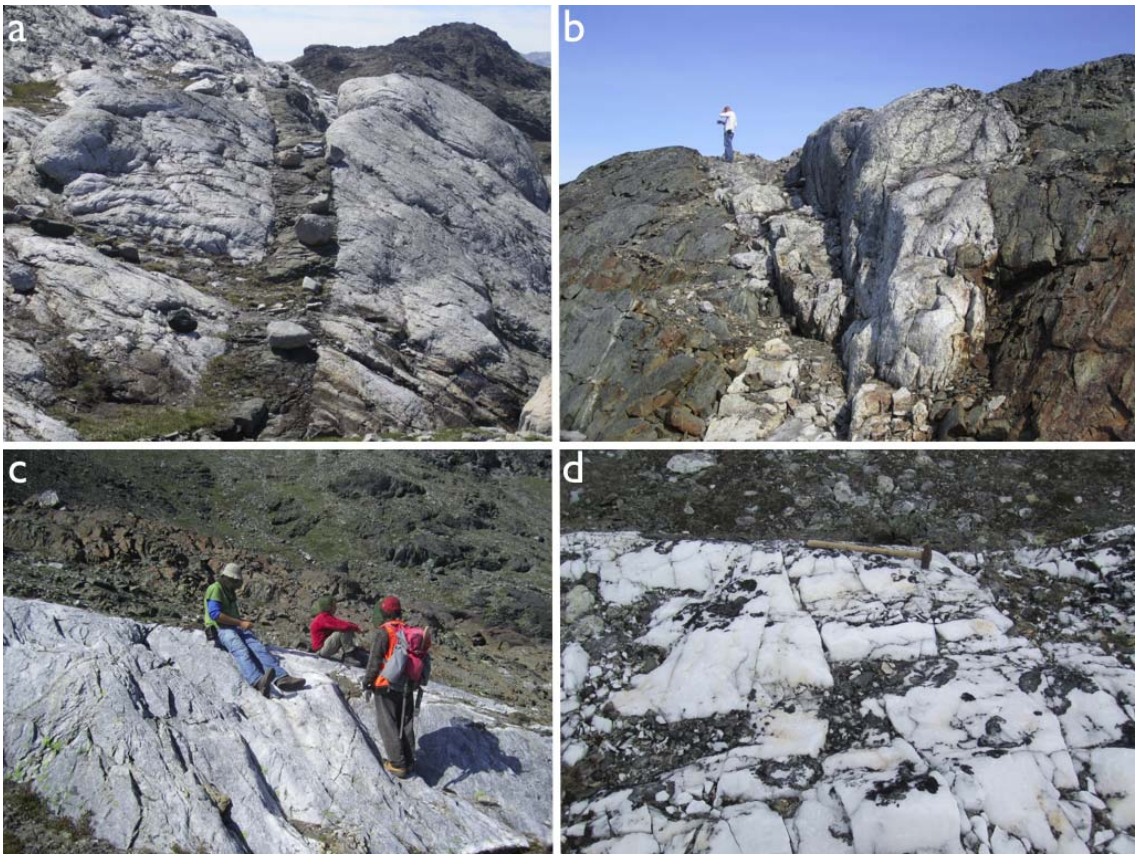

Figure 2. *Rock units. (a) Diabase dyke. (b) Pegmatite. (c) Blue quartz. (d) Milky quartz.*

Foliations and Lineations

Three distinct foliations were identified in the Akuliaq peninsula, defined as S_1, S_2 and S_3. The S_1 foliation is defined by hornblende and preserved only in a few locations developed in rootless isoclinal folds and is layer-parallel. This S_1 foliation was only measurable in 3 locations. It has strikes from SE to S with dips noted at 6°, 32°, and 64° to the W.
The S_2 foliation is the dominant fabric in the Akuliaq peninsula, and is mainly defined by hornblende and was parallel to compositional banding in places. The S_2 foliation generally strikes SW, and dips from 25°-70° to the NW (see Figure 4 below)

The S_3 foliation also is only locally developed and defined, again, by hornblende. It strikes to the WNW and has steep dips from 74°-88°. These S_3 foliations are parallel to the axial planes of open, m-scale folds (see below). Figure 2 is a stereographic projection of the foliations in the Akuliaq Peninsula.

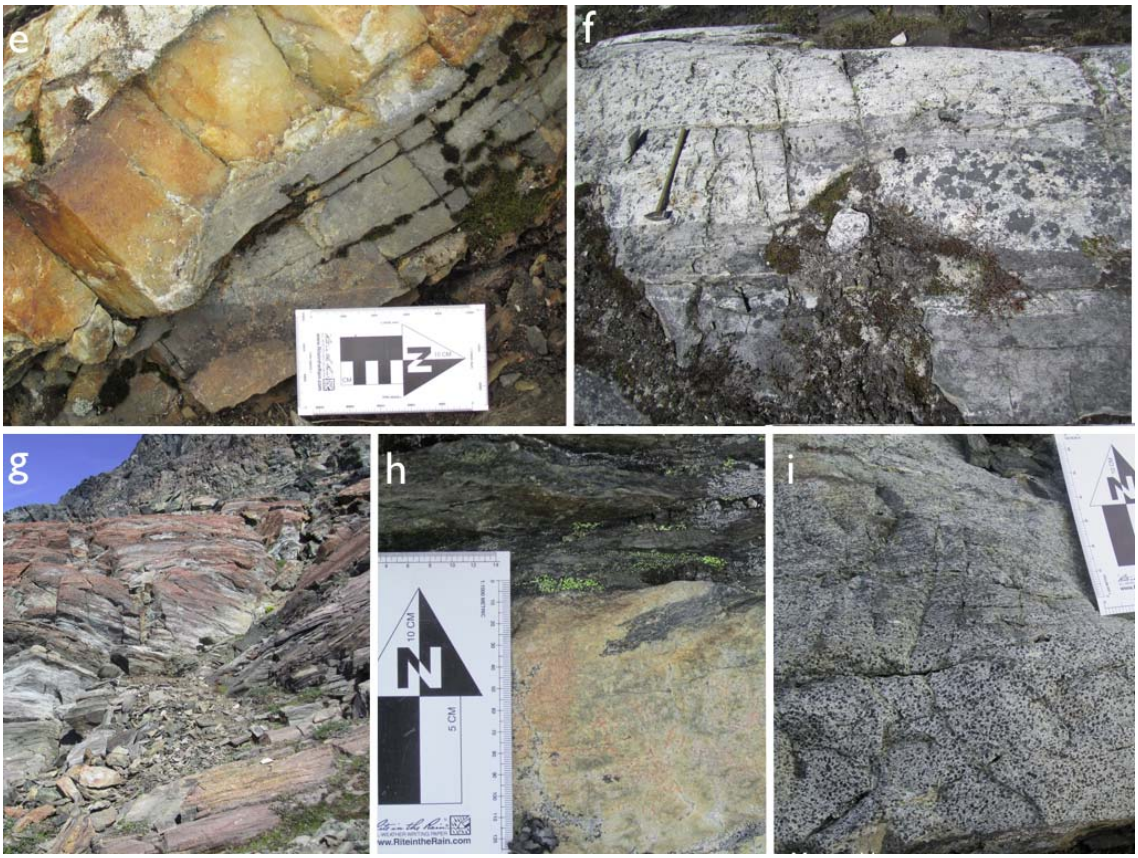

Figure 3. *Rock units. (e) Rusty quartz. (f) TTG gneiss and amphibolite contact. (g) Ultramafics. (h) Amphibolite and aplitic sill contact. (i) Metagabbro.*

A lineation (L_2) is associated with the S_2 foliation that is generally down-dip, but locally can be oblique to sub-horizontal (L_3) and is defined by hornblende and plagioclase crystals. These oblique to sub-horizontal lineations plunge to the north and were only observed within E-W shear zones that can be seen on the map (Appendix C). Figures 6 and 7 show the orientation of the lineations in the Akuliaq Peninsula.

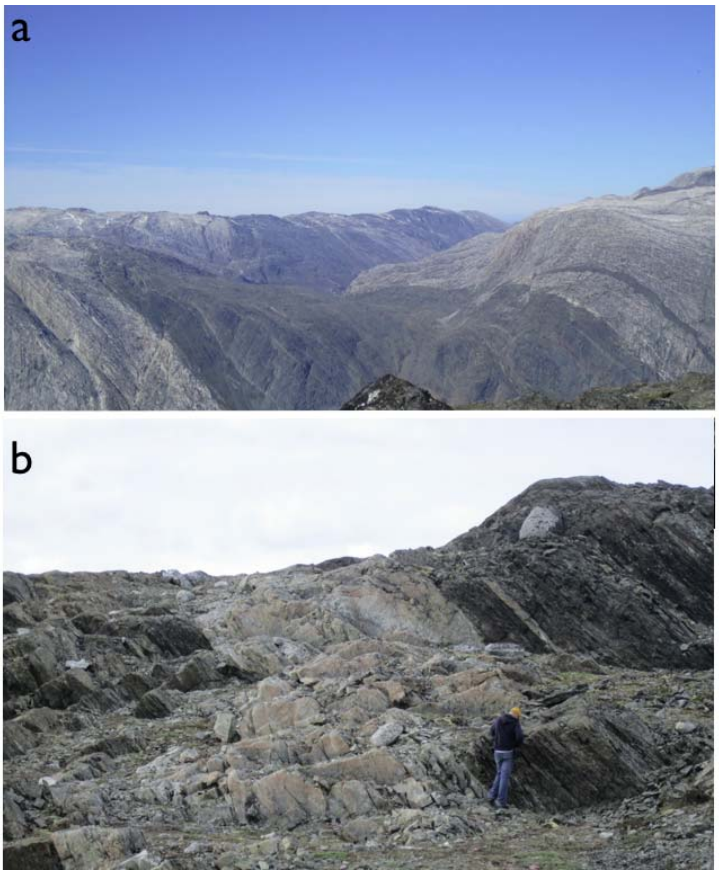

Figure 4. *Both (a) and (b) show the dominant S_2 foliation fabric facing SW.*

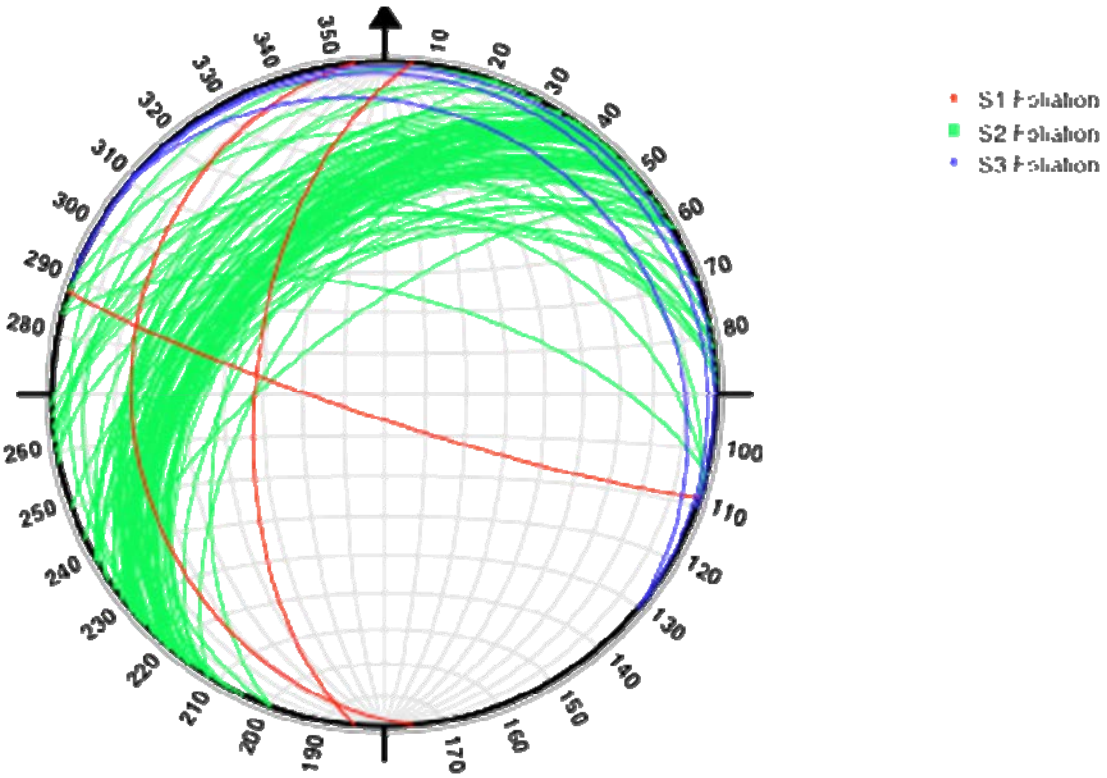

Figure 5. *Equal area projection of foliations found in Akuliaq.*

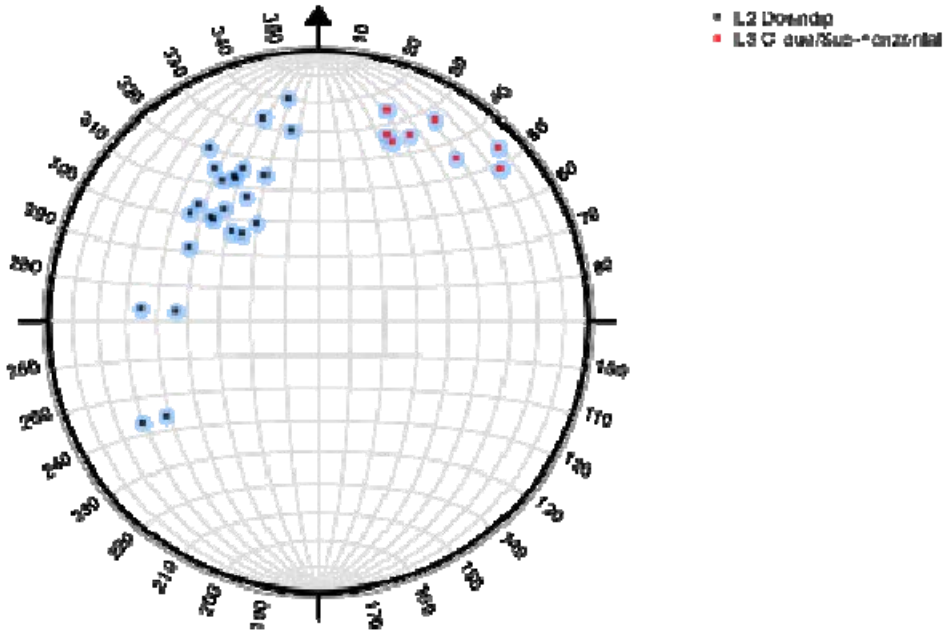

Figure 6. ***Equal area projection of lineations in Akuliaq.***

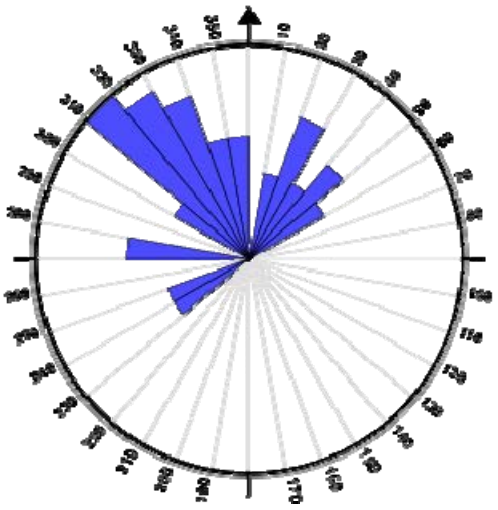

Figure 7. ***Rose Diagram showing frequency and direction of lineations.***

Folds

Three distinct fold types were observed in the region describing some of the principal stress that acted upon the rocks in the Akuliaq Peninsula. They have been termed F_1, F_2, and F_3. The F_1 folds are cm-scale, rootless, and isoclinal, are contained within the S_2 foliation, and are often refolded within F_2. The fold axes that could be measured for F_1 plunge to the S between 25° and 58°(Fig. 8).

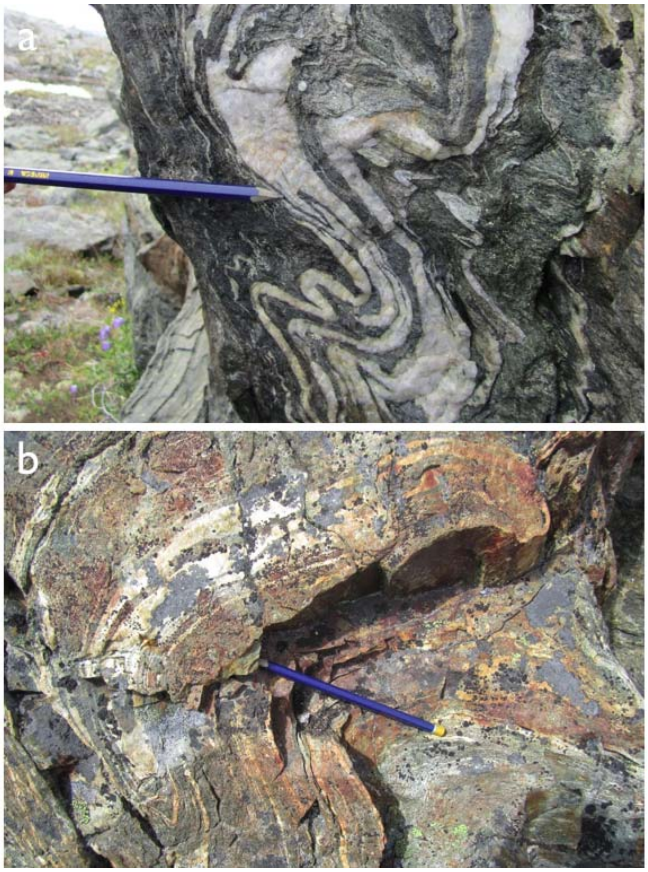

Figure 8. *Both (a) and (b) show rootless isoclinal F_1 folds within F_2 folds.*

Tight to open, asymmetric, cm- to m-scale F_2 folds are developed throughout the area, and have fold axes that generally plunge 30° to 60° to the N and NW, and seem to be parallel with the L_2 lineations. In some locations, F_2 folds are associated with parasitic “Z” and “S” folds as well as crenulations. These exhibit the same axial trace and orientation as the F_2 folds they accompany (Figs. 9, 10, and 11). These have been termed F_{2b}.

Open m-scale F_3 folds were observed and have fold axes that generally plunge from 40-60° to the west. The F_2 folds can be seen inside some of these F_3 folds (Figs. 12 and 13).

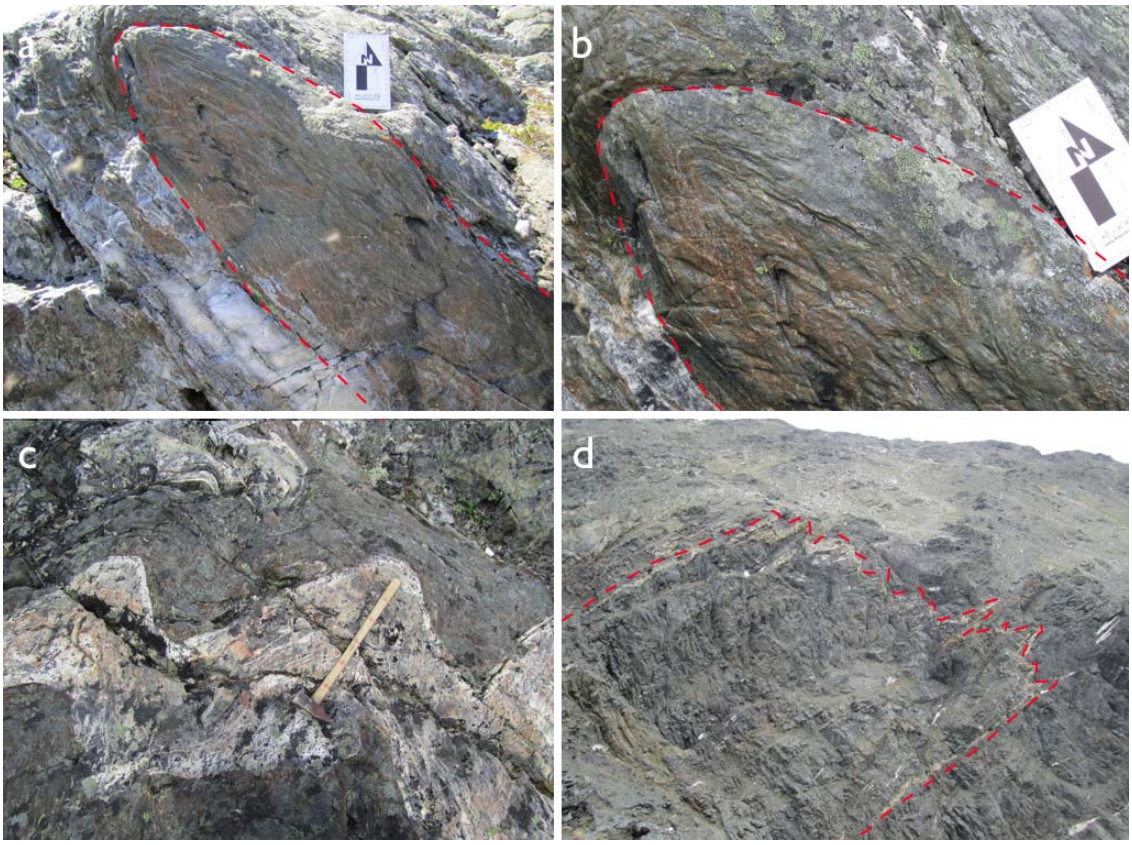

Figure 9. *(a) and (b) F_2 folding in amphibolite. (c) F_2 folding in aplitic sill. (d) F_2 folding with parasitic Z and S folds.*

Figure 10. *F_2 fold displaying a Z fold.*

Figure 11. *(a) and (b) both show crenulations within F_2.*

Figure 12. *(a) Larger open F_3 fold. (b) Tight to open F_2 within F_3.*

Figure 13. *Sheath folding located at N 62°04'25.6" and W 49°04'18.3" showing F_3.*

Shears/faults

The Akuliaq Peninsula contains two major shear zones (Fig. 14) that run NE-SW, and several other E-W shear zones that can be seen on the structural map (Appendix C). Associated with the NE-SW shears regularly along their length were mylonitic zones. In places where E-W shear zones intersect the NE-SW shears there was also evidence of cataclasites occurring regularly.

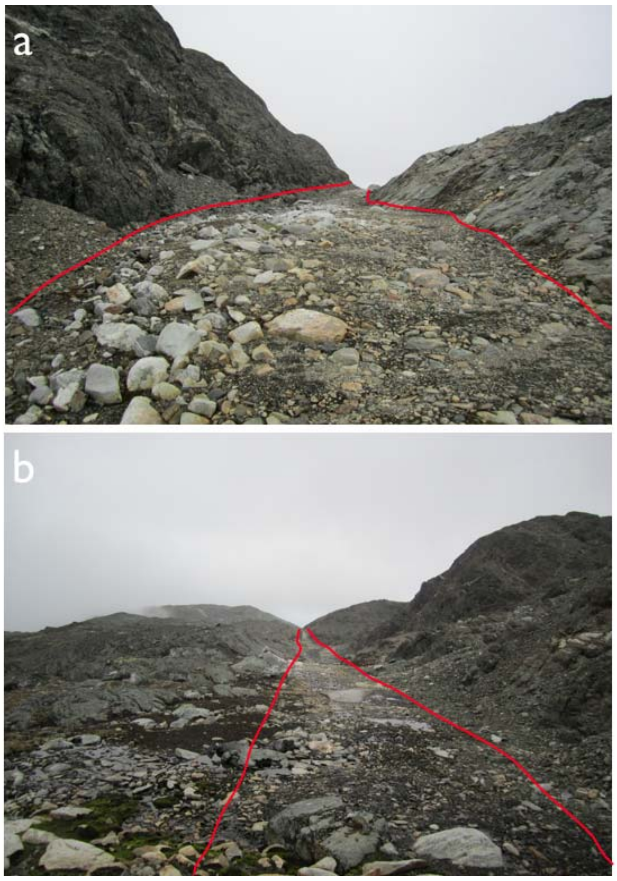

Figure 14. *NE-SW trending major shear zone. (A) Facing NE. (B) Facing SW.*

Kinematic indicators

The NE-SW and E-W shear zones contain several shear sense indicators indicate structural movement in the region. These have been observed and recorded in various locations throughout the Peninsula. They include: sigma clasts, delta clasts, S-C fabrics, S-C' fabrics, bedding offsets perpendicular to lineations for the NE-SW shear zones (Figs. 15 and 16). Oblique to sub-horizontal lineations and possible intrusion offsets can be seen occurring in the E-W shear zones.

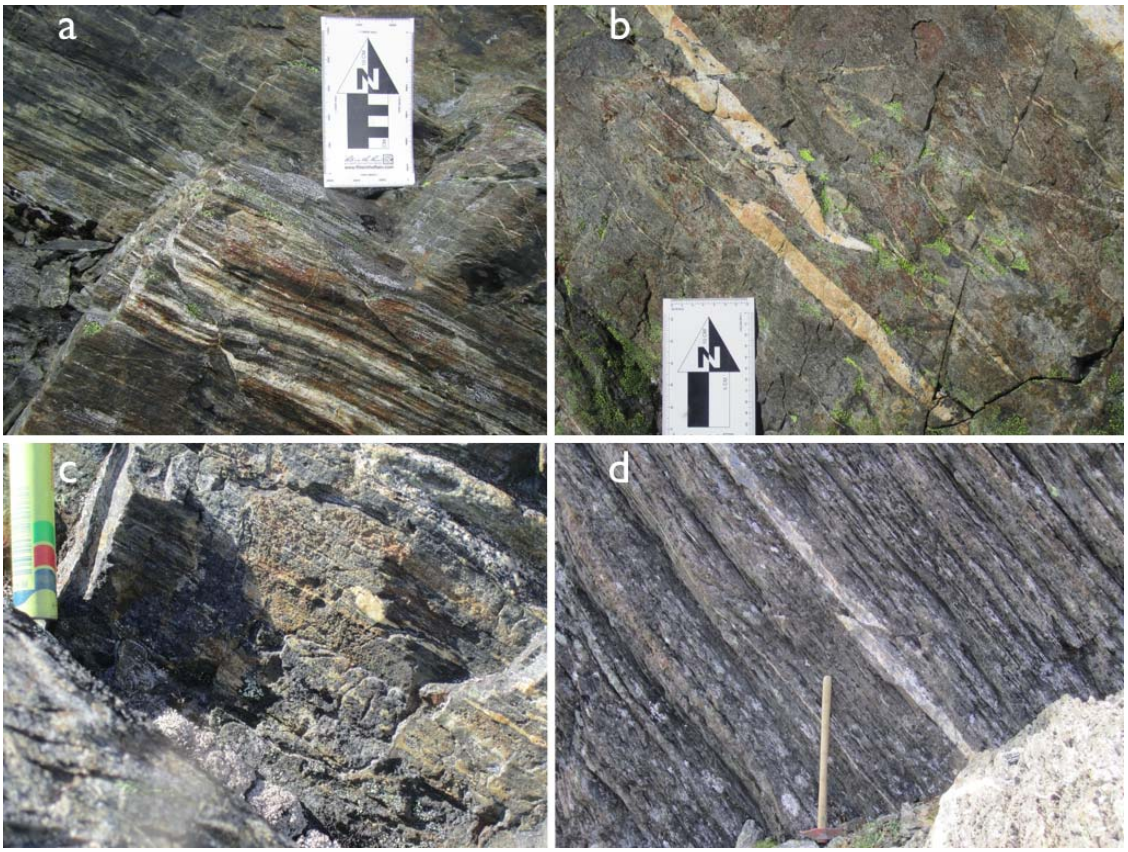

Figure 15. *(a), (b), and (d) showing brittle offsets perpendicular to lineations. (c) Delta clast. All examples are facing South, generally parallel with strike.*

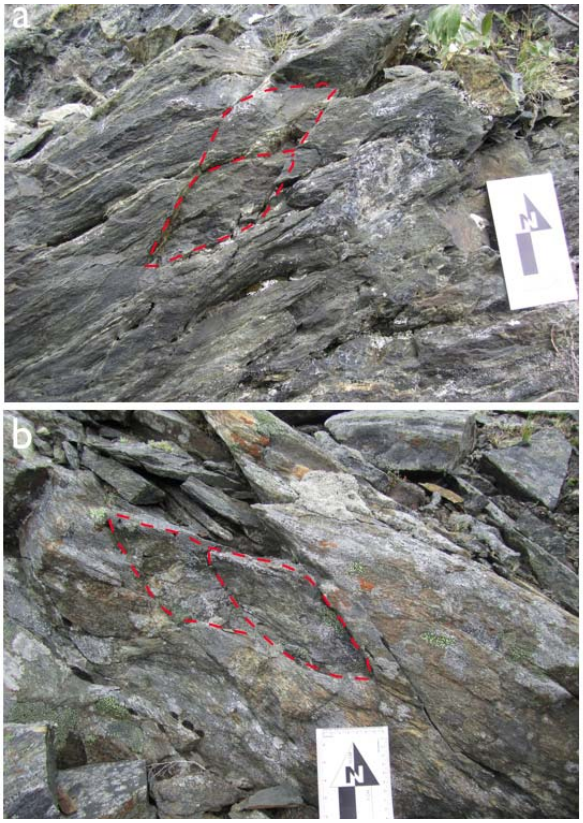

Figure 16. *S-C' fabrics perpendicular to lineations and parallel to strike. (a) Facing north. (b) Facing south.*

Gold mineralisation

As a result of work carried out by NunaMinerals between 2005 and 2008, gold mineralisation was identified along shear zones and at intersections between shear zones. Gold concentrations of between 0.6 and 11.8 ppm were found (Slowey & Goodman, 2008). To try to add to, and further understand, possible controls on gold mineralisation in shear zones, twelve quartz samples were sent to ActLabs in Ancaster. The results are presented in Table 1.

Table 1. *Gold results from twelve quartz samples taken throughout Akuliaq*

	Au	Mass	Latitude	Longitude
	ppb	g	North	West
Detection Limit	1			
Analysis Method	FA-INAA			
495510	2	30.3	62°05'36.5"	49°02'56.2"
495556	2	30.4	62°05'12.5"	49°04'22.8"
495558	3	30.1	62°05'14.7"	49°04'19.0"
495567	3	30.6	62°05'11.2"	49°04'27.8"
495568	3	30.1	62°05'14.2"	49°04'20.5"
495570	2	30.9	62°05'14.2"	49°04'21.6"
495587	2	30.0	62°05'36.9"	49°02'35.6"
495588	3	30.8	62°05'36.9"	49°02'35.6"
495590	2	30.7	62°05'39.2"	49°02'27.9"
495594	3	30.3	62°05'59.8"	49°02'04.4"
476703	2	30.3	62°05'22.6"	49°03'18.3"
477546	1	30.1	62°05'57.7"	49°02'27.4"

Discussion

Escher (1971) proposed that the rocks of the Akuliaq peninsula had been affected by five deformation events (D_1-D_5). This was based on the belief that the TTG gneisses were older than the amphibolites in the region. However, more recent investigations, principally field relationships, have suggested that the TTG gneisses are younger (Friend & Nutman, 2001). This implies that Escher's D_1/D_2 and D_3/D_4 actually occurred at the same time, as can be seen by the replication of data in his paper.

Rather, three deformation events (D_1, D_2 and D_3) are proposed based on the observations from this study, taking TTG gneiss age into account. These deformation events and accompanying structural history of each event are chronologically as follows:

$\underline{D_1}$: S_1 foliations occurred and were axial planar to the folds occurring in F_1. These presently are locally observed as rootless isoclinal folds. Some layer parallel S_1 foliation is still

observed in rare localities. The L_1 lineations could have formed along with S_1 but no evidence for their existence was found.

$\underline{D_2}$: S_1 was transposed by F_2 and S_2 became the dominant fabric in the Akuliaq peninsula, defined by hornblende and was parallel to mm- to cm-scale compositional banding in places. A major top-to-the-west extensional shearing event occurred due to E-W compression and local/regional F_2 folding was seen. It can be observed that F_2 has an axial trace parallel to that of S_2 in tight to open, cm- to m-scale F_2 folds. The F_2 folds have associated parasitic "Z" and "S" folds, as well as crenulations that show a deformation of S_2. The parasitic folds exhibit the same axial traces and general orientation as the F_2 folds, making them a progression of F_2 termed F_{2b}. Top-to–the-west shearing is shown by the major shear sense indicators in and around NE-SW trending shear zones: sigma clasts, delta clasts, S-C and S-C' fabrics, offsets and boudinage formations. The L_2 lineations formed in conjunction with this event, and are defined by hornblende and plagioclase crystals.

$\underline{D_{3a}}$: Open, metre-scale F_3 folding and dextral shearing occurred due to a N-S compressional event. These dextral shear zones generally trend E-W. Dextral shearing is shown by offsetting fabrics and oblique to sub-horizontal lineations, defined again by hornblende and plagioclase crystals. Oblique to sub-horizontal lineations plunge to the north and only seem to occur within E-W dextral shear zones showing a rotation of L_2 into L_3. This, in turn, suggests that the strike-slip shearing occurred in response to ongoing N-S compression. This D_3 shearing was accompanied by the development of late, open, m-scale F_3 folds, which refolded F_2 folds in some localities, creating sheath folds. S_3 occurs locally in areas along F_3 fold axial traces showing their correlation with one another, meaning S_3 is axial planar to F_3.

$\underline{D_{3b}}$: There is some evidence for reactivation of the NE-SW trending shear zones, which could be a younger brittle overprint. Evidence for this is possible brittle overprinting of previously ductile areas and cataclasite formation.

Gold mineralisation in the area associated with the rusty quartz veins seems to be closely linked to shear zones and shear zone intersections, according to the values presented by NunaMinerals (Slowey & Goodman, 2008). The lack of correlative results from our geochemistry and that of NunaMinerals indicates a need for more and larger samples.
The milky, blue, and rusty quartz all show indication of occurring during D_2 from their orientation and structural data and would have formed from fluids entering during extensional top-to-the-west shearing and associated ramp structures, or fluid entering dilation zones associated with D_2 shear zones and at shear intersections.

The study area represents an Archaean fold and thrust belt and these rocks most likely formed as a Mesoarchaean oceanic crust. Figure 16, below, is an idealised stratigraphic column of the Akuliaq Peninsula.

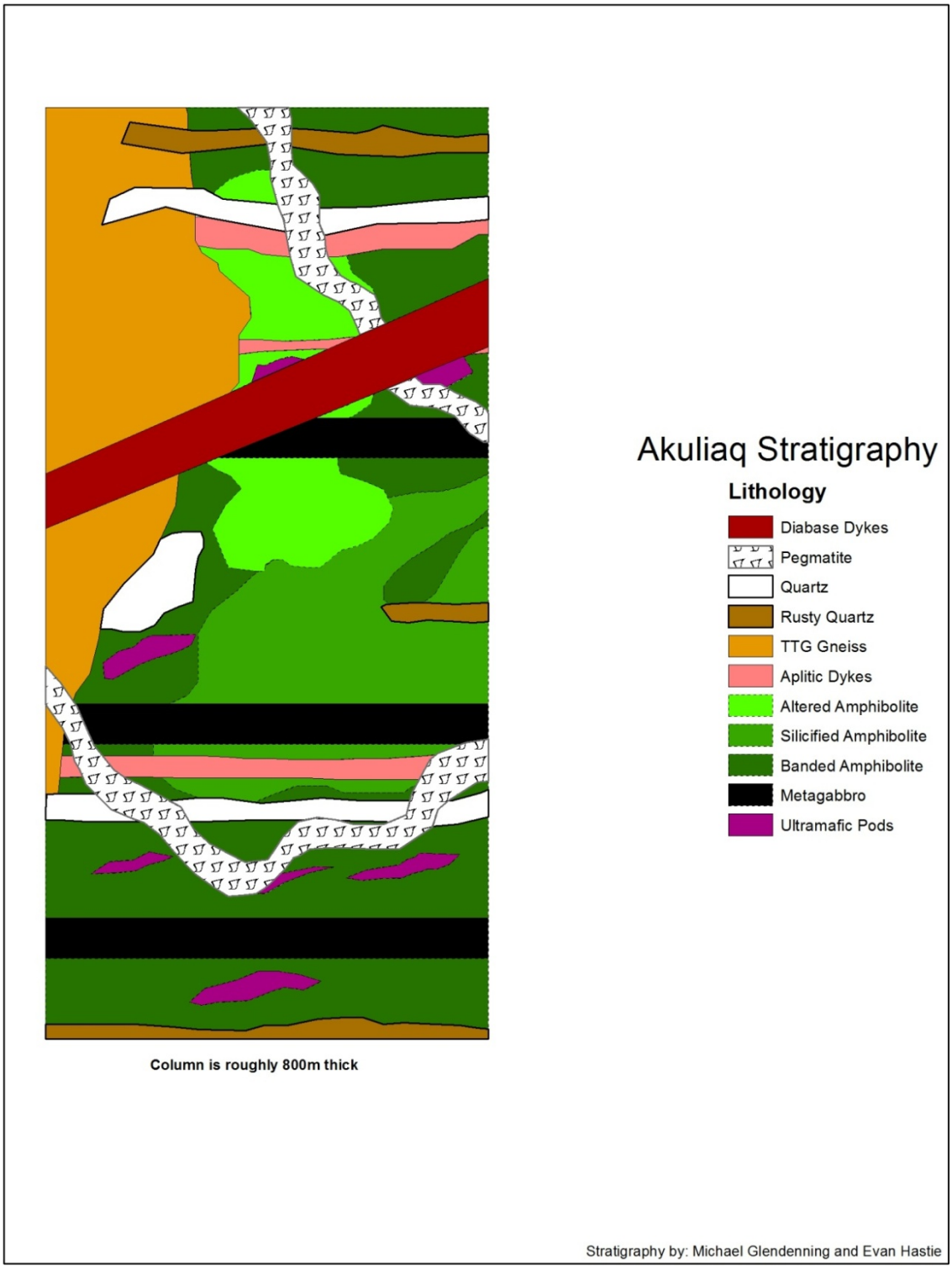

Figure 17. *Idealized stratigraphic column of Akuliaq showing cross-cutting relationships.*

Conclusions

The structural characteristics of rocks in the Akuliaq Peninsula can be explained in terms of three deformation events: D_1, D_2, and D_3. An early S_1 foliation is only locally preserved in rootless isoclinal F_1 folds that are contained in the S_2 foliation. The S_2 foliation is the dominant fabric in the Akuliaq Peninsula, and is mainly defined by hornblende and was parallel to mm- to cm-scale compositional banding in places. The S_2 foliation generally trends NE-SW, and dips from 25-70° to the NW. The associated lineation (L_2) is generally down-dip, but locally can be oblique to sub-horizontal (L_3) and is defined by hornblende and plagioclase crystals. These oblique to sub-horizontal lineations plunge to the north and only seem to occur within E-W dextral shear zones showing a rotation of L_2 into L_3 (D_3). This, in turn, suggests that the strike slip shearing occurred in response to ongoing N-S compression, (i.e. the oblique lineations are L_3 lineations). The majority of shear-sense indicators (i.e. S-C' fabrics, offsetting perpendicular to lineations, etc.) suggest a top-to-the-west sense of movement during D_2. Mylonitic shear zones and cataclasites that occur at shear zone intersections indicate an early-ductile to late-brittle progression to the shearing. The notable exception to this being some cataclasites in the SE were ductile overprinted after they were brecciated. Tight to open, cm- to m-scale F_2 folds are developed throughout the area, and have fold axes that generally plunge 30-60°to the N and NW and seem to be parallel with the L_2 lineations. The youngest stage of deformation (D_3) is characterised by a set of dextral shear zones that crosscut the S_2 foliation at high angles and generally trend E-W. This D_3 shearing was accompanied by the development of late, open F_3 folds, which refolded some F_2 folds to form sheath folds. These F_3 folds have fold axes that generally plunge from 40-60° to the west. In a few localities near D_3 shear zones, hornblende defines an S_3 foliation that trends E-W, and L_3 lineations which trend N-S. These S_3 foliations are parallel to the axial planes of the open F_3 folds, which also indicate a N-S compression event. Late reactivation of NE-SW shear zones could also have been responsible for some of the brittle shear sense indicators that indicate younger brittle overprint in these shear zones.

A new and significantly more detailed map has been created during this project and possible structural controls on gold include: fluids entering during extensional top-to-the-west shearing and associated ramp structures, or fluid entering dilation zones associated with D_2 shear zones and at shear intersections. The geological setting that the Akuliaq Peninsula formed in, as indicated by the structural and lithological evidence, would have been an Archaean fold-and-thrust belt as part of a Mesoarchaean oceanic crust.

References

Escher, J.C. 1971: The Geology of Akuliaq: With particular bearing on the origin and evolution of the supracrustal Kvanefjord belt, Frederiskshab area, South-West Greenland. Thesis, (PhD). Universite de Lausanne.

Friend, C.R.L. & Nutman, A.P. 2001: U-Pb zircon study of tectonically bounded blocks of 2940-2840 Ma crust with different metamorphic histories, Paamiut region, South-West Greenland: implications for the tectonic assembly of the North Atlantic craton. Precambrian Research, **105**, 143-164.

McGregor, V.R. & Friend, C.R.L. 1992: Late Archaean prograde amphibolite- to granulite-facies relations in the Fiskenæsset region, southern West Greenland. Journal of Geology, **100**, 207–219.

McGregor, V.R. & Friend, C.R.L. 1997: Recognition of rocks totally retrogressed from granulite facies and reinterpretation of the large-scale Archaean structure in the Paamiut region, South-West Greenland. Precambrian Research, **86**, 59–70.

Passchier, C.W., & Trouw, R.A.J. Microtectonics. Berlin, Germany: Springer, 2005.

Robb, L.Introduction to ore forming processes. Malden, MA, U.S.A.: Blackwell Publishing, 2005.

Slowey, E., & Goodman, R., 2008. A valuation of NunaMinerals interest in exploration licenses in Greenland, March 2008. CSA Report No. 38311078.

Appendix A

Sample Data

Sample #	Rock Name	Latitude	Longitude
477501	Aplitic Lens	62^{0}05'35.7" N	49^{0}03'07.0" W
477502	Amphibolite	62^{0}05'35.7" N	49^{0}03'07.0" W
477503	Amphibolite	62^{0}05'35.7" N	49^{0}03'07.0" W
477504	Rusty Quartz	62^{0}05'35.7" N	49^{0}03'07.0" W
477505	Quartz	62^{0}05'37.0" N	49^{0}03'11.0" W
477506	Quartz	62^{0}05'37.0" N	49^{0}03'11.0" W
477507	Amphibolite	62^{0}05'36.0" N	49^{0}03'21.0" W
477508	Mylonite	62^{0}05'43.5" N	49^{0}03'13.6" W
477509	Altered Amphibolite	62^{0}05'34.5" N	49^{0}03'21.3" W
477510	Rusty Quartz	62^{0}05'23.8" N	49^{0}03'55.9" W
477511	Rusty Quartz	62^{0}05'23.8" N	49^{0}03'55.9" W
477512	Altered Amphibolite	62^{0}05'34.3" N	49^{0}03'06.1" W
477513	Diabase Dyke	62^{0}05'28.0" N	49^{0}02'58.6" W
477514	Rusty Quartz	62^{0}05'24.9" N	49^{0}02'56.2" W
477515	Amphibolite	62^{0}05'24.0" N	49^{0}02'48.0" W
477516	Silicified Amphibolite	62^{0}05'22.0" N	49^{0}02'44.3" W
477517	Meta Ultramafic	62^{0}05'20.0" N	49^{0}02'42.8" W
477518	Altered Amphibolite	62^{0}05'11.4" N	49^{0}02'46.3" W
477519	Silicified Amphibolite	62^{0}05'06.2" N	49^{0}02'51.6" W
477520	Amphibolite	62^{0}05'35.0" N	49^{0}02'55.8" W
477521	Amphibolite	62^{0}05'56.0" N	49^{0}02'43.9" W
477522	Silicified Amphibolite	62^{0}06'05.1" N	49^{0}02'51.8" W
477523	White Pegmatite	62^{0}06'11.2" N	49^{0}03'04.5" W
477524	Amphibolite	62^{0}06'11.0" N	49^{0}01'33.6" W
477525	White Pegmatite	62^{0}05'34.7" N	49^{0}02'35.7" W
477526	Amphibolite	62^{0}05'34.7" N	49^{0}02'35.7" W
477527	Silicified Amphibolite	62^{0}04'33.8" N	49^{0}04'39.4" W
477528	Amphibolite	62^{0}04'40.4" N	49^{0}03'58.3" W
477529	Amphibolite	62^{0}04'33.0" N	49^{0}04'38.5" W
477530	Amphibolite	62^{0}04'33.0" N	49^{0}04'38.5" W

477531	Banded Amphibolite	62^{0}05'37.0'' N	49^{0}02'26.0'' W
477532	Diabase Dyke	62^{0}05'37.1'' N	49^{0}02'25.6'' W
477533	Silicified Amphibolite	62^{0}05'32.8'' N	49^{0}02'18.3'' W
477534	White Pegmatite	62^{0}05'32.8'' N	49^{0}02'18.3'' W
477535	Blue Quartz	62^{0}04'39.8' N	49^{0}04'37.6'' W
477536	Meta Ultramafic	62^{0}04'30.7'' N	49^{0}04'17.3'' W
477537	Diabase Dyke	62^{0}04'30.7'' N	49^{0}04'17.3'' W
477538	Amphibolite	62^{0}04'30.7'' N	49^{0}04'17.3'' W
477539	White Pegmatite	62^{0}04'27.0'' N	49^{0}04'13.0'' W
477540	TTG Gneiss	62^{0}04'27.0'' N	49^{0}04'13.0'' W
477541	White Pegmatite	62^{0}04'20.5'' N	49^{0}04'23.5'' W
477542	TTG Gneiss	62^{0}06'11.7'' N	49^{0}03'30.3'' W
477543	TTG Gneiss	62^{0}06'11.7'' N	49^{0}03'30.3'' W
477544	Amphibolite	62^{0}06'22.5'' N	49^{0}02'50.9'' W
477545	Meta Gabbro	62^{0}06'30.2'' N	49^{0}01'56.4'' W
477546	Blue Quartz	62^{0}05'57.7'' N	49^{0}02'27.4'' W
477547	Aplitic Lens	62^{0}05'56.4'' N	49^{0}03'19.6'' W
477548	Aplitic Lens	62^{0}05'57.7'' N	49^{0}03'35.3'' W
477549	Altered Amphibolite	62^{0}05'49.5'' N	49^{0}03'25.4'' W
477550	Altered Amphibolite	62^{0}05'46.2'' N	49^{0}03'27.9'' W
477551	Altered Amphibolite	62^{0}05'46.2'' N	49^{0}03'27.9'' W
477552	Quartz	62^{0}05'21.7'' N	49^{0}03'56.7'' W
477553	Mylonite	62^{0}05'15.5'' N	49^{0}04'56.7'' W
477554	Quartz	62^{0}05'15.5'' N	49^{0}04'56.7'' W
477555	Amphibolite	62^{0}05'15.5'' N	49^{0}04'56.7'' W
477556	Quartz	62^{0}05'15.5'' N	49^{0}04'56.7'' W
477557	Diabase Dyke	62^{0}05'15.5'' N	49^{0}04'56.7'' W
477558	Silicified Amphibolite	62^{0}05'03.9'' N	49^{0}04'20.3'' W
477559	Diabase Dyke	62^{0}05'03.9'' N	49^{0}04'20.3'' W
477560	Banded Amphibolite	62^{0}05'03.9'' N	49^{0}04'20.3'' W
477561	Diabase Dyke	62^{0}05'03.9'' N	49^{0}04'20.3'' W
477562	Ultra Mafic	62^{0}04'51.1'' N	49^{0}04'53.7'' W
477563	Altered Amphibolite	62^{0}05'00.7'' N	49^{0}04'58.1'' W
477564	Altered Amphibolite	62^{0}05'00.7'' N	49^{0}04'58.1'' W
477565	Quartz	62^{0}05'00.7'' N	49^{0}04'58.1'' W
477566	Altered Amphibolite	62^{0}05'00.7'' N	49^{0}04'58.1'' W
477567	Diabase Dyke	62^{0}05'03.9'' N	49^{0}04'20.3'' W
477568	Altered Amphibolite	62^{0}05'46.0'' N	49^{0}03'28.0'' W
477569	Altered Amphibolite	62^{0}05'46.0'' N	49^{0}03'28.0'' W
477570	Aplitic Lens	62^{0}05'07.5'' N	49^{0}03'50.9'' W
477571	Altered Amphibolite	62^{0}04'50.8'' N	49^{0}03'42.0'' W
477572	White Pegmatite	62^{0}04'50.8'' N	49^{0}03'42.0'' W
477573	White Pegmatite	62^{0}04'50.8'' N	49^{0}03'42.0'' W
477574	Altered Amphibolite	62^{0}04'50.0'' N	49^{0}03'37.7'' W
477575	Altered Amphibolite	62^{0}04'50.0'' N	49^{0}03'37.7'' W
477576	White Pegmatite	62^{0}04'53.0'' N	49^{0}03'44.2'' W
477577	Diabase Dyke	62^{0}05'18.2'' N	49^{0}03'22.1'' W

477578	Aplitic Lens	62^{0}05'18.2" N	49^{0}03'22.1" W
477579	Amphibolite	62^{0}05'18.2" N	49^{0}03'22.1" W
477580	White Pegmatite	62^{0}06'11.1" N	49^{0}03'04.4" W
477581	Aplitic Lens	62^{0}06'09.0" N	49^{0}03'01.3" W
477582	Altered Amphibolite	62^{0}06'05.1" N	49^{0}02'28.1" W
477583	Altered Amphibolite	62^{0}05'59.1" N	49^{0}02'27.3" W
477584	Blue Quartz	62^{0}05'59.1" N	49^{0}02'27.3" W
477585	Aplitic Lens	62^{0}05'48.4" N	49^{0}03'04.7" W
477586	Altered Amphibolite	62^{0}06'05.1" N	49^{0}02'28.1" W
477587	Meta Gabbro	62^{0}06'03.2" N	49^{0}02'08.1" W
477588	Diabase Dyke	62^{0}06'08.1" N	49^{0}01'24.0" W
477589	Diabase Dyke	62^{0}06'08.1" N	49^{0}01'24.0" W
477590	Milky Quartz	62^{0}05'30.8" N	49^{0}04'07.7" W
477591	Milky Quartz	62^{0}05'30.8" N	49^{0}04'07.7" W
477592	Altered Amphibolite	62^{0}05'30.8" N	49^{0}04'07.7" W
477593	Altered Amphibolite	62^{0}05'26.1" N	49^{0}04'23.1" W
477594	Amphibolite	62^{0}05'26.1" N	49^{0}04'23.1" W
477595	Quartz	62^{0}05'21.8" N	49^{0}04'23.9" W
477596	Altered Amphibolite	62^{0}05'17.6" N	49^{0}04'23.0" W
477597	Rusty Quartz	62^{0}05'18.9" N	49^{0}04'13.4" W
477598	Meta Gabbro	62^{0}05'23.1" N	49^{0}04'13.4" W
477599	Altered Amphibolite	62^{0}05'23.1" N	49^{0}04'13.4" W
495501	Diabase Dyke	62^0 05'21.6" N	49^{0}03'20.7" W
495502	Altered Amphibolite	62^0 05'17.6" N	49^{0}04'23.0" W
495503	Amphibolite	62^0 05'18.9" N	49^{0}04'13.4" W
495504	Altered Amphibolite	62^0 04'37.2" N	49^{0}04'22.3" W
495505	Diabase Dyke	62^0 04'35.9" N	49^{0}04'13.6" W
495506	TTG Gneiss	62^0 04'31.4" N	49^{0}04'04.7" W
495507	Pegmatite	62^0 04'23.7" N	49^{0}03'59.4" W
495508	Diabase Dyke	62^0 04'29.1" N	49^{0}03'59.0" W
495509	Meta Gabbro	62^0 04'56.7" N	49^{0}04'03.4" W
495510	Milky Quartz	62^0 05'36.5" N	49^{0}02'56.2" W
495511	Altered Amphibolite	62^0 05'35.4" N	49^{0}02'43.3" W
495512	Diabase Dyke	62^0 05'36.8" N	49^{0}02'31.6" W
495513	Aplitic Lens	62^0 05'34.7" N	49^{0}02'35.6" W
495514	Quartz	62^0 05'34.7" N	49^{0}02'35.6" W
495515	TTG Gneiss	62^0 09'05.11" N	48^{0}42'13.4" W
495516	Altered Amphibolite	62^0 09'07.0" N	48^{0}42'20.5" W
495517	Banded Amphibolite	62^0 09'07.0" N	48^{0}42'21.5" W
495518	White Pegmatite	62^0 09'06.4" N	48^{0}42'22.9" W
495519	Aplitic Lens	62^0 09'05.9" N	48^{0}42'24.2" W
495520	TTG Gneiss	62^0 06'21.5" N	49^{0}02'13.0" W
495521	TTG Gneiss	62^0 06'32.8" N	49^{0}01'39.1" W
495522	TTG Gneiss	62^0 06'27.6" N	49^{0}01'12.0" W
495523	Amphibolite	62^0 06'14.9" N	49^{0}03'37.2" W
495524	Rusty Quartz	62^0 05'42.6" N	49^{0}02'21.9" W
495525	TTG Gneiss	62^0 06'14.3" N	49^{0}03'24.3" W

495526	Pegmatite	62^0 06'23.8" N	49^{0}02'56.9" W
495527	TTG Gneiss	62^0 06'29.5" N	49^{0}02'49.0" W
495528	Rusty Quartz	62^0 05'19.1" N	49^{0}04'13.2" W
495529	Altered Amphibolite	62^0 05'19.1" N	49^{0}04'13.2" W
495530	Amphibolite	62^0 05'19.1" N	49^{0}04'13.2" W
495531	Meta Gabbro	62^0 05'19.1" N	49^{0}04'13.2" W
495532	Banded Amphibolite	62^0 05'19.1" N	49^{0}04'07.9" W
495533	Amphibolite	62^0 05'19.1" N	49^{0}04'07.9" W
495534	Amphibolite	62^0 05'19.1" N	49^{0}04'07.9" W
495535	Amphibolite	62^0 05'15.9' N	49^{0}04'03.0" W
495536	Rusty Quartz	62^0 05'15.9' N	49^{0}04'03.0" W
495537	Amphibolite	62^0 05'15.9' N	49^{0}04'03.0" W
495538	Amphibolite	62^0 05'15.9' N	49^{0}04'03.0" W
495539	Rust Quartz	62^0 05'15.9' N	49^{0}04'03.0" W
495540	Aplitic Lens	62^0 05'15.9' N	49^{0}04'03.0" W
495541	Quartz	62^0 05'15.9' N	49^{0}04'03.0" W
495542	Blue Quartz	62^0 05'11.4" N	49^{0}04'19.5" W
495543	Rusty Quartz	62^0 05'15.9' N	49^{0}04'03.0" W
495544	Amphibolite	62^0 05'31.5" N	49^{0}02'30.5" W
495545	Altered Amphibolite	62^0 05'32.2" N	49^{0}02'26.4" W
495546	Rusty Quartz	62^0 05'32.2" N	49^{0}02'20.2" W
495547	Amphibolite	62^0 05'33.8" N	49^{0}02'14.7" W
495548	Amphibolite	62^0 05'32.9" N	49^{0}02'12.4" W
495549	Rusty Quartz	62^0 05'50.2" N	49^{0}02'45.2" W
495550	Banded Amphibolite	62^0 05'35.2" N	49^{0}03'10.4" W
495551	Amphibolite	62^0 05'35.2" N	49^{0}03'10.4" W
495552	Meta Gabbro	62^0 05'28.3" N	49^{0}03'28.4" W
495553	Banded Amphibolite	62^0 05'11.0" N	49^{0}03'38.4" W
495554	Banded Amphibolite	62^0 05'06.3" N	49^{0}03'30.0" W
495555	Rusty Quartz	62^0 05'12.5" N	49^{0}04'22.8" W
495556	Rusty Quartz	62^0 05'12.5" N	49^{0}04'22.8" W
495557	Rusty Quartz	62^0 05'12.5" N	49^{0}04'22.8" W
495558	Rusty Quartz	62^0 05'14.7" N	49^{0}04'19.0" W
495559	Rusty Quartz	62^0 05'14.7" N	49^{0}04'19.0" W
495560	Rusty Quartz	62^0 05'17.0" N	49^{0}04'07.5" W
495561	Rusty Quartz	62^0 05'35.6" N	49^{0}03'07.4" W
495562	Meta Gabbro	62^0 05'27.5" N	49^{0}03'28.0" W
495563	Rusty Quartz	62^0 05'27.5" N	49^{0}03'28.0" W
495564	Amphibolite	62^0 05'11.3" N	49^{0}03'37.1" W
495565	Amphibolite	62^0 05'08.6" N	49^{0}03'30.6" W
495566	Altered Amphibolite	62^0 05'11.2" N	49^{0}04'27.8" W
495567	Rusty Quartz	62^0 05'11.2" N	49^{0}04'27.8" W
495568	Rusty Quartz	62^0 05'14.2" N	49^{0}04'20.5" W
495569	Rusty Quartz	62^0 05'14.2" N	49^{0}04'20.5" W
495570	Rusty Quartz	62^0 05'14.2" N	49^{0}04'21.6" W
495571	Rusty Quartz	62^0 05'21.0" N	49^{0}04'04.0" W
495572	Amphibolite	62^0 05'21.0" N	49^{0}04'04.0" W

495573	Altered Ultramafic	62^0 04'38.7" N	49^{0}04'43.8" W
495574	Hornblendite	62^0 04'38.7" N	49^{0}04'43.8" W
495575	Amphibolite	62^0 04'34.4" N	49^{0}04'50.7" W
495576	Altered Ultramafic	62^0 04'38.7" N	49^{0}04'44.0" W
495577	Serpentinite	62^0 04'38.7" N	49^{0}04'44.0" W
495578	Actinolite	62^0 04'38.7" N	49^{0}04'44.0" W
495579	Actinolite	62^0 04'38.7" N	49^{0}04'44.0" W
495580	Hornblendite	62^0 04'34.3" N	49^{0}04'52.2" W
495581	Mylonite	62^0 04'31.8" N	49^{0}04'11.8" W
495582	Pegmatite	62^0 04'20.9" N	49^{0}04'25.4" W
495583	Rusty Quartz	62^0 05'35.8" N	49^{0}02'46.1" W
495584	Rusty Quartz	62^0 05'35.8" N	49^{0}02'46.1" W
495585	Pillow Basalt	62^{0}05'29.7" N	49^{0}02'46.3" W
495586	Amphibolite	62^0 05'06.9" N	49^{0}02'41.2" W
495587	Rusty Quartz	62^0 05'36.9" N	49^{0}02'35.6" W
495588	Rusty Quartz	62^0 05'36.9" N	49^{0}02'35.6" W
495589	Rusty Quartz	62^0 05'36.9" N	49^{0}02'35.6" W
495590	Rusty Quartz	62^0 05'39.2" N	49^{0}02'27.9" W
495591	Rusty Quartz	62^0 05'40.4" N	49^{0}02'27.4" W
495592	Rusty Quartz	62^0 05'43.0" N	49^{0}02'26.6" W
495593	Rusty Quartz	62^0 05'45.5" N	49^{0}02'26.0" W
495594	Rusty Quartz	62^0 05'59.8" N	49^{0}02'04.4" W
495595	Rusty Quartz	62^0 05'59.8" N	49^{0}02'04.4" W
495596	Amphibolite	62^0 06'11.5" N	49^{0}01'36.7" W
495597	Pillow Basalt	62^0 05'29.6" N	49^{0}02'45.4" W
495598	Pillow Basalt	62^0 05'29.6" N	49^{0}02'45.4" W
495599	Pillow Basalt	62^0 05'28.3" N	49^{0}02'48.3" W
476701	Pillow Basalt	62^{0}05'28.3" N	49^{0}02'48.3" W
476702	Pillow Basalt	62^{0}05'28.3" N	49^{0}02'48.3" W
476703	Rusty Quartz	62^{0}05'22.6" N	49^{0}03'18.3" W
476704	Rusty Quartz	62^{0}05'22.0" N	49^{0}03'18.4" W
476705	Rusty Quartz	62^{0}05'20.9" N	49^{0}03'21.5" W
476706	Rusty Quartz	62^{0}05'19.1" N	49^{0}03'23.5" W
476707	Unknown Purple Mineral	62^{0}05'06.3" N	49^{0}03'31.2" W
476708	Rusty Quartz	62^{0}04'50.7" N	49^{0}04'04.3" W
476709	Pegmatite	62^{0}05'33.9" N	49^{0}02'21.1" W
476710	Aplite/Pegmatite	62^{0}05'33.9" N	49^{0}02'21.1" W

Appendix B

Foliation Data

Strike (degrees)	Dip (degrees)	Pole Strike	Pole Dip	Latitude N	Longitude W
214	34	124	90	62 05 35.7	49 03 07
240	34	150	56	62 05 35.7	49 03 07
239	50	149	40	62 05 37	49 03 11
262	53	172	37	62 05 34	49 03 21
212	44	122	46	62 05 43.5	49 03 13.6
208	64	118	26	62 05 32.7	49 03 13.6
220	48	130	42	62 05 33.1	49 03 20.7
219	40	129	50	62 05 33.5	49 03 21.8
224	50	134	40	62 05 36.4	49 03 36.7
218	48	128	42	62 05 34.3	49 03 06.1
226	45	136	45	62 05 30.2	49 03 01.5
227	40	137	50	62 05 29.5	49 03 00.9
229	45	139	45	62 05 26.3	49 02 58.7
232	48	142	42	62 05 22.6	49 02 44.3
216	41	126	49	62 05 10.6	49 02 55.2
220	45	130	45	62 05 08.3	49 02 46.2
221	43	131	47	62 05 10.6	49 02 50
230	40	140	50	62 05 06.2	49 02 55.5
223	58	133	32	62 05 13.8	49 02 51.6
212	43	122	47	62 05 16.7	49 03 03
240	38	150	52	62 05 35	49 02 55.8
216	40	126	50	62 05 56	49 02 43.9
222	40	132	50	62 06 09.6	49 03 01
212	44	122	46	62 06 23.5	49 02 22.8
218	43	128	47	62 04 41.6	49 04 24.4
228	40	138	50	62 05 26.4	49 02 18.3
234	42	144	48	62 04 47.7	49 03 57.2
228	42	138	48	62 04 39.0	49 04 37.9
228	39	138	51	62 04 17	49 04 28
229	40	139	50	62 06 22.5	49 02 50.9
230	44	140	46	62 06 22.5	49 01 34.3
240	46	150	44	62 05 56.7	49 03 20.7
220	50	130	40	62 05 57.7	49 03 35.3
220	50	130	40	62 05 16.6	49 03 56.7
220	60	130	30	62 05 16.6	49 03 56.7
218	43	128	47	62 04 46.4	49 04 40.5
218	45	128	45	62 06 11.6	49 01 56.7
226	55	136	35	62 05 38.5	49 03 45.8
220	52	130	38	62 05 27.1	49 03 40.9
200	38	110	52	62 04 37.2	49 04 22.3
218	44	128	46	62 04 27.8	49 03 42.1
224	46	134	44	62 05 36.1	49 02 49.7
240	32	150	58	62 06 20.1	49 01 14.9
228	48	138	42	62 05 36.7	49 03 03

220	45	130	45	62 05 36.7	49 03 03
222	42	132	48	62 06 32.9	49 01 38.9
215	39	125	51	62 05 38.2	49 02 40.4
226	58	136	32	62 05 31.8	49 02 31.4
217	44	127	46	62 05 32.2	49 02 26.4
218	40	128	50	62 05 34	49 02 08
237	45	147	45	62 05 39.1	49 02 06.4
212	28	122	62	62 05 56.4	49 02 13.8
234	20	144	70	62 06 14.3	49 01 54.5
228	48	138	42	62 05 36.7	49 03 02.7
285	48	195	42	62 05 33.4	49 03 24.5
200	62	110	28	62 05 32.8	49 03 23.6
264	45	174	45	62 05 28.7	49 03 26.8
222	42	132	48	62 05 09.9	49 03 46.6
240	46	150	44	62 05 09.9	49 03 46.6
220	45	130	45	62 05 11.4	49 03 36.8
232	33	142	57	62 05 11.4	49 03 36.8
224	55	134	35	62 05 08.6	49 03 30.6
236	59	146	31	62 05 06.4	49 03 33.5
268	56	178	34	62 04 38.7	49 04 44
227	45	137	45	62 04 33.7	49 04 53.3
229	37	139	53	62 04 27.3	49 04 12.7
218	50	128	40	62 06 01.1	49 01 42.8
240	48	150	42	62 06 25.9	49 01 22.7
244	38	154	52	62 05 00.2	49 03 39.7
216	55	126	35	62 04 59.8	49 03 41.7
262	55	172	35	62 04 59.4	49 03 50.3
250	35	160	55	62 05 27.8	49 03 38.4
205	84	115	6	62 04 28.9	49 04 10.1
220	76	130	14	62 04 28.9	49 04 10.1
284	25	194	65	62 04 28.1	49 04 11.6
231	40	141	50	62 04 28.1	49 04 11.6
260	40	170	50	62 04 28.1	49 04 11.6
266	45	176	45	62 04 28.1	49 04 11.6
258	62	168	28	62 04 28.1	49 04 11.6
288	66	198	24	62 04 28.1	49 04 11.6
216	59	126	31	62 04 28.1	49 04 11.6
212	56	122	34	62 05 33.2	49 02 20.6
175	65	85	25	62 05 31	49 03 24.5
108	6	18	84	62 04 24.8	49 04 19.6
310	74	220	16	62 05 33.9	49 02 21.1
308	85	218	5	62 05 33.9	49 02 21.1
290	88	200	2	62 05 33.9	49 02 21.1
185	32	95	58	62 05 34.9	49 03 21.3

Lineation Data

L Trend (degrees)	L Plunge (degrees)	Latitude N	Longitude W
314	44	62 05 36.7	49 03 02.7
30	15	62 04 26.4	49 04 11.6
340	42	62 04 27.9	49 04 04.7
300	44	62 05 11.4	49 03 36.8
328	55	62 05 08.6	49 03 30.6
274	46	62 05 06.4	49 03 33.5
40	22	62 04 34.3	49 04 53.4
240	26	62 05 31.8	49 02 31.4
238	34	62 05 32.2	49 02 20.2
274	35	62 05 34	49 02 08
330	39	62 05 33.4	49 03 24.5
314	38	62 05 32.8	49 03 23.6
320	45	62 05 28.7	49 03 26.8
330	46	62 05 28.7	49 03 26.8
316	52	62 05 28.7	49 03 26.8
330	38	62 05 28.3	49 03 27.1
326	32	62 05 28.3	49 03 27.1
314	45	62 06 25.9	49 01 22.7
310	38	62 06 25.9	49 01 22.7
352	18	62 05 27.2	49 03 14.1
328	25	62 05 16.3	49 03 29.2
50	13	62 05 00.2	49 03 39.7
326	37	62 06 00.5	49 01 46.2
319	55	62 06 01.1	49 01 42.8
18	19	62 04 59.8	49 03 41.7
22	29	62 04 28.9	49 04 10.1
26	24	62 04 28.9	49 04 10.1
20	27	62 04 28.1	49 04 11.6
345	23	62 04 23.3	49 04 15.1
352	29	62 05 37.4	49 02 37.7
334	37	62 05 37.4	49 02 37.7
46	8	62 05 11.4	49 03 36.8

Fold Axis Data

Fold Axis	Plunge	Latitude N	Longitude W
342	26	62 05 33.4	49 03 24.5
318	38	62 05 33.4	49 03 24.5
355	33	62 05 32.8	49 03 23.6
325	30	62 05 31	49 03 24.5
334	40	62 05 31	49 03 24.5
328	44	62 05 31	49 03 23.3
328	32	62 05 31	49 03 23.3
322	46	62 05 30.4	49 03 23.7
337	38	62 05 28.3	49 03 27.1
309	45	62 06 25.9	49 01 22.7
317	79	62 06 11.9	49 03 9.5
306	53	62 06 11.9	49 03 9.5
327	35	62 06 01.7	49 03 01.2
294	36	62 05 27.2	49 03 14.1
358	25	62 05 57.4	49 02 05
322	32	62 05 57.4	49 02 05
345	35	62 06 00.5	49 01 46.2
323	15	62 06 01.1	49 01 42.8
345	45	62 06 01.1	49 01 42.8
342	13	62 06 01.1	49 01 42.8
45	66	62 04 28.9	49 04 10.1
29	21	62 04 28.9	49 04 10.1
228	68	62 04 28.1	49 04 11.6
346	16	62 04 28.1	49 04 11.6
284	25	62 04 28.1	49 04 11.6
145	57	62 04 28.1	49 04 11.6
231	40	62 04 28.1	49 04 11.6
260	40	62 04 28.1	49 04 11.6
266	45	62 04 28.1	49 04 11.6
258	62	62 04 28.1	49 04 11.6
288	66	62 04 28.1	49 04 11.6
190	62	62 04 28.1	49 04 11.6
220	55	62 04 28.1	49 04 11.6
216	59	62 04 28.1	49 04 11.6
288	52	62 04 24.8	49 04 19.6
242	70	62 04 24.8	49 04 19.6
278	55	62 04 24.8	49 04 19.6
292	31	62 05 33.9	49 02 21.1
247	36	62 05 33.9	49 02 21.1
256	29	62 05 33.9	49 02 21.1
250	39	62 05 33.9	49 02 21.1
336	36	62 05 40.8	49 02 07.4
342	28	62 05 56.4	49 02 13.8
346	24	62 05 56.4	49 02 13.8
344	15	62 06 14.3	49 01 54.5
332	26	62 05 58.6	49 02 21

352	30	62 05 46.3	49 02 57.2
18	11	62 05 34.9	49 03 21.3
13	1	62 05 34.9	49 03 21.3
2	12	62 05 34.9	49 03 21.3
302	46	62 05 34.6	49 03 22
11	36	62 05 34.1	49 03 22.6
19	25	62 04 33.7	49 04 53.3
355	14	62 04 33.7	49 04 53.3
25	14	62 04 33.7	49 04 53.3
356	39	62 04 30.5	49 04 44.5
316	62	62 04 30.5	49 04 44.5
195	25	62 04 30.4	49 04 18.0
270	49	62 04 30.4	49 04 18.0
258	21	62 04 30.4	49 04 18.0
258	33	62 04 30.4	49 04 18.0
272	44	62 04 30.4	49 04 18.0
274	53	62 04 30.4	49 04 18.0
254	48	62 04 30.4	49 04 18.0
254	47	62 04 30.4	49 04 18.0
322	25	62 04 20.9	49 04 25.4
41	11	62 04 34.3	49 04 53.4
42	25	62 04 34.3	49 04 53.4
360	51	62 05 32.2	49 02 26.4
322	56	62 05 34	49 02 14.9
346	31	62 05 34	49 02 14.9
288	38	62 05 37.9	49 02 6.4
280	42	62 05 37.9	49 02 6.4
316	46	62 05 39.1	49 02 06.4
330	50	62 05 38.9	49 03 45.8
340	41	62 05 34.1	49 02 26
208	10	62 05 11.4	49 03 36.8
212	5	62 04 38.7	49 04 44
196	0	62 04 38.7	49 04 44

Geological map and cross sections

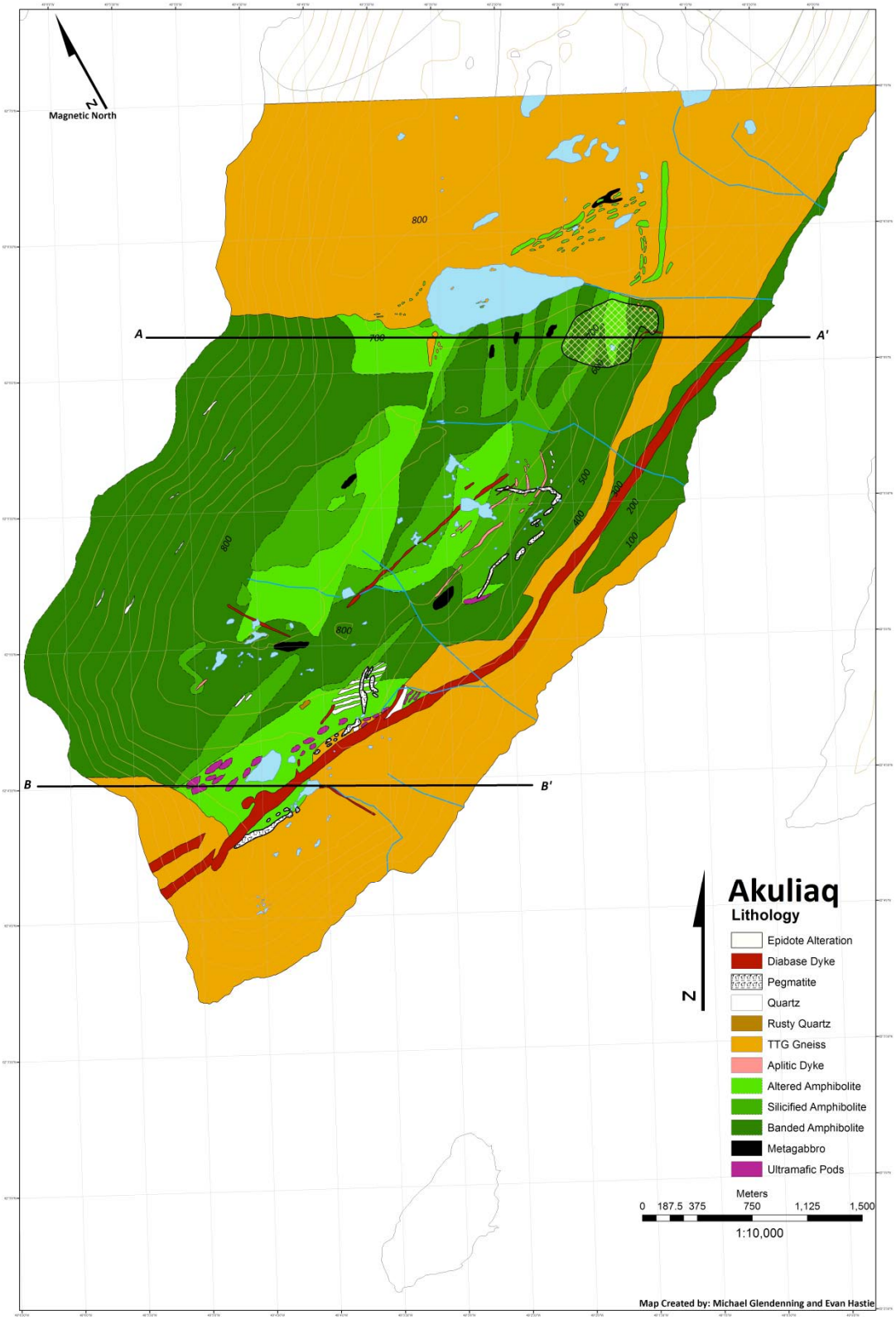

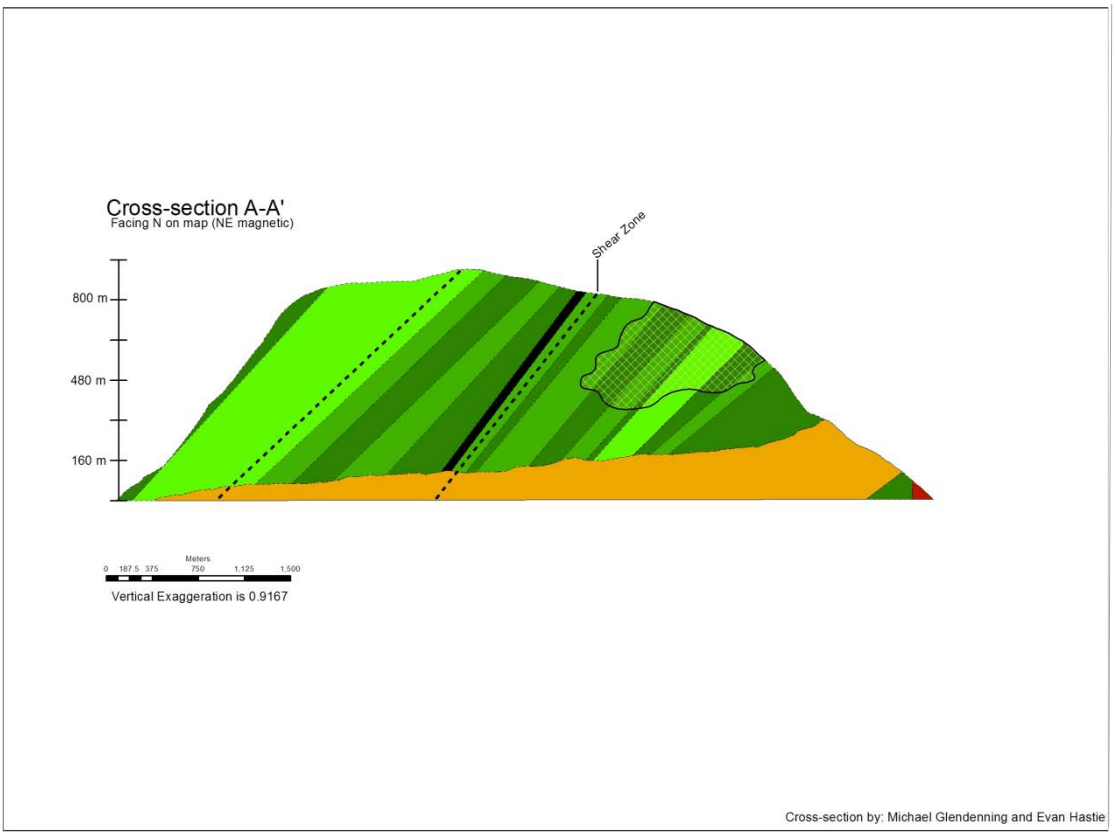
Cross-section A-A'
Facing N on map (NE magnetic)
Shear Zone
800 m
480 m
160 m
Meters
0 187.5 375 750 1,125 1,500
Vertical Exaggeration is 0.9167
Cross-section by: Michael Glendenning and Evan Hastie

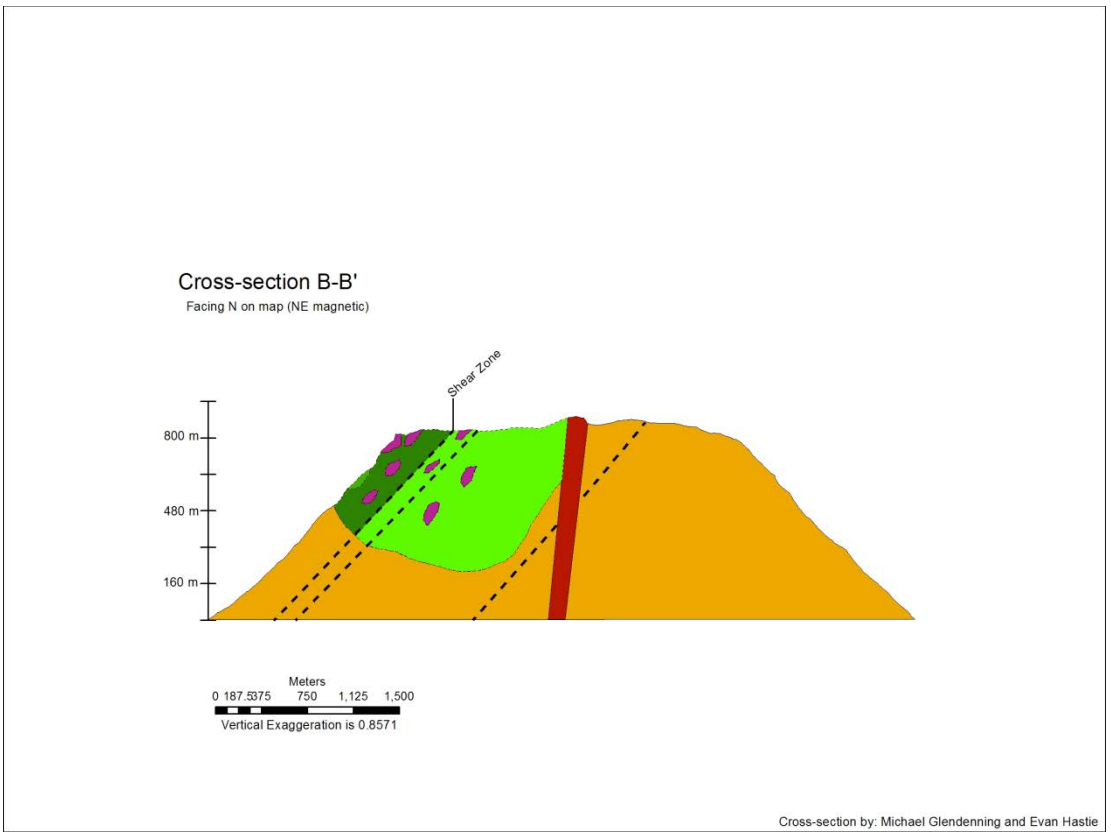
Cross-section B-B'
Facing N on map (NE magnetic)
Shear Zone
800 m
480 m
160 m
Meters
0 187.5375 750 1,125 1,500
Vertical Exaggeration is 0.8571
Cross-section by: Michael Glendenning and Evan Hastie

Mapping and petrographic analysis of the lithology of Akuliaq Peninsula, Paamiut Region, Southwest Greenland (Glendenning)

Michael Glendenning

Department of Earth and Environmental Sciences, University of Windsor, Windsor, Ontario

Abstract

This study focused on the geological history of Akuliaq Peninsula, Paamiut Region, SW Greenland, using a combination of field work, geochemistry and petrography. Lithology was mapped in the field and transferred to a 1:10000 scale map and a 1:2500 small scale map with a focus on rock units, metamorphism and Au mineralisation. This involved the use of the Ganfeld field mapping system which is being developed by the Danish and Greenlandic Geological Survery and the Geological Survey of Canada. Petrographic slides were used to collect detailed information regarding each rock unit. Geochemistry was used to determine gold values of known mineralised sites. As a result of this study the nature of the Au mineralisation is known along with the nature of the complex metamorphism and the relationship between tonalite-trondhjemite-granodiorite gneiss and the greenstones. The conclusion of this study supports the current theory that the tonalite-trondhjemite-granodiorite gneiss is intruding into the greenstones and that the Au mineralisation is a result of quartz-carbonate vein formation resulting from ductile/brittle-ductile shearing.

Introduction

As modern society becomes more advanced and nations struggle to compete for the remaining natural resources, exploration is an invaluable tool. This increase in demand has lead to an increased strain on current ore deposits and reserves. As these producing sites are depleted it is left to the exploration industry to seek out new deposits in more remote areas.

Akuliaq Peninsula in southwest Greenland, roughly 30 km NE from the town of Paamiut in the Kvanefjord region, is part of a greenstone belt that was originally mapped and studied in the 1960's by Jan C. Escher as part of his PhD thesis (Fig. 1). The data and maps provided by the Geological Survey of Denmark and Greenland, known as GEUS, were last updated when J.C. Escher originally published his data in the early part of the 1970's. Studies conducted by C.R.L. Friend & A.P. Nutman on the North Atlantic Craton suggest that the Paamiut region is the product of crustal accretion (Friend & Nutman, 2001). The Paamiut block was emplaced into its current position after a metamorphic event at about 2820 Ma (Friend & Nutman, 2001).

Akuliaq was relatively unexplored until the start of the 21st century when NunaMinerals leased the land rights to the Kvanefjord region for the purpose of Au exploration (Slowey & Goodman, 2008). According to initial reports the stratigraphic sequence is dominated by fine-grained amphibolites with subordinate medium-grained leuco-amphibolites, lenticular ultramafics and carbonate rocks (Slowey & Goodman, 2008). Basic rocks on the southern portion of Akuliaq host concordant quartz veins along with widespread carbonate and chlorite alteration (Slowey & Goodman, 2008). Slowely & Goodman reported that Au mineralisation occurs in two main settings and is generally associated with the major North- Northeast striking Vesterland shear zone of Palaeoproterozoic age (Slowey & Goodman, 2008). Au occurs in disseminated sulphides in quartz-ankerite lenses which tend to be discontinuous and may form vein systems (Slowey & Goodman, 2008). The dominant sulphide mineral is pyrite and secondary pyrrhotite with the best samples returning up to 11.7 g/t Au (Slowey & Goodman, 2008). The second occurrence is in rusty, folded beds within amphibolites and associated with carbonatised rocks and small quartz veins (Slowey & Goodman, 2008). Sulphides are finely disseminated pyrite or pyrrhotite with the best samples returning anywhere from 0.5 to 4.0 g/t Au (Slowey & Goodman, 2008). Currently the Akuliaq mineralisation is in the grassroots exploration phase (Slowey & Goodman, 2008).

Due to the nature of tonalite-trondhjemite-granodiorite gneiss (TTG) formation it is generally accepted that these rocks are younger than the amphibolites; it has yet to be proven with precise dating. This is a problem that the geologists and geoscientists at GEUS are trying to address using zircon age dating techniques on both units.

This study is being conducted because of the inadequacies in mapping technology during the 1960s. The area is being updated using new digital technologies which integrate field GIS software with active GPS receivers to generate a more accurate and useful map.

Objectives

Accurate and relative geological mapping plays a vital role in economic geology and mineral exploration. The purpose of this project was to remap the rock units and structural features of Akuliaq within the NunaMinerals prospecting area as a part of a larger regional mapping project currently being conducted by GEUS. The collected data was used to generate maps on the scale of 1:10000 and 1:2500 along with cross-sections of the study area. Thin sections of selected specimens were cut and studied to assess the mineralogical and textural characteristics of the rock types in the area.

Methods

Sample collection

All specimens were collected in June and July of the 2011 field season from the Akuliaq Peninsula near Paamiut in southwestern Greenland. The study area is approximately 3 km wide and 6 km long (Fig. 2). Sample sites were chosen specifically in order to collect representative specimens from the entire study area. Hand samples were organised based on

the GEUS standard sample booklets. Each sample was tagged with a seven digit number unique to that sample along with a field name and brief description. Samples are listed in the Appendix in Table 1 with a brief description of each and Table 2 contains the samples along with the coordinates of the sample location.

Mapping was carried out during the same period and the classification of rock units was aided by the simultaneous sampling. Appendices A, B and C are a compendium of both the structural and petrographic data that were collected during fieldwork. All field terms that were used while mapping have also been used in this thesis to characterise each rock unit.

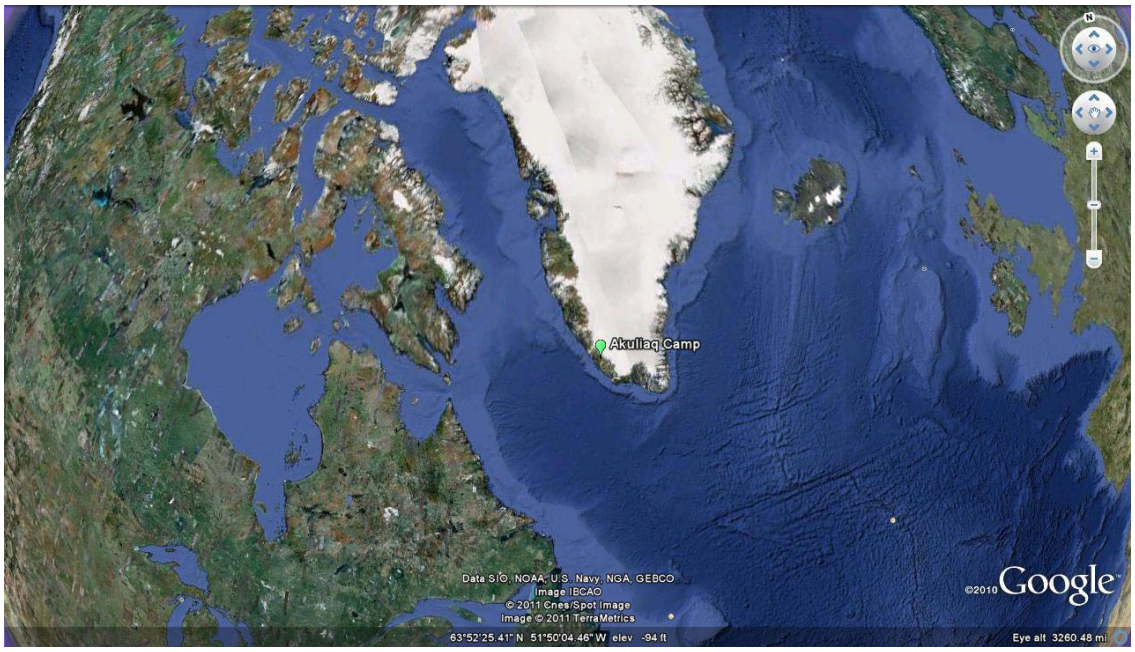

Figure 1. *Location of the study area in SW Greenland.*

Sample preparation

In preparation for transmitted and reflected light microscopy each selected sample had to be cut to roughly the size of a standard microscope slide. Sample selection was almost entirely random with the focus being primarily on the selection of representative samples from around the study area. One set of samples was specifically selected to determine the potential nature of alteration in amphibolites proximally and distally to a mineralised quartz vein; this set and the rest of the samples are summarised in Table 3. All sample cutting was done using a diamond edged blade and a water-cooled saw which is located on site in the Department of Earth and Environmental Science, University of Windsor. Polished thin sections were prepared by Vancouver Petrographics Ltd, Vancouver, BC.

Figure 2. *Study area on Akuliaq Peninsula (see geological map in the appendix for scale).*

Ten selected samples were analysed for their Au content by Activation Labs Ltd. (Ancaster, Ontario). The method for gold analysis was 1A1 – Au Fire Assay – INAA which digests a sample size of 30g in a mixture of fire assay fluxes which binds to Ag and heated to 1060°C. The lighter molten material is moulded and the Pb is absorbed which allows Au recovery.

Map data were collected in the field using the Ganfeld ArcPad system that was provided by GEUS. All of the collected map data were stored on disk and transferred to ESRI ArcMap v.9.3.1. The data was compiled and the maps generated using ArcMap v.9.3.1. digitising was carried out manually using a CalComp Drawing Board II and accompanying digitiser puck directly into ArcMap. The maps are presented according to GEUS map standards at 1:10000 and 1:2500 scale (see Appendices B, C and G). Field photography is used to help document relationships and lithologic boundaries between units (refer to Appendix A). Photos are numbered and catalogued for use by GEUS and for the purpose of this thesis.

Results

Field relations and petrography

The mapping clarified the lithologic relationships allowing relative chronological relationships to be determined. The study area consists of greenstones which contain lenticular ultramafics, metagabbros and three subtypes of amphibolite, aplitic dykes, tonalite-trondjhemite-granodiorite gneiss, quartz and rusty quartz veins, pegmatitic dykes and diabase dykes.

Greenstones – Field Relations

This is the most common unit in the study area and typically has sharp contacts with other lithologies. These greenstones have a general dip of roughly 45° to the North with a strike of approximately 250° to the North. The subtypes of the amphibolite are banded amphibolite, silicified amphibolites and altered amphibolite and these units typically grade from one type to another with no clear defined contact between the units. In the field the banded subtype has a well-developed foliation, giving it a schistose texture. The silicified subtype has a weak-foliation and was noticeably harder than its altered counterpart and appeared to contain additional quartz. The unit has an aphanitic texture which is characterised by a grain-size on the mm-scale. The altered subtype is the least deformed and typically contains pillow structures. These pillows typically occur in areas distal to shear zones in the centre of the peninsula and sometimes in close proximity to metagabbros. The altered subtype has a weak-foliation, mm-sized grains and an aphanitic texture. The term 'altered' is used to break up the amphibolites into three subtypes to allow for the field terms to be carried over and applied to both the map and this thesis; in essence it is just amphibolite. Metagabbros are characterised by a pebbly texture due to the presence of large porphyroblasts of amphibole or hornblende. Typically they can be found as small bodies within altered or silicified amphibolites. Lenticular ultramafics are large 'egg-shaped' pods emplaced in the greenstones. These rocks contain carbonates which have been preferentially weathered leaving a pitted texture (Fig. 3).

Greenstones – Petrography

The amphibolite subtypes tend to have similar assemblages, and differ in the relative abundance of the minerals. The banded subtype has a typical assemblage of 50% amphibole, 15% quartz, 25% plagioclase, 5% biotite and 5% calcite. The unit is foliated and the grain boundaries are sutured which indicates strain on the assemblage. Minor epidote alteration of plagioclase is present. Calcite has precipitated between grains and biotite has replaced plagioclase and amphibole. The silicified subtype has a typical assemblage of 65% amphibole, 15% quartz, 15% plagioclase and 5% biotite. This subtype shows a weak foliation with subhedral to anhedral grains. Quartz has precipitated throughout the rock and some plagioclase is replaced by biotite. The altered subtype has a typical assemblage of 50% amphibole, 30% plagioclase, 5% quartz and 5% biotite. Minor epidote alteration of plagioclase is present. Grains are typically subhedral to anhedral with minor quartz and minor biotite alteration. The grains show a very weak foliation. Metagabbro is similar to the amphibolite units. The typical metagabbro assemblage is 55% amphibole, 25% plagioclase, 10% quartz and 10% biotite. Minor epidote alteration is present. This unit shows no foliation and grains are euhedral to subhedral with irregular grain contacts. Biotite has replaced plagioclase (Fig. 4).

Ultramafics are characterised by two separate assemblages. One assemblage consists of approximately 90% amphibole and 10% plagioclase and the second assemblage is a mixture of serpentine- and epidote-group minerals. The first assemblage is a hornblendite and the second is interpreted as a serpentinite. The hornblendites typically have subhedral grains showing no foliation with irregular grain boundaries. Opaque minerals probably magnetite and hematite, appear between and within grains of amphibole. The serpentinites contain igneous minerals and grains are anhedral showing a strong foliation. It appears that the grains 'flow' around the opaques present (Fig. 5).

Figure 3. *A) Lenticular ultramafics set into greenstones within a shear zone on the western point of the peninsula; B) Metagabbro with large amphibole/hornblende grains which act as a lithologic indicator; C) Lenticular ultramafics with scale to emphasize the size of each pod; D) Relic pillow texture preserved in amphibolite outside of shear zones.*

Energy dispersive spectroscopy (EDS) data was collected on an environmental scanning electron microscope (ESEM) in the Great Lakes Institute for Environmental Research using the same polished thin-section prepared by Vancouver Petrographics and carbon coated for elemental analysis. The data suggests that the unknown mineral is biotite which is replacing the plagioclase. This plagioclase is texturally similar to sillimanite but is very close to being almost pure end member anorthite (Table 5).

Sample 495544, a metagabbro, contains lath-shaped minerals resembling biotite but do not show the biotite interference colours and are colourless under plane polarized light; SEM data was collected to clarify what this mineral is as it is observed in a few other samples. Some of these minerals are being replaced by biotite. Some relict pyroxene grains are present. Some plagioclase is present but usually in minor quantities except for sample 495514, silicified amphibolite, which contains a vein of plagioclase and quartz. This vein shows relic igneous textures as there are numerous zoned plagioclase crystals that are also euhedral to subhedral with clear contacts between grains (Fig. 4).

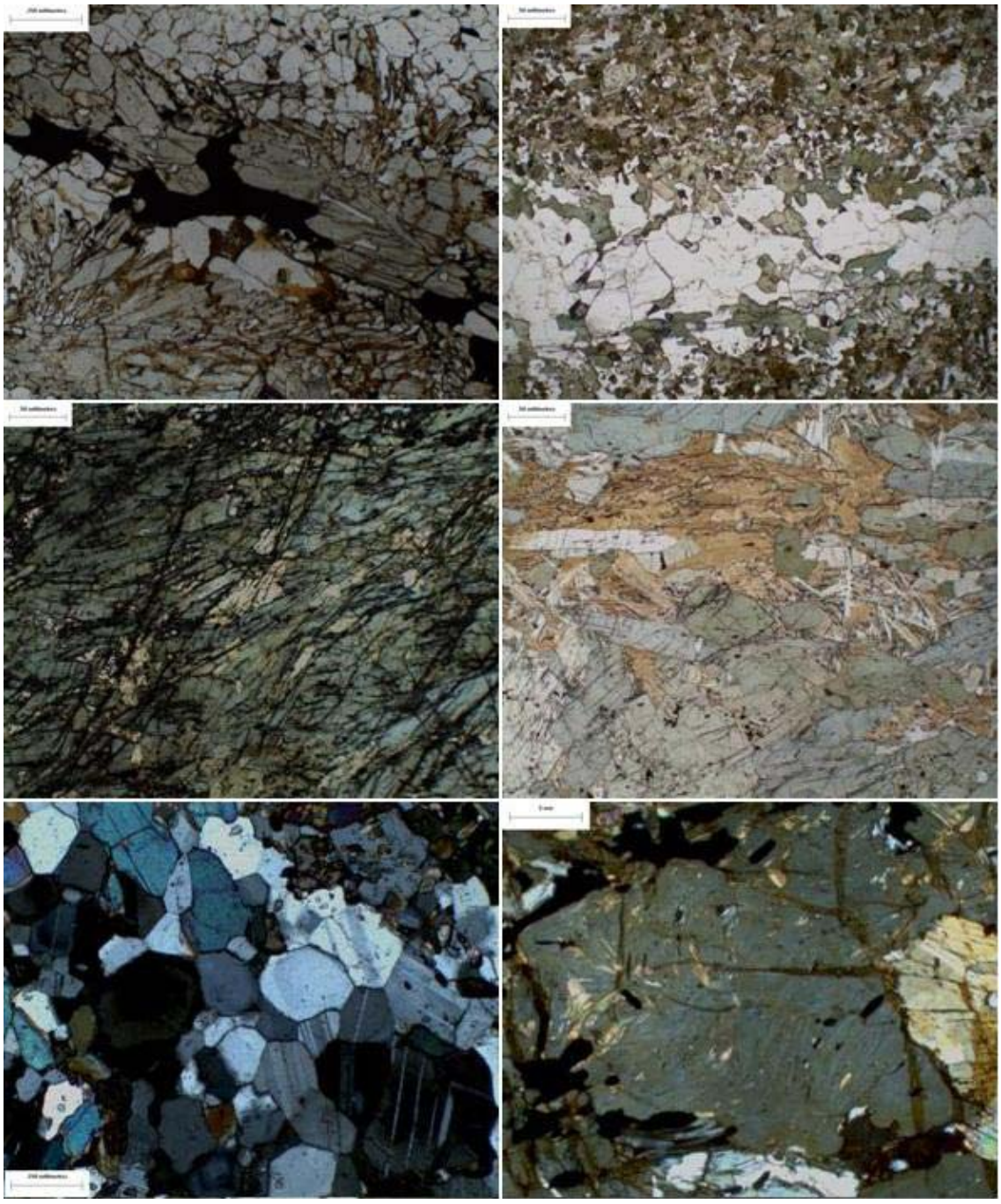

Figure 4. *A) Altered amphibolite showing weak foliation (5x's magnification); B) Silicified amphibolite with large amounts of quartz precipitation; C) Banded amphibolite showing foliation; D) Metagabbro showing weak foliation with plagioclase being altered to biotite; E) A sample from the cross-cutting vein that shows clear grain boundaries and zoning of plagioclase which suggests a period of crystal/melt interaction; F) Pervasive alteration present in amphibole grains as biotite replaces the amphibole from within.*

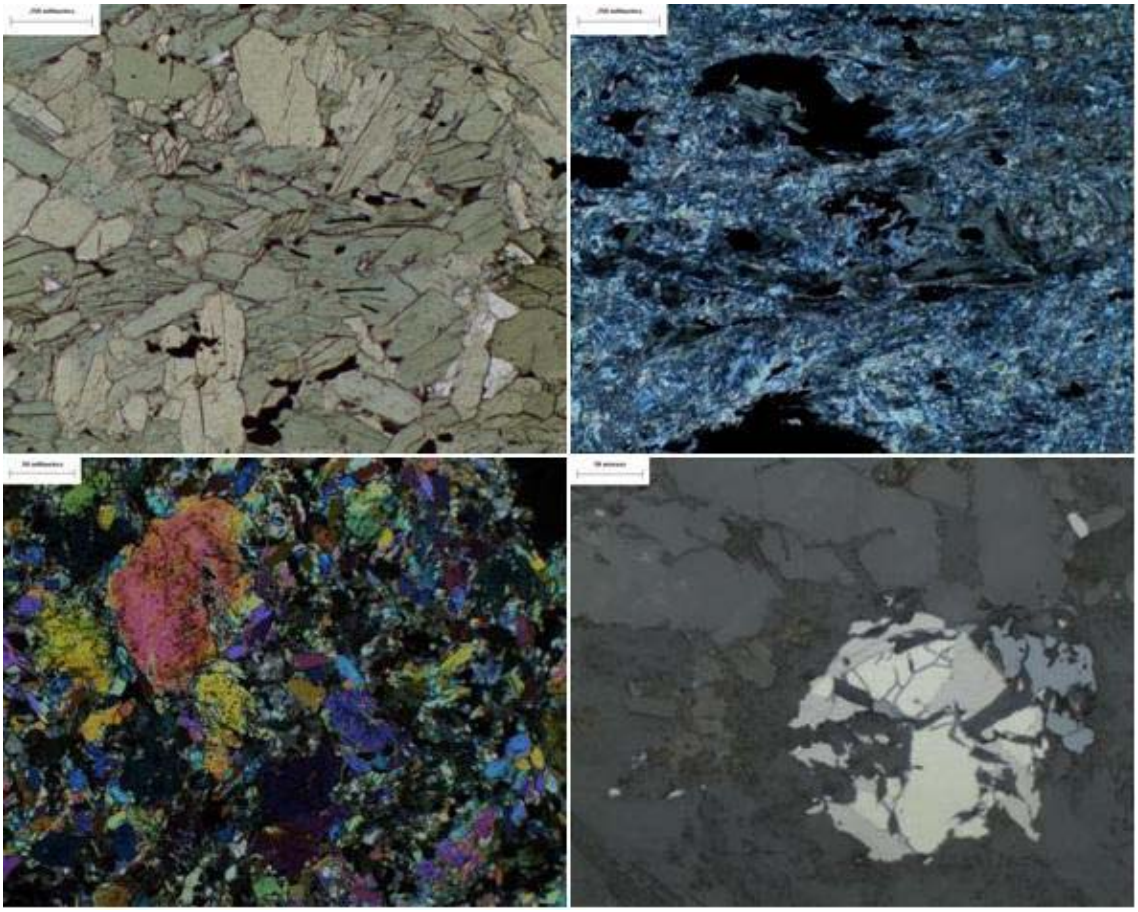

Figure 5. *A) Hornblendite showing no preferred orientation with overgrowths of magnetite; B) Highly altered metamorphic ultramafic containing serpentinite, epidote, and magnetite with the development of a slight lepidoblastic texture; C) Actinolite showing alteration as minerals precipitate pervasively within grains of amphibole; D) Altered ultramafic showing the replacement of pyrite by magnetite.*

Figure 6. *A) Aplitic dyke cross-cutting greenstones; B) Contact between the greenstones and aplitic dykes showing relic intrusive texture.*

Aplitic dykes – field relations

The aplitic dykes are boudinaged, sometimes occur as rods and cross-cut the greenstones. These dykes show the same foliation orientation as the greenstones. Texturally these units appear to be ‘sugary’ with some potassic alteration which is characterised as a red tint in the field. Commonly they are associated with barren quartz veins in the central portion of the peninsula (Fig. 6).

Aplitic dykes – petrography

The aplite assemblage consists of 40% quartz, 40% feldspar and 10% biotite. Epidote alteration of plagioclase is present and is characterised by their anomalous interference colour and deformation lamellae. Grains are generally subhedral to anhedral and are foliated. Foliation is partially defined by the presence of biotite laths, which have replaced plagioclase. Zoning is present in some larger plagioclase grains and is emphasised by the presence of alteration minerals within the zoned regions of the mineral grain (Fig. 7).

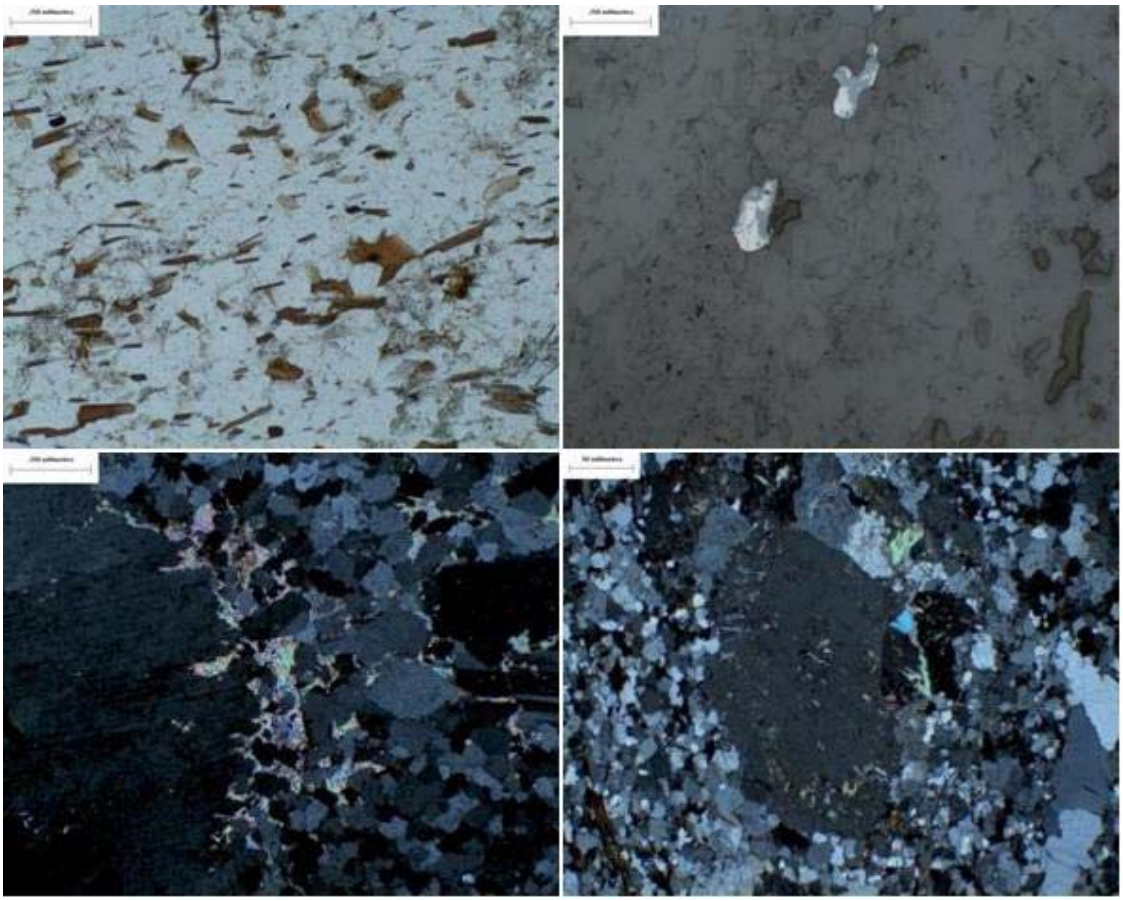

Figure 7. *A) Aplite showing lepidoblastic texture which is exaggerated by the biotite laths replacing the plagioclase; B) Replacement of pyrite by hematite; C) Pervasive alteration of plagioclase to epidote along grain boundaries with some minor infiltration of the grain itself; D) Presence of biotite and epidote alteration within the structure of the crystal emphasis the zoning that is present within the plagioclase crystal.*

Tonalite-Trondjhemite-Granodiorite gneiss – field relations

Despite being named TTG, the unit is entirely made of granodiorite with minor hornblende banding. The unit is cut by pegmatitic dykes and diabase dykes on the western portion of the peninsula and contains a large shear zone, containing large amounts of amphibolite, on

the eastern side of the peninsula. All contacts with other units are now shear zones, such that no relict igneous contacts survived (Fig. 8).

Tonalite-Trondjhemite-Granodiorite gneiss - petrography

The TTG gneisses have an assemblage of 50% feldspar, 35% quartz and 15% amphibole. The amphibole commonly manifests as bands or circular patches. Alteration, characterised by clinozoisite and muscovite are present as 'flag-like' grains that contain deformation lamellae indicating strain. Epidote and biotite alteration of feldspars is common and are also characterised by deformation lamellae structures mentioned above. Patches of chlorite and hematite appear to be later as they consist of small lath-like grains that overlap each other and replace or overprint the host assemblage of plagioclase**.** The amphiboles appear to define the foliation present in the TTG's. Many of the grains show sutured boundaries and are subhedral to anhedral. Grains of anti-perthite with microcline exsolution are present in a few samples (Fig. 9).

Figure 8. *A) TTG gneiss being cut by a diabase dyke with greenstones present at the top of the photo; B) View across the fjord that shows the intrusive nature of the TTG as the boundary appears fairly sharp; C) Typical shear zone commonly found between TTG's and greenstones; D) Shear zone with bands of greenstone and TTG that underwent ductile deformation.*

Quartz veins – field relations

Three types of quartz veins have been identified in the area. Rusty quartz is orange to brassy in colour and is typically associated with sulphides and occurs as boudinaged veins metre-size boudins. The 'dirty' nature of the quartz is due to a mixture of iron, sulphides and oxides with hematite, pyrite, pyrrhotite and minor chalcopyrite and arsenopyrite. In some regions of the peninsula pyrite was replaced by arsenopyrite, which was identified

from its silver colour and lath-like habit. Milky quartz is white and barren of sulphides. Typically, it occurs as rods or sheets that are intercalated with amphibolites on a metre scale. Some milky quartz veins exhibit varying degrees of folding. Blue quartz is more common than milky quartz and commonly 'rims' milky quartz veins but also occurs as massive veins and rods larger than 10 m or much smaller centimetre-wide veins cutting through the greenstones and aplitic dykes (Fig. 10).

Quartz veins – petrography

Quartz veins are almost 100% quartz with very minor amounts of other minerals that occur in mm-wide veins. Typically, the quartz grains are euhedral to subhedral with no fracturing present but generally show undulose extinction. In the rusty quartz samples it is common to see veins of hematite with pyrite. Under transmitted light these appear opaque but under intense light it is clear that some iron is present as hematite red staining appears along the edges of these veins. Grain boundaries are commonly sutured which indicates shear stress (Fig. 11).

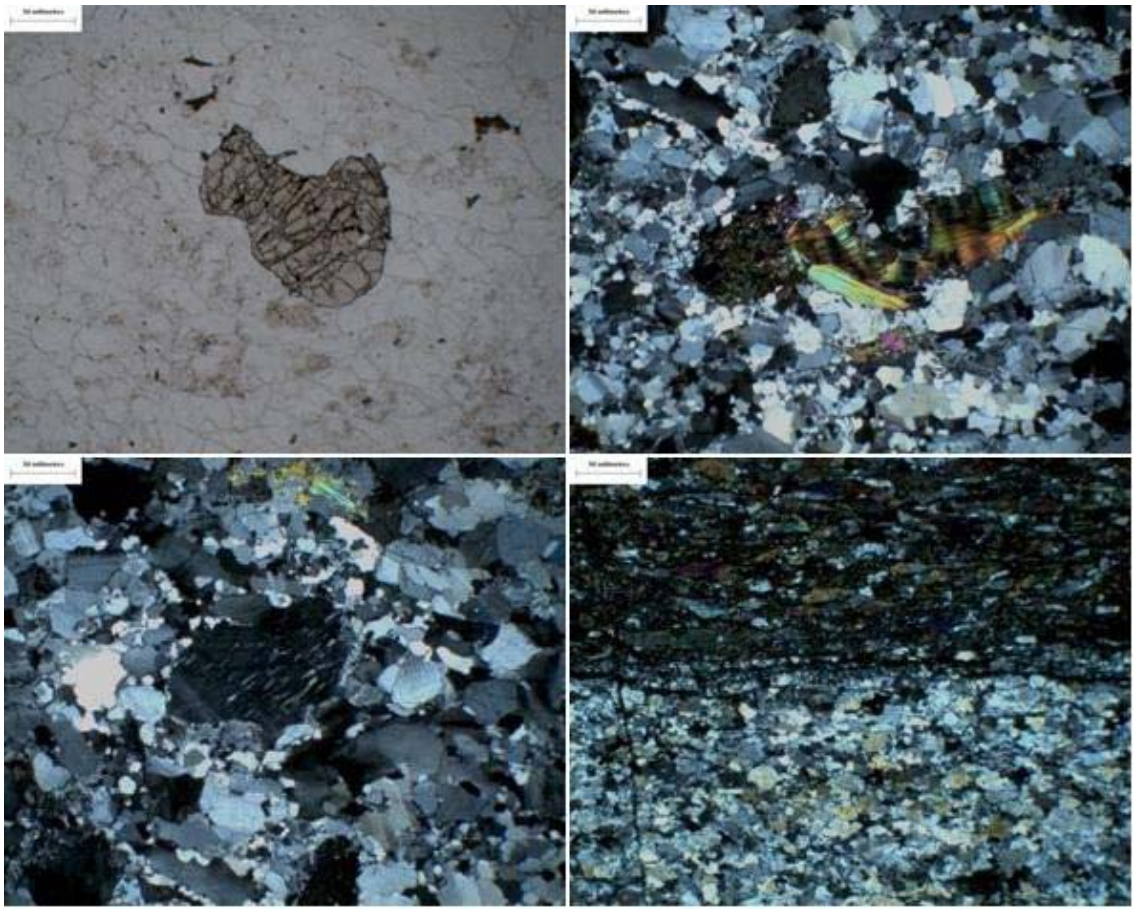

Figure 9. *A) Garnet within TTG gneiss; B) Deformation lamellae of muscovite and epidote with a pocket of chlorite; C) Perthite with albite lamellae and microcline along the mineral boundaries; D) Gneissic banding between a plagioclase quartz rich layer and a heavily deformed layer of amphibole.*

Pegmatitic dykes – field relations

Pegmatite occurs as large intrusive dykes throughout the south side of the peninsula and cross-cuts all of the previously discussed units. The pegmatite has cm-size grains of quartz, plagioclase, muscovite and tourmaline with some mm-size garnets. The pegmatite shows minor deformation (Fig. 12A).

Figure 10. *A) Mineralised quartz containing large amounts of sulphide minerals in contact with greenstones and aplite; B) Partially mineralised quartz with interbedded mylonite containing garnets; C) Large barren quartz rod; D) Deformed quartz which would be much older than the linear veins observed throughout the region.*

Pegmatitic dykes – petrography

The pegmatite consists of ~ 50% plagioclase, 35% quartz, 10% muscovite and 5% accessory minerals. Typically, the pegmatites are characterised by coarse grains of plagioclase, quartz and muscovite with minor amounts of fluorite. The grains are generally subhedral to anhedral with no foliation. Suturing between grain boundaries is common and is an indicator of deformation. Strain is also indicated by deformation lamellae within quartz and plagioclase. These lamellae are commonly within grains of epidote or clinozoisite which have replaced plagioclase. Some plagioclase and quartz grains are zoned and retain some of their original igneous texture. The large tourmaline grains exhibit a poikilitic texture with quartz, epidote and clay mineral inclusions. Zoning occurs in less deformed tourmaline grains (Fig. 13).

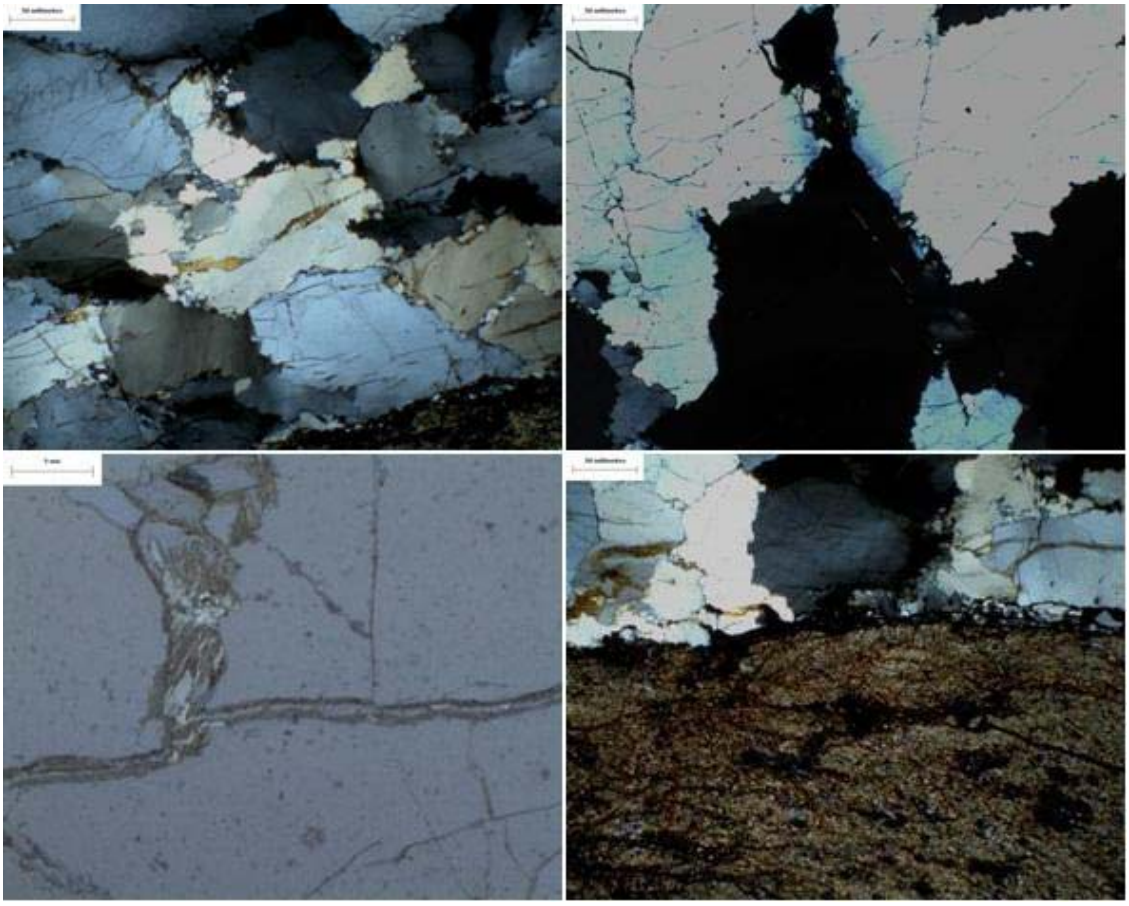

Figure 11. *A and B) Strained quartz showing sutured boundaries and slight deformation lamellae within some grains; C) Hematite within micro veins that cut through and between quartz grains; D) Sutured boundary between an amphibolite proto-mylonite and strained quartz.*

Diabase dikes – field relations

The diabase dykes cross-cut every unit and are commonly exposed as linear undeformed features that can be traced for kilometres in some cases. The largest dyke is roughly 5 – 8 metres wide. A small dyke in the western portion of the peninsula contains large phenocrysts of plagioclase and is the only mapped dyke in the area that contains such phenocrysts (Fig. 14).

Figure 12. *A) Pegmatitic dyke cross-cutting greenstones against regional foliation; B) Large tourmaline crystal within a pegmatitic dyke.*

Diabase dikes – petrogaphy

The diabase assemblage consists of 60% pyroxene and 40% plagioclase with minor alteration minerals present. The original ophitic texture is well preserved and characterised by the plagioclase laths enveloped by clinopyroxene. The laths typically exhibit albite twinning and are euhedral and the clinopyroxene is subhedral to anhedral. Large clinopyroxene grains are present and characterised by simple twinning under crossed-polars. Minor calcite is present between grains and some epidote has replaced plagioclase.

Sample 477562 is an early diabase dyke that shows alteration and relict igneous textures. This sample shows plagioclase being altered to clinozoisite. Many opaques are present in sample 477562 making it difficult to determine what other minerals might be present, but the relict ophitic texture is clearly identifiable (Fig. 15).

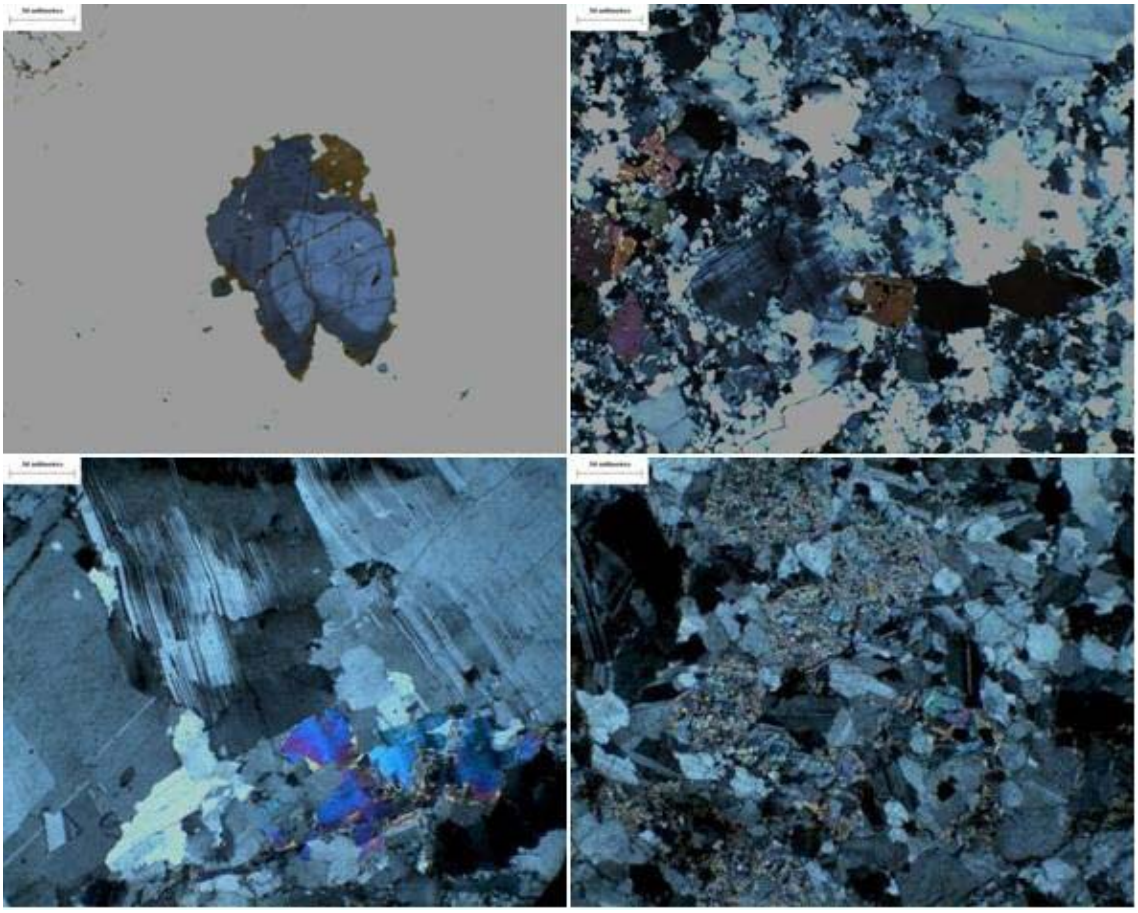

Figure 13. *A) Zoned tourmaline within a pegmatitic dyke; B) Typical regional pegmatite rich in plagioclase, quartz and microcline with minor alteration minerals including muscovite and epidote; C) Deformation lamellae in plagioclase which shows that this unit was exposed to a deformation event; D) Relic tourmalines? that have been completely replaced by epidote(?) and muscovite(?).*

Figure 14. - *A) Diabase dyke cutting through amphibolite with no deformation; B) Diabase dyke cutting through a shear zone containing TTG and amphibolites.*

Alteration on Akuliaq

Many of the rocks have been metamorphosed to greenschist facies. This is characterised by the presence of chlorite and epidote throughout the study area. Some areas show greenschist overprinting of the amphibolite facies which is characteristic in the areas hosting silicified and banded amphibolite subtypes. On the eastern portion of the peninsula there is a large area showing epidosite facies metamorphism. This is characterised by large veins of epidote within the greenstones. This area is the only part of the peninsula where epidosite is present. Garnets are present in close proximity to quartz veins within silicified units and are commonly anhedral. Carbonatisation is common around shear zones and is characterised by pitted textures within the greenstone units where the carbonates have been weathered out (Fig. 16).

Geochemistry

Geochemistry results from Activation Labs were conducted on twelve 30 g samples of quartz. The results show that gold concentrations in these few samples range from 1 to 3 ppb, with an average of 2 ppb (Table 4). ActLabs used the fire assay method coupled with instrumental neutron activation analysis method (FA/INAA) on both the experimental and control runs with a detection limit of 1 pbb.

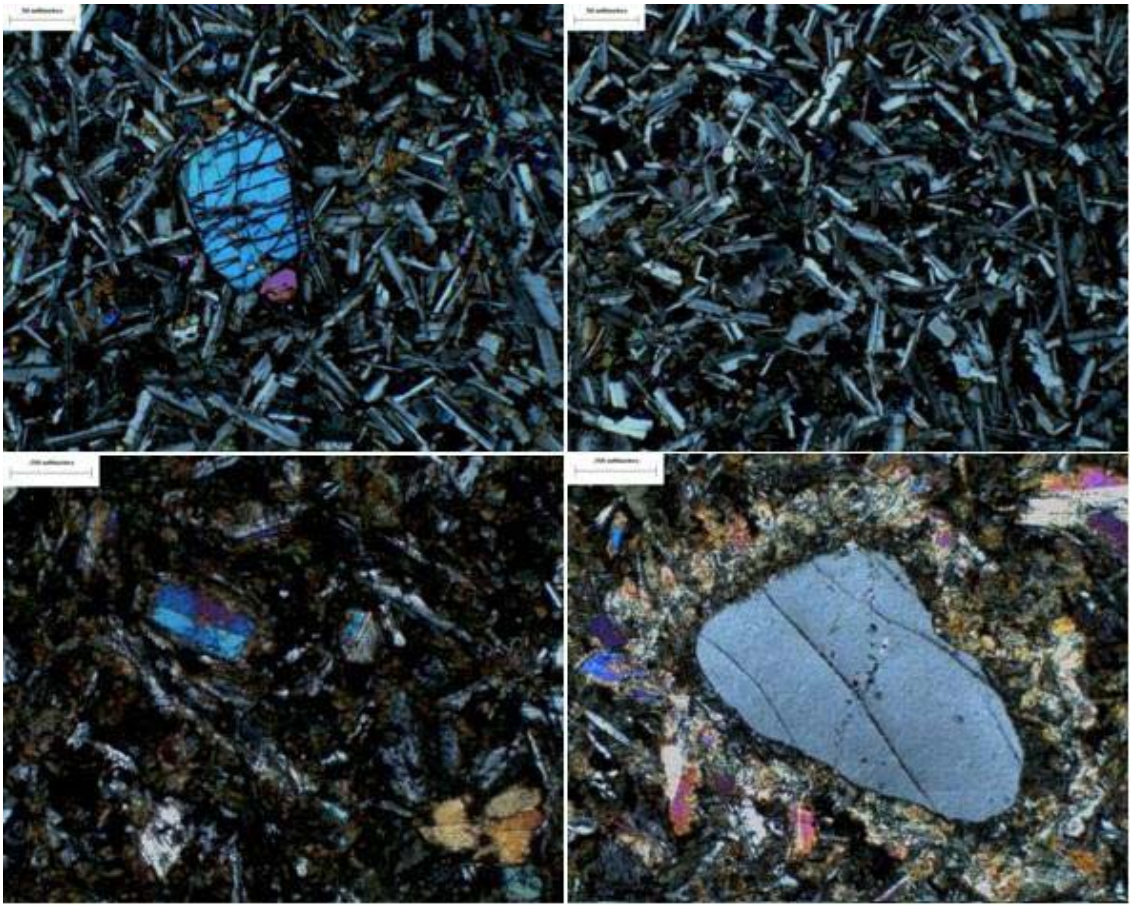

Figure 15. *A) Plagioclase laths enveloped in clinopyroxene showing ophitic texture and a single pyroxene grain; B) Plagioclase laths showing ophitic texture; C) Altered diabase with relic ophitic texture with augite and a large amount of iron bearing opaques; D) A single plagioclase crystal with an alteration halo consisting of mostly chlorite and epidote which has overgrown the augite around the mineral.*

Discussion

The chronology of Akuliaq begins with the greenstone unit. The greenstone unit contains three subdivisions of amphibolites, as well as metagabbros, and lenticular ultramafic units. This could correspond to a dismembered ophiolite sequence which consists of massive gabbroic units, lenticular ultramafics, and pillow basalts (Chiarenzelli & Moores, 2004; Dilek & Polat, 2008). Ophiolites are considered to be masses of oceanic crust and upper mantle that have been obducted onto the edge of a continent or incorporated into mountain belts (Chiarenzelli & Moores, 2004; Dilek & Furnes, 2011; Robertson, 2004). This sequence of metagabbros, amphibolites with relict pillow textures and lenticular ultramafics make up the oldest unit on Akuliaq peninsula and as such have been subjected to every deformation event that occured in the region (Fig. 3 and Appendices A and C).

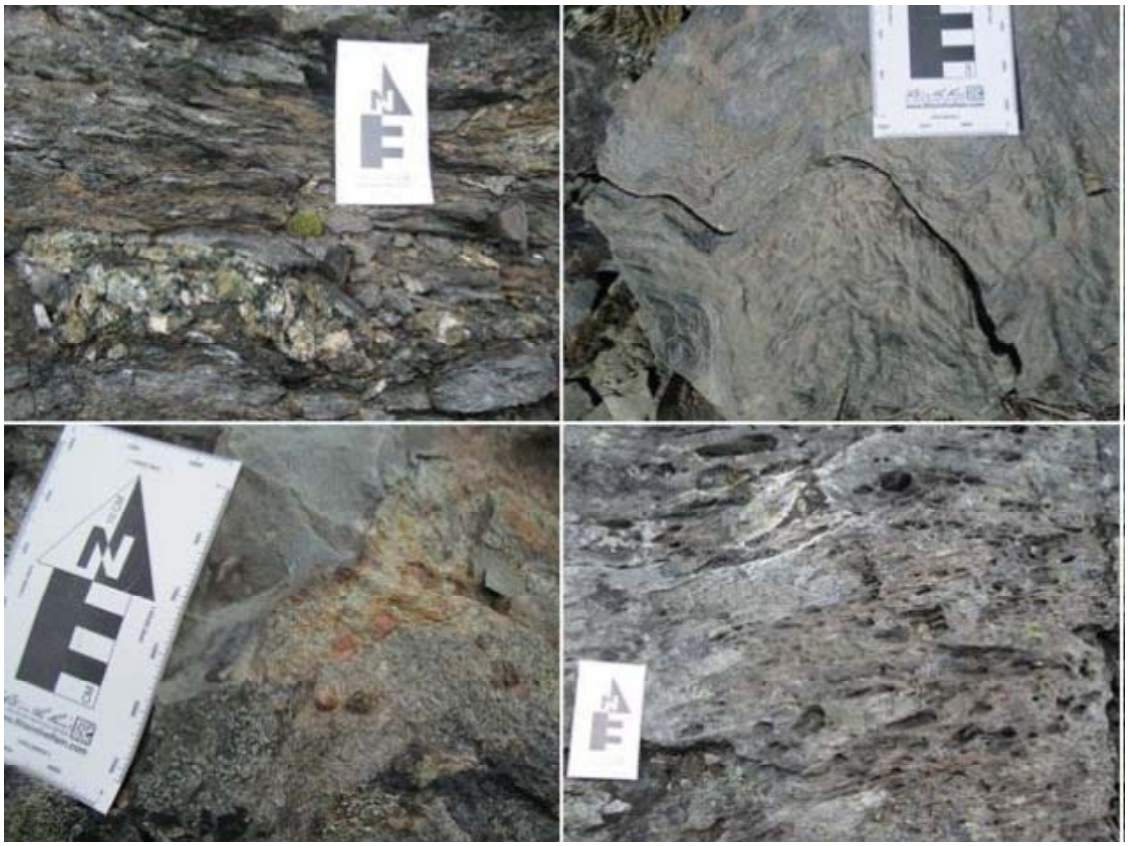

Figure 16. *A) Epidote alteration east of camp; B) Greenschist alteration that is commonly preserved in the western portion of the peninsula; C) Garnet that is commonly found near quartz veins suggesting a hydrothermal nature; D) Carbonatisation of the amphibolites which is characterised by a pitted texture on the country rocks.*

The aplite dykes cross-cut the amphibolites and metagabbro units but do not intersect any lenticular ultramafic units. However, because these units are part of the same lithotectonic package, it is reasonable to surmise that the aplite dykes are a younger feature (Fig. 6 and Appendices A and C). It is less likely that the aplitic dykes are older than the lenticular ultramafics because of the association that occurs between the ultramafics and the rest of the ophiolite-related units.

Intrusion of the TTG unit can be explained using models that describe Archean tectonics and mantle convection. It is theorised that the Archean experienced vigorous convection, which rapidly recycled and produced oceanic crust (Eriksson & Catuneanu, 2004; Frei et al, 2009; Moyen et al, 2009). Subduction of this warm crust resulted in shallow dipping subduction wedges with high geothermal gradients (Eriksson & Catuneanu, 2004; Moyen et al, 2009). Unlike modern subducting plates that only experience small degrees of partial melting, Archean plates more than likely experienced much higher degrees of partial melting (Moyen et al, 2009). The resulting melts generated Archean TTG suites that probably formed as small island arcs and that coalesced into Archean microcontinents (Dilek & Polat, 2008; Moyen et al, 2009). Work conducted on the Fiskenæsset complex by A. Polat and others during the 2009 field season suggests that the Fiskenæsset complex was generated by slab-dominated melting, reflecting high Archean geothermal gradients (Polat et al, 2011). Typically anorthosites were generated from highly aluminous slab-derived melts

between 3700 Ma and 2700 Ma which is roughly the same time the Paamiut block was emplaced (Friend & Nutman, 2001; Polat et al, 2011). Similar processes could potentially explain the aluminous minerals in the pegmatitic dykes and the TTGs.

In this model, the TTG in this area could have been generated through crustal underplating under an ophiolite that had been thrust up onto the edge of an Archean microcontinent (Robertson, 2004; Rushmer, 2009). Partial assimilation of the ophiolite country rocks by the TTG magma can explain the amphibole banding. Unfortunately no igneous contacts remain as all of the contacts between the TTG and the rest of the units were deformed by shear zones (Fig. 8 and Appendices A and C).

The quartz veins are typically sheets, rods, or boudinaged. Generally the boudinaged quartz veins are on the order of metres wide, and are commonly sulphide-bearing and referred to as ‘rusty’ or ‘dirty’ quartz. These veins are orange or brassy in colour and are a source of Au and sulphide minerals; commonly pyrite and pyrrhotite. The sheeted veins and quartz rods contain either blue or milky quartz and are generally barren of sulphides. Due to the distribution of quartz veins throughout the peninsula it can be suggested that the same fluids that caused silicification and carbonatisation of the amphibolites on the north side of the peninsula were probably derived from seafloor hydrothermal cells. These ‘dirty’ veins do not occur as sheeted systems or quartz rods; only the barren veins do. The barren veins are quite possibly older than the mineralised quartz veins because some veins varying degrees of folding which is not present in the mineralised vein systems. These mineralised quartz veins have a foliation orientation that is consistent with the greenstones, suggesting that their orientation was controlled by the regional tectonic fabric in the host rocks and/or they formed in the same stress regime that formed the regional foliation. Through the following observations it is clear that there are numerous quartz forming events and at least three were identified while in the field. The first event is characterised by folded milky or blue quartz veins and small chevron-like folded milky quartz veins within large amphibolite bodies, primarily on the western edge of the peninsula near the large diabase dyke. The large quartz rods were also emplaced during this event. This can be seen in the distortion of the foliation proximal to the quartz rods which would have occurred during the development of the rod. The second event was the emplacement of the large vein sets that contain both barren and mineralised veins, and that are commonly parallel to the major foliation in the area. The last event produced small, cm-scale quartz veins that cross cut the greenstones and aplitic dykes and occur throughout the peninsula.

The pegmatite dykes are a much younger feature than the previously described units and show minimal deformation. These dykes consist mostly of feldspar and quartz, with lesser tourmalines. Typically pegmatites are associated with volatile-rich magmas, which suggests that a later magmatic body was present in the area during the formation of this unit. The volatile-rich nature of the parent magma is manifested as tourmaline, which indicates elevated boron concentrations. In addition the occurrence of garnet and muscovite suggest an aluminous melt. In some places the pegmatite cross-cuts sheeted barren quartz veins. Interestingly, there were no pegmatites in the same region as the ‘dirty’ quartz veins (Fig. 12 and Appendices A and C).

The youngest unit is the diabase dyke that is undeformed and cross-cuts all the major units in the area. There is one sample that could be an altered diabase but there was no field

evidence for diabase alteration. Aside from acting as the youngest feature on the peninsula these diabase dykes have no economic importance (Fig. 14 and Appedix C). Studies conducted by Friend & Nutman (2001) on the North Atlantic craton suggests that metamorphism occurred before the Paamiut block accreted onto the landmass that is now modern Greenland. This accretion occurred at roughly 2820 Ma meaning that the Paamiut block, which was originally an Archean microcontinent, was metamorphosed to lower amphibolite facies at roughly 3000 Ma (Friend & Nutman, 2001). In the field it was documented that the northern and western portions contained greenschist facies assemblages. It was characterised by intense chlorite alteration along with radial patches actinolite in areas of more intense chlorite alteration. A sudden decrease in the pressure and temperature regime would affect the entire peninsula, unless it was subsequently tilted from a vertical orientation to its current orientation. To support the subsequent tilting of the peninsula there is a region of epidosite on the eastern portion of the peninsula. This area does not appear to have reached amphibolite grade metamorphism and shows no retrogression to greenschist facies which supports that it is actually epidote facies rather than an alteration. The small area even has differing structural characteristics with foliations that are different to the rest of the peninsula. Commonly, the aplitic dykes show signs of epidote alteration in this area of the peninsula and in a few cases the smaller veins have been almost totally replaced by epidote. The remainder of the peninsula is lower-amphibolite upper-greenschist with little visible chlorite alteration and largely massive amphibolites. Silicification is commonly associated with the central portion of the peninsula in areas bounded by shear zones. Carbonatisation occurs in many of the amphibolites proximal to the major NE-SW trending shear zones. The thin sections generally contain calcite filling void spaces and field evidence shows pitted surfaces from preferential carbonate dissolution from the rocks. Therefore it can be concluded that the northern and western portions of the peninsula contain greenschist assemblages, carbonatisation is generally localised near the shear zones, silicification is dispersed throughout the centre of the peninsula, epidosite occurs towards the east of the peninsula and the remainder of the peninsula is typically greenstone with less intense alteration.

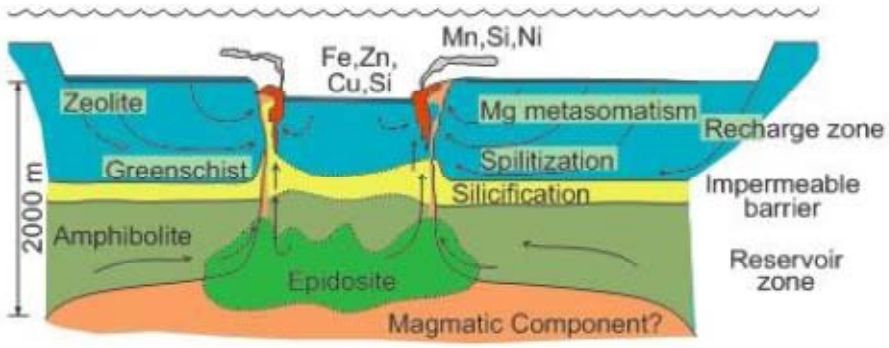

Figure 17. *Seafloor hydrothermal cells commonly associated with VMS; note the presence of the described greenschist, silicified, amphibolite and epidosite regions.*

It is possible that the metamorphism is associated with sub-seafloor hydrothermal alteration of the early Archean oceanic slab. This oceanic crust would have been subjected to seafloor hydrothermal cells similar to those that develop below volcanic-hosted massive sulphide deposits (Galley et al, 2007). Hydrothermal cells would act to hydrate the slab and assist in metamorphism up to amphibolite and epidote-amphibolite facies (Fig. 17). This

period of hydration is supported by the presence of amphibole, biotite, chlorite, muscovite and epidote which remained in the country rock. This is plausible if the replacement minerals present in thin section are not post-obduction. Figure 4d shows a thin section of metagabbro containing large, euhedral grains of biotite that appear to be in equilibrium with the surrounding minerals, unlike figure 7a which shows biotite grains replacing plagioclase and with a partially defined foliation that is not shared by the rest of the assemblage. As metamorphism from greenschist to lower amphibolite facies progressed, the rocks would have dehydrated. This metamorphic fluid would be released into the surrounding host rock and flowed towards the surface via fractures and dialatant zones in the shear zones and their host rocks. This fluid is suggested to have hosted gold and other solutes which would have been precipitated as quartz veins.

These quartz veins are part of a greenstone-hosted quartz-carbonate vein system, analogous to those that are commonly associated with large shear zones in greenstone belts. As the metamorphic fluid travels up the shear zones it precipitates quartz and Au. Commonly the country rocks undergo silicification and carbonatisation due to fluid-rock interaction. Carbonatisation is characterised by an influx of carbonates into the rock through fluid movement. In the field this is characterised as a pitted texture which suggests that the carbonates were dissolved out of the greenstones during weathering. Silicification is easiest seen under thin-section and is characterised by an increase in quartz precipitation within void space and between grains. In the field the rocks are commonly harder than the altered units with less schistosity than banded units (Fig. 18).

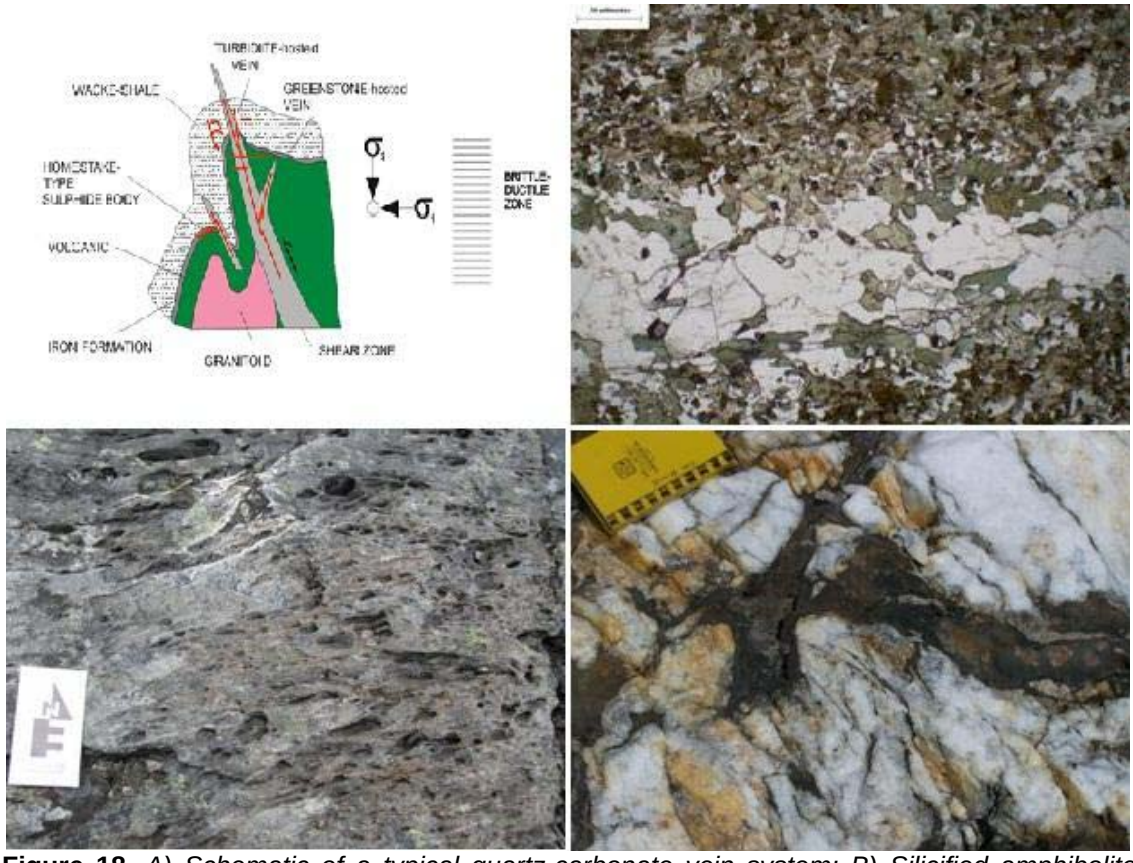

Figure 18. *A) Schematic of a typical quartz-carbonate vein system; B) Silicified amphibolite showing silicification which is characteristic of quartz-carbonate gold systems; C) Carbonatization as seen in the field, characterised by the pitted texture; D) Rusty quartz vein in a shear zone hosting a mylonite.*

Conclusions

The mapping of Akuliaq peninsula is a vital piece to the Akuliaq prospect and in the interpretation of the petrographic data. This data will be used by NunaMinerals in the planning and probable execution of drill programs. It will also be used to update the GEUS map records for the area which was last updated in the late 1960's during Jon C. Escher's PhD thesis. The petrography has provided important new insights into alterations within the region. The primary objective of the project was to develop a new map for GEUS so they could update their database using up-to-date mapping techniques. The Ganfeld system that was deployed during the entire season is still in the research and development phase. As part of the project the field teams were required to provide feedback to be used for future updates to the system. This feedback is important to both GEUS and the Geological Survey of Canada as both surveys are working together to develop this system further.

Active field mapping was important in the development of new rock divisions within the peninsula which were not included in the previous GEUS supplied map from J.C. Escher's PhD thesis. The secondary objective to the mapping portion of the project was to plot the discontinuous mineralised and barren quartz veins throughout the peninsula. These veins clearly follow strike of 270° N and are numerous which suggests that at one time they may have been continuous veins of quartz. The cross-sections that were created using this map will be used to help determine target areas for exploration drilling programs to continue to map the mineralised zones. This is an important step forward towards the completion of the grassroots program on the Akuliaq prospect.

Petrography was used to determine metamorphic events and mineral abundances within the samples. Zoning and sharp contacts are synonymous with direct crystallisation from a source melt, while ophitic textures are clearly igneous in nature. Lepidoblastic textures are a clear indication of deformation events and commonly deformation lamellae can be observed in the sample. Secondary minerals from the epidote group suggest that metamorphism reached epidote facies or that they are the by-product of the hydration of plagioclase which may have been caused by hydrothermal fluids. Continued examination of these samples may be used to fully understand and map the alteration history of the lithology.
This exercise demonstrates the need for geological mapping followed up by petrographic and geochemical studies when prospecting. This research significantly decreases the amount of risk involved during exploration and can be used to generate data sets that can be referenced during later stages of the operation. Continued exploration and geochemical analysis will assess the feasibility of pursuing further development of the Akuliaq prospect.

Appendix – C: Stratigraphy

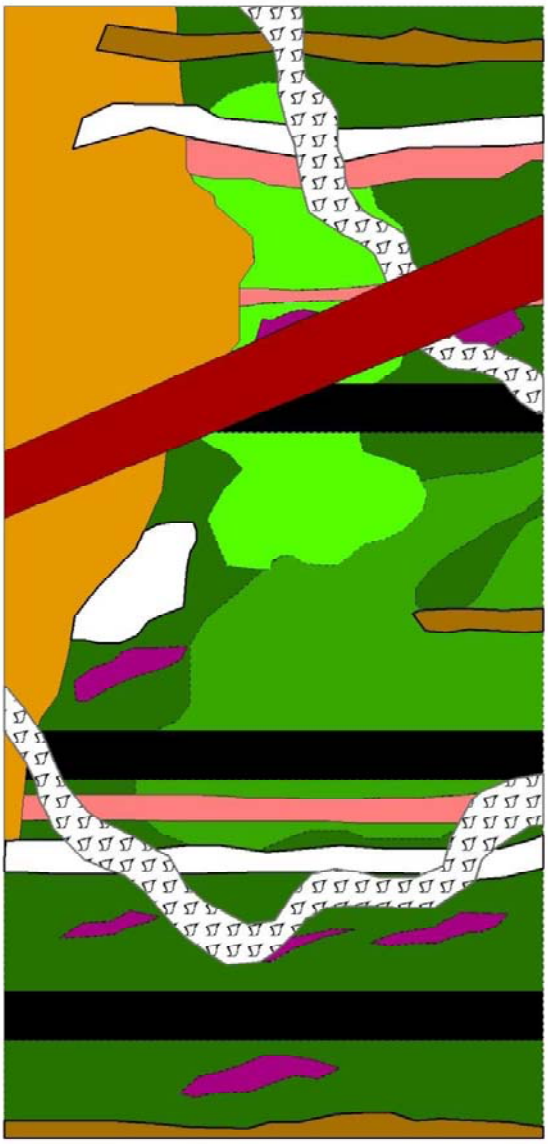

Column is roughly 800m thick

Akuliaq Stratigraphy

Lithology

- Diabase Dykes
- Pegmatite
- Quartz
- Rusty Quartz
- TTG Gneiss
- Aplitic Dykes
- Altered Amphibolite
- Silicified Amphibolite
- Banded Amphibolite
- Metagabbro
- Ultramafic Pods

Stratigraphy by: Michael Glendenning and Evan Hastie

Appendix – D: Cross section

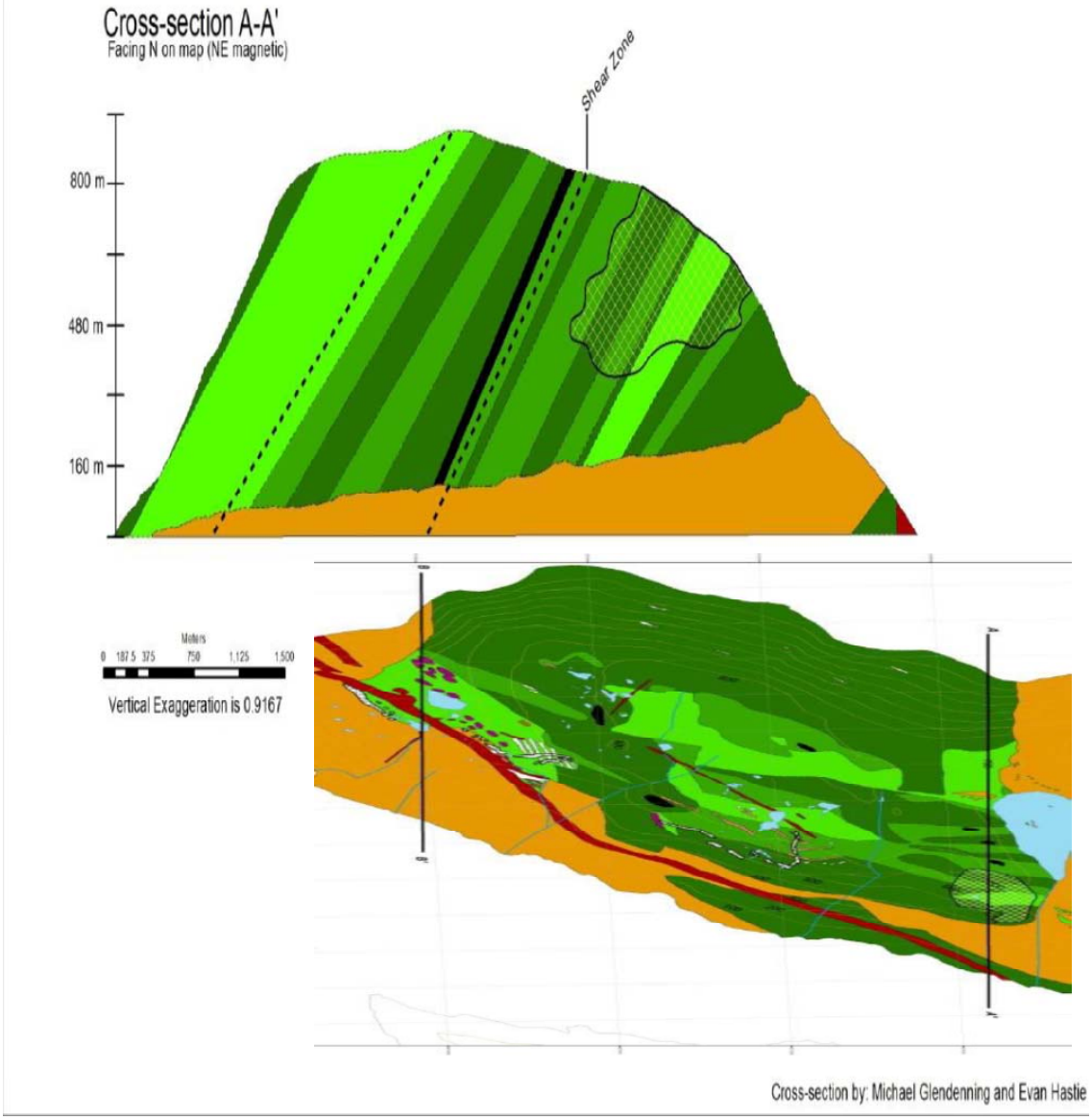

Appendix – E: Cross section

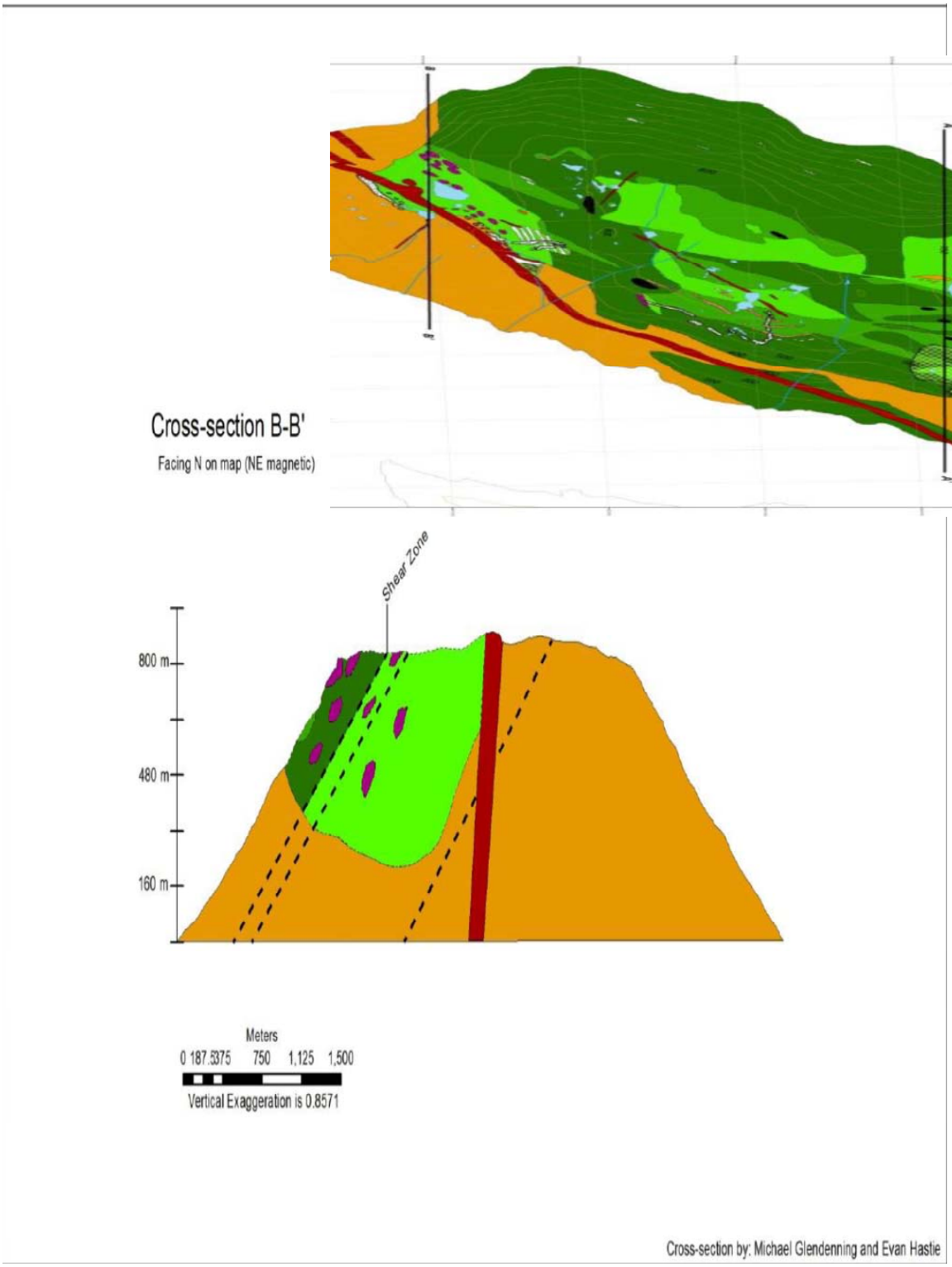

Table 1. *Sample localities*

Sample #	Rock name	Latitude	Longitude
477501	Aplitic Lens	62°05'35.7" N	49°03'07.0" W
477502	Amphibolite	62°05'35.7" N	49°03'07.0" W
477503	Amphibolite	62°05'35.7" N	49°03'07.0" W
477504	Rusty Quartz	62°05'35.7" N	49°03'07.0" W
477505	Quartz	62°05'37.0" N	49°03'11.0" W
477506	Quartz	62°05'37.0" N	49°03'11.0" W
477507	Amphibolite	62°05'36.0" N	49°03'21.0" W
477508	Mylonite	62°05'43.5" N	49°03'13.6" W
477509	Altered Amphibolite	62°05'34.5" N	49°03'21.3" W
477510	Rusty Quartz	62°05'23.8" N	49°03'55.9" W
477511	Rusty Quartz	62°05'23.8" N	49°03'55.9" W
477512	Altered Amphibolite	62°05'34.3" N	49°03'06.1" W
477513	Diabase Dyke	62°05'28.0" N	49°02'58.6" W
477514	Rusty Quartz	62°05'24.9" N	49°02'56.2" W
477515	Amphibolite	62°05'24.0" N	49°02'48.0" W
477516	Silicified Amphibolite	62°05'22.0" N	49°02'44.3" W
477517	Meta Ultramafic	62°05'20.0" N	49°02'42.8" W
477518	Altered Amphibolite	62°05'11.4" N	49°02'46.3" W
477519	Silicified Amphibolite	62°05'06.2" N	49°02'51.6" W
477520	Amphibolite	62°05'35.0" N	49°02'55.8" W
477521	Amphibolite	62°05'56.0" N	49°02'43.9" W
477522	Silicified Amphibolite	62°06'05.1" N	49°02'51.8" W
477523	White Pegmatite	62°06'11.2" N	49°03'04.5" W
477524	Amphibolite	62°06'11.0" N	49°01'33.6" W
477525	White Pegmatite	62°05'34.7" N	49°02'35.7" W
477526	Amphibolite	62°05'34.7" N	49°02'35.7" W
477527	Silicified Amphibolite	62°04'33.8" N	49°04'39.4" W
477528	Amphibolite	62°04'40.4" N	49°03'58.3" W
477529	Amphibolite	62°04'33.0" N	49°04'38.5" W
477530	Amphibolite	62°04'33.0" N	49°04'38.5" W
477531	Banded Amphibolite	62°05'37.0" N	49°02'26.0" W
477532	Diabase Dyke	62°05'37.1" N	49°02'25.6" W
477533	Silicified Amphibolite	62°05'32.8" N	49°02'18.3" W
477534	White Pegmatite	62°05'32.8" N	49°02'18.3" W
477535	Blue Quartz	62°04'39.8' N	49°04'37.6" W
477536	Meta Ultramafic	62°04'30.7" N	49°04'17.3" W
477537	Diabase Dyke	62°04'30.7" N	49°04'17.3" W
477538	Amphibolite	62°04'30.7" N	49°04'17.3" W
477539	White Pegmatite	62°04'27.0" N	49°04'13.0" W
477540	TTG Gneiss	62°04'27.0" N	49°04'13.0" W
477541	White Pegmatite	62°04'20.5" N	49°04'23.5" W

477542	TTG Gneiss	62°06'11.7" N	49°03'30.3" W
477543	TTG Gneiss	62°06'11.7" N	49°03'30.3" W
477544	Amphibolite	62°06'22.5" N	49°02'50.9" W
477545	Meta Gabbro	62°06'30.2" N	49°01'56.4" W
477546	Blue Quartz	62°05'57.7" N	49°02'27.4" W
477547	Aplitic Lens	62°05'56.4" N	49°03'19.6" W
477548	Aplitic Lens	62°05'57.7" N	49°03'35.3" W
477549	Altered Amphibolite	62°05'49.5" N	49°03'25.4" W
477550	Altered Amphibolite	62°05'46.2" N	49°03'27.9" W
477551	Altered Amphibolite	62°05'46.2" N	49°03'27.9" W
477552	Quartz	62°05'21.7" N	49°03'56.7" W
477553	Mylonite	62°05'15.5" N	49°04'56.7" W
477554	Quartz	62°05'15.5" N	49°04'56.7" W
477555	Amphibolite	62°05'15.5" N	49°04'56.7" W
477556	Quartz	62°05'15.5" N	49°04'56.7" W
477557	Diabase Dyke	62°05'15.5" N	49°04'56.7" W
477558	Silicified Amphibo-lite	62°05'03.9" N	49°04'20.3" W
477559	Diabase Dyke	62°05'03.9" N	49°04'20.3" W
477560	Banded Amphibolite	62°05'03.9" N	49°04'20.3" W
477561	Diabase Dyke	62°05'03.9" N	49°04'20.3" W
477562	Ultra Mafic	62°04'51.1" N	49°04'53.7" W
477563	Altered Amphibolite	62°05'00.7" N	49°04'58.1" W
477564	Altered Amphibolite	62°05'00.7" N	49°04'58.1" W
477565	Quartz	62°05'00.7" N	49°04'58.1" W
477566	Altered Amphibolite	62°05'00.7" N	49°04'58.1" W
477567	Diabase Dyke	62°05'03.9" N	49°04'20.3" W
477568	Altered Amphibolite	62°05'46.0" N	49°03'28.0" W
477569	Altered Amphibolite	62°05'46.0" N	49°03'28.0" W
477570	Aplitic Lens	62°05'07.5" N	49°03'50.9" W
477571	Altered Amphibolite	62°04'50.8" N	49°03'42.0" W
477572	White Pegmatite	62°04'50.8" N	49°03'42.0" W
477573	White Pegmatite	62°04'50.8" N	49°03'42.0" W
477574	Altered Amphibolite	62°04'50.0" N	49°03'37.7" W
477575	Altered Amphibolite	62°04'50.0" N	49°03'37.7" W
477576	White Pegmatite	62°04'53.0" N	49°03'44.2" W
477577	Diabase Dyke	62°05'18.2" N	49°03'22.1" W
477578	Aplitic Lens	62°05'18.2" N	49°03'22.1" W
477579	Amphibolite	62°05'18.2" N	49°03'22.1" W
477580	White Pegmatite	62°06'11.1" N	49°03'04.4" W
477581	Aplitic Lens	62°06'09.0" N	49°03'01.3" W
477582	Altered Amphibolite	62°06'05.1" N	49°02'28.1" W
477583	Altered Amphibolite	62°05'59.1" N	49°02'27.3" W
477584	Blue Quartz	62°05'59.1" N	49°02'27.3" W
477585	Aplitic Lens	62°05'48.4" N	49°03'04.7" W
477586	Altered Amphibolite	62°06'05.1" N	49°02'28.1" W
477587	Meta Gabbro	62°06'03.2" N	49°02'08.1" W
477588	Diabase Dyke	62°06'08.1" N	49°01'24.0" W

477589	Diabase Dyke	62°06'08.1" N	49°01'24.0" W
477590	Milky Quartz	62°05'30.8" N	49°04'07.7" W
477591	Milky Quartz	62°05'30.8" N	49°04'07.7" W
477592	Altered Amphibolite	62°05'30.8" N	49°04'07.7" W
477593	Altered Amphibolite	62°05'26.1" N	49°04'23.1" W
477594	Amphibolite	62°05'26.1" N	49°04'23.1" W
477595	Quartz	62°05'21.8" N	49°04'23.9" W
477596	Altered Amphibolite	62°05'17.6" N	49°04'23.0" W
477597	Rusty Quartz	62°05'18.9" N	49°04'13.4" W
477598	Meta Gabbro	62°05'23.1" N	49°04'13.4" W
477599	Altered Amphibolite	62°05'23.1" N	49°04'13.4" W
495501	Diabase Dyke	62° 05'21.6" N	49°03'20.7" W
495502	Altered Amphibolite	62° 05'17.6" N	49°04'23.0" W
495503	Amphibolite	62° 05'18.9" N	49°04'13.4" W
495504	Altered Amphibolite	62° 04'37.2" N	49°04'22.3" W
495505	Diabase Dyke	62° 04'35.9" N	49°04'13.6" W
495506	TTG Gneiss	62° 04'31.4" N	49°04'04.7" W
495507	Pegmatite	62° 04'23.7" N	49°03'59.4" W
495508	Diabase Dyke	62° 04'29.1" N	49°03'59.0" W
495509	Meta Gabbro	62° 04'56.7" N	49°04'03.4" W
495510	Milky Quartz	62° 05'36.5" N	49°02'56.2" W
495511	Altered Amphibolite	62° 05'35.4" N	49°02'43.3" W
495512	Diabase Dyke	62° 05'36.8" N	49°02'31.6" W
495513	Aplitic Lens	62° 05'34.7" N	49°02'35.6" W
495514	Quartz	62° 05'34.7" N	49°02'35.6" W
495515	TTG Gneiss	62° 09'05.11" N	48°42'13.4" W
495516	Altered Amphibolite	62° 09'07.0" N	48°42'20.5" W
495517	Banded Amphibolite	62° 09'07.0" N	48°42'21.5" W
495518	White Pegmatite	62° 09'06.4" N	48°42'22.9" W
495519	Aplitic Lens	62° 09'05.9" N	48°42'24.2" W
495520	TTG Gneiss	62° 06'21.5" N	49°02'13.0" W
495521	TTG Gneiss	62° 06'32.8" N	49°01'39.1" W
495522	TTG Gneiss	62° 06'27.6" N	49°01'12.0" W
495523	Amphibolite	62° 06'14.9" N	49°03'37.2" W
495524	Rusty Quartz	62° 05'42.6" N	49°02'21.9" W
495525	TTG Gneiss	62° 06'14.3" N	49°03'24.3" W
495526	Pegmatite	62° 06'23.8" N	49°02'56.9" W
495527	TTG Gneiss	62° 06'29.5" N	49°02'49.0" W
495528	Rusty Quartz	62° 05'19.1" N	49°04'13.2" W
495529	Altered Amphibolite	62° 05'19.1" N	49°04'13.2" W
495530	Amphibolite	62° 05'19.1" N	49°04'13.2" W
495531	Meta Gabbro	62° 05'19.1" N	49°04'13.2" W
495532	Banded Amphibolite	62° 05'19.1" N	49°04'07.9" W
495533	Amphibolite	62° 05'19.1" N	49°04'07.9" W
495534	Amphibolite	62° 05'19.1" N	49°04'07.9" W
495535	Amphibolite	62° 05'15.9' N	49°04'03.0" W
495536	Rusty Quartz	62° 05'15.9' N	49°04'03.0" W
495537	Amphibolite	62° 05'15.9' N	49°04'03.0" W

495538	Amphibolite	62° 05'15.9' N	49°04'03.0'' W
495539	Rust Quartz	62° 05'15.9' N	49°04'03.0'' W
495540	Aplitic Lens	62° 05'15.9' N	49°04'03.0'' W
495541	Quartz	62° 05'15.9' N	49°04'03.0'' W
495542	Blue Quartz	62° 05'11.4'' N	49°04'19.5'' W
495543	Rusty Quartz	62° 05'15.9' N	49°04'03.0'' W
495544	Amphibolite	62° 05'31.5'' N	49°02'30.5'' W
495545	Altered Amphibolite	62° 05'32.2'' N	49°02'26.4'' W
495546	Rusty Quartz	62° 05'32.2'' N	49°02'20.2'' W
495547	Amphibolite	62° 05'33.8'' N	49°02'14.7'' W
495548	Amphibolite	62° 05'32.9'' N	49°02'12.4'' W
495549	Rusty Quartz	62° 05'50.2'' N	49°02'45.2'' W
495550	Banded Amphibolite	62° 05'35.2'' N	49°03'10.4'' W
495551	Amphibolite	62° 05'35.2'' N	49°03'10.4'' W
495552	Meta Gabbro	62° 05'28.3'' N	49°03'28.4'' W
495553	Banded Amphibolite	62° 05'11.0'' N	49°03'38.4'' W
495554	Banded Amphibolite	62° 05'06.3'' N	49°03'30.0'' W
495555	Rusty Quartz	62° 05'12.5'' N	49°04'22.8'' W
495556	Rusty Quartz	62° 05'12.5'' N	49°04'22.8'' W
495557	Rusty Quartz	62° 05'12.5'' N	49°04'22.8'' W
495558	Rusty Quartz	62° 05'14.7'' N	49°04'19.0'' W
495559	Rusty Quartz	62° 05'14.7'' N	49°04'19.0'' W
495560	Rusty Quartz	62° 05'17.0'' N	49°04'07.5'' W
495561	Rusty Quartz	62° 05'35.6'' N	49°03'07.4'' W
495562	Meta Gabbro	62° 05'27.5'' N	49°03'28.0'' W
495563	Rusty Quartz	62° 05'27.5'' N	49°03'28.0'' W
495564	Amphibolite	62° 05'11.3'' N	49°03'37.1'' W
495565	Amphibolite	62° 05'08.6'' N	49°03'30.6'' W
495566	Altered Amphibolite	62° 05'11.2'' N	49°04'27.8'' W
495567	Rusty Quartz	62° 05'11.2'' N	49°04'27.8'' W
495568	Rusty Quartz	62° 05'14.2'' N	49°04'20.5'' W
495569	Rusty Quartz	62° 05'14.2'' N	49°04'20.5'' W
495570	Rusty Quartz	62° 05'14.2'' N	49°04'21.6'' W
495571	Rusty Quartz	62° 05'21.0'' N	49°04'04.0'' W
495572	Amphibolite	62° 05'21.0'' N	49°04'04.0'' W
495573	Altered Ultramafic	62° 04'38.7'' N	49°04'43.8'' W
495574	Hornblendite	62° 04'38.7'' N	49°04'43.8'' W
495575	Amphibolite	62° 04'34.4'' N	49°04'50.7'' W
495576	Altered Ultramafic	62° 04'38.7'' N	49°04'44.0'' W
495577	Serpentinite	62° 04'38.7'' N	49°04'44.0'' W
495578	Actinolite	62° 04'38.7'' N	49°04'44.0'' W
495579	Actinolite	62° 04'38.7'' N	49°04'44.0'' W
495580	Hornblendite	62° 04'34.3'' N	49°04'52.2'' W
495581	Mylonite	62° 04'31.8'' N	49°04'11.8'' W
495582	Pegmatite	62° 04'20.9'' N	49°04'25.4'' W
495583	Rusty Quartz	62° 05'35.8'' N	49°02'46.1'' W
495584	Rusty Quartz	62° 05'35.8'' N	49°02'46.1'' W
495585	Pillow Basalt	62°05'29.7'' N	49°02'46.3'' W

495586	Amphibolite	62° 05'06.9'' N	49°02'41.2'' W
495587	Rusty Quartz	62° 05'36.9'' N	49°02'35.6'' W
495588	Rusty Quartz	62° 05'36.9'' N	49°02'35.6'' W
495589	Rusty Quartz	62° 05'36.9'' N	49°02'35.6'' W
495590	Rusty Quartz	62° 05'39.2'' N	49°02'27.9'' W
495591	Rusty Quartz	62° 05'40.4'' N	49°02'27.4'' W
495592	Rusty Quartz	62° 05'43.0'' N	49°02'26.6'' W
495593	Rusty Quartz	62° 05'45.5'' N	49°02'26.0'' W
495594	Rusty Quartz	62° 05'59.8'' N	49°02'04.4'' W
495595	Rusty Quartz	62° 05'59.8'' N	49°02'04.4'' W
495596	Amphibolite	62° 06'11.5'' N	49°01'36.7'' W
495597	Pillow Basalt	62° 05'29.6'' N	49°02'45.4'' W
495598	Pillow Basalt	62° 05'29.6'' N	49°02'45.4'' W
495599	Pillow Basalt	62° 05'28.3'' N	49°02'48.3'' W
476701	Pillow Basalt	62°05'28.3'' N	49°02'48.3'' W
476702	Pillow Basalt	62°05'28.3'' N	49°02'48.3'' W
476703	Rusty Quartz	62°05'22.6'' N	49°03'18.3'' W
476704	Rusty Quartz	62°05'22.0'' N	49°03'18.4'' W
476705	Rusty Quartz	62°05'20.9'' N	49°03'21.5'' W
476706	Rusty Quartz	62°05'19.1'' N	49°03'23.5'' W
476707	Unknown Purple Mineral	62°05'06.3'' N	49°03'31.2'' W
476708	Rusty Quartz	62°04'50.7'' N	49°04'04.3'' W
476709	Pegmatite	62°05'33.9'' N	49°02'21.1'' W
476710	Aplite/Pegmatite	62°05'33.9'' N	49°02'21.1'' W

Table 2. *Sample descriptions*

Sample #	Rock name	Description
477501	Aplitic Lens	w/ Blue Quartz and Arseno-pyrite
477502	Amphibolite	w/ Blue Quartz and Altera-tion
477503	Amphibolite	w/ Biotite, Carbonates, and probably silicifed
477504	Rusty Quartz	w/ Sulphides, possible VG
477505	Quartz	w/ Mylonite
477506	Quartz	w/ Mylonite
477507	Amphibolite	w/ Ankerite Veins
477508		Mylonite
477509	Altered Amphibolite	w/ Pyrrhotite
477510	Rusty Quartz	Alteration w/ Sulphides & Carbonates
477511	Rusty Quartz	Alteration w/ Sulphides & Carbonates
477512	Altered Amphibolite	w/ Sulphides and Micas
477513		Diabase Dyke
477514	Rusty Quartz	Alteration w/ Sulphides
477515	Amphibolite	w/ Rusty Alteration + Sul-phides
477516	Silicified Amphibolite	w/ Contact Relation (Aplitic Lens)
477517		Meta Ultramafic
477518	Altered Amphibolite	w/ Quartz, Sulphides and Felsics
477519		Silicified Amphibolite
477520		Amphibolite
477521	Amphibolite	Biotitie/Phlogopite Alteration
477522		Silicified Amphibolite
477523	White Pegmatite	w/ Muscovite and Cordierite
477524		Amphibolite
477525	White Pegmatite	w/ Tourmaline
477526		Amphibolite
477527	Silicified Amphibolite	w/ Sulphides
477528	Amphibolite	w/ Cholrite Alteration (Folded)
477529	Amphibolite	Alteration w/ Folded Blue Quartz
477530	Amphibolite	w/ Actinolite and Tourmaline
477531		Banded Amphibolite
477532		Diabase Dyke
477533	Silicified Amphibolite	w/ Sulphides
477534	White Pegmatite	w/ Tourmaline
477535	Blue Quartz	w/ Cordierite
477536		Meta Ultramafic
477537		Diabase Dyke

477538	Amphibolite	Altered w/ Biotite or Muscovite
477539		White Pegmatite
477540		TTG Gneiss
477541		White Pegmatite
477542	TTG Gneiss	Amphibolite Contact (Structural Contact?)
477543	TTG Gneiss	w/ Hematite Staining
477544	Amphibolite	w/in TTG area (Structural Contact?)
477545		Metagabbro
477546		Blue Quartz
477547		Aplitic Lens
477548		Aplitic Lens
477549	Altered Amphibolite	w/ Blue Quartz and Carbonates
477550	Altered Amphibolite	w/ Marble or Calcite
477551	Altered Amphibolite	w/ Marble or Calcite
477552	Quartz	w/ Mylonite
477553		Mylonite
477554	Quartz	From channel cut (NUNA Sampling Plan)
477555	Amphibolite	From channel cut (NUNA Sampling Plan)
477556	Quartz	Honey Combed
477557	Diabase Dyke	w/ Sulphides
477558	Silicified Amphibolite	w/ Mylonitization
477559	Diabase Dyke	w/ Plag and Magnetic Minerals
477560	Banded Amphibolite	Contact w/ 477599
477561	Diabase Dyke	w/ Plag and Magnetic Minerals
477562		Ultra Mafic
477563	Altered Amphibolite	w/ Sulphides (Arsenopyrite and Chalcopyrite)
477564	Altered Amphibolite	w/ Marble or Calcite and Mylonite
477565	Quartz	Honeycombed w/ Amphibolite and Calcite
477566	Altered Amphibolite	w/ Sulphides
477567	Diabase Dyke	w/ Plag and Magnetic Minerals
477568	Altered Amphibolite	w/ Sulphides
477569	Altered Amphibolite	w/ Calcite or Marble and Quartz
477570		Aplitic Lens
477571		Altered Amphibolite
477572		White Pegmatite
477573	White Pegmatite	Contact w/ Amphibolite

477574	Altered Amphibolite	Chlorite Alteration
477575	Altered Amphibolite	Chlorite Alteration
477576	White Pegmatite	w/ Cordierite
477577		Diabase Dyke
477578		Aplitic Lens
477579	Amphibolite	Chlorite Alteration w/ Ankerite
477580		White Pegmatite
477581		Aplitic Lens
477582	Altered Amphibolite	w/ Rusty Quartz and Sulphides
477583	Altered Amphibolite	w/ Blue Quartz
477584		Blue Quartz
477585		Aplitic Lens
477586	Altered Amphibolite	w/ Rusty Quartz, Sulphides and Garnet
477587		Metagabbro
477588	Diabase Dyke	Small Scale
477589		Diabase Dyke
477590		Milky Quartz
477591	Milky Quartz	Contact w/ Amphibolite
477592		Altered Amphibolite
477593	Altered Amphibolite	w/ Sulphides
477594	Amphibolite	w/ Ankerite
477595	Quartz	Honey Combed
477596	Altered Amphibolite	w/ Calcite, Quartz and Feldspar
477597	Rusty Quartz	VG
477598		Metagabbro
477599	Altered Amphibolite	w/ Quartz, Sulphides and Carbonates
495501		Diabase Dyke
495502	Altered Amphibolite	w/Calcite, Quartz and Feldspar
495503	Amphibolite	w/Garnet (Transported)
495504	Altered Amphibolite	w/ Quartz and Sulphides
495505		Diabase Dyke
495506		TTG Gneiss
495507		Pegmatite
495508		Diabase Dyke
495509		Metagabbro
495510		Milky Quartz
495511	Altered Amphibolite	w/ Sulphides
495512		Diabase Dyke
495513		Aplitic Lens
495514	Quartz	w/ Ultramafic
495515		TTG Gneiss
495516	Altered Amphibolite	w/ Biotite and Garnet
495517	Banded Amphibolite	w/ Quartz and Biotite
495518		White Pegmatite
495519		Aplitic Lens

495520	TTG Gneiss	(Tonalite?)
495521		TTG Gneiss
495522	TTG Gneiss	w/ Biotite
495523	Amphibolite	w/ Epidote (retrograde?)
495524	Rusty Quartz	w/ Altered Amphibolite
495525		TTG Gneiss
495526		Pegmatite
495527		TTG Gneiss
495528		Rusty Quartz
495529	Altered Amphibolite	w/ Ankerite and Sulphides
495530	Amphibolite	w/ Ankerite veinlets?
495531		Metagabbro
495532		Banded Amphibolite
495533	Amphibolite	w/ Ankerite veinlets?
495534	Amphibolite	w/ Platy Texture
495535	Amphibolite	w/ Actinolite
495536		Rusty Quartz
495537	Amphibolite	w/ Milky Quartz
495538	Amphibolite	w/ Sulphides and Honey-combed Quartz
495539	Rust Quartz	w/ Honeycombing
495540		Aplitic Lens
495541	Quartz	w/ Honeycombing, Purple Mineral , and Epidote
495542	Blue Quartz	w/ Interbedded Amphibo-lite
495543	Rusty Quartz	w/ Amphibolite
495544	Amphibolite	w/Platy Texture
495545	Altered Amphibolite	w/ Garnet
495546	Rusty Quartz	w/ Altered Amphibolite
495547	Amphibolite	w/ Garnet
495548	Amphibolite	w/ Tourmaline
495549		Rusty Quartz
495550		Banded Amphibolite
495551	Amphibolite	Carbonitized
495552		Metagabbro
495553	Banded Amphibolite	Mylonite
495554	Banded Amphibolite	w/ Garnet and Interesting Texture
495555	Rusty Quartz	VG
495556	Rusty Quartz	VG
495557	Rusty Quartz	w/ Altered Amphibolite and VG
495558	Rusty Quartz	VG
495559	Rusty Quartz	VG
495560	Rusty Quartz	VG
495561	Rusty Quartz	VG
495562		Metagabbro
495563	Rusty Quartz	w/ Blue Quartz

495564	Amphibolite	w/Garnet, Epidote, and Purple-Mineral
495565	Amphibolite	w/ Garnet and Interesting Texture
495566	Altered Amphibolite	w/ Rusty Quartz
495567	Rusty Quartz	VG
495568	Rusty Quartz	VG
495569	Rusty Quartz	VG
495570	Rusty Quartz	VG
495571	Rusty Quartz	VG
495572	Amphibolite	w/ Hydrothermal Garnets
495573	Altered Ultramafic	w/ Magnetite
495574		Hornblendite
495575	Amphibolite	w/ Epidote Alteration
495576	Altered Ultramafic	w/ Magnetite and Chalcopyrite
495577		Serpentinite
495578	Actinolite	w/ Pyroxene and Olivine
495579	Actinolite	w/ Pyroxene and Olivine
495580		Hornblendite
495581	Mylonite	w/ Sigma Clast
495582	Pegmatite	w/ "Pinhead" Garnets
495583	Rusty Quartz	VG
495584	Rusty Quartz	VG
495585	Pillow Basalt	Folded
495586	Amphibolite	w/ Hydrothermal Garnets and Noted Texture
495587	Rusty Quartz	VG
495588	Rusty Quartz	VG
495589	Rusty Quartz	VG
495590	Rusty Quartz	VG
495591	Rusty Quartz	VG
495592	Rusty Quartz	VG
495593	Rusty Quartz	VG
495594	Rusty Quartz	VG
495595	Rusty Quartz	VG
495596	Amphibolite	w/ Greenschist retrograde
495597		Pillow Basalt
495598		Pillow Basalt
495599		Pillow Basalt
476701		Pillow Basalt
476702		Pillow Basalt
476703	Rusty Quartz	VG
476704	Rusty Quartz	w/ Hydrothermal Garnet Contact
476705	Rusty Quartz	VG
476706	Rusty Quartz	VG
476707	Unknown Purple Mineral	w/ Garnet, Epidote, Hornblende
476708	Rusty Quartz	VG
476709	Pegmatite	w/ Cordierite, Tourmaline,

476710	Aplite/Pegmatite	Garnet w/ Cordierite

Table 3. *Petrography*

Sample#	Thin section	Description
495505	Diabase Dyke	Ophitic texture with some alteration; clinozoisite present
495514	Amphibolite	Large vein of plag + quartz with zoned plag; amphibole + relic OPX
495519	Aplitic Lens	Primarily plag + quartz + biotite with lepidoblastic texture
495522	TTG Gneiss	Primarily plag + quartz + minor amph; clinozoisite lamalle
495533	Amphibolite	Many generations of amphibole, some opaques
495536	Rusty Quartz	Quartz with Fe rich veins and altered severely altered amphiboles
495544	Amphibolite	Amphibole + biotite + calcite +-anorthite
495572	Amphibolite	Amphiboles with reaction rim present
495573	Altered Ultramafic	Mostly amphiboles with minor plag and opaques
495577	Serpentinite	Highly mylonitized which destroyed the original texture
495578	Actinolite	Some OPX with actinolite
495588	Rusty Quartz	Quartz + Veins of Fe-rich material
495593	Amphibolite	Amphibole rich with diffusion between grain boundaries
476710	Pegmatite	Tourmaline + plag + quartz with major grain diffusion +-fluorite
477501	Aplitic Lens	Primarily plag + quartz + biotite with lepidoblastic texture
477513	Diabase Dyke	Mylonitized; +- olivine, + amphibole, + plag
477517	Meta Ultramafic	Mylonitized; + amphibole, + plag, + clinozoisite, + relic pyroxene
477523	White Pegmatite	Quartz, + plag, + clinozoisite. Major diffusion along boundaries
477525	White Pegmatite	Relic tourmaline + quartz + plag
477536	Amphibolite	Amphibole + plag +- calcite
477542	TTG Gneiss	Lepidoblastic texture; amphibole banding; mostly plag + quartz
477545	Meta Gabbro	Large amphibole grains, +- anorthite, +- clinozoisite
477553	Mylonite	Heavily mylonitized sample with microstructures
477561	Diabase Dyke	Ophitic texture with plag lathes + amphibole; minor OPX
477562	Altered Diabase	Relic ophitic texture with major diffusion along boundaries
477570	Aplitic Lens	Primarily plag + quartz + biotite with lepidoblastic texture
477585	Aplitic Lens	Primarily plag + quartz + biotite with lepidoblastic texture
477593	Altered Amphibolite	Amphibole rich with diffusion between grain boundaries

Table 4. *Activation labs fire assay report*

Analyte Symbol	*Au*	*Mass*
Unit Symbol	*ppb*	*g*
Detection Limit	*1*	
Analysis Method	*FA-INAA*	*FA-INAA*
495510	2	30.3
495556	2	30.4
495558	3	30.1
495567	3	30.6
495568	3	30.1
495570	2	30.9
495587	2	30
495588	3	30.8
495590	2	30.7
495594	3	30.3
476703	2	30.3
477546	1	30.1

Table 5. *ESEM data*

Date: 2-Mar-2011

kV: 13.00 Tilt: 0.00 Take-off: 35.02 AmpT: 51.2

Detector Type: SUTW, Resolution: 129.14 Lsec: 29

Sapphire

EDAX ZAF Quantification (Standardless)

Oxides

Element	Wt%	Mol%	K-Ratio	Z	A	F
Na2O	1.23	1.51	0.0054	0.9661	0.6079	1.0044
Al2O3	52.82	39.37	0.2265	0.9559	0.8438	1.0045
SiO2	34.83	44.06	0.1202	0.9813	0.7521	1.0006
CaO	11.11	15.06	0.0729	0.9473	0.9685	1
Total		100		100		

Element	Net Inte.	Bkgd Inte.	Inte. Error	P/B
NaK	32.62	28.64	4.9	1.28
AlK	1412.33	41.37	0.51	34.14
Sik	669.91	42.43	0.76	15.79
CaK	195.33	16.67	1.43	11.72

References

Chiarenzelli, J.R. & Moores, E.M., 2004, The Precambrian Earth: Tempos and Events: Precambrian Ophiolites. Developments in Precambrian Geology, v.12, p.213-217.

Dilek, Y. & Furnes, H., 2011, Ophiolite genesis and global tectonics: Geochemical and tectonic fingerprinting of ancient oceanic lithosphere. GSA Bulletin March 2011, v.123, no.3-4, p.387-411.

Dilek, Y. & Polat, A., 2008, Suprasubduction zone ophiolites and Archean tectonics. Geology May 2008, v.36, p.431-432.

Eriksson, P.G. & Catuneanu, O., 2004, The Precambrian Earth: Tempos and Events: A Commentary on Precambrian Plate Tectonics. Developments in Precambrian Geology, v.12, p.201-213.

Frei, R., Polat, A. & Fryer, B., 2009, Evidence for recycling of Eoarchean (3700 Ma) Continental Crust into Mesoarchean (3075 Ma) Mantle, Ivisaartoq Greenstone Belt, SW Greenland. In, McCausland, P.J., Ernst, R. & Bleeker, W. (presiding) Proceedings of the “American Geophysical Union” Joint Assembly 2009 (AGU website).

Friend, C.R.L. & Nutman, A.P., 2001, U-Pb zircon study of tectonically bounded blocks of 2940 – 2840 Ma crust with different metamorphic histories, Paamiut region, South-West Greenland: implications for the tectonic assembly of the North Atlantic craton. Precambrian Research, v.105, no. 2-4, p.143-164.

Galley, A. Hannington, M. & Jonasson, I., 2007, Volcanogenic-associated massive sulphide deposits (VMS); in Mineral Deposits of Canada A Synthesis of Major Deposit Types, District Metallogeny, the Evolution of Geological Provinces and Exploration Methods, (ed.) W.D. Goodfellow; Geological Association of Canada, Mineral Deposits Division, no.5, p.141-161.

Moyen, J., Stevens, G. & Kisters, A.F., 2009, TTG as Archean syn-orogenic granitoids. In, McCausland, P.J., Ernst, R. & Bleeker, W. (presiding) Proceedings of the “American Geophysical Union” Joint Assembly 2009 (AGU website).

Polat, A., Fryer, B.J., Appel, P.W.U., Kalvig, P. & Kerrich, R., 2011, Geochemistry of anorthositic differentiated sills in the Archean (~2970 Ma) Fiskenæsset Complex, SW Greenland: Implications for parental magma compositions, geodynamic setting, and secular heat flow in arcs. Lithos, v.123, p.50-72.

Robertson, A., 2004, Development of concepts concerning the genesis and emplacement of Tethyan ophiolites in the Eastern Mediterranean and Oman regions. Earth Science Reviews, v.66, p.331-387.

Rushmer, T., 2009, Petrogenesis of TTG magmatism: Generating chemical diversity in different tectonic settings. Geochimica et Cosmochimica Acta (GCA), v.73, issue 13 supplement 1, p.1135.

Slowey, E. & Goodman, R., 2008, A valuation of NunaMinerals interest in exporation licenses in Greenland, March 2008. CSA Report No. 3831/078.

Structural geology and emplacement of the Tartoq Group, SW Greenland (Kisters *et al*.)

Alexander F.M. Kisters[1], Kristoffer Szilas[2] & Vincent J. van Hinsberg[3]

[1] Department of Earth Sciences, Stellenbosch University, Matieland 7602, South Africa

[2] Geological Survey of Denmark and Greenland – GEUS, Øster Voldgade 10, DK-1350, København, Denmark

[3] Department of Earth Sciences, University of Oxford, South Park Road, Oxford, United Kingdom

Introduction

The Tartoq Group comprises a series of kilometre-scale, pre-Ketilidian supracrustal belts around the Sermiligaarsuk Fjord in SW Greenland (Higgins & Bondesen 1966). The rocks are commonly described as greenschist to lower-amphibolite-grade supracrustals that are in tectonic contact with and/or intruded by the surrounding TTG's. The low grades of metamorphism and preservation of primary textures in the supracrustals have long been noted as being unique, but, to date, there is only little information in the literature as to the origin and significance of the Tartoq Group within the broader geological framework of SW Greenland. A U-Pb zircon age of 2944±7 Ma from a discordant TTG sheet within the supracrustals was interpreted by Nutman & Kalsbeek (1994) to indicate the minimum age of the Tartoq Group, underlining the probably Neoarchaean age of the supracrustal succession.

The present report describes the main structural elements and lithological inventory of the Tartoq Group, also with the aim to characterise the evolution and tectonic setting of the supracrustals. The report is based on field work carried out over a period of ca. three weeks between June 20 and July 14 2010, covering the four larger belts of the Tartoq Group including, from W to E, Nuuluk, Iterlak, Sioralik and Midternæs N (Fig. 1). Field work focused on the structural inventory of the belts along selected traverses and the nature of TTG-greenstone contacts. For compilations of the geology of individual belts, the reader is referred to reports by e.g. Higgins & Bondesen (1966) and Higgins (1968). More detailed lithological and petrographic descriptions can be found in e.g. van Hinsberg et al. (2010). Specific aspects addressing the economic geology of the Tartoq Group can be found in, *inter alia*, Appel & Secher (1984), Evans & King (1993) and Petersen (1993). Nutman & Kalsbeek (1994) and Nutman et al. (2004) provide the, to date, only geochronological constraints on the Tartoq Group rocks.

Synopsis of the regional structural inventory

Supracrustals of the Tartoq Group occur in six main belts or slivers, forming allochtonous, infolded inliers in the TTG-dominated terrain around the Sermiligaarsuk Fjord (Fig. 1). In contrast to previous assertions, metamorphic grades are highly variable between the different belts, ranging from lower-greenschist to lower-granulite facies grades (Van Hinsberg et al., 2010). Importantly, most supracrustals preserve evidence of pro- and retrograde assemblages and P-T paths during their emplacement, an aspect that is critical when interpreting the emplacement and tectonic setting of the Tartoq Group. The majority of contacts between the TTG's and greenstones are structural, but many, if not most, of these contacts have been overprinted by late-stage intrusives, forming km-wide intrusive breccias and stockworks surrounding, but also within the supracrustal belts (Fig. 1).

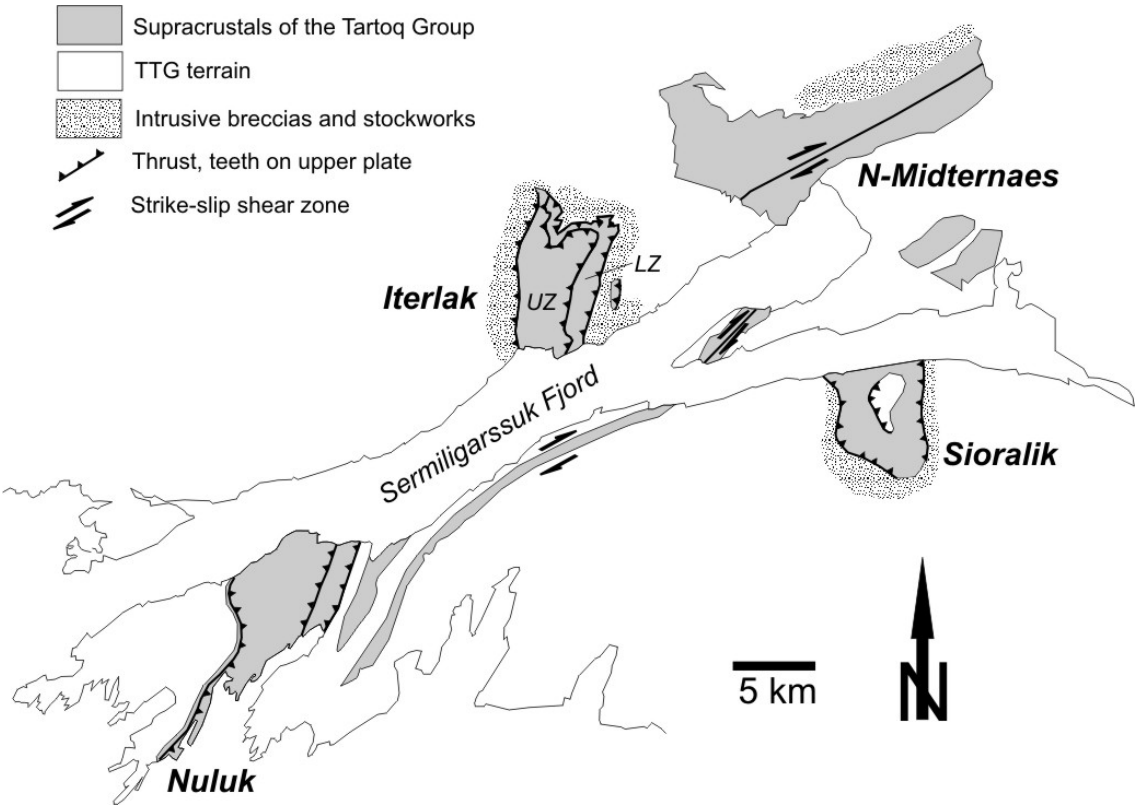

Figure 1. *Simplified map of the Tartoq Group, showing the distribution of the main supracrustal belts around the Sermilligarssuk Fjord (modified from Higgins 1968, and own work). UZ/LZ – upper and lower zone of the Iterlak belt.*

The Tartoq Group has undergone two main phases of deformation, D1 and D2, only followed by late-stage brittle faulting (D3), the latter of which is considered to have had only minor influence on the present-day configuration of the belts. This notation of successive deformation phases is used to establish a broad chronology of events that would also allow for the correlation of deformation phases between individual belts. It should be emphasized that the main deformation phases describe a continuum and a progressive deformation path, also evidenced by the progressive overprint of fabric-forming mineral assemblages. Evidence of these deformation phases is preserved in most belts, but the degree of later overprints on earlier assemblages and fabrics is highly variable. As a result, a clear distinction of fabrics is not always possible.

D1: Early imbrication (D1a) and exhumation (D1b)

The earliest deformation phase (D1) can be subdivided into a D1a (or early) and D1b (or late) deformation phase. A D1c deformation can be distinguished in the Sioralik belt, based on the preservation of distinct and overprinting mineral assemblages.

D1a fabrics (D1a) are characterised by higher-T mineral assemblages and textures commensurate with crystal-plastic deformation processes and, broadly speaking, amphibolite-facies conditions of deformation. This includes the pervasive recrystallization and grain refinement of feldspar in mylonites or S1a and L1a fabrics defined by the preferred orientation of e.g. hornblende. D1 is expressed by (1) a variably developed, bedding- and/or layer-subparallel foliation (S1); (2) mineral stretching and rodding lineations (L1), resulting in locally developed constrictional-type fabrics, particularly in D1 high-strain zones; (3) metre- to kilometre-scale recumbent folds (F1) that refold bedding; (4) associated low-angle shear zones; and (5) mainly SE-facing vergence folds. Throughout this report, fabrics are labeled D1a fabrics (e.g. S1a or L1a), if the fabrics are defined by higher-grade parageneses. D1b fabrics (S1b and L1b) are defined by lower-grade, greenschist facies assemblages.

D1a shear zones are identified by mylonitic and ultramylonitic textures. In many places, D1a mylonite zones are delineated by the presence of highly-sheared felsic gneiss units. The close spatial association of these gneisses (quartz-plagioclase ± muscovite mylonites) with D1a shear zones, their discontinuous geometry and TTG-like composition (Szilas, 2010, pers. comm.) may also suggest that the gneisses represent TTG slivers, marking the early imbrication of Tartoq Group rocks with the surrounding TTG's. This interpretation is favoured in this report.

D1b: Later fabrics (D1b) are commonly brittle and retrograde, partly or completely overprinting earlier D1a fabrics. D1b mineral assemblages are dominated by chlorite and an associated carbonate alteration, pointing to broadly greenschist-facies conditions of deformation. D1b structures in all greenstone belts, except for Midternæs N, indicate an overall SE vergence and top-to-the-SE kinematics. D1b fabrics are largely coaxial with D1a fabrics, but the brittle nature of fabrics and associated retrogression of earlier fabrics indicate the formation of D1b fabrics during the exhumation of the supracrustals. D1b fault zones are defined by narrow (<2 m) ultracataclasites and narrow (cm- to dm) to up to several hundred metre wide cataclasite zones. The latter may show regional extents and cataclasite textures (e.g. broken and/or rounded feldspar clasts in a fine-grained, chloritic matrix) have previously been interpreted as e.g. indicating the presence of prominent pyroclastic sequences within the greenstones (e.g. in Midternæs N). The majority of shear-sense indicators are S-C' fabrics (*extensional crenulation cleavages*) pointing to top-to-the-E and SE kinematics, consistent with W- and NW-plunging mineral stretching lineations (L1b), and SE-verging folds (F1b). In Iterlak, metre- to decametre-scale low-angle normal faults occur in the immediate hangingwall of D1b cataclasite zones. The normal faults displace earlier S1a fabrics, but are refolded by F2 folds, also indicating a D1b timing. These features consistently point to the fact that despite the thrust-sense of movement, imbrication occurred during extensional shearing and concomitant with the exhumation of the rocks. Dextral-strike slip kinematics are indicated by pervasive S-C and S-C' fabrics in steeply-dipping, E trending segments of supracrustal belts (e.g. Midternæs N). These subvertical, E-trending

belts show the orientation and kinematics of lateral ramp structures during the overall E-verging imbrication (see also Petersen 1993).

Cataclasites are commonly characterised by a chlorite-rich matrix, even where leucocratic pegmatites and gneisses are the protoliths, indicating a pervasive Mg- and Fe- metasomatism during fluid flow. In greenstones, deformation and associated fluid flow have resulted in the pervasive alteration of the supracrustals, resulting in vuggy, or “knobbly” textures that obliterate primary structures. Where greenstones have been altered to chlorite-carbonate schist, the deformation is ductile, resulting in highly-foliated greenschist packages. This is particularly well developed in the central-eastern parts of Nuuluk, where deformation along D1b thrusts and associated fluid flow resulted in local mineralisation, as well as in the strike-slip shear zones of Midternæs N. The D1b related retrogression is near-pervasive in the western belts, but much more localized in the E (e.g. Sioralik) (van Hinsberg et al., 2010).

Both D1a and D1b resulted in the imbrication of greenstone packages. The common association of basaltic flows, sediments and volcaniclastics (?) and ultramafic rocks suggest an oceanic origin of the Tartoq Group (van Hinsberg et al., 2010). This does not, however, imply that individual greenstone packages share the same evolution (see discussion). Evidence of the D1 deformation has been identified in Nuuluk, Iterlak and Sioralik, and structures describe very similar patterns in these belts. N-Midternæs shows D1b structures, but with different orientations and kinematics, mainly related to its different orientation. D1 a/b shear and fault zones also account for the juxtaposition of the TTG terrain with the greenstones of the Tartoq Group. Similar to structural relationships recorded within the supracrustals, the TTG-greenstone contacts also record earlier high-T fabrics overprinted by retrograde fabrics and brittle-ductile or brittle deformation fabrics.

For the most part, the originally tectonic contacts are overprinted by intrusive contacts of either TTG’s into greenstones (Nuuluk, Iterlak, and N-Midternæs) or extensive leucopegmatite stockworks (Sioralik). The prolonged and syn-tectonic intrusion of either TTG’s or pegmatites during and after D1 is a characteristic feature of all supracrustal belts of the Tartoq Group.

D2: refolding and partial reactivation of D1 structures

The subsequent D2 deformation resulted in the refolding of earlier D1 structures by N to NE trending, both E and W verging, doubly-plunging (mainly SW, but also NE), m- to km-scale folds (F2), associated axial planar foliations (S2) and intersection, crenulation and mineral lineations (L2). D2 represents most likely a continuation of the D1 event, recording the progressive shortening and co-axial refolding of imbricates and recumbent folds during and following the lock-up of the low-angle thrusts. D2 is again associated with the formation of brittle cataclasites and associated fluid flow and alteration. For the most part, the supracrustals of the Tartoq Group are preserved in F2 synclinoria, which suggests the originally wider extent and distribution of the greenstones in the region.

Later normal faulting is recorded in all greenstone belts of the Tartoq Group. The timing of the low-temperature brittle faulting is not clear, but it clearly overprints earlier D1 and D2

related structures and fabrics. Mafic dyke swarms of variable orientation have intruded the TTG-greenstone terrain and are possibly associated with the late normal faulting.

Geology of individual supracrustal belts of the Tartoq Group

Nuuluk

Nuuluk is the westernmost supracrustal belt (Fig. 1), measuring ca. 10 by 4 km. Its western contact is made up of a sequence of interlayered greenstones and TTG- gneisses. In the E, the main belt is also made up by a series of thin supracrustal slivers intercalated with TTG gneisses that structurally underlie the main belt (Fig. 2). The supracrustals show overall N to NE trends and bedding and/or layering define a km-scale NNE trending, SW plunging synclinorium (F2), with N and E dips in the W and mainly W dips in the E. D1a,b thrusts, associated S1b foliations together with F2 folds and an axial planar S2 foliation result in the prominent E to SE-vergence of the Nuuluk belt (Fig. 2). Based on lithological and structural characteristics, the Nuuluk supracrustal belt and surrounding TTG gneiss terrain has been subdivided, from W to E, into six, roughly parallel domains. The six domains are briefly described in the following:

Western basement gneisses

The western basement gneisses comprise banded gneisses and leucogneisses that contain xenoliths of an earlier generation of medium-grey trondhjemitic gneisses and greenstones. Contacts between the main phase of leucogneisses and older gneisses and greenstones are clearly intrusive, but xenoliths can be seen to have been tectonically transposed into the shallowly W-dipping gneisssosity, which gives rise to the lithological banding. The presence of biotite and hornblende (?) in the gneisses suggests broadly amphibolite-facies grades for the basement gneisses. In places, the interlayered TTG-greenstone sequence has been folded by NE-trending, shallow NE- and SW-plunging, SE-verging folds (F1b) (Fig. 3a). The 1:100.000 scale geological map (61 V. 1 SYD Ivigtut, Berthelsen & Henriksen 1975) shows steep W dips of the gneisses closer to the Atlantic seaboard, indicating the presence of a corresponding NNE-trending and plunging F2 antiform some 3-4 km to the W of the F2 Nuuluk synclinorium. The far western parts of the Nuuluk belt are located in the N-plunging hinge and on the E limb of this synform. The vergence of F1b folds indicates that they are not parasitic folds related to the later F2 folding (Fig. 2).

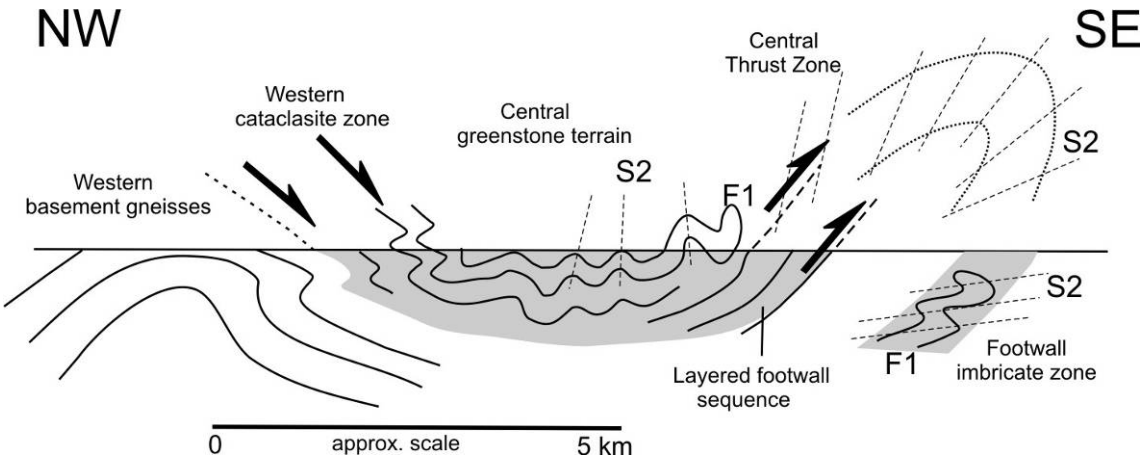

Figure 2. *Schematic cross section through the Nuuluk belt, illustrating the main lithological and structural zones described in the text.*

Western cataclasite zone

The western cataclasite zone is made up of interlayered leucogneisses and greenstones that have been affected by a near-pervasive cataclastic overprint over a width of at least 1-1.5 km. Gneisses dominate in the W, but greenstones become massive and are far more dominant towards the E. Primary layering, where identified, shows gentle, mainly E and SE dips, but is openly folded by N to NE trending, gently doubly-plunging F2 folds. The cataclastic nature of most rocks is indicated breccia-like textures, pervasively developed cataclastic textures evidenced by the presence of rounded feldspar clasts in a chloritic matrix, narrow, cm-scale bands of foliated to massive cataclasites, anastomosing blackish-greenish ultracataclasite bands or m-wide cataclasite networks grading into breccias (Fig. 3b,c). Quartz veining and epidote formation is common and, in places, sulphide mineralisation (pyrite, chalcopyrite) is recorded in quartz veins and cataclasite zones. The matrix of cataclasites shows the pervasive formation of chlorite even in leucogneisses that originally show very little if any mafic minerals. Feldspar in cataclastically deformed gneisses is commonly reddish-pinkish. Quartz may show ribbon formation that also define an anastomosing foliation wrapping around feldspar clasts (Fig. 3c). This western cataclasite zone largely corresponds to what has been mapped as ‘quartz-diorite’ on the Ivigtut 1:100.000 geological map (Berthelsen & Henriksen 1975).

Central greenstone terrain

The central greenstone terrain underlies much of the higher lying plateau of the Nuuluk belt. It is mainly made up of what appears to be massive basaltic (sensu lato) volcanic flows and interlayered sediments, although the identification of the latter is not always unambiguous. Most of the greenstone rocks are pervasively altered showing a vuggy and distinctly blocky or ‘knobbly’ weathering. This type of alteration and resulting weathering is even more pronounced in some of the eastern zones and will be discussed in more detail below. For the most part, the greenstones show greenschist-facies assemblages, dominated by chlorite, carbonate and minor epidote. Quartz and quartz-carbonate veins are common throughout the sequence. In places, however, large, >10m thick and up to 250 m long slivers of massive and unaltered amphibolites are interlayered with the greenstones. The central greenstone terrain shows a general increase in fabric and strain intensity from W to E. Bedding and layering in the W are very shallow and, again, gently folded by upright

to E-verging F2 folds. In places, the low fabric intensities allow to identify an early generation of tight, recumbent F1 folds that show half wavelengths of 5-10m and amplitudes in excess of several tens of metres (Fig. 3d). Towards the E, F2 folds become tighter, associated with a pronounced vergence to the E and SE. Here, folding is commonly associated with small-scale, tight, SW-plunging crenulations and a WNW-dipping axial-planar foliation (S2). Rock types include chlorite –carbonate and talc-carbonate schists. Despite the stronger fabric intensities, numerous localities contain structures interpreted to represent pillows. The presence of distinct, m-wide, shallow- to moderately W dipping high-strain zones is marked by a pervasive, W-dipping foliation (S1b foliation). The increase in fabric intensity marks the transition to the Central Thrust Zone to the immediate E.

The Central Thrust Zone

The Central Thrust Zone is well exposed in an up to 150 m high, NE-trending cliff section, parallel to the regional strike of the strata in the central-eastern parts of the Nuuluk belt (Fig. 3e). Deformation is indicated by the presence of highly-foliated greenschists, anastomosing foliation patterns enclosing lensoid low-strain domains, the truncation and/or duplication of units and the occurrence of large, 10's to 100's of metre long lenses of sheared felsic rocks at different levels within the high-strain domain, indicating the imbrication of these lenses. Two planar fabrics (S0/1b and S2) are commonly developed. Within the Central Thrust Zone, S0 shows shallower dips towards the W and WNW compared to the commonly steeper, NW dipping S2, but S0/1 and S2 may also be parallel to each other, underlining the coaxial nature of D1 and D2. Small-scale crenulations (F2) are formed by the refolding of S0/1b by S2 and are particularly prominent where the two fabrics enclose relatively large angles. Shear sense indicators such as S-C, S-C' fabrics and sigma clasts, the SE vergence of folds and, in places, a prominent NW-plunging down-dip rodding lineation (Fig. 3f) suggest a top-to-the-E or SE thrust sense of shear along the Central Thrust Zone.

The footwall of the Central Thrust Zone is marked by highly strained chlorite- and chlorite-carbonate schists. Up to several m-wide, strongly recrystallized marble horizons are in sharp contact with relatively undeformed, low-strain greenstones, but isolated marble lenses also occur at structurally higher levels and within the main thrust. These marbles are interpreted to be hydrothermal in origin having formed during thrust-related fluid infiltration. While the footwall contact of the Central Thrust Zone is well defined by the strong fabric gradient, the hangingwall contact against structurally overlying, highly-foliated and crenulated greenstones of the eastern parts of the central greenstone terrain is rather gradual. Hence, the thickness of the Central Thrust Zone cannot be ascertained, but it is assumed to be at least 300 m.

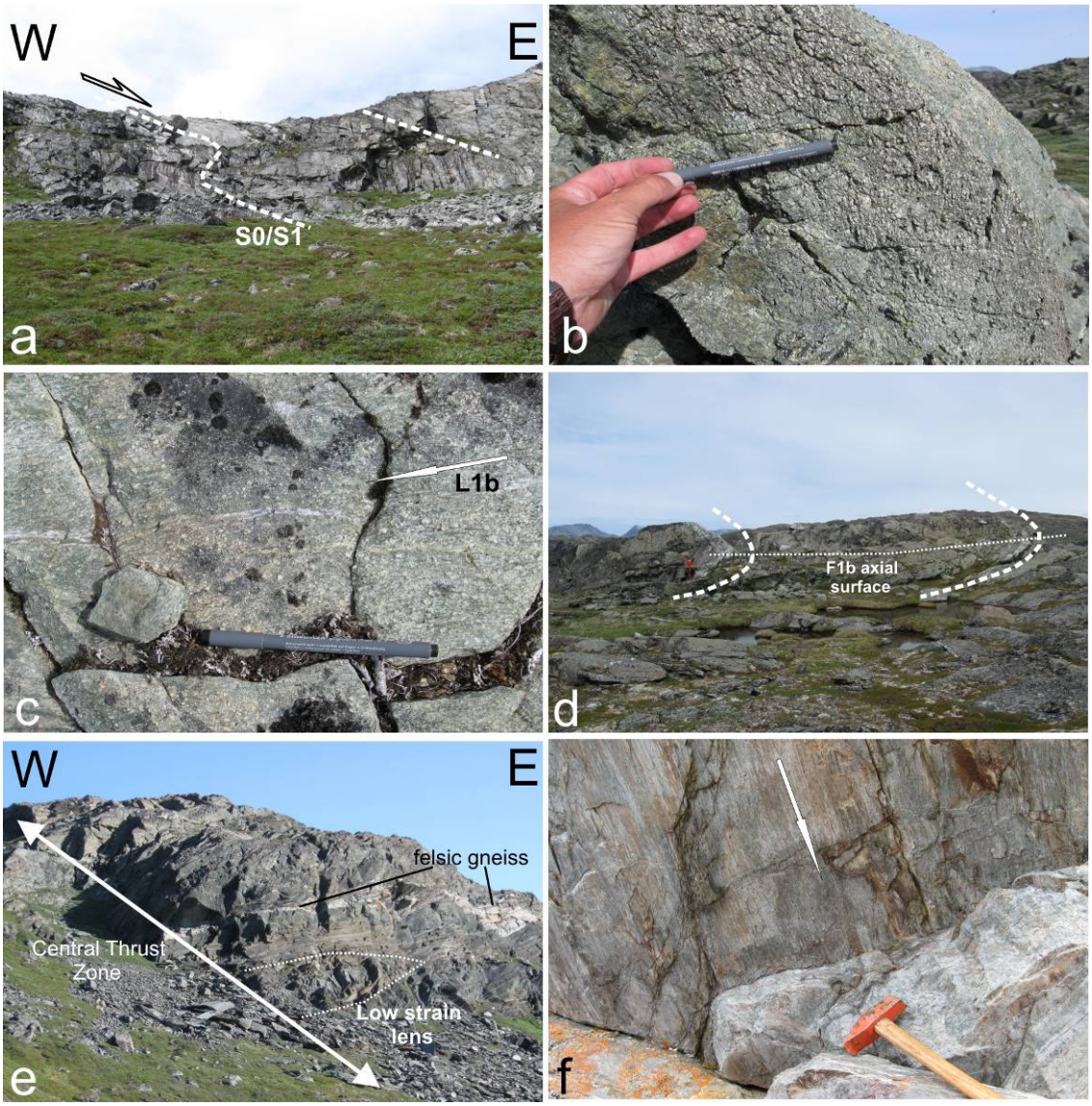

Figure 3. *(a) SE-verging fold (F1b) refolding layered TTG-greenstone succession in the western basement gneisses. Cliff is approximately 30 m high. (b) Cataclasite in the western cataclasite zone. Note the abundance of feldspar in a chloritic matrix, indicating the deformation of originally TTG gneisses; (c) Brittle-ductile cataclasite – quartz ribbons occur adjacent to feldspar clasts set in a chloritic matrix. Plan view, arrow indicates stretching lineation; (d) recumbent F1 fold in the central greenstone domain; person for scale on the left hand side of the photo; (e) cliff exposure of the central thrust zone. Note the dramatic thickness variation of the mylonitic gneiss lens in the central parts of the thrust zone; (f) down-dip rodding lineation in highly foliated schists contained within the Central Thrust Zone.*

The layered footwall sequence

The layered footwall sequence forms the easternmost zone of the main Nuuluk belt in the footwall of the Central Thrust Zone. This zone is made up of a thick succession of pervasively altered greenstones, probably basaltic flows and interlayered sediments. The pervasive alteration results in the blocky weathering of the greenstone sequence that has almost obliterated any primary features (Fig. 4a). In places, the open vugs and fractures that cause the blocky weathering pattern can be seen to be filled by brownish weathering carbonates.

Fabric intensities seem generally low in this sequence, although the blocky weathering complicates the identification of fabrics. The rather massive greenstones give locally way to well-foliated (S1/2) greenschists and carbonate-rich greenschists. The latter show a distinctive brownish weathering (Fig. 4b). These high-strain zones (D1b/2) are parallel to the regional strata, showing moderate NW dips and NE trends. The foliation (S1b/2) in these zones anastomoses around low-strain pods and zones of particularly high strain intensity commonly coincide with pervasive carbonate alteration (Fig. 4b). Boudinaged and/or folded quartz veins are common and also testify to the focused fluid flow in these zones that are known to contain elevated Au contents. Individual high-strain zones may be up to 20 m wide, but the composite zones made up of up to three or four high-strain strands may be up to 60-70 m wide. In places, a prominent down-dip lineation (L1b/2) on foliation/bedding planes is defined by tremolite (?) and/or rodded chlorite-carbonate aggregates, giving rise to constrictional-type fabrics. The most prominent high-angle fracture set hosting the pervasive carbonate alteration is normal to this lineation, also indicating the syn-D1b (possibly as late as D2) timing of the main phase of alteration (Fig. 4a).

The E contact of the main Nuuluk belt with the structurally underlying TTG gneisses is very sharp and tectonic in nature, showing steep W dips. Cataclastic bands and breccias have affected the TTG gneisses over a width of several tens of metres (Fig. 4c). Brittle-ductile fabrics are developed in the supracrustals and S-C fabrics point to top-to-the-SE transport of the greenstones over the gneisses. This basal contact preserves amphibolite-facies assemblages, although greenschist-facies retrogression is near pervasive.

Footwall Imbricate Zone

The footwall imbricate zones describes a series of very low-grade metamorphic greenstone slivers that are structurally located below the main Nuuluk belt, separated from the belt by a ca. 500m wide zone of cataclastically deformed TTG gneisses and greenstone xenoliths (Fig. 2). The greenstones comprise well banded rocks of presumable volcanic and/or volcaniclastic origin as well as slivers of quartz-rich sediments.

The structural geology of the footwall imbricate zone is distinct from that of the main belt. Bedding (S0) is steep to overturned and is cross-cut, refolded and crenulated by the shallow NW dipping S2 fabric. The angular and cross-cutting relationship between S0/1 and S2 is underlined by the refolding of early (F1), tight- to isoclinal folds with steeply-dipping axial planes by the shallowly-dipping S2 foliation (Fig. 4d), which is ubiquitous in the footwall imbricate zone. This is in marked contrast with structural relationship recorded in the main belt, where early recumbent folds (F1) are refolded by later upright- to E-verging F2 folds and the associated S2 foliation. This relationship and the, in general, shallower attitude of S2 with respect to the steep SE and NW dipping S0/S1 suggest that the entire sequence may form part of the overturned limb of a km-scale, (S)E-verging antiform that follows on from the central synclinorium, which underlies the main part of the belt (Fig. 2).

Given (1) the overall, rather open synformal geometry of the first-order structure underlying the Nuuluk belt, (2) the generally only shallow- to moderate dips, and (3) the presence of early recumbent folds that refold the sequence on a variety of scales, the greenstone sequence exposed at Nuuluk must be assumed to be < 1 km thick and, in all likelihood, considerably thinner (ca. 400-500m).

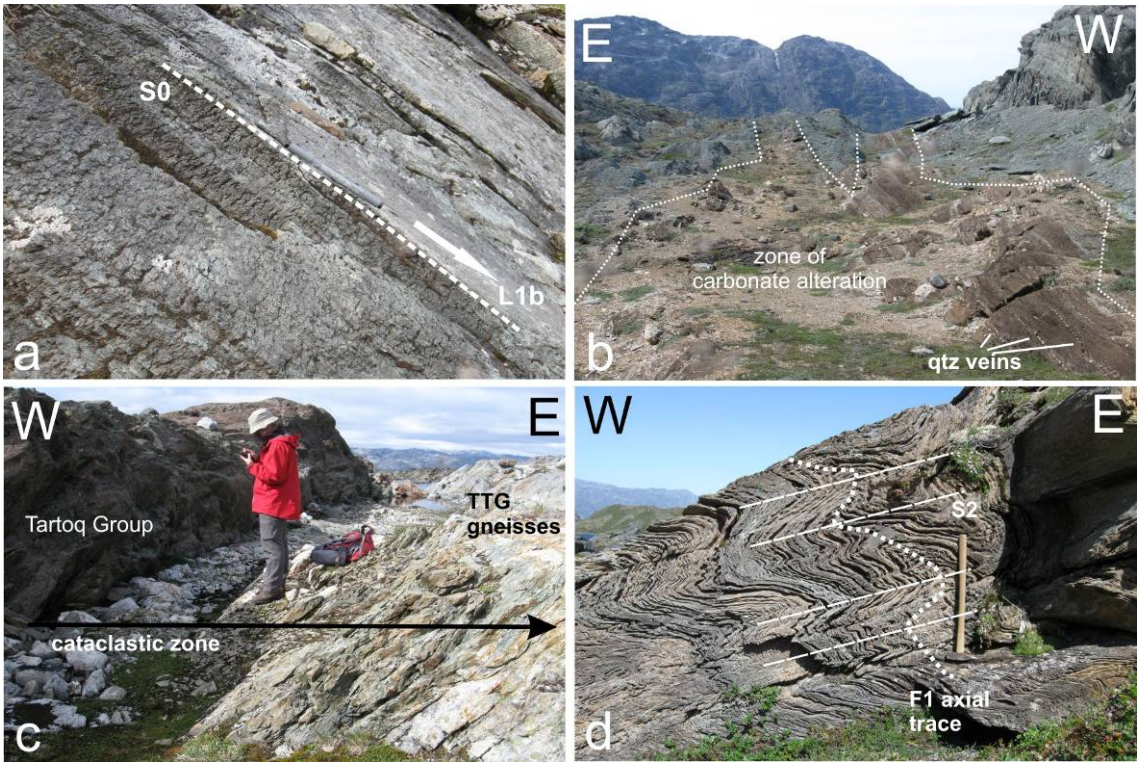

Figure 4. *(a) The pervasive "knobbly" appearance of greenstones is caused by the preferential weathering of carbonate-filled fractures, the main set being perpendicular to the stretching lineation (L1b, arrow). Cross-sectional view, looking SW, layered footwall sequence. (b) Anastomosing zones of brownish carbonate alteration and quartz veining in greenschists of the layered footwall sequence; (c) Sharp tectonic contact between greenstones and TTG's in the E of the main Nuuluk belt. The cataclastic deformation is zone extends for > 50 m into the footwall TTG's; (d) near-upright, isoclinal F1 fold refolded by shallowly-dipping S2 foliation. Note that S2 is shallower than S0, indicating that this part of the Nuuluk belt in the footwall imbricate zone forms the overturned limb of a SE-verging F2 antiform (see Fig. 2)*.

Iterlak

The NNE-trending Iterlak belt is situated along the northern shoreline of the Sermiligaarsuk Fjord (Fig. 1). It measures ca. 7 by 3.5 km and is surrounded by TTG gneisses.

Lithological inventory

Iterlak is made up of massive to foliated greenstones and greenschists of broadly basaltic origin, forming laterally continuous, sill-like flows. The greenstones are pervasively altered, showing the vuggy or knobbly textures related to the weathering of carbonate-filled fractures and pods within the greenstones also developed in Nuuluk. Cross-cutting dykes are locally observed, but are volumetrically very subordinate. Interflow sediments are suspected in the succession, but could not be identified with certainty as a result of the pervasive alteration and multiphase deformation. Conglomerate horizons have been described in previous studies (e.g. Higgins 1968), but could not be confirmed in this study. Banded iron

formations occur sporadically, but it is not clear whether they are primary sedimentary precipitates or alteration features (e.g. van Hinsberg et al., 2010). Felsic and often mylonitic gneisses ("quartz-muscovite gneiss" after Higgins 1968) are lithologically very prominent, somewhat discontinuous marker horizons within the metamafic sequence, similar to those at Nuuluk (Fig. 3e). The rocks are leucocratic gneisses, made up of mainly plagioclase, quartz and muscovite. The mylonitic foliation is defined by quartz and quartz-feldspar ribbons and the pervasive crystal-plastic deformation of all mineral components. In contrast, the immediately adjoining metamafics are, for the most part, devoid of similar high-strain fabrics and the mylonites seem to be delineating early, low-angle D1a shear zones (see below). Ultramafic rocks are distinct, showing a reddish-brownish weathering on surface, whereas fresh serpentinites are greenish-black with a distinct luster. They occur as either narrow, discontinuous horizons or as more massive pods. Gabbroic rocks are common and most easily distinguished by their coarse grain size, preserving primary magmatic textures, showing original pyroxene intergrown with plagioclase. Based on the pyroxene to plagioclase ratio, leucograbbros can be distinguished from more melanocratic varieties. The supracrustal rocks of the Tartoq Group are intruded by later mafic dykes.

Within the Iterlak belt, two main lithological packages can be distinguished, henceforth referred to as Upper and Lower Zone rocks (Figs. 1 and 5). They are distinguished by (1) their different lithological inventory. Upper Zone rocks contain a thick succession of layered greenstones, correlated with basaltic flows. Lower Zone rocks contain greenstones, but with significantly more abundant ultramafic and gabbroic rocks. Provided that the Iterlak greenstone package represents sections of oceanic crust, Upper Zone rocks would correspond to the upper parts of the crust, whereas Lower Zone rocks correspond to deeper parts of the crust and possibly including mantle sections; and (2) different grades of metamorphism and/or retrogression. Upper Zone rocks contain evidence of originally amphibolite-grade assemblages and fabrics, but the rocks are almost pervasively retrogressed to greenschist-facies assemblages. In the Lower Zone, rocks are also retrogressed, but to a lesser extent and primary amphibolite-facies assembages are far more widespread and original protoliths of e.g. gabbroic and/or ultramafic rocks are clearly discernable. The boundary between the Upper and Lower Zone is a low-angle shear zone, either delineated by the mylonitized felsic gneiss unit (D1a shear zone) or a m-wide ultracataclasite horizon (D1b) (Fig. 5, and see below).

Structural geology of the Iterlak belt

The Iterlak supracrustal belt consists of two fault-bounded and imbricated tectonostratigraphic packages, i.e. the Upper and the Lower Zone (UZ and LZ; see above; Fig. 5). The Upper Zone is exposed along the W and NW margins and occupying large portions of the central parts of the belt. The Lower Zone is exposed as a narrow strip along the N and E margins of the belt, where it is in sheared contact with the structurally underlying TTG gneisses (Fig. 1). The belt has been affected by a very similar sequence of deformational events (D1-D2) compared to Nuuluk, although the expression of the deformational events differs in detail.

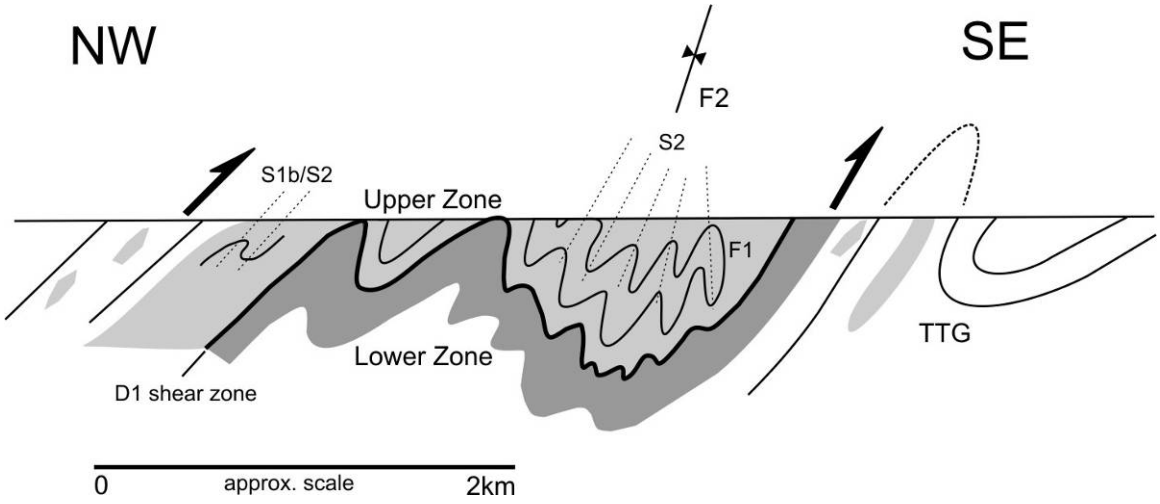

Figure 5. *Simplified cross section through the central-northern parts of the Iterlak belt, illustrating the presence of two fault-bounded lithological sections (Upper and Lower Zone) underlying the belt. The structural geology of Iterdlak is remarkably similar to that of the Nuuluk belt, showing the refolding of earlier, recumbent F1 fold nappes by F2 folds, although the overall SE vergence of structures at Iterlak is less pronounced compared to Nuuluk.*

D1: The early D1a deformation phase is associated with (1) an early, bedding parallel foliation (S1a) and, in places, rodding lineation (L1a,b), (2) bedding-parallel shear zones, manifested by mylonites and ultramylonites (D1a shear zones). D1a shear zones (or felsic gneisses/schists) occur as semiconcordant, up to 30 m wide, strongly drawn out and discontinuous units with the greenstones. For the most part, the felsic gneisses display penetrative mylonitic and, locally, ultramylonitic fabrics showing quartz-ribbons, pervasively-recrystallized feldspar textures and intrafolial folds (Figs. 6a,b). Pervasive mineral and/or mineral-stretching lineations give, in places, rise to rodded textures in mylonites and protomylonites. Mineral lineations plunge at moderate- to steep angles to the W and SW. In metamafic units, L1 lineations are defined by mainly amphibole, although mineral assemblages are dominated by retrograde chlorite and carbonate that form pseudomorphs after the higher-grade assemblages (Fig. 6c). The D1a shear zones are considered to form the boundary between rocks of the Upper and Lower Zone; and (3) a phase of tight, recumbent folding (F1a) that is evident on an outcrop scale (Fig. 6d), but also indicated by the regional refolded fold pattern defined by felsic units within the otherwise mafic-dominated sequence (Fig. 5). F1a folds cannot be identified with certainty in the lower sequence.

D1b fabrics are parallel to earlier D1a structures, but characterised by lower-grade, commonly greenschist-facies mineral parageneses and brittle deformation textures. Quartz- and quartz-carbonate veining is common and the majority of pegmatites seem to have been emplaced during D1b, indicated by their progressive deformation through D1b structures. Cataclasites are common and range from distributed, several tens of metre wide cataclasite zones that have affected intrusive pegmatites and greenstone alike (Fig. 6e), to narrow, metre-wide blackish-greenish ultracataclasites. An up to 1.5 m wide band black ultracataclasite is particularly prominent in the field and can be traced for several hundred metres along strike (Fig. 6f).

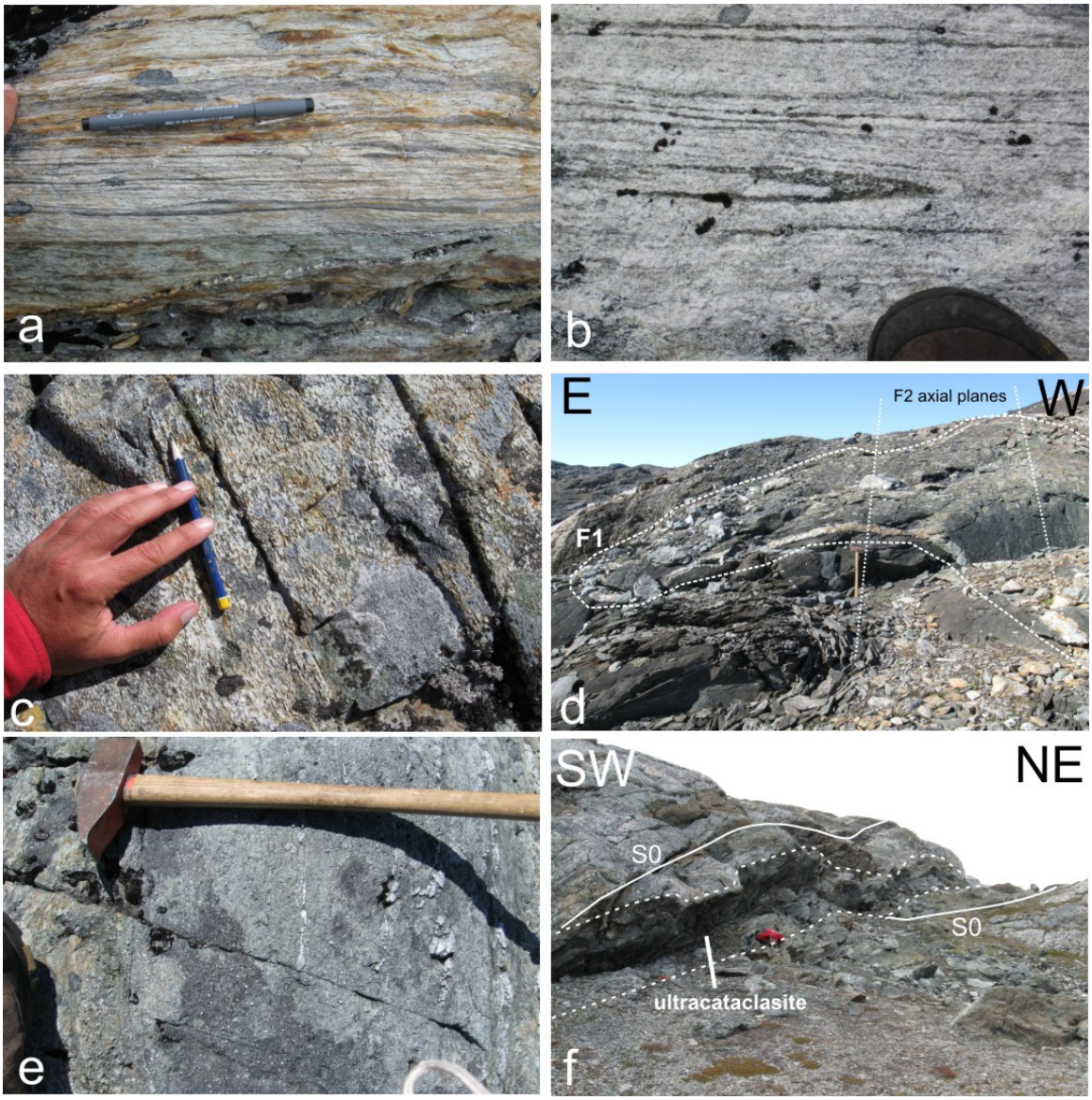

Figure 6. (*a) Banded, mylonitic gneiss delineating the presence of D1a shear zones often lined with gneiss slivers; (b) Isoclinal, intrafolial and rootless fold in transposed mylonitic foliation of sheared gneisses (D1a shear zones); both a and b are plan views; (c) Pervasive mineral lineation (L1a/b) defined by originally hornblende (parallel to pencil, plunging SW), pseudomorphed by chlorite (Upper Zone); (d) Early F1 recumbent fold (annotated by dashed line) refolded by nearly upright F2 folds (stippled, axial surface of F2) (Upper Zone); (e) Cataclastically deformed 'greenstone' – note: the abundance of feldspar clasts suggest the protolith to be a pegmatite or TTG, despite the abundance of chlorite in the matrix; (f) Trace of the central ultracataclasites. The cataclasite is only 1-2m thick, but can be traced for several hundred metres along strike, separating different lithological packages and truncating bedding (S0) in the hangingwall and its footwall.*

This ultracataclasite band is subparallel to bedding of the layered greenstones in the hangingwall, but has a sharp, highly discordant and sheared footwall contact against greenstones, serpentinites and TTG gneisses, highlighting the structural significance of this unit. The ultracataclasite is located structurally below the D1a mylonites and, as such, in the Lower Zone, indicating that the Lower Zone is likely to represent a structurally more complex and imbricated unit. In numerous places, the hanging-wall of the ultracataclasite

shows the development of dm- to m-scale, remarkably well-preserved low-angle normal faults (Fig. 7). Normal faulting is indicated by the displacement of the primary layering and the rotation of blocks in the hangingwall of the faults. Individual normal faults seem to merge with the underlying ultracataclasite that appears to form the first-order detachment, but this relationship could not be directly confirmed in any of the exposures. The syn-D1b timing of the normal faults and their relationship to the ultracataclasite is suggested by the displacement of earlier S1a fabrics along the faults that are, in turn, refolded by F2 folds (see below). In this particular outcrop (Fig. 7), normal faults show S dips (average dip direction/dip 190/40). Rotating the faults to their pre-D2 orientation about the SW plunging F2 fold axes yields W to WNW dips, depending on the angle of rotation, and top-to-the-NW kinematics. This aspect is important for the later discussion of the overall emplacement of the Tartoq Group. Similar D1b normal faults can be mapped throughout the N and E parts of the Iterlak belt.

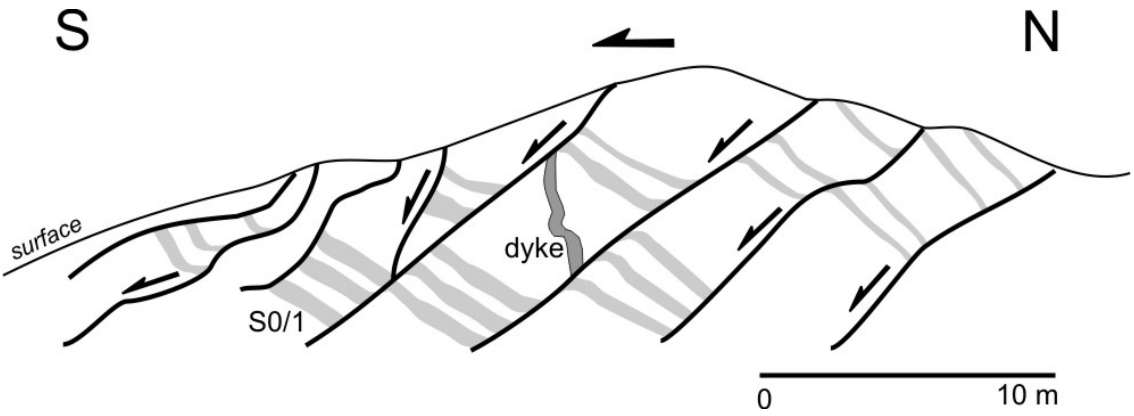

Figure 7. *Series of low-angle normal faults displacing and tilting the layering of the greenstones in a domino-type fashion (cross-sectional view). Normal faulting is commonly associated found in the hangingwall of faults/shear zones that bound and juxtapose lithological packages in the Iterlak belt. The main ultracataclasite (Fig. 6f) is located some 10-15 m into the footwall of this outcrop.*

D2: The second deformation phase finds its main manifestation in the refolding of earlier D1 structures by NE-trending, SW-plunging folds (F2) that have affected the entire supracrustal sequence as well as wall-rock gneisses outside the belt. F2 folds at Iterlak show an almost identical orientation to those mapped at Nuuluk. The largest of these folds is a synformal structure in the central-eastern parts of the belt, showing a half-wavelength of ca. 1.5 km. This fold largely determines the overall synformal geometry of the belt (Fig. 5). A smaller first-order antiform-synform pair with half-wavelengths of between 700 and 200 m is developed towards the W. The F2 folding event has affected all rocks, expressed by the close-to tight folding of the layered sequence on all scales and the tight crenulation of earlier fabrics (Fig. 8a). This includes the D1b-related alteration, also suggesting that the main phase of retrogression and carbonate alteration causing the knobbly weathering of greenstones has a pre-D2 timing. F2 folding is associated with an axial planar foliation (S2) (Fig. 8b). The S2 foliation is steep, showing both NW and SE dips. NW dips and SE vergence of folds dominate in the W part of the belt, but folds become more upright, showing even NW vergence in the E parts of the belt. The lack of a regionally prominent and consistent vergence of D2 structures in Iterlak differs from the structural pattern at Nuuluk, where D2

structures show a very pronounced SE vergence. A prominent intersection lineation between bedding (S0) and S2 plunges at moderate angles to the SW, parallel to F2 fold plunges.

TTG-greenstone contacts

The contacts between the main supracrustal belt and the TTG terrain are sharp and clearly tectonic, marked by highly-foliated chlorite schists or serpentinites in the greenstones.

In the W, the Iterlak belt is structurally overlain by foliated and banded TTG gneisses along a moderate- to steep W- to NW-dipping contact (Fig. 5). The high-strain nature of this contact is illustrated by the isoclinal folding and transposition of greenstones slivers, intrusive TTG apophyses and pegmatites over a width of at least 50-80 m along this contact. Shear sense indicators and the vergence of folds indicate to-top-the-SE kinematics, in which the gneisses have been thrust over the greenstones. This agrees with a prominent, down-dip mineral stretching lineation on foliation planes. On a broader scale, however, TTG gneisses along this W contact are riddled with greenstone fragments, ranging in size from minute inclusions to several tens of metre wide fragments that can be followed for hundreds of metres along strike. It would appear that the greenstones represent xenoliths within intrusive TTG's, but the commonly flattened fragments have invariably been rotated into parallelism with the TTG gneissosity, so that primary contact relationships are ambiguous. The fragments are almost invariably amphibolites, but their margins and contacts against the enveloping TTG's are mostly retrogressed to chlorite schists (Fig. 8c). These retrogressed margins are commonly not wider than 25-30 cm.

The E margin of the Iterlak belt against the TTG gneisses is exposed along a steep cliff. The contact trends NNE, and shows both steep NW as well as SE dips. This suggests that the greenstones structurally overlie TTG gneisses, but that this contact is, in places, overturned (Fig. 5). Folds show moderate SW plunges and are upright or verge to the NW, associated with a steep SE dipping axial planar foliation (S2). Contacts between the main Iterlak belt and the surrounding TTG's are sharp and tectonic, but the actual contact zone is several hundred metres wide, characterised by the imbrication of greenstone slivers with the TTG gneisses. As is the case along the E contact, greenstones are mainly at amphibolite grades, but variably retrogressed along anastomosing brittle-ductile shear zones and foliation planes (Fig. 8d, e). Deformation in the gneisses is mainly brittle and characterised by either pervasive cataclastic textures in the gneisses or networks of cataclasites and breccias. Shear sense indicators are mainly preserved in the supracrustal sequence. S-C fabrics indicate mainly top-to-the-(S)E thrust kinematics along NW dipping contacts (Fig. 8f). In places, a dextral strike-slip component is indicated in addition to the thrust-sense of shear.

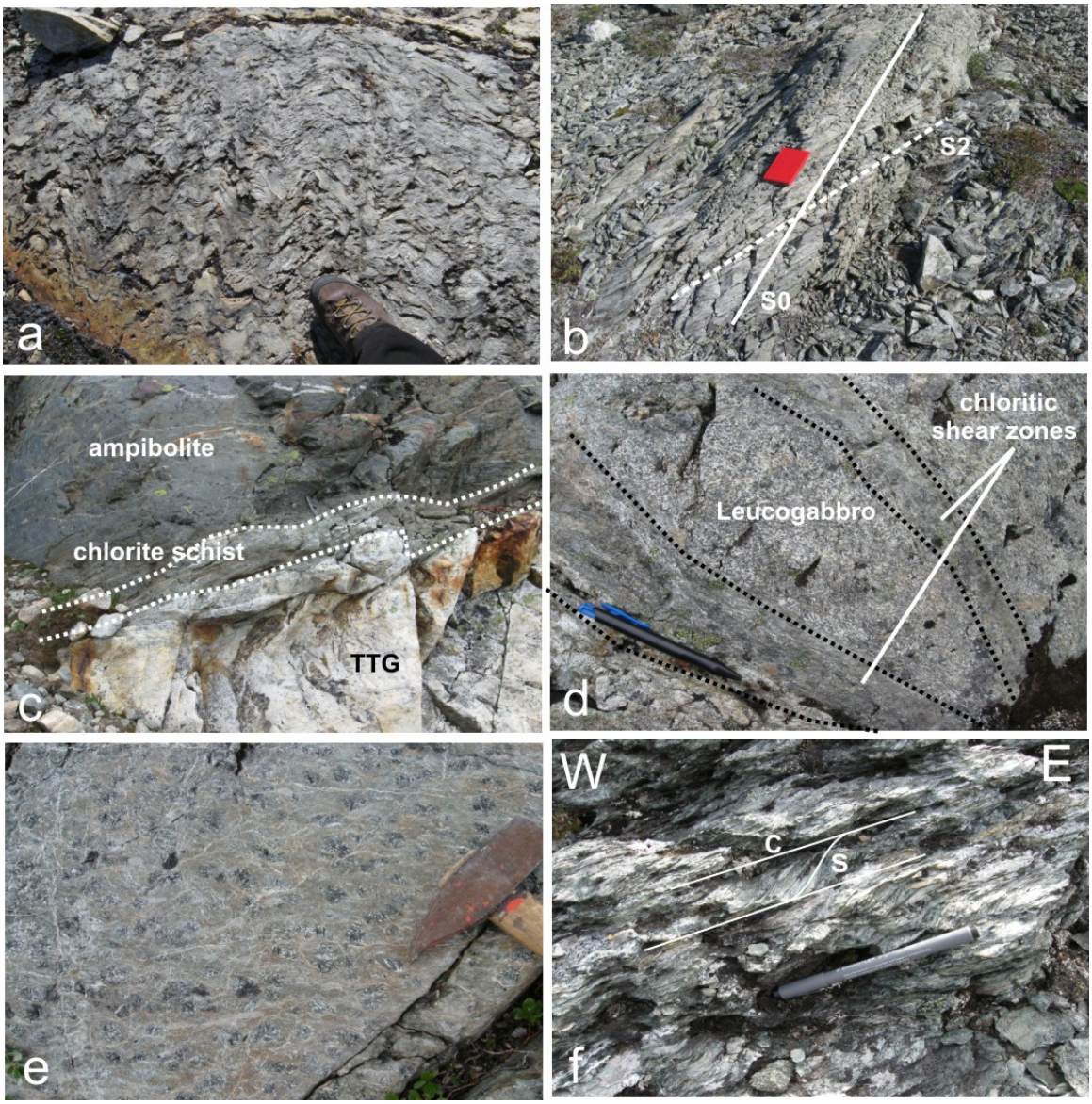

Figure 8. *(a) F2 crenulation folding of earlier S0/S1 and D1b related alteration. F2 folds show consistent SW plunges (Upper Zone, UZ); (b) Intersection of S0/S1 and S2, resulting in pencil cleavage-type weathering (UZ); (c) Contact zone between a greenstone xenolith and TTG gneisses in the W hangingwall of the Iterlak belt. Note that the 'greentones' are at amphibolite grade, showing a narrow, retrogressed margin of chlorite where they are in contact with the TTG's; (d) Relatively unaltered pod of leucogabbro enveloped by retrograde, chloritic shear zones, forming a regional-scale pattern of anastomosing, retrograde faults and shear zones (Lower Zone, LZ); (e) pervasively retrogressed gabbroic rock, made up of relics of fresh pyroxene (black) in a chloritic matrix (green) and enveloped by a network of carbonate veins (white); (f) S-C fabrics (annotated) in chlorite schist 1 m above the E greenstone-TTG contact, indicating top-to-the-E thrust sense of movement.*

Sioralik

The Sioralik belt is located to the S of the Sermiligaarsuk Fjord, measuring ca. 4 by 4 km (Fig. 1). In contrast to other belts of the Tartoq Group, Sioralik is, for the most part, made

up of high-grade supracrustals. In-situ partial melting and garnet-clinopyroxene assemblages in amphibolites are widespread and testify to the, at least, upper amphibolite-facies conditions of metamorphism. Van Hinsberg et al. (2010) determined peak P-T conditions of P > 6-7 kbar and T ca. 850°C. Although a greenschist-facies retrogression of the rocks is common, it is mainly localized along the margins of the Sioralik block against the TTG gneisses. Within the belt, the retrograde overprint is largely confined to relatively narrow (5-15 m wide) high-strain zones marked by chlorite schists. Both the structural foot- and hangingwall of the belt are well preserved, in contrast to the other belts where only the footwall seems exposed. Similar to other belts of the Tartoq Group, the Sioralik supracrustals are also preserved in a F2 synclinorium, with moderate E dips in the W and steep- to overturned, both W and E dips in the E (Fig. 9).

The sequence at Sioralik seems to define a broad stratigraphy (Fig. 9). The western and structurally seemingly lower parts of the belt are made up of a well-bedded and, in places, finely- laminated sequence of amphibolite-facies, metasedimentary and/or volcaniclastic rocks with intercalated ortho-amphibolites, reaching a thickness of ca. 100 - 150 m. The volcanosedimentary succession is structurally overlain towards the E by a 200-300 m thick succession of interbedded amphibolites, metagabbros and lenses and/or laterally extensive horizons of ultramafic rocks. The latter are mainly serpentinites or talc-carbonate schists. Van Hinsberg et al. (2010) interpret this sequence as a section through Archaean oceanic crust, which would suggest that the succession at Sioralik is, in its current position, overturned.

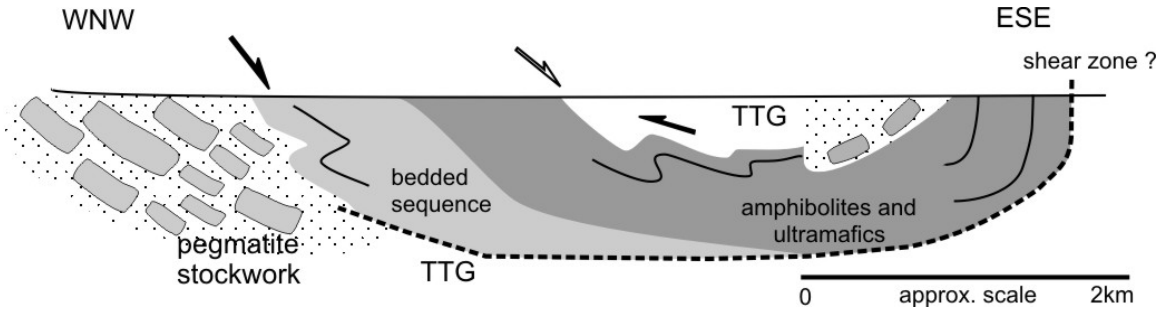

Figure 9. *Schematic cross-section through the central parts of the Sioralik belt. Note that large parts of the belt have been pervasively intruded by pegmatites and leuco-granites. Black arrows indicate the vergence and likely kinematics of high-grade structures (D1a and b), open arrow indicates the kinematics of retrograde fabrics along the upper greenstone granite contact.*

Structural geology

Bedding is clearly indicated by compositional and pronounced colour variations in metasedimentary succession, but also in layered ortho-amphibolites, ranging from mm-wide laminations to dm- thick beds (Fig. 10a). In the W parts of Sioralik, prominent packages of what is interpreted to represent volcaniclastics or sediments can be followed for several hundred metres without any significant structural disturbance, indicating that the sequence is, in large parts, intact.

D1: D1-related fabrics and structures formed under amphibolite- and/or granulite-grade conditions. A pervasive bedding-parallel foliation (S1) is defined by the grain-shape preferred orientation of biotite and amphibole. In places, S1 is accentuated by the presence of thin, foliation-parallel quartzo-feldspathic leucosomes. Garnet aggregates rimmed by plagioclase overgrow the S1 foliation and retain their round to ovoid shapes (Fig. 10b). Intrafolial, isoclinal folds (F1a) are present, particularly in the well-layered metasediments (Fig. 10c), but large-scale recumbent nappes in the greenstone sequence, such as at Iterlak, could not be identified.

Throughout the belt, S0/S1 has been refolded by NE-trending and plunging folds (F1a). Fold wavelengths range from decimetre to tens of metres and fold shapes vary from open and moderately inclined to tight and recumbent Tight F1a folds are associated with an axial planar foliation (S1b) that shows both NW and SE dips. F1a folding formed under peak-metamorphic conditions as is indicated by (1) the common localization of in-situ partial melts in F1a fold hinges (Fig. 10d) and (2) an axial planar foliation, S1a, defined by e.g. the preferred orientation of amphibole in layered amphibolites. The folds are associated with an intersection lineation (L2i: S0/S1) and a stretching lineation (L1m), both of which are parallel to the fold axes. F1a folds are particularly prominent close to the lower and upper contacts between the Sioralik supracrustals and gneisses or pegmatites. Importantly, F1a folds in the structural foot- and hangingwall verge in opposite directions (Figs. 9 and 10e, f). Fold vergence is to the E and SE close to the base of the succession in the finely laminated rocks along the W contact. In contrast, folds verge to the W and NW close to the upper contact of the supracrustals against the gneisses in e.g. layered amphibolites in the central parts of the belt (Fig. 10e, f). In the structural footwall of Sioralik, m-scale S-C' fabrics (*extensional shear bands*) are common, indicating top-to-the-SE kinematics, consistent with the SE vergence of F1a folds in this area (11a, b). The shear bands affect amphibolites, are not associated with a retrogression of the rocks and appear to have formed during high-grade metamorphism.

D1b structures overprint D1a structures and are commonly defined by brittle and brittle-ductile fabrics and greenschist-facies assemblages that replace the widespread high-grade assemblages. The most common manifestation of the D1b deformation is highly-foliated chlorite schists and/or cataclasites (Fig. 11c, d). The most prominent of these is located at the hangingwall contact of the Sioralik supracrustals against the overlying TTG gneisses (see above). Importantly, the top-to-the-SE kinematics recorded by S-C' fabrics along this contact indicate the reversal of shear compared to that indicated by the NW vergence of F1b folds immediately below this contact and in high-grade amphibolites (Figs. 11c, d, and see below).

D2: The regional synformal structure in which Sioralik is preserved is also interpreted to have formed during D2 (D2 late), forming a NNE rending, doubly-plunging synform, resulting in the overall keel-like structure.

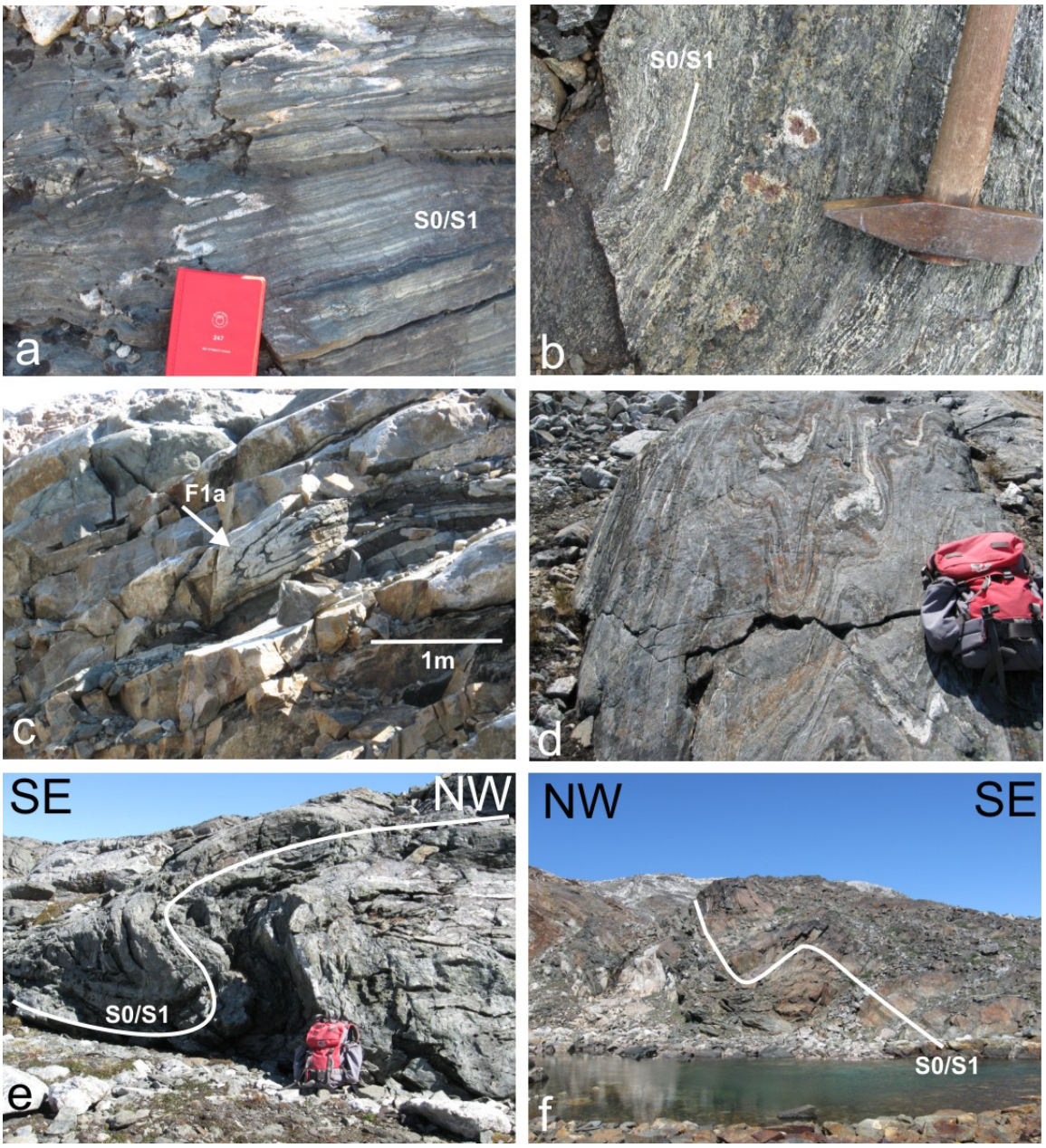

Fig. 10: *(a) Bedding is indicated by mm- to cm- scale compositional variations, particularly in the western parts of Sioralik, and interpreted to be underlain by a volcaniclastic an/or sedimentary succession. Note the tightly folded cross-cutting aplite vein that gives an indication of the strain the rocks have experienced; (b) Plagioclase-rimmed garnet porphyroblasts are common in parts of the amphibolitic sequence. Here, the porphyroblasts overgrow the foliation; (c) Isoclinal F1a fold in bedded supracrustals, testifying to the partial transposition of the sequence; (d) Leucosomes contained in F1a fold hinges of banded amphibolites. The presence of green clinopyroxene and garnet in the leucosomes and immediately adjacent wall rocks suggests the in-situ generation of the melts and only small-scale segregation into the hinge zones; (e) Shallowly-plunging, SE-verging F1a folds are common in the western, structurally lower parts of Sioralik; (f) Shallowly NW-verging folds dominate in the structurally higher section of Sioralik, developed in the central parts of the belt and mainly in mafics and ultramafics. Note: in the far background and underlying the central, large-scale pegmatite stockworks brecciating the supracrustals form the structural top of the Sioralik belt.*

TTG-greenstone contacts

The western contact of the Sioralik block is made up of a > 1 km wide intrusive stockwork in which quartz-feldspar ± muscovite pegmatites intrude and brecciate the well-banded greenstones (Figs. 9 and 11c, d). The pegmatites may constitute > 80% of individual outcrops, but large xenoliths of the Tartoq Group describe a ghost stratigraphy with no or only minor rotation of the angular wall-rock xenoliths. Much of the intrusive sequence shows N and NW trends and moderate E and NE dips, parallel to the main part of the Sioralik block to the E. The actual contact between the main Sioralik belt and pegmatites is sharp, although numerous and up to 50 m wide pegmatite dykes and sills are intrusive into the belt and can be seen to be connected to the underlying pegmatite stockwork. The pegmatites may sharply cross-cut the supracrustal succession at high angles, but pegmatites are also folded and/or boudinaged and even transposed (F1a) into the bedding-parallel foliation (S1). This suggests a protracted emplacement history and the largely syn-tectonic intrusion of pegmatites (syn- to late D1, pre D2). The eastern contact of Sioralik with the surrounding TTG terrain is sharp. This contact is dominated by highly sheared, mylonitized and transposed, subvertical amphibolites.

Deformation in the TTG gneisses to the immediate E is, in contrasts brittle-ductile, characterised by abundant, steeply-dipping and contact-parallel cataclasite zones that can be recorded over a width of several hundred metres. The absence of the prominent metasedimentary pile forming the W parts of Sioralik along the E contact also suggests that the footwall contact may have excised the sequence and possibly along these cataclasite zones.

The upper contact between the greenstones and overlying pegmatites and TTG's is exposed in the central parts of Sioralik, mapped on regional maps as a klippen structure made up of a central gneiss klippe surrounded by underlying supracrustals (see also above). This contact is very sharp in the N (Fig. 11c). It is marked by the presence an up to 25 m thick unit of highly foliated chlorite schist that overprints upper-amphibolite facies metamafic rocks in the immediate footwall. The structural hangingwall is made up of cataclastically deformed leucogneisses. The actual contact between the supracrustals and the gneisses is knife-sharp and marked by a 20cm wide ultracataclasites (Fig. 11c). S-C' fabrics are common in the chlorite schists and indicate top-to-the-SE kinematics in their present orientation (Fig. 11d). The southern extent of this contact is somewhat diffuse and rather developed as an intrusive breccia, very similar to the W contact and structural footwall, in which massive pegmatite sills and subordinate dykes intrude and brecciate the greenstone sequence with no clear upper contact exposed.

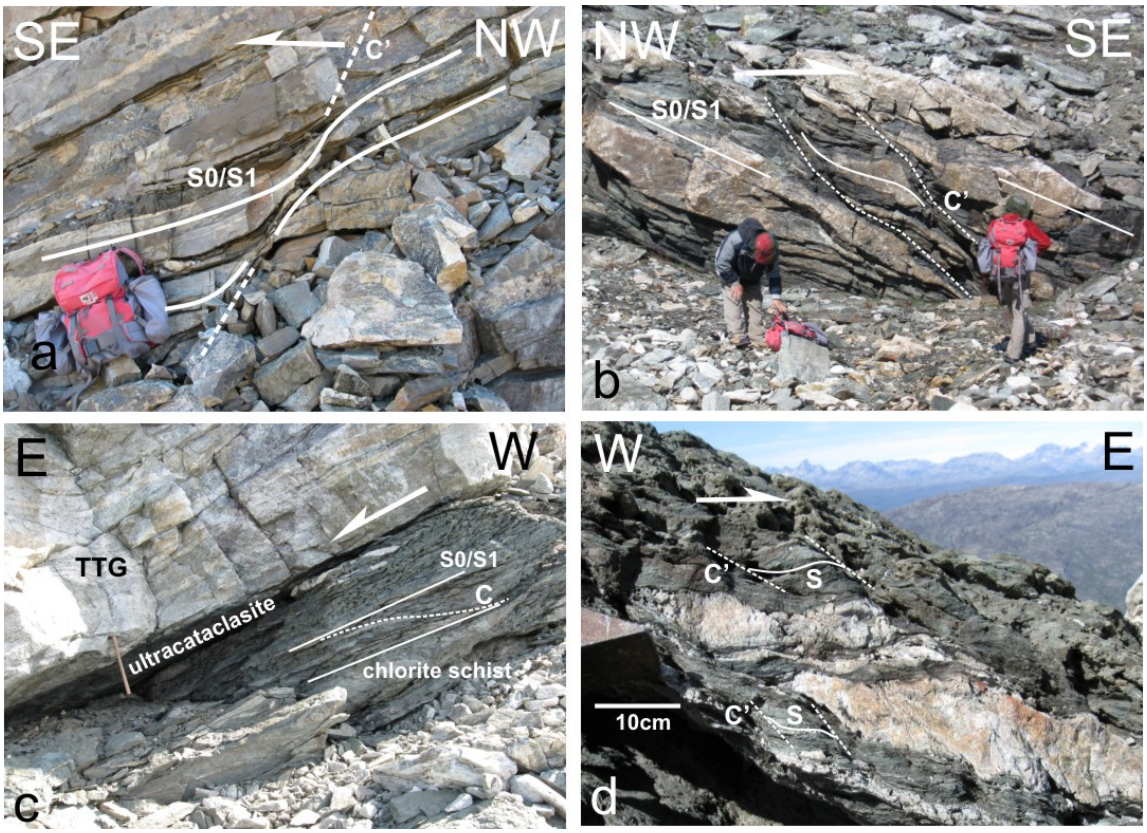

Figure 11. (*a) Metre-scale extensional shear bands (S-C') in bedded metasediments in the central-western parts of Sioralik are common, consistently indicating top-to-the-SE kinematics; (b) Similar shear bands as in (a). (c) Knife-sharp contact between chlorite schists of the Sioralik belt and TTG gneisses. The chlorite schist package forms a ca. 25m thick unit retrogressing upper-amphibolite facies amphibolites in the footwall of this structural hanging-wall contact. S-C and S-C' fabrics (in (d)) are common in the schists and consistently indicate top-to-the-SE kinematics. Note that this sense of displacement is exactly opposite to what is indicated by e.g. the vergence of F1a folds at this structural level, formed at higher grades. TTG gneisses are strongly cataclastic and brecciated.*

Midternæs N

Midternæs N is the largest supracrustal belt of the Tartoq Group, measuring ca. 12 by 4 km, located N of the Sermiligaarsuk Fjord. Unlike the N- to NE-trending belts of Nuuluk, Iterlak and Sioralik that have been preserved in km-scale F2 synclinoria, Midternæs N and rocks within the belt show ENE trends and steep- to subvertical dips throughout.

Lithological inventory

The lithological inventory of Midternæs N is similar to that of the other belts. The rocks also show greenschist-facies grades, but there is clear evidence for originally higher metamorphic grades with locally preserved amphibolite-facies assemblages. The sequence is dominated by massive flows of probably basaltic origin. Contacts between individual flows are commonly well preserved, although carbonate alteration and the associated knobbly weathering of rocks recorded at e.g. Nuuluk and Iterlak has pervasively overprinted primary

textures. In places, pillow textures are well preserved (A. Polat, pers. comm.), testifying to the origin of at least parts of the layered succession as submarine basalts. Ultramafic rocks include serpentinites and talc-carbonate schists that occur as elongated lenses and pods. The ultramafic rocks are commonly zoned, showing highly-sheared and retrogressed margins against the wall rocks and more massive central parts that preserve original textures. Brownish weathering carbonates occur as layer-parallel stringers and horizons or as massive pods, several tens of metres in diametre (Fig. 12a). Contacts between the carbonate rocks and wall rocks are commonly gradational and carbonates progressively replace the original wall rocks along foliation planes and/or S-C planes, ultimately resulting in near massive carbonate bodies in the centre of the pods (Fig. 12b). This strongly suggests a hydrothermal origin of the carbonates and the syn- D1b/ D2 timing of alteration and fluid flow.

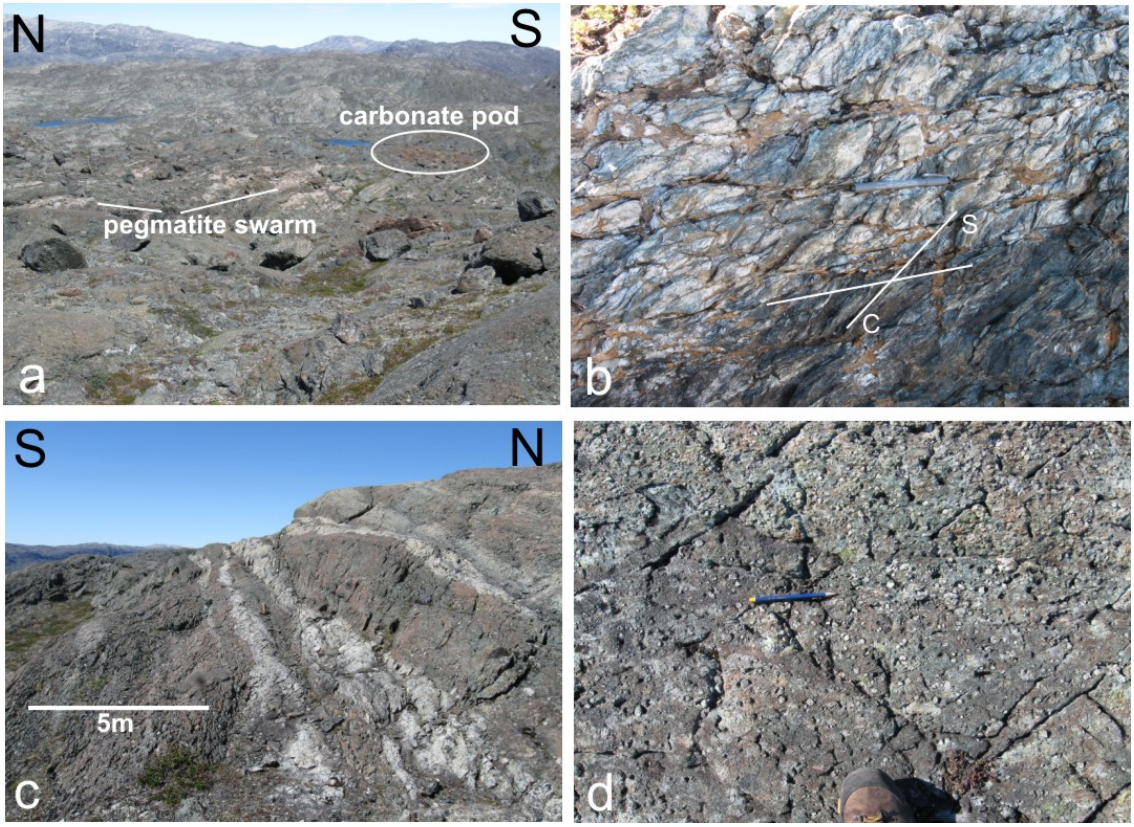

Figure 12. *(a) Regional view across the central-northern parts of Midternæs illustrating the occurrence of massive carbonate pods (brownish weathering) and layer-parallel pegmatite clusters; (b) S-C fabric development in talc-carbonate schist. Dextral strike-slip kinematics prevail throughout the belt. Note the lining of S and C planes with brownish weathering carbonate; (c) bedding-parallel clusters of pegmatites occur throughout Midternæs N. The pegmatites are almost invariably deformed, indicating a syn- to late tectonic timing of emplacement; (d) Cataclasite – note the large angular- to rounded feldspar clasts set in a fine-grained chloritic matrix. The occurrence of feldspars suggests that the protolith of the cataclasite was a pegmatite. Many of these rocks had previously been mapped as 'pyroclastics' in regional and company maps.*

In contrast to Nuuluk and Iterlak, but similar to Sioralik, Midternæs N is intruded by abundant pegmatites. The leucocratic quartz-feldspar pegmatites occur as isolated, mainly layer- concordant or gently cross-cutting sills and/or dykes or swarms of closely spaced sills and dykes (Fig. 12c). Individual pegmatites are between 0.2 to 10 m wide. The majority of pegmatites has been deformed and is either affected by a brecciation and cataclastic deformation and/or folding and boudinage. Field work suggests that pegmatites formed a volumetrically much more significant component in Midternæs N. However, the pervasive cataclastic deformation and growth of chlorite in the finer-grained matrix of cataclasites has largely obliterated their original distribution and extent (Fig. 12d). In fact, areas that have been mapped as 'pyroclastic rocks' on existing maps, based on the occurrence of large, rounded feldspars in a chloritic matrix probably all represent broad cataclasite zones (Fig. 12d). The northern margin of Midternæs N is developed as an intrusive breccia over a width of at least 1 to 1.5 km. The breccias result from the intrusion of TTG's into greenstones, and large areas of the greenstone belt are, in fact, agmatitic breccias. The actual margin of the greenstone belt is taken, where greenstones only occur as isolated rafts in leucogcratic TTG's (Fig. 13a).

Structural geology

Greenstones at Midternæs N trend ENE and dip steeply to the NW and SE. The layering contains tight folds on a variety of scales with half wavelengths ranging from dm to > 100m (Fig. 13b). This fold generation is here referred to as F1b, although a direct correlation with similar folds in the other belts is not possible. This also suggests that the sequence at Midternaeas N belt has been structurally duplicated and the stratigraphic correlation of units is tentative at best. In outcrop, the folds show an axial planar foliation, which is subparallel to bedding S0 (Fig. 13b). An earlier fold generation is represented by sheath-fold like structures (Fig. 13c) that only seem to be preserved in higher-grade rocks, mainly amphibolites, along the N margin of the greenstone belt, where it has been intruded by TTG's. These structures (F1a) refold an earlier layering/foliation and are refolded by the ENE-trending F1b folds. The plunge of the cone axes of the sheath folds is to the SW. Talc – carbonate schists, in particular, preserve well-developed S-C and S-C' fabrics pointing consistently to detxtral strike-slip kinematics along the subvertical, ENE-trending sequence (Fig. 13d). Carbonate alteration can be seen to be introduced along these shear zones, progressively replacing the shear fabrics. The most pervasive deformation is related to the formation of cataclasites that affect up to 100 m wide corridors throughout the belt (Fig. 12d).

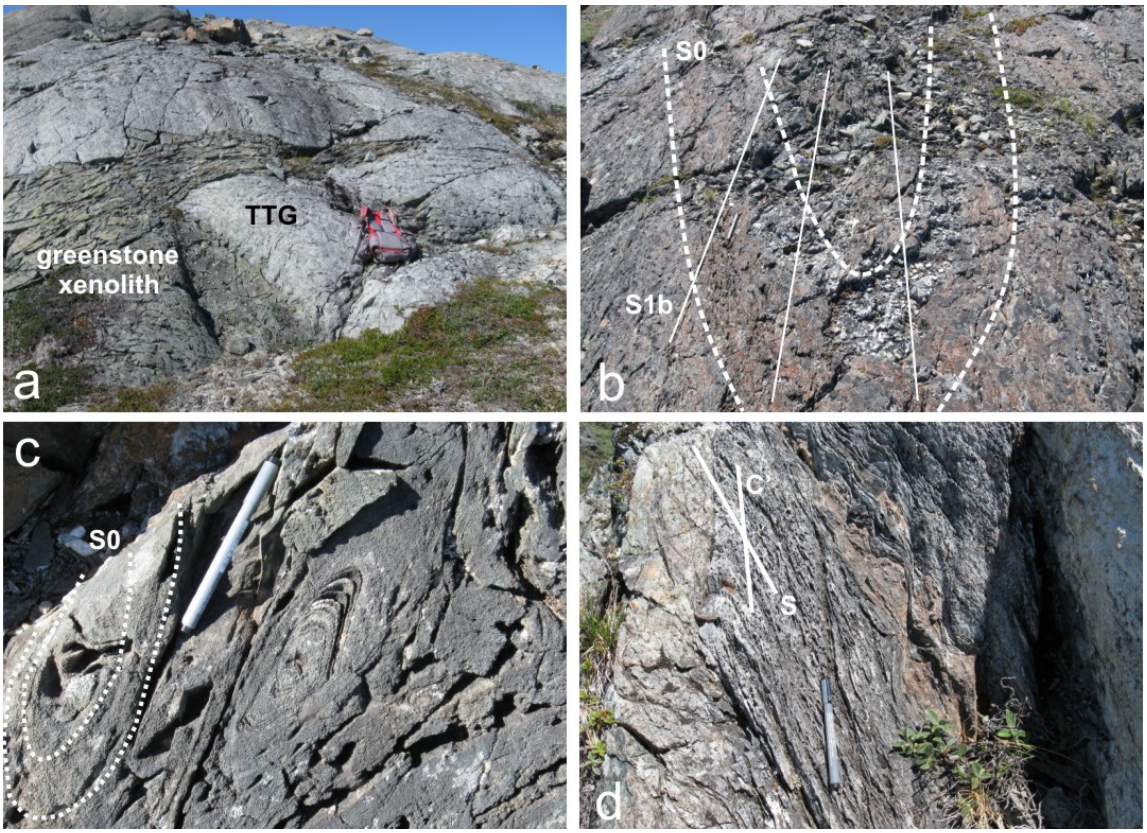

Fig. 13: (*a) Intrusive breccia of leucocratic TTG into greenstone. These intrusive breccias form an > 1.5 km wide zone along the northern margin of Midternæs; (b) Tight- to isoclinal folds (F1b) refold the supracrustals and probably result in a significant duplication of the sequence. Folds occur on all scales, from m-scale (this photo), to the half-wavelengths of hundreds of metres; (c) Small-scale sheath folds (here termed F1a) are common in amphibolite-facies rocks along the northern margin of Midternæs that have escaped later retrogression and deformation. Central sheath fold (to the right-hand side of pen) is juxtaposed against another sheath fold (folded S0 annotated) to the left of the pen; (d) S-C' fabrics (annotated) are common in less competent talc-carbonate schists, consistently pointing to dextral strike-slip kinematics along the ENE trending rocks of Midternæs.*

Discussion: models for the emplacement of the Tartoq Group

Several observations can be made and inferred from the structural reconnaissance mapping:

1. The supracrustal belts of the Tartoq Group are mainly made up of metavolcanic rocks. Basaltic flows (sensu lato) are, by far, the dominant rock type. Ultramafic rocks include mainly serpentinites and talc-carbonate schist, which form a volumetrically significant component in e.g. Iterlak and Sioralik. Probable interflow sediments and/or volcaniclastics are volumetrically very subordinate. Overall, the lithological inventory of the Tartoq Group suggests that the rocks represent relics of oceanic crust. A detailed petrographic and geochemical characterization of the rocks is prepared by Szilas (in prep.).
2. In their present position, the supracrustal belts are preserved in infolded synclinoria (F2) (see also Higgins 1968). There is evidence in the E parts of Nuuluk and, in

particular, at Sioralik that suggest that parts of the greenstone slivers contain overturned strata, forming part of large, regional-scale nappe structures.

3. Despite their considerable outcrop widths of several kilometres, the original and true thicknesses of all of the greenstone belts must be considered to be significantly less and probably in the order of only a few hundred metres (300-500 m), certainly less than 1 km. The apparent thickness is due to the early imbrication and isoclinal folding (D1a/b) of lithologies, resulting in the structural duplication of the greenstones, and later refolding into near-upright to SE-verging, shallowly-plunging F2 folds.
4. The supracrustal belts record a wide range of P-T conditions from lower- and mid-greenschist facies conditions (Nuuluk, and partly in Iterlak and Midternæs N) to upper-amphibolite and lower-granulite grades in Sioralik (e.g. Van Hinsberg et al., 2010). All of the lower-grade supracrustal belts contain variably preserved evidence of originally higher metamorphic grades. Irrespective of their original peak-metamorphic grades, the greenstones have uniformly undergone a greenschist-facies retrogression. Importantly, high-grade (D1a) and retrograde (D1b and D2) fabrics are largely coaxial, suggesting that burial (D1a) and exhumation (D1b) were part of one progressive deformation path. Different peak P-T conditions point to different burial conditions, but similar retrograde conditions indicate the final emplacement and exhumation of the greenstone slivers to similar upper-crustal depths (< 10-12 km) where the belts are now juxtaposed against each other.
5. Deformation along the bounding, but also internal shear zones point to dominantly top-to-the-SE thrust kinematics. High-strain fabrics in top-to-the-SE cataclasites and chloritic shear zones (D1b) are mainly characterised by extensional fabrics (cm- to m-scale S-C' fabrics and/or synthetic normal faults. The well preserved normal faults in the hangingwall of D1b cataclasites in Iterlak (Fig. 7) show top-to-the W kinematics in their pre-D2 orientation. All this agrees with the progressive retrograde overprint of fabrics, i.e. the D1b deformation is associated with the progressive exhumation of the supracrustals to shallower crustal levels.
6. Both the structural hanging and footwall of a supracrustal belt are only preserved in Sioralik. Structural as well as lithostratigraphic relationships point to the fact that the preserved parts of Sioralik represent the erosional relic of an overturned limb of a recumbent nappe (Fig. 14). In this scenario, the present hangingwall of the greenstone sequence would, in fact, represent the structural footwall of the supracrustal sequence against underlying TTG gneisses (Fig. 14). This is consistent with (a) the opposite vergence of F1a folds at the top and the bottom part of the succession, and (b) the occurrence of the well-bedded volcanosedimentary sequence structurally below the mafic and ultramafic dominated succession at Sioralik. Importantly, the NW vergence of F1a folds in the mafic sequence is opposite to the top-to-the-SE kinematics preserved by S-C' fabrics in retrograde greenschists along the greenstone-TTG contact (Figs. 10e, f and 11c, d). This may reflect the initial burial (subduction) of the supracrustals (Fig. 14b), followed by return flow and exhumation of the rocks in the subduction channel (Fig. 14c).

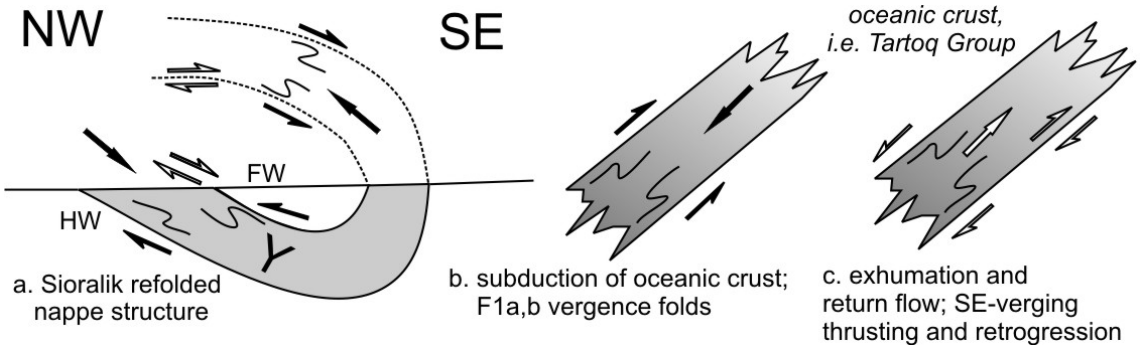

Figure 14. *(a) Simplified section of the Sioralik belt, showing the main structural features (vergence of high-grade structures (solid arrows) and retrograde structures (open arrow) as well as presumed younging direction (Y); the full arrows indicate the polarity of subduction prior to refolding; HW: hangingwall, FW: footwall; (b) schematic sketch showing a section of the downgoing plate and associated formation of D1a structures in the supracrustals during NW-direction subduction, i.e. prior to exhumation and refolding; (c) schematic sketch showing the exhumation path of the oceanic slab and associated development of structures during SE direction extrusion and return flow in the subduction channel. The structures recorded in Sioralik (shown in a) are in agreement with structures that could be expected during the burial (in b) and exhumation (c) of the rocks and the progressive refolding of the structures in a SE-facing (extruding) nappe. Similar scenarios have been described for recent scenarios in subduction zone channels such as the Alps or Oman (e.g. Searle et al., 2004; Agard et al., 2009)*

7. There is unambiguous textural and mineralogical evidence for partial melting of amphibolites in the high-grade parts of Sioralik, including in-situ leucosomes and the presences of peritectic phases such as garnet and clinopyroxene associated with the quartz-feldspar leucosomes (Fig. 10d). This represents a very rare case where in-situ melting of mafic, in all likelihood, Archaean oceanic crust can be demonstrated in outcrop. These outcrops must be considered critical for Archaean plate-tectonic models since they may illustrate processes of in-situ slab melting of subducting oceanic crust (see also below).
8. The close association and intrusion of TTG's and pegmatites into and along the Tartoq Group appears to be critical for the exhumation of the supracrustals. Agard et al. (2009) recently reviewed the exhumation mechanisms of oceanic crust in subduction zones. They concluded that the exhumation of negatively buoyant oceanic crust due to return flow in the subduction channel is far less likely compared to e.g. the exhumation of buoyant continental crust or sediments, the latter of which are by far the most dominant components of HP terranes. In fact, relics of oceanic crust are only expected to be returned if they are associated with more buoyant material such as hydrated serpentinites or enveloped in sedimentary mélanges, where they form isolated blocks or slivers. Moreover, the detachment of slivers of oceanic crust from the downgoing slab is unlikely to be a continuous process, but rather fortuitous both in space and time (e.g. Agard et al., 2009, 2010). These observations from recent subduction zone environments have two implications for the evolution of the Tartoq Group. Firstly, the metamafic sequence is almost invariably intruded by synkinematic TTG's and/or pegmatites. The Sioralik block, in particular, has been extensively intruded by syn- to late- tectonic pegmatites not only along its contacts, but pegmatites also form extensive stockworks within the belt. The intru-

sion of the leucocratic melts have most likely contributed to the buoyancy of the oceanic slivers during the earlier stage of burial and/or exhumation. The greenschist-facies retrogression of the mainly mafic sequence and the associated hydration and carbonatization of the rocks has probably assisted the buoyancy-driven exhumation, but this has occurred only during the later stages and once the rocks were already on their exhumation path. Secondly, the probably rather accidental separation of oceanic slivers from the subducting slab means that different supracrustal slivers of the Tartoq Group may not share a common origin and preserve, for instance, (1) different levels of the oceanic crust, or remnants of an oceanic plateau, or mid-ocean ridges, that (2) may only show broadly similar ages and are not necessarily related to the same stage of subduction or crust formation. This is consistent with suggestions by e.g. Nutman et al. (2004) who indicated that the Tartoq Group S and N of the Sermiligaarsuk Fjord may consist of differently aged supracrustal successions.

9. Most greenstone belts, except for possibly Sioralik, have experienced a near-pervasive fluid infiltration during their exhumation. The brittle-ductile conditions of deformation (i.e. regionally developed cataclasites) have most likely assisted this pervasive fluid flow. The ubiquitous chloritization of cataclastically deformed, even leucocratic TTG's or pegmatites suggests that fluid infiltration was associated with a pronounced metasomatism, particularly of Fe and Mg. The structural controls of Au mineralised vein systems by D1b shear zones suggest that Au was introduced during this exhumation stage and fluid infiltration. Economic-grade Au mineralisation is considered to be preferably focused into second-order ductile-brittle structures, such as the footwall of the main central thrust zone at Nuuluk.

Towards a tectonic model

The field and mainly structural observations presented in this report provide evidence that can be used to describe a broad structural evolution and possible geotectonic setting for rocks of the Tartoq Group. Detailed P-T-t and geochronological work is in progress and should help to place tighter constraints on this tentative model, while geochemical and isotope geochemical data should shed light on the origin of the Tartoq Group.

Stage 1: Formation of the Tartoq Group

The dominance of basaltic lavas, mainly sills, associated ultramafic rocks and possible volcaniclastics and sediments suggest that the rocks formed in an oceanic environment. However, details as to the origin of the Tartoq Group and different components of the supracrustals must remain speculative in this report. A Neoarchaean age (> 2944 Ma) of formation is indicated by U-Pb zircon ages of a supposedly intrusive TTG into the greenstones (Nutman & Kalsbeek 1994).

Stage 2: Burial and subduction

Metamorphism of the Tartoq Group indicates the burial of the supracrustals. Metamorphic parageneses commonly define pervasive fabrics (S1a, F1a), indicating that this metamorphism occurred in a dynamic setting. The vergence of folds (F1a and, to a certain extent, F1b) is particularly informative and may hold clues as to the structural setting and kinematics of this burial. F1a folds, as defined here, affect higher-grade fabrics and contain axial planar foliations defined by commonly amphibolite-facies assemblages. These folds are

interpreted to be associated with either the burial of the Tartoq Group or, at least, the early stages of exhumation. Where both the structural hanging- and footwalls of the Tartoq Group are exposed (e.g. at Sioralik), F1a folds verge in opposite directions along the upper and lower contacts (Figs. 10e, f and 14). In all other cases, where only the structural footwall of the belts is exposed, the folds show a consistent vergence to the SE, although later D2 folds may result in the reorientation of folds. The D1 deformation also results in the imbrication of supracrustal packages of possibly different origin or crustal level (i.e. Lower and Upper Zone units in Iterlak) and, in the process, the formation of a first generation of large-scale nappes (part of F1a). The burial and imbrication of supracrustal units is interpreted to have occurred along a W- to NW-dipping subduction zone (Fig. 15a). This scenario is compatible with the presence of overwhelmingly SE-verging F1 structures, the presence of high-grade S-C' fabric in e.g. Sioralik (Figs. 11a, b), the opposite vergence of F1 folds along the upper and lower contact of Sioralik (Fig. 14) and the imbrication of units along low-angle shear zones (D1a) and formation of associated nappes (F1a). Different peak-metamorphic conditions recorded in the greenstone slivers point to the fact that different levels of the subducted slab were detached from the downgoing slab and subsequently exhumed by return flow in the subduction channel (Fig. 15b). At Sioralik, in-situ partial melting of the amphibolites can be observed. Initial estimates of the P-T conditions point to partial melting at P > 6-7 kbar and T ca. 850° C. Although pressure conditions are not well constrained at this stage, P-T conditions point to unusually high apparent geotherms if a subduction environment is assumed. This may reflect (1) subduction of already hot oceanic crust, and/or (2) the intrusion of synkinematic leucocratic melts and associated advective heating. Both features are likely to have resulted in shallow subduction (Fig. 15). The thickness of the supracrustal slivers of the Tartoq Group is about 300-500m for the different greenstone belts, which is entirely within the range of oceanic slivers typically exhumed along subduction zones (0.1-1km, e.g. Agard et al., 2009).

Stage 3: Exhumation and retrogression

Shallow subduction is inevitably associated with high-shear stresses at the interface between the downgoing and the overriding plate. In this zone, slivers of the downgoing plate may be detached and returned against the subduction direction in the subduction channel ("subduction extrusion", Searle et al., 2004; Agard et al., 2010). This process is mainly buoyancy driven, which also explains the scarcity of oceanic crust in HP and UHP terrains worldwide. Structures (D1b) formed during this time are compatible with SE-directed exhumation of the slivers of the Tartoq Group during NW-directed subduction. The model implies that the structural footwalls of the slivers are bounded by thrusts recording, in the case of the Tartoq Group, top-to-the-SE kinematics. The hangingwall, in contrast, should show the formation of normal faults and top-to-the-NW shearing that accommodates the exhumation and accretion of the slivers to the base of the overriding plate. The true hangingwall of the greenstone slivers is only exposed in the W parts of Sioralik, which, in turn is intruded by pegmatite stockworks, so that original structural relationships may be obscured. Top-to-the-W kinematics during D1b normal faulting is, however, well preserved in Iterlak (Fig. 7). Moreover, all greenstone belts record extensional structures during the exhumation-related D1b deformation and ubiquitous S-C' fabrics and extensional shear bands (all belts).

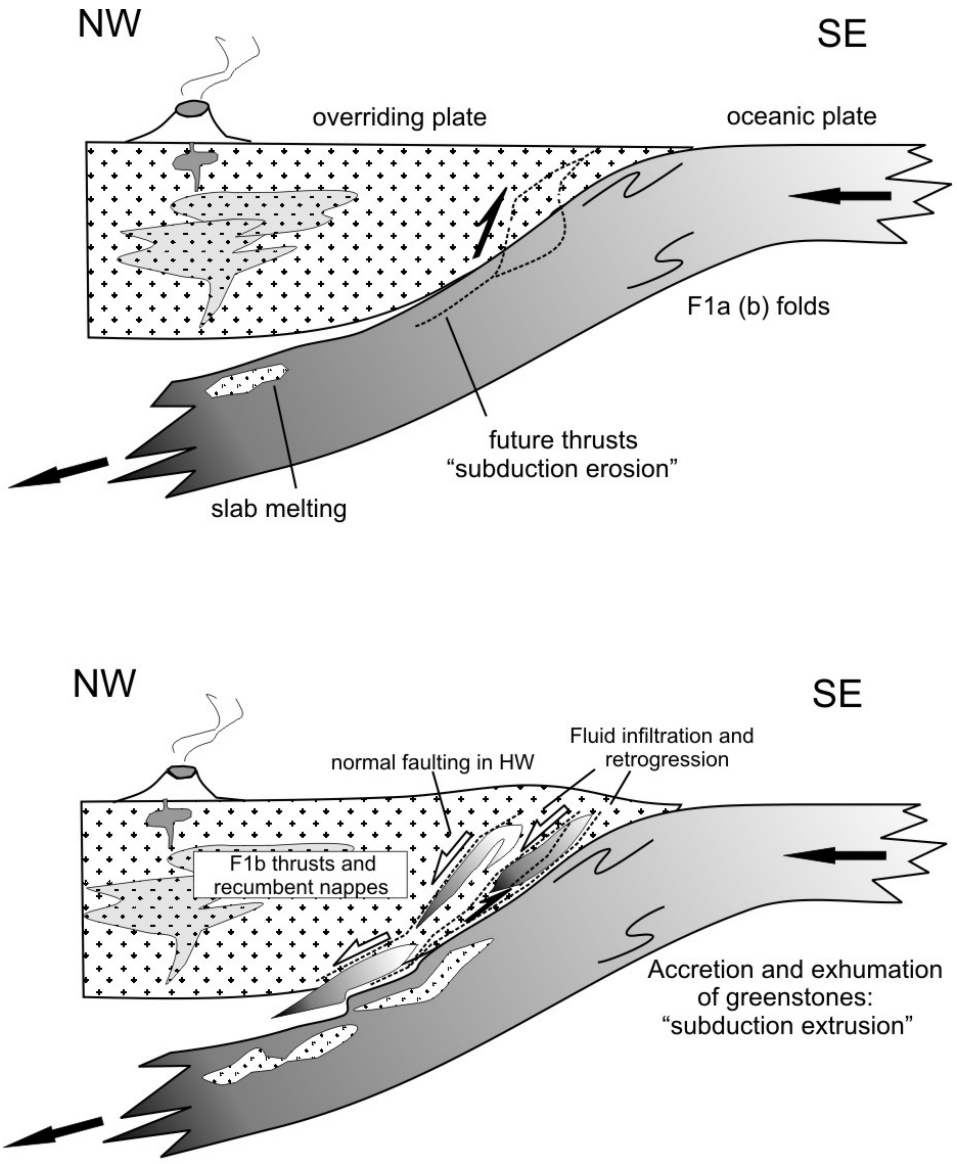

Figure 15. (*a) Top – Schematic section showing the NW-directed subduction of oceanic crust beneath the leading edge of a W continent or magmatic arc. Folds depict the formation and geometry of vergence folds (F1a) that are expected to form due to subduction. Also shown are the traces of future thrusts, along which the Tartoq Group slivers are detached from the downgoing plate during shallow subduction. The overriding plate is likely to be made up of older and synconvergent TTG's that are emplaced during subduction; (b) bottom – detachment of oceanic slivers from the downgoing plate and return flow and accretion of the slivers to the base of the overriding plate. Note that thrust sense of movement is recorded in the footwall of the slivers, while the hangingwall is bounded by normal faults. The hangingwall contacts are not exposed in the Tartoq Group slivers, but normal faulting and widespread extensional shear bands in D1b (exhumation-related) fabrics point to the extensional component during exhumation. Fluid infiltration occurs during exhumation of the greenstones, facilitated by the generally more brittle deformation.*

As speculated above, the synkinematic emplacement of TTG's and pegmatites are likely to have contributed to this buoyancy-assisted return flow. D1b structures form during this time (Fig. 15b), and the exhumation of the supracrustals is indicated by the overprint of earlier, higher-grade D1a structures by D1b structures. It should be emphasized that D1a and b form part of a continuum. Although similarly developed across all greenstone belts, a correlation of D1a and b across the belts must remain tentative. A clear distinction of fabrics is, for example, difficult in Nuuluk, Iterlak and Midternæs N, where low-grade metamorphic assemblages are widespread. In these cases, it is, at this stage, not even clear as to what extent greenschist-facies assemblages represent retrograde or peak assemblages. A distinction of fabrics is less ambiguous in e.g. Sioralik where high-and low-grade assemblages and fabrics are well defined.

The later stages of exhumation of the rocks to shallower crust levels are characterised by brittle deformation and the development of pervasive cataclasite networks. The coaxial refolding of the thin greenstone slivers results in the formation of second-generation nappe structures during subduction extrusion that refold earlier nappes (Fig. 15b). These stages are associated with a massive fluid infiltration and, in fact, metasomatism, leading to the chloritization of even leucopegmatites and TTG's. The pervasive knobbly alteration of the greenstones, i.e. carbonate and quartz-carbonate veining has occurred during this stage, as well as the locally observed gold mineralisation that exploits D1b ductile-brittle shear zones (e.g. at Nuuluk).

Geochronological results of the surrounding TTG basement will be summarised in a separate report (Szilas, in prep.), but the TTG basement is likely to be more heterogeneous than currently shown on regional maps. It likely consists of older TTG's, forming the leading edge of the overriding plate in the W, and a variety of syn- to late-tectonic TTG's intruding the Tartoq Group, representing the magmatic products of the convergent arc during Tartoq Group subduction. It may be argued that the paucity of metasediments in the greenstone sequences is due to partial melting of the sediments prior to the onset of melting of the mafic oceanic crust. These melts may, in fact, be represented by the extensive pegmatite stockworks that have intruded all belts. However, this aspect requires further geochemical, petrographic and geochronological work.

On a regional scale, the Nuuluk, Iterlak and Sioralik belts show N to NE trends and structures are characteristic of a frontal orientation with respect to the SE imbrication and vergence of structures. Midternæs N, in contrast shows rather E strikes and lithologies are steep. Kinematics are characterised by dextral strike-slip movement rather than top-to-the-E and SE thrusting. This orientation and the invariably strike-slip kinematics correlate with Midternæs N and similar, narrow, highly drawn out greenstone slivers occupying the position of regional-scale lateral ramp systems that formed at low angle or even parallel within the overall E and SE verging imbricate stack.

Stage 4: Refolding

D1 structures are mainly low-angle structures, such as low-angle shear zones, bedding-parallel fabrics or recumbent nappes. These structures are refolded by N- to NE-trending, both SW and NE plunging and predominantly SE verging F2 folds (Fig. 16). In fact, the Sioralik, Nuuluk and Iterlak belts owe their preservation to the presence of F2 synclinoria, being responsible for the infolding of the supracrustals into the TTG's. However, rather than

representing a gentle phase of refolding, greenstones to the E of Nuuluk appear to form an overturned limb of an F2 antiform. The SE vergence of F2 folds and possibly nappes and the N- to NE fold trends suggest the D2 to be largely coaxial with the earlier D1 imbrication of greenstone slivers. As such, the subsequent F2 folding is interpreted to have formed during progressive shortening, once D1 structures exhumed to shallower crustal levels had locked up for further lateral translation. This final stage of deformation may herald an actual collisional event, but this must remain speculative.

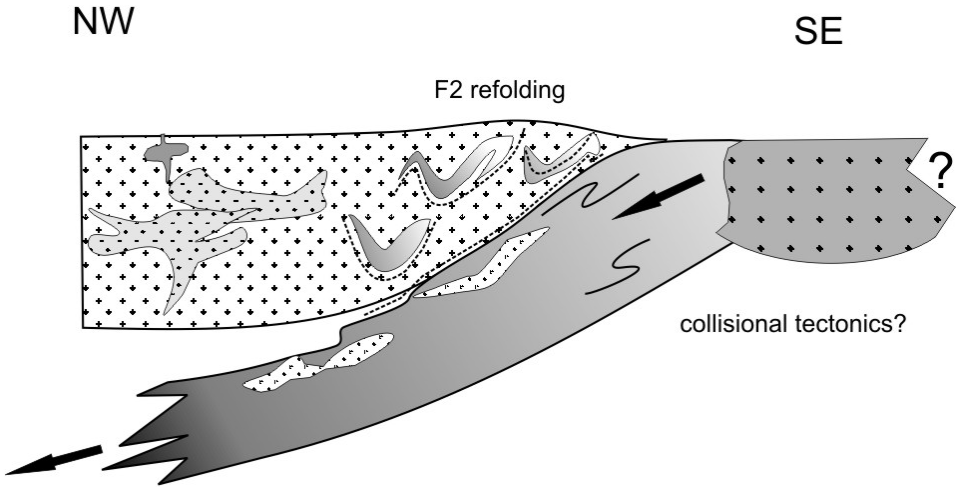

Figure 16. *F2 refolding of earlier D1 structures. The late-stage refolding may indicate a final collisional event.*

Summary

Structural work around the Sermiligaarsuk Fjord in south Western Greenland suggests that rocks of the Tartoq Group may represent the vestiges of a remarkably well-preserved Neoarchaean subduction zone channel. The supracrustals represents slivers of oceanic crust. The structural and metamorphic record of the supracrustals is consistent with their burial and exhumation of oceanic crust during NW-directed subduction. This was followed and overlapped with the SE-directed return flow and accretion of the supracrustals to the base of an overriding TTG terrain located to the W. In-situ partial melting of granulite-grade amphibolites documents the melting of the oceanic slab during subduction. Both the burial and exhumation of oceanic slivers was accompanied by the emplacement of leucocratic melts (TTG's and pegmatites) into the supracrustals. This is taken as further indication that tectonic processes occurred along a convergent margin. Exhumation of the slivers in the subduction channel to shallow-crustal levels is associated with the formation of pervasive, km-scale cataclasite networks, associated fluid infiltration and pervasive to localized retrogression of the rocks and, in places, economic-grade gold mineralisation.

Acknowledgements

This work was made possible through the support from Marianne, Jakob and Klaus at base camp and their relentless efforts to keep us fed, informed and connected to the outside world. Denis Schlatter, Kirsty Reynolds, Annika Dziggel and Ali Polat are thanked for making this not only a highly enjoyable, but also very productive field season through many laughs and thought-provoking discussions. Jochen Kolb and Thomas Kokfeldt, excursion leaders of the 2010 field season, are thanked for the flawless organization and getting the project off the ground. Many thanks to all other participants of the trip who we only met during short transfer windows to and fro or in Greenland, for their collegiality and good spirit. Brian Windley is thanked for many constructive comments on an earlier version of this report.

References

Agard, P., Yamato, P., Jolivet, L. & Burov, E. (2009). Exhumation of oceanic blueschists and eclogites in subduction zones: timing and mechanisms. Earth Science Reviews 92, 53-79.

Agard, P., Searle, M.P., Alsop, I.G. & Dubacq, B. (2010). Crustal stacking and expulsion tectonics during continental subduction: P-T deformation constraints from Oman. Tectonics 29, TC5018.

Appel, P.W.U. & Secher, K. (1984). On a gold mineralization in the Precambrian Tartoq Group, SW Greenland. Journal of the geological Society of London 141, 273-278.

Berthelsen, A. & Henriksen, N. (1975). Geological map of Greenland, 1:100,000 Ivittuut 61 V.1 Syd (with description), Geological Survey of Greenland, Copenhagen, 169 pp.

Evans, D.M. & King, A.R. (1993). Sediment and shear-hosted gold mineralization of the Tartoq Group supracrustals, southwest Greenland. Precambrian Research 62, 61-82.

Higgins, A.K. & Bondensen, E. (1966). Supracrustals of pre-Ketilidian age (the Tartoq Group) and their relationships in the ivigtut region South-West Greenland. Rapport Gronlands Geol. Unders. 8, 21p.

Higgins, A.K. (1968). The Taroq Group on Nuna qaqortoq and the Iterdlak area, southern West Greenland. Rapport Gronlands Geol. Unders. 17, 17p.

Nutman, A.P. & Klasbeek, K. (1994). A minimum age of 2944±7Ma for the Tartoq Group, South West Greenland. Rapport Gronlands Geol. Unders. 161, 35-38.

Nutman, A.P., Friend, C.L.R., Barker, S.L.L. & McGregor, V.R. (2004). Inventory and assessment of Palaeoarchaean gneiss terrains and detrital zircons in southern West Greenland. Precambrian Research 135, 281-314.

Petersen, J.S. (1993) Gold mineralization in the Tartoq Group greenstones, Southwest Greenland – results of structural, geochemical and geophysical exploration studies 1991. Exploration report Nunaoil A/S, 44p.

Searle, M.P., Warren, C.J., Waters, D.J. & Parrish, R.R. (2004). Structural evolution, metamorphism and restoration of the Arabian continental margin, Saih Hatat region, Oman Mountains. Journal of Structural Geology 26, 451-473.

Van Hinsberg, V.J., Szilas, K. & Kisters, A.F.M (2010). The Tartoq Group, SW Greenland: mineralogy, textures and a preliminary metamorphic to hydrothermal history. GEUS report, 24p.

Summary of 2010 field work in the Tartoq Group, Paamiut region, SW Greenland (Polat & Dziggel)

Ali Polat[1] & Annika Dziggel[2]

[1]Department of Earth and Environmental Sciences, University of Windsor, Windsor, ON, Canada

[2]Institute of Mineralogy and Economic Geology, RWTH Aachen University Wüllnerstr. 2, 52064 Aachen, Germany

Introduction

Field work in the summer of 2010 was undertaken in the Neoarchaean Tartoq Group, the Paamiut region, southern West Greenland (Fig. 1). The field work was conducted in three areas (camps) between July 2 and July 14, 2010 (Fig. 1).

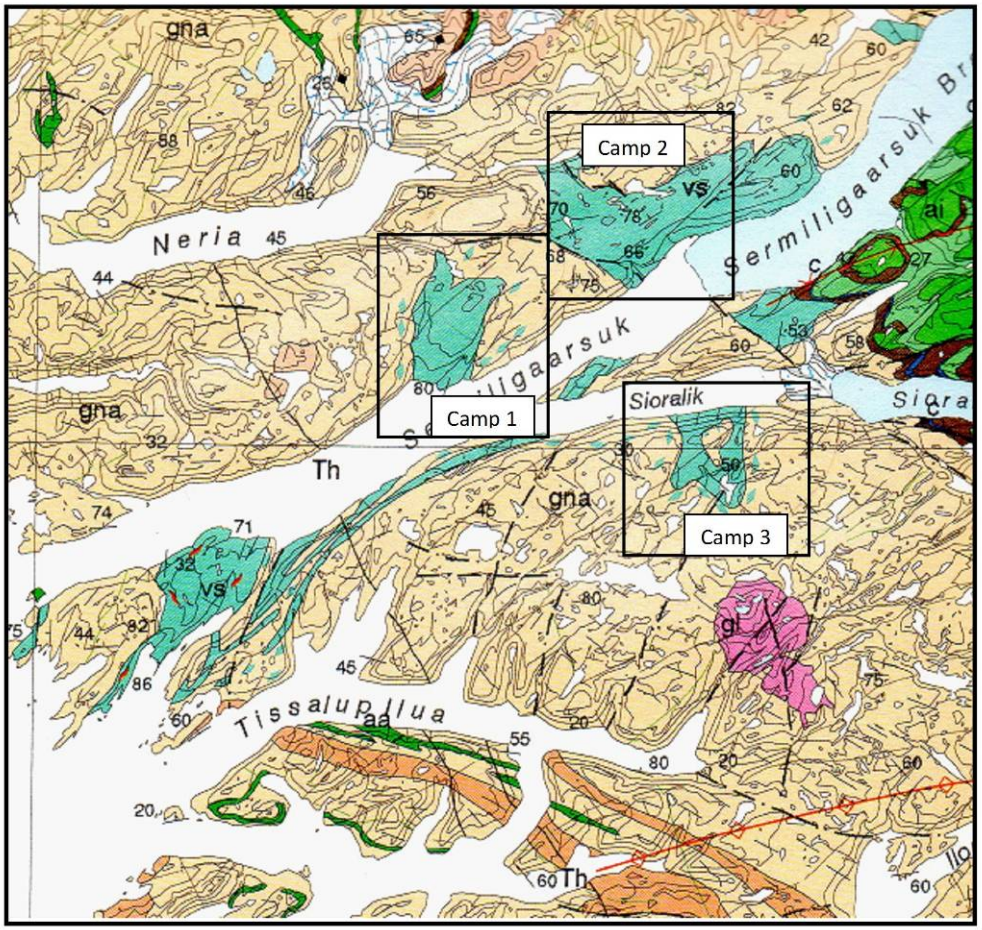

Figure 1. *Geological map of the Tartoq area. Rectangles show the outline of the investigated and sampled camp sites (greenstones).*

The field work was focused mainly on understanding the field characteristics and sampling of ultramafic to felsic rocks for geochemical analyses. Sample descriptions and GPS coordinates are presented in Tables 1, 2 and 3, and in the field notes. Eighty-nine samples were collected for detailed petrographic and geochemical studies, including major and trace element (REE, HFSE, LILE, transition metals), and Nd, Pb and Hf isotope analyses. Whole-rock geochemical data will be used to understand the petrogenesis of supracrustal rocks in the Tartoq Group. The samples were collected from the least to most altered outcrops to assess the effect of metamorphism on element mobility before petrogenetic and geodynamic interpretation. In the following sections, the field characteristics of the rocks occurring in the three camp sites are summarised.

Camp 1 (Iterlak)

This camp site was located at N61°33'36.2" and W48°34'39.0", and field work was carried out between July 2 and 6, 2010. In the camp area, chlorite schists, chlorite-sericite-carbonate schists, meta-gabbros, felsic quartz-feldspar-muscovite-sericite schists, intermediate schists, ultramafic rocks, and intermediate to felsic dykes and sills constitute the major rock types (Figs. 2 and 3). The mineral assemblages indicate greenschist facies metamorphism, no higher metamorphic grade has been observed. In general, the contacts between different rock units are strongly deformed. These contacts often display multiple phases of folding, shearing, mylonitisation and transposition (Figs. 2 and 3). Because of intense deformation and metamorphism, primary magmatic relationships between different units (e.g., mafic, ultramafic, felsic rocks) have mostly been modified. The chlorite schists occur as several metres to several tens of metres thick layers (Figs. 1 and 2), and are mainly fine-grained to mylonitic. They are intercalated with up to 50 m thick, medium- to coarse-grained gabbros in which the primary magmatic textures are generally well-preserved. The mineral assemblages in the mafic rocks comprise chlorite, quartz, plagioclase, calcite, opaques and minor epidote. The felsic schists form important marker horizons within the mafic sequence. The rocks are fine-grained to mylonitic, commonly crenulated and consist of quartz, plagioclase, muscovite, chlorite, opaques, tourmaline and minor biotite, in decreasing order of abundance. Evans & King (1993) interpreted these rocks as being derived from felsic volcaniclastic material, however, geochemical data suggest that these rocks may instead reflect strongly deformed equivalents of the surrounding TTG gneisses (Szillas, personal communication 2010).

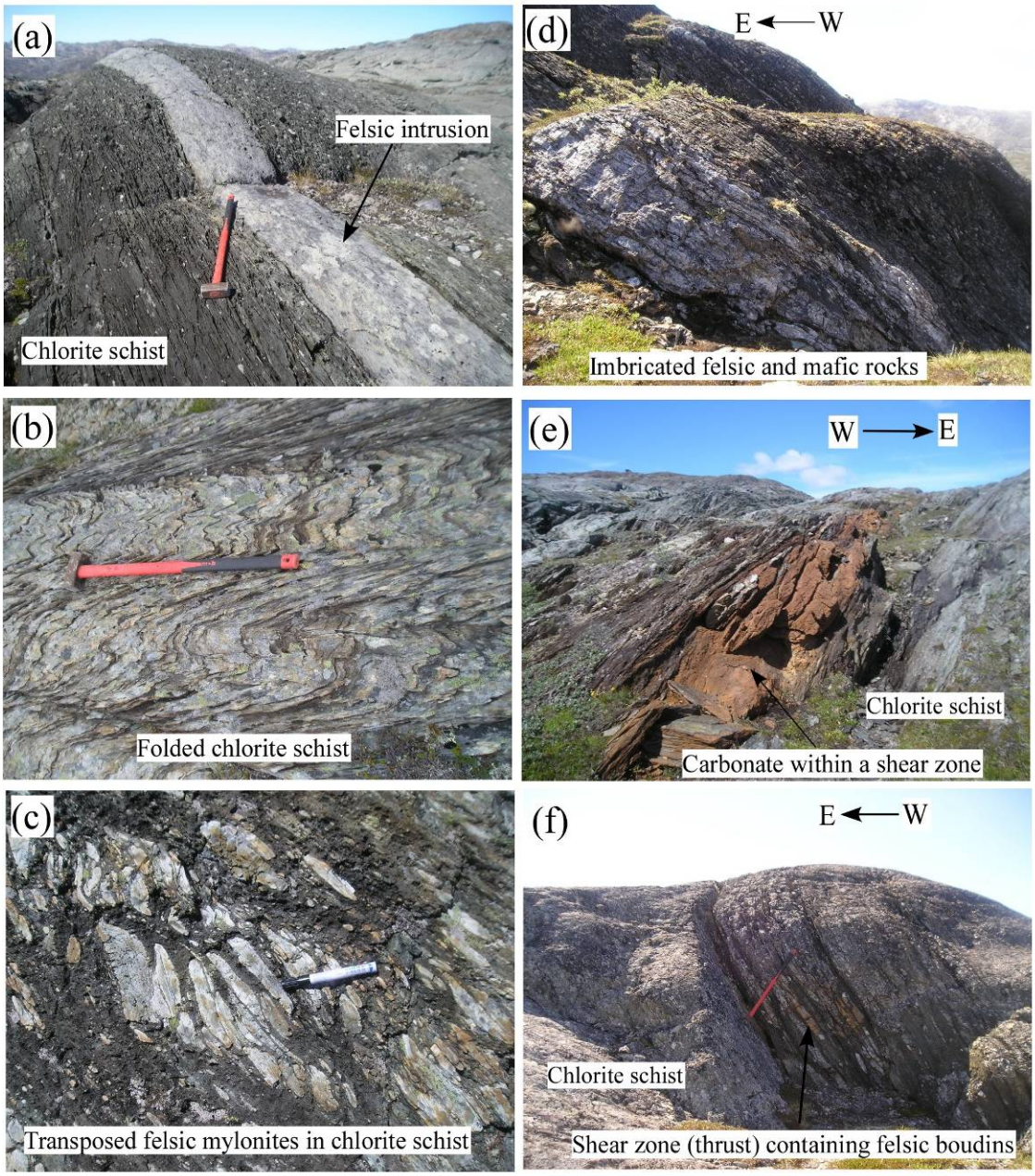

Figure 2. *Field photographs of various rock types and structures in the Camp 1 area, Tartoq Group.*

Dismembered, up to 100 m thick and boudinaged layers of intermediate schists occur in the eastern part of the area investigated. The intermediate schists comprise a heterogeneous sequence of quartzo-feldspatic rocks that contain variable amounts of chlorite, muscovite, calcite and opaques. A characteristic feature of these rocks is the local presence of cm- to dm large and commonly rounded clasts of fine-grained (chert-like) felsic material, that often do not display an internal foliation (Fig. 3). In matrix-dominated portions, the clasts are strongly flattened, and resemble pyroclastic material (Fig. 2). In cross-section, the clasts define a prominent stretching lineation.

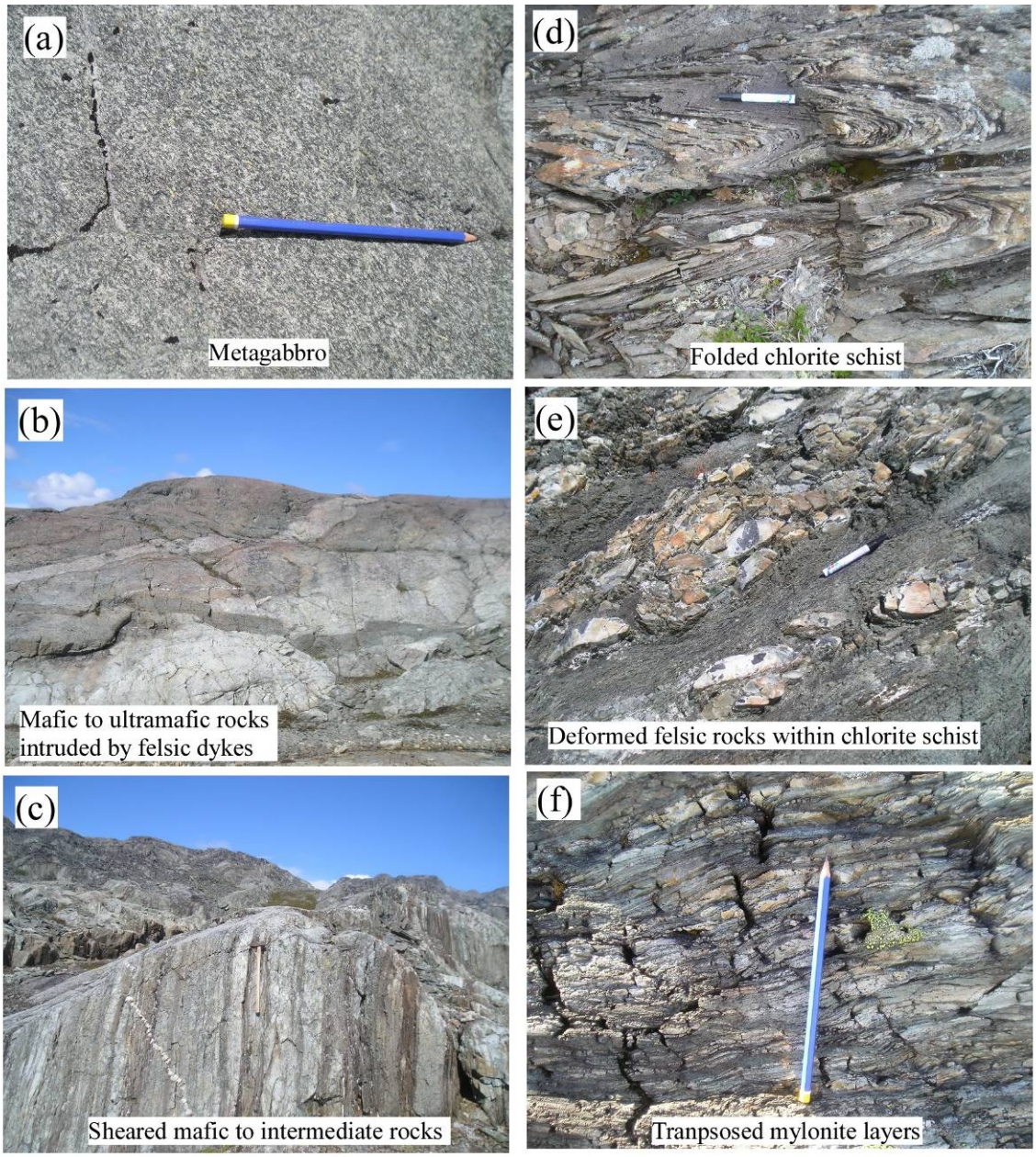

Figure 3. *Field photographs of various rock types and structures in the Camp 1 area, Tartoq Group.*

Bookshelf-type segmentation of the clasts is characterised by small-scale synthetic and antithetic normal faults that are at high angles to the mineral stretching lineation. Higgins (1968) interpreted these rocks as deformed conglomerates, i.e. to be of clastic sedimentary origin. However, based on the lack of compositional diversity within the clasts as well as the tectonic nature of the rocks, we interpret the rocks as cataclasites, i.e. tectonic breccias/conglomerates. Carbonates occur mainly along shear zones as several centimetres to several metres thick and several metres to several hundred metres long lenses or veins (Figs. 2 and 3). The strongly sheared wall rocks are silicified and carbonated chlorite schists and locally contain hydrothermal fuchsite. Both veins and the wall rocks contain pyrrhotite. Except for rare possible pyroclastic structures and gabbroic textures in a few locations (Fig. 3), no primary magmatic textures or structures have been preserved in the area. Forty-two samples were collected for geochemical analyses and petrographic studies.

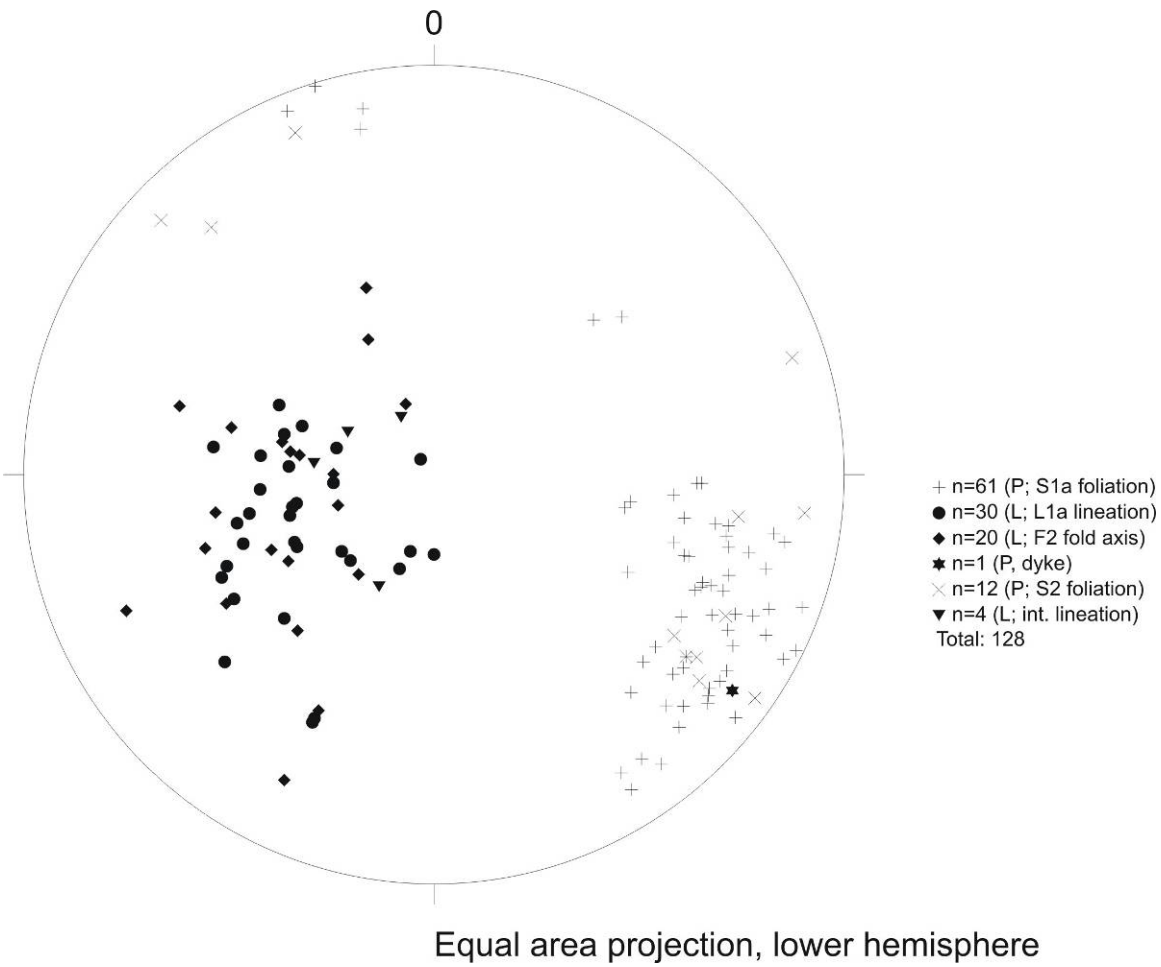

Figure 4. *Stereographic projection of structural data collected at Iterlak.*

Following the structural scheme of Kisters et al. (this volume), the dominant fabric is a pervasive, mainly moderately west to north-west dipping S1a foliation (Figs. 3 and 4). The fabric intensity of the S1a foliation is strongly heterogeneous and is best-developed in bedding-parallel mylonitic shear zones (i.e. the felsic schists), where it is mainly defined by chlorite, muscovite and quartz- and feldspar aggregates. The associated mineral stretching lineations plunge at moderate to steep angles to the west and southwest (Fig. 4). Shear sense indicators point to a top to the east and southeast sense of movement. The D1a fabrics are overprinted by an S2 foliation. The S2 foliation is often parallel to D1a and is axial-planar to mainly SW-plunging, close- to tight F2 folds. The F2 folding has been preserved on all scales, and is marked by a prominent crenulation cleavage in schists and mylonites. The vergence of the F2 folds is to the SE. Because the folding also affected the carbonate veins and lenses, the alteration and associated mineralisation must predate the F2 folding. The axial-planar, subvertical S2 foliation dips at moderate to steep angles to the NW and SE.

Camp 2 (Midternæs N)

The second camp site was located at N61°36'51.9" and W48°21'51.6", which is about 12 km northeast of the first camp site (Fig. 1). The two camp areas are separated by orthogneisses (Fig. 1). We arrived in the second campsite on July 6 and left the camp on July

10, 2010. The camp area is characterised dominantly by variably deformed and hydrothermally altered pillow basalts and basaltic lava flows, chlorite schists, chlorite-sericite-quartz-carbonate schists and minor ultramafic (peridotite) rocks (Fig. 5). Contacts between the generally east-west striking rock types are typically characterised by intense deformation and display carbonate alteration. Chlorite schists exhibit crenulation cleavage and chevron folding throughout the study area. Many chlorite schist outcrops contain 1-3 % sulphide minerals. Peridotites occur as several tens of metres thick lenses in the northern part of the area. The pillow basalts and basaltic lava flows commonly contain cm-large plagioclase crystals that overgrow e.g. the cores and rims of individual pillows. The rocks are also cut by quartz- and carbonate veins and have a light-greenish or yellowish colour, indicating that they were exposed to extensive hydrothermal alteration. The pillow cores mainly consist of quartz, chlorite, plagioclase, muscovite, calcite and epidote. The plagioclase crystals are variably replaced by fine-grained aggregates of muscovite (sericite) and/or epidote and zoisite. The pillow rims are composed mainly of chlorite and epidote and have a thickness of 1 and 5 centimetres.

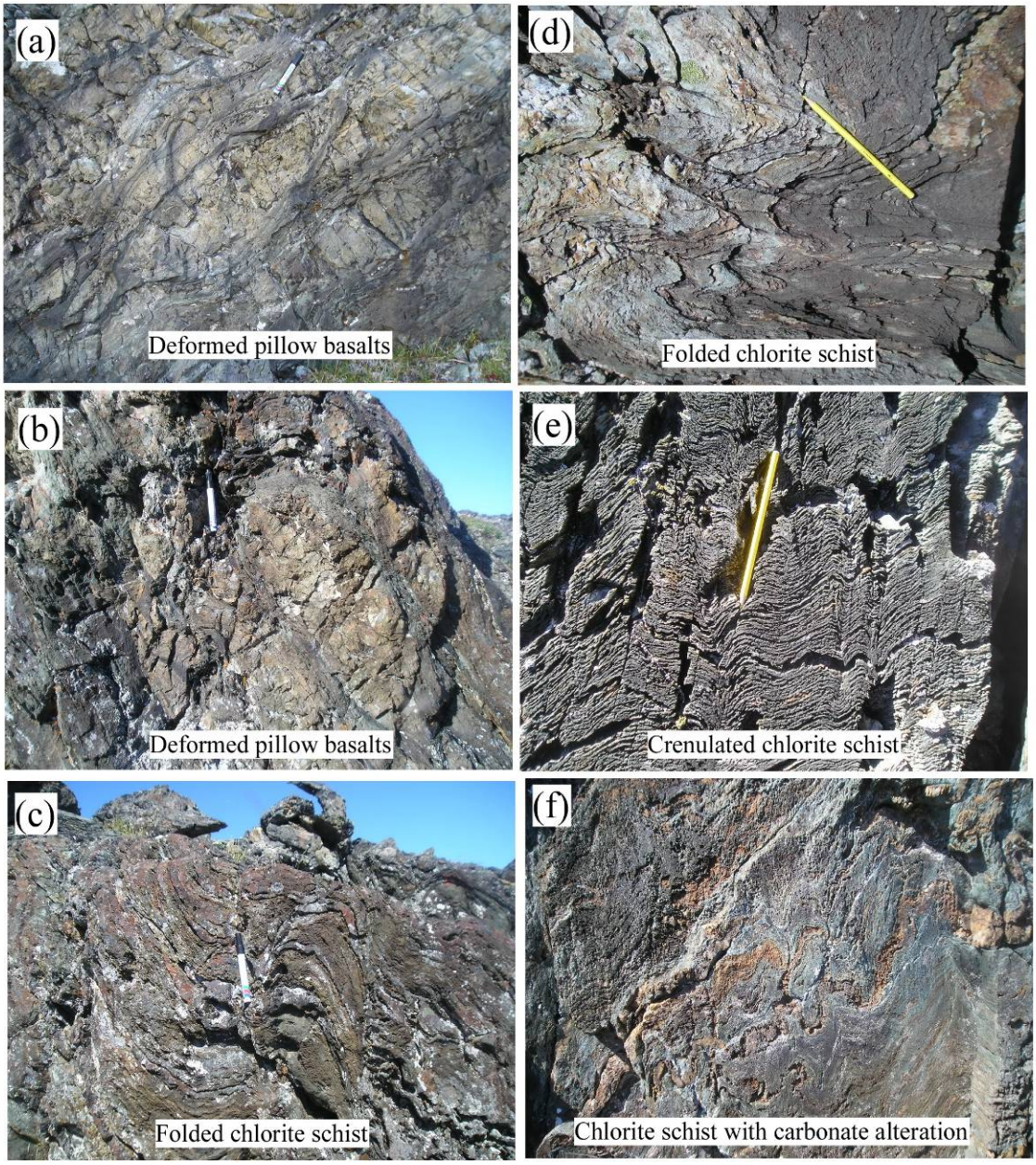

Figure 5. *Field photographs of various rock types and structures in the Camp 2 area, Tartoq Group.*

Based on the mineralogy and field characteristics, we interpret the rocks as spilites formed during seafloor hydrothermal alteration. A total of 30 samples, including chlorite schist, peridotite, chlorite-sericite-quartz-carbonate schist and pillow core and pillow rim, were collected from the camp 2 area for geochemical analyses and petrographic studies (Table 2).

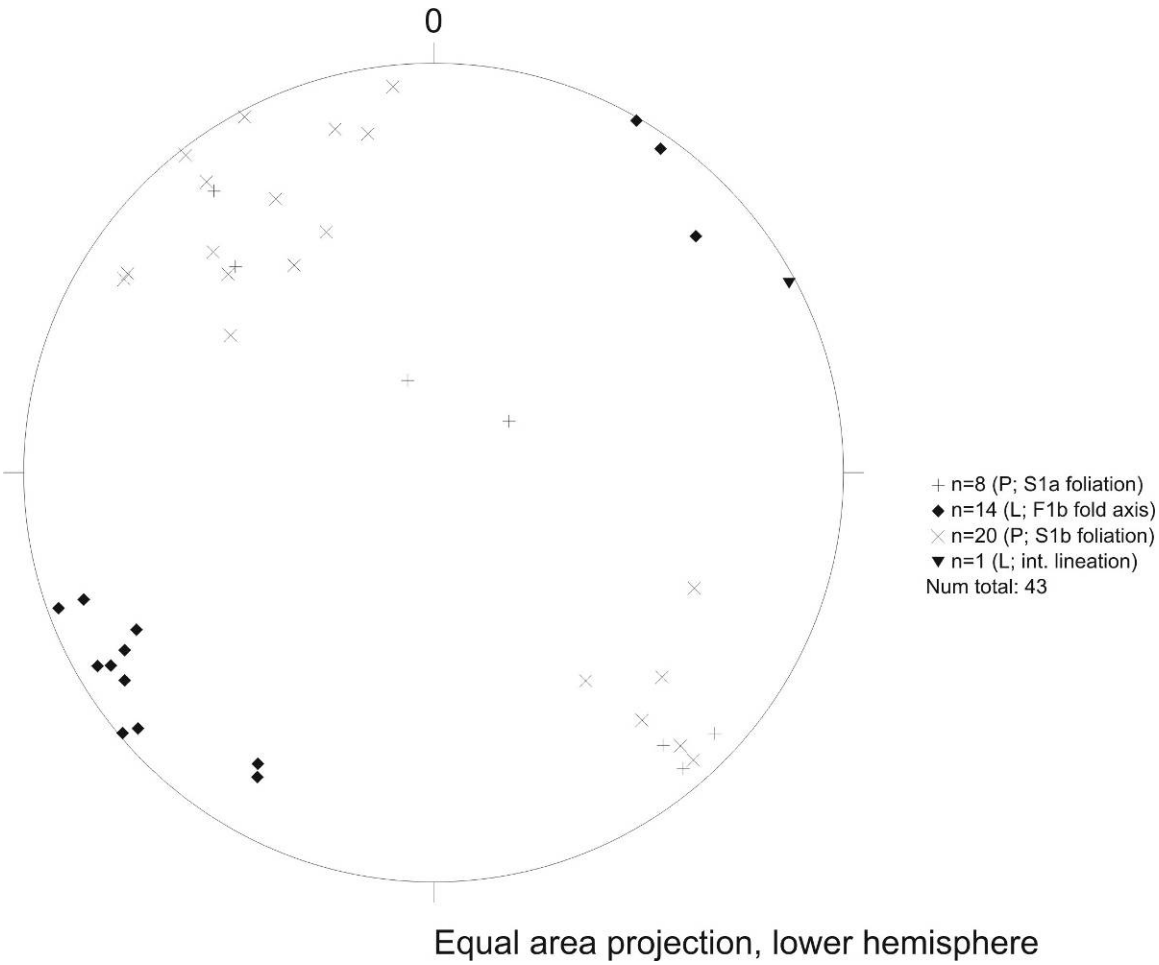

Figure 6. *Stereographic projection of structural data collected at Midternæs N.*

The structural inventory of Midternæs N can be explained in terms of two deformation events. However, due to major differences in the overall orientation and kinematics, a direct correlation with similar structures in the other belts is currently not possible (Kisters et al., this volume). The earliest fabric preserved in the belt is a variably dipping foliation that is here referred to as the S1a foliation. This early foliation is parallel to bedding and/or lithological layering (Fig. 5) and is locally associated with a generation of early recumbent (F1a) folds. The S1a foliation has been refolded by a second generation of open to tight folds that may correlate with the D1b deformation in the other belts (Kisters et al., this volume). The D1b folds are associated with an axial-planar foliation. The S1b foliation dips at moderate to steep angles to the NW and SE, almost parallel to the S2 foliation at Iterlak (Fig. 6). Mineral lineations are absent. The fold axes of the generally NE-trending folds are sub-horizontal and plunge at shallow angles to the SW and NE. Shear sense indicators (mainly S-C' fabrics) indicate dextral strike-slip kinematics.

Camp 3 (Sioralik)

We moved to the third camp on July 10 and left the camp on July 14, 2010. The camp was situated at N61°29'21.8" and W48°18'57.4". The third camp area has higher grade (amphibolite facies) metamorphic rocks than the first and second camp areas. Rock types in the area are composed predominantly of banded amphibolites, ultramafic rocks (peridotites,

serpentinites, talc-actinolite schists), rusty quartzo-feldspathic-mica schists, pegmatites, and orthogneisses (Fig. 7). Contacts between orthogneisses and the members of the supracrustal rocks are generally characterised by strong deformation and/or have been intruded by syn- to late-tectonic pegmatites. Contacts between different rock units of the supracrustal rocks are also marked by deformation (Fig. 7). Foliation-parallel, up to several metre thick and boudinaged pegmatites are widespread. The metamorphic grade seems to increase from mid- amphibolite facies conditions in the western and central parts to upper amphibolite facies metamorphism and local migmatisation in the east. The banded amphibolites are generally fine-grained to mylonitic and have a peak metamorphic mineral assemblage of hornblende + plagioclase + quartz ± clinopyroxene ± garnet. The peak assemblage and plagioclase in particular has been variably and locally extensively replaced by greenschist facies minerals, including epidote, zoisite, colourless amphibole (likely actinolite), titanite, calcite and, locally, chlorite and biotite. A prominent, foliation-parallel “rust zone” occurs in the central part of Sioralik (e.g. at N61°29'83.8" and W48°19'44.3"), where it can be followed for several hundred metres along strike (Fig. 7). The sulphide mineralisation is associated with laminated quartz-veins that are hosted by mainly gneisses and amphibolites. The mineralised samples mainly consist of quartz, feldspar (strongly altered to sericite and epidote), opaques, garnet, biotite, tourmaline and chlorite. Chlorite, muscovite, and biotite define a well-developed foliation. However, chlorite typically replaces muscovite and biotite, as well as garnet along fractures, suggesting that it formed during retrogression. A total of seventeen samples were collected from the third camp site for petrologic and petrographic studies (Table 3).

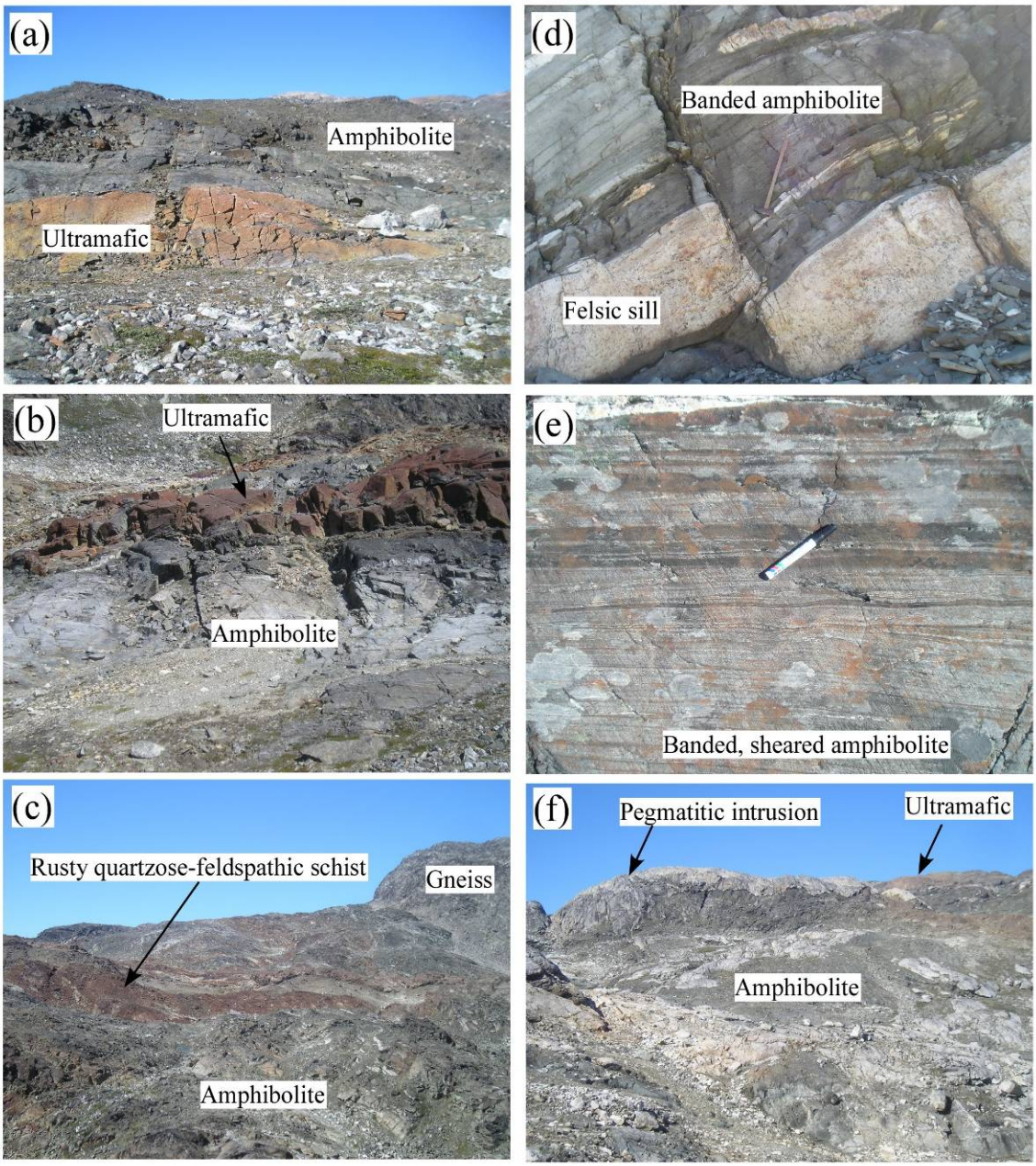

Figure 7. *Field photographs of various rock types and structures in the Camp 3 area, Tartoq Group.*

The dominant fabric in the amphibolites and associated supracrustal rocks is a variably dipping S1a foliation (Fig. 8). The S1a foliation in the central parts of Sioralik mainly dip moderately to the E and NE, but records steep westerly dips in the east close to the contact with the TTG gneisses. The S1a foliation is defined by peak metamorphic minerals such as amphibole and biotite and has been refolded by NE-plunging F1a folds (see Kisters et al., this volume, for a detailed description). Shear sense indicators (S-C' fabrics) in the central part of the belt indicate top-to-the-SE kinematics. The early high-T fabrics are variably overprinted by greenschist facies mylonites and cataclasites that are commonly parallel to the S1a foliation. This later overprint is also marked by the presence of steep, SE dipping brittle normal faults in some of the amphibolites.

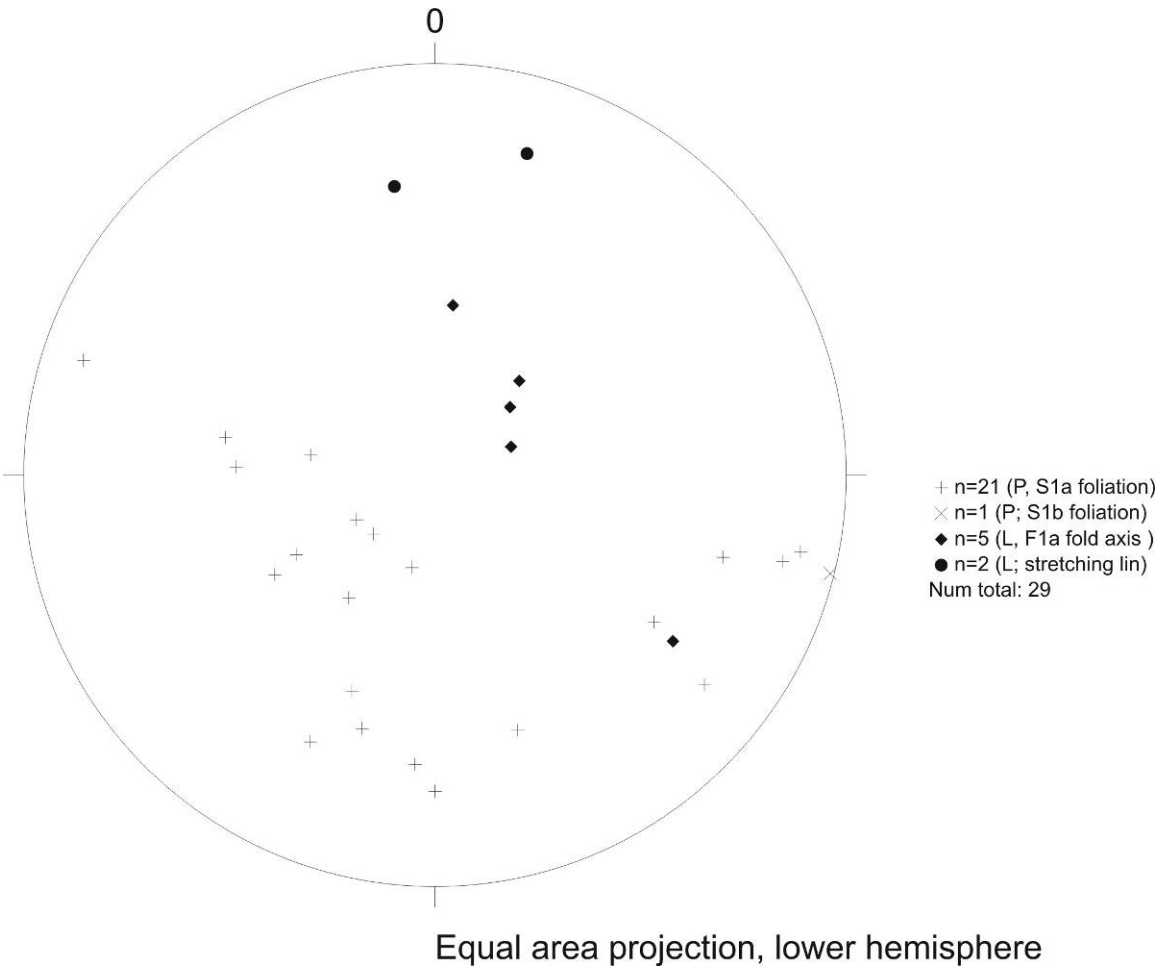

Figure 8. *Stereographic projection of structural data collected at Sioralik.*

References

Evans, D.M. & King, A.R. 1993: Sediment and shear-hosted gold mineralization of the Tartoq Group supracrustals, southwest Greenland. Precambrian Research 62, 61-66.

Higgins, A.K. (1968). The Taroq Group on Nuna qaqortoq and the Iterdlak area, southern West Greenland. Rapport Gronlands Geol. Unders. 17, 17p.

Gold occurrences of the Tartoq area (Kolb)

Jochen Kolb

Geological Survey of Denmark and Greenland – GEUS, Øster Voldgade 10, DK-1350, København, Denmark

Several gold occurrences hosted in the Tartoq Group are known and explored in the Sermiligaarsuk Fjord area, South West Greenland, since the early 1970'ies (Appel & Secher 1984; Evans & King 1993). Their origin and genesis have been disputed, using orogenic gold, submarine exhalative and diagenetic models (Appel & Secher 1984; Evans & King 1993). Since gold exploration was not successful in the area and this was partly caused by a lacking conclusive genetic model for the gold mineralisation, GEUS revisited the area in 2010 and re-evaluated existing data. I the following the main results are summarised. Detailed information is found on the DVD including theses, conference contributions and a GIS project.

Six gold occurrences are distinguished from west to east, including the Nuuluk and the Iterlak gold prospects, and the Akuliarusaq, the Amitsuarsua, the Bikuben, and the Naalagaaffik gold occurrences (Fig. 1).

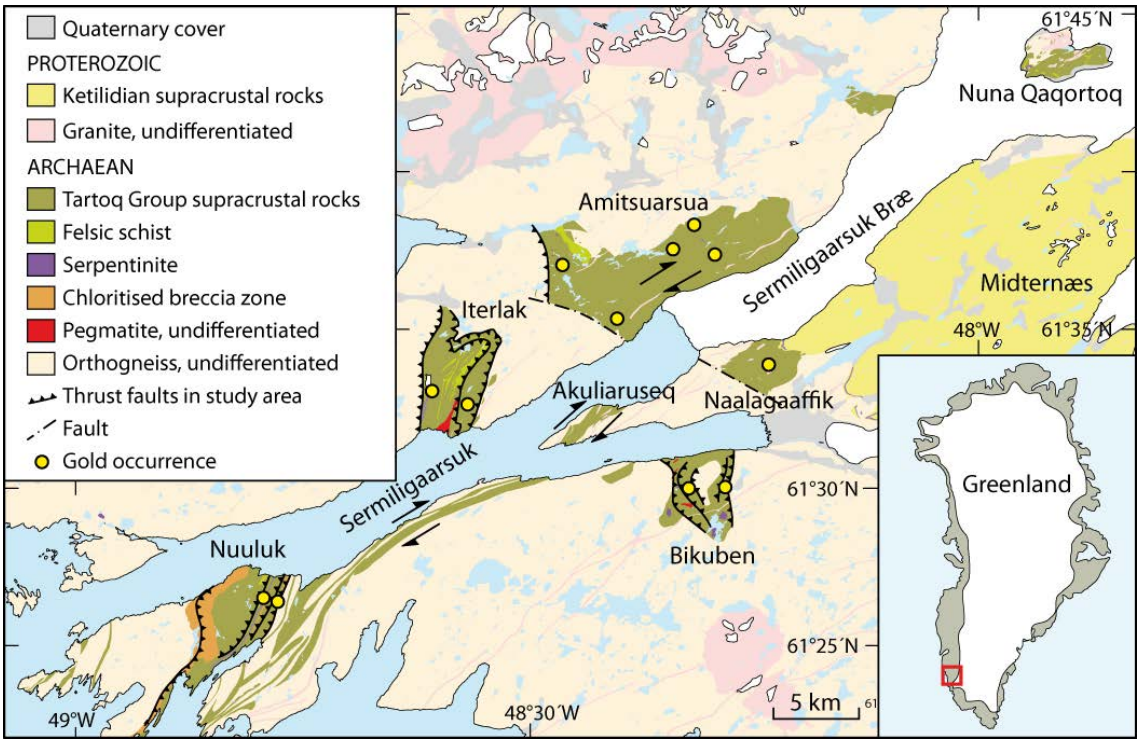

Figure 1. *Schematic geological map of the Tartoq gold province (modified after, Escher & Jensen 1974; Henriksen 1968; Jensen 1975).*

Nuuluk gold prospect

Nuuluk, to the south of Sermiligaarsuk Fjord, is characterised by metavolcanic rocks that are metamorphosed to greenschist facies grade and thrust over an Archaean gneiss basement to the east (Fig. 1, Kisters et al., this volume, Szilas *et al.* 2011; van Hinsberg *et al.* 2010). They are mainly tholeiitic basalts to basaltic andesites.

Gold is hosted in two distinct NNE-SSW trending, moderately WNW-dipping, 50-100 m wide and 5 km long zones, namely the western and eastern carbonate zones (Petersen & Madsen 1995). These zones are located 100-200 m in the foot wall of D_{1b} thrust zones (cf.; Fig. 1 in Kisters et al., this volume). The spacing between the two zones is about 500 m and, within the two zones, again two parallel gold horizons with a spacing of approximately 25 m are distinguished (Hoffritz 2011). The structure of the western carbonate zone is probably characterised by an isoclinal F_1 fold that formed in the foot wall of the main thrust (Hoffritz 2011).

The western carbonate zone comprises hydrothermally altered greenschist, magnetite greenschist and graphite greenschist (Fig. 2). The distal hydrothermal alteration assemblage comprises carbonate (calcite, dolomite or ankerite depending on host rock composition), chlorite, pyrite and tourmaline in foliation parallel veins and extension veins. Tourmaline thermometry together with pseudosection modelling suggests 380°C ± 50°C and < 2 kbar for this hydrothermal alteration (van Hinsberg *et al.* 2010). The proximal alteration zone comprises ankerite, muscovite (fuchsite), chlorite, quartz, pyrite, arsenopyrite, pyrrhotite, chalcopyrite, tennantite and gold (see also, Appel & Secher 1984; Evans & King 1993). Arsenopyrite thermometry suggests 350-450°C for the hydrothermal alteration and mineralisation (Evans & King 1993). The gold mineralisation is disseminated in the hydrothermally altered magnetite and graphite greenschists (Fig. 3).

The eastern carbonate zone is characterised by up to 20 cm wide quartz veins hosted in hydrothermally altered greenschist (Fig. 2). The hydrothermal alteration assemblages are similar in both carbonate zones. Here, the proximal alteration zone surrounds quartz veins that host the bulk of the hydrothermal gold mineralisation (Fig. 3).

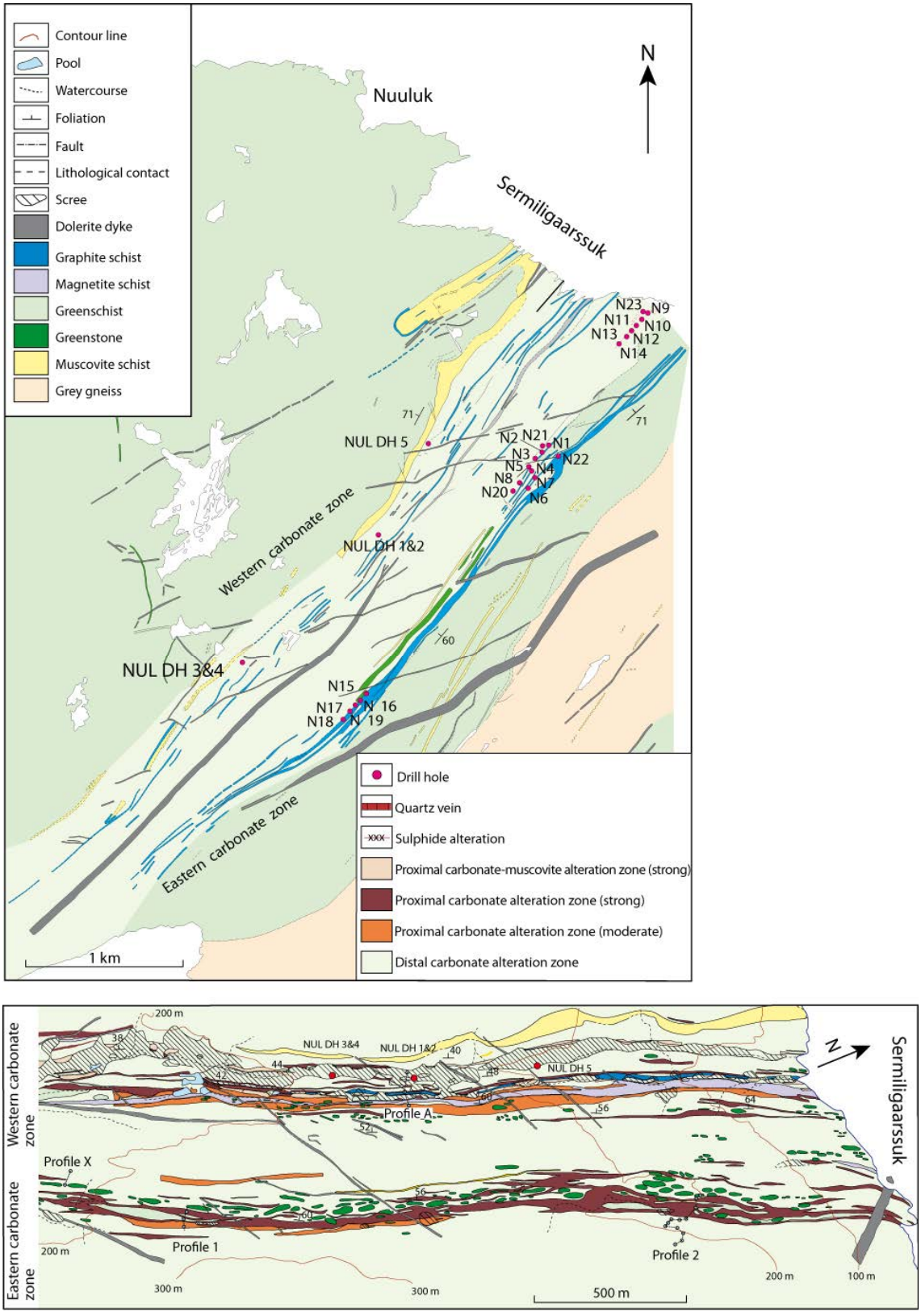

Figure 2. *Geological map of the Nuuluk area showing the distribution of hydrothermal alteration zones and the location of drill holes (modified after, King 1985; Petersen 1991, 1992).*

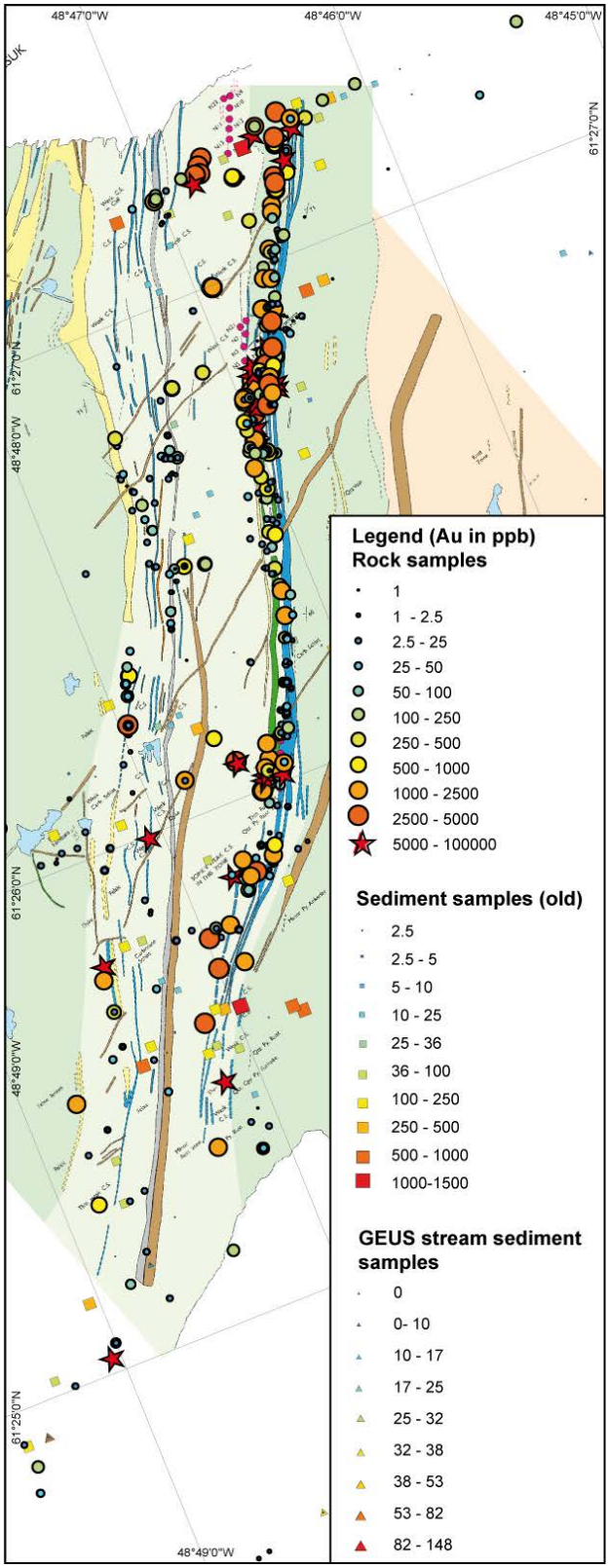

Figure 3. *Gold analyses plotted on the map from Figure 2 using data from various internal reports and the GEUS data base (Anonymous 1985; Edsen & Halkjær 1992; Geisler 1972, 1973, 1974, 1975; Gowen 1992, 1993; King 1983, 1985; Petersen 1991, 1992; Steenfelt 2001).*

Gold and silver show a good correlation in the hydrothermally altered samples. Although gold shows only weak correlation with arsenic and copper a halo of elevated As and Cu occurs in the gold zone which suggests that the auriferous fluids were also enriched in these elements. Mass change calculations reveal that the hydrothermal alteration from the western carbonate zone is characterised by gain in K and CO_2 and loss of Na, whereas the eastern carbonate zone is characterised by K, Si, Na, Fe and CO_2 gains (Schlatter, unpubl. data). The hydrothermal gold mineralisation at Nuuluk, consequently, represents a typical mesozonal orogenic gold prospect associated with regional-scale carbonate-chlorite-pyrite alteration and thrusting. The gold mineralisation is hosted in either geochemically favourable rocks, i.e. graphite and magnetite greenschists, or more competent greenschists in the form of quartz veins in the foot wall of the main thrust zones.

Iterlak gold prospect

Iterlak to the north of the Sermiligaarsuk Fjord comprises greenschist, meta-gabbro, muscovite schist, serpentinite, talc schist, banded iron formation and pegmatite (Fig. 4; see also Kisters et al., this volume; Polat & Dziggel, this volume). The peak metamorphic grade varies from greenschist facies conditions in the west to amphibolite facies conditions in the east (van Hinsberg *et al.* 2010). A regional hydrothermal alteration comprises a carbonate-chlorite-pyrite assemblage (Reynolds 2011). Three NNE-SSW trending thrust zones are distinguished, at the Iterlak belt – gneiss contact and within the belt marked by muscovite schist, which represents sheared grey gneiss (Fig. 1; see also Kisters et al., this volume). The belt represents a F_2 synclinorium, where the greenstone rocks are preserved (Kisters et al., this volume).

Gold is hosted in two NNE-SSW trending, approximately 100 m wide and 200-400 m long zones, namely the Western Valley zone and the Eastern Valley zone (Fig. 5, see also, Appel & Secher 1984; Evans & King 1993; Petersen & Madsen 1995). These zones are located in the foot wall of the larger thrust zones. Higher gold values are also recorded from carbonate-sericite alteration zones in the belt.

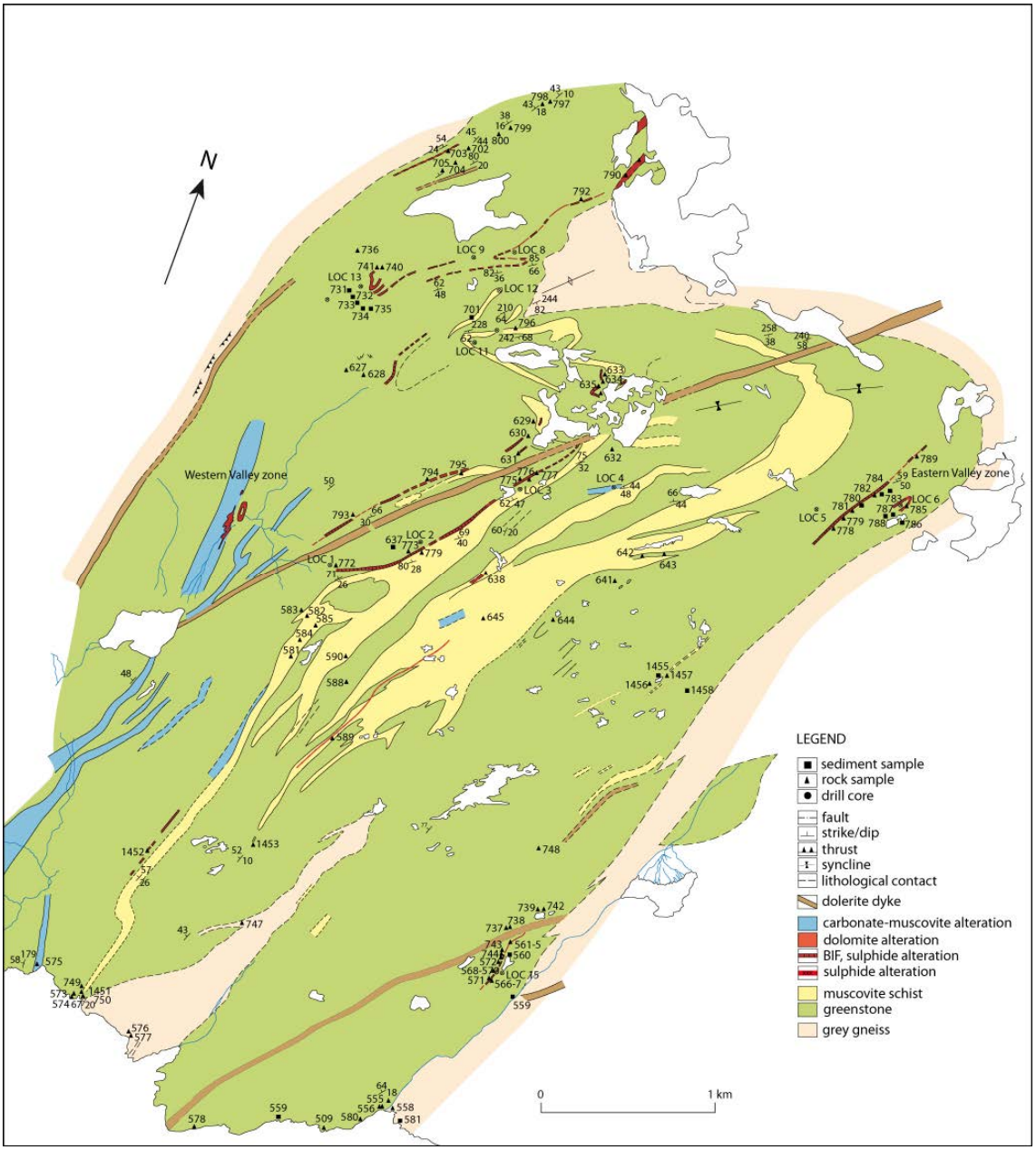

Figure 4. *Geological map of the Iterlak area showing the distribution of hydrothermal alteration zones and the location of drill holes (modified after, King 1985; Petersen 1991, 1992).*

The Western Valley zone comprises hydrothermally altered greenschist and banded iron formation (Fig. 4). VLF-data suggests a 400 m by 50 m lens-shaped body of hydrothermally altered banded iron formation tapering in both lateral directions (Petersen & Madsen 1995). The proximal carbonate-sericite alteration zone consists mainly of fine-grained muscovite (sericite), quartz, ankerite, pyrite and minor chlorite (Reynolds 2011). The ankerite is concentrated in small, foliation-parallel quartz-ankerite veins, which may not be well-developed. In this case, the proximal alteration zone is dominated by sericite and quartz (Reynolds 2011). An originally magnetite-grunerite-quartz banded iron formation is completely altered to banded quartz-pyrite rocks (Fig. 4). Quartz-rich units show a fine banding by sulphides, whereas units with 30-50 Vol.% sulphides show approximately 0.5 mm, euhedral pyrite and minor chalcopyrite (Evans & King 1993; Petersen & Madsen 1995; Reynolds 2011). The pyrite grains have inclusions of pyrrhotite, sphalerite and boulangerite

($Pb_5Sb_4S_{11}$, Evans & King 1993). Gold mineralisation occurs in the proximal alteration zones and altered banded iron formation, mainly in quartz-rich samples, i.e. quartz-ankerite veins (cf., Evans & King 1993). In the carbonate-sericite alteration zone up to 25% volume increase is associated with K, Ba, Cs, Rb, LOI enrichment and loss of Mg, Ca and Na (Reynolds 2011). Locally, Fe, Al and Ti are slightly enriched (Reynolds 2011). Gold enrichment is associated with high base metal contents and LOI, indicating hydrothermal alteration, but is also located in Fe-rich samples (Reynolds 2011). The latter suggests that precipitation of gold from the hydrothermal fluids was triggered by the Fe-rich lithologies like the banded iron formation and possibly Fe-rich greenschists.

The Eastern Valley zone is characterised by hydrothermally altered greenstone, talc schist and banded iron formation (Fig. 4). The proximal alteration zone is confined to talc schist, forming a talc-ankerite-sericite-chlorite-pyrite assemblage (Reynolds 2011). The banded iron formation shows a pyrite and minor chalcopyrite alteration. The hydrothermal alteration was not complete leaving magnetite as a primary or a metamorphic mineral in the banded iron formation and talc schist behind. Gold enrichment is most pronounced in magnetite-rich talc schist, where magnetite is replaced by up to 7 mm, euhedral pyrite (Reynolds 2011). The proximal hydrothermal alteration caused a slight mass increase together with Ca, Cu, LOI and minor K enrichment and depletion in Mg (Reynolds 2011).

The hydrothermal gold mineralisation at Iterlak, consequently, represents a typical mesozonal orogenic gold prospect associated with regional-scale carbonate-chlorite-pyrite alteration and thrusting. The gold mineralisation is hosted in geochemically favourable rocks, i.e. banded iron formation and magnetite-rich talc schist.

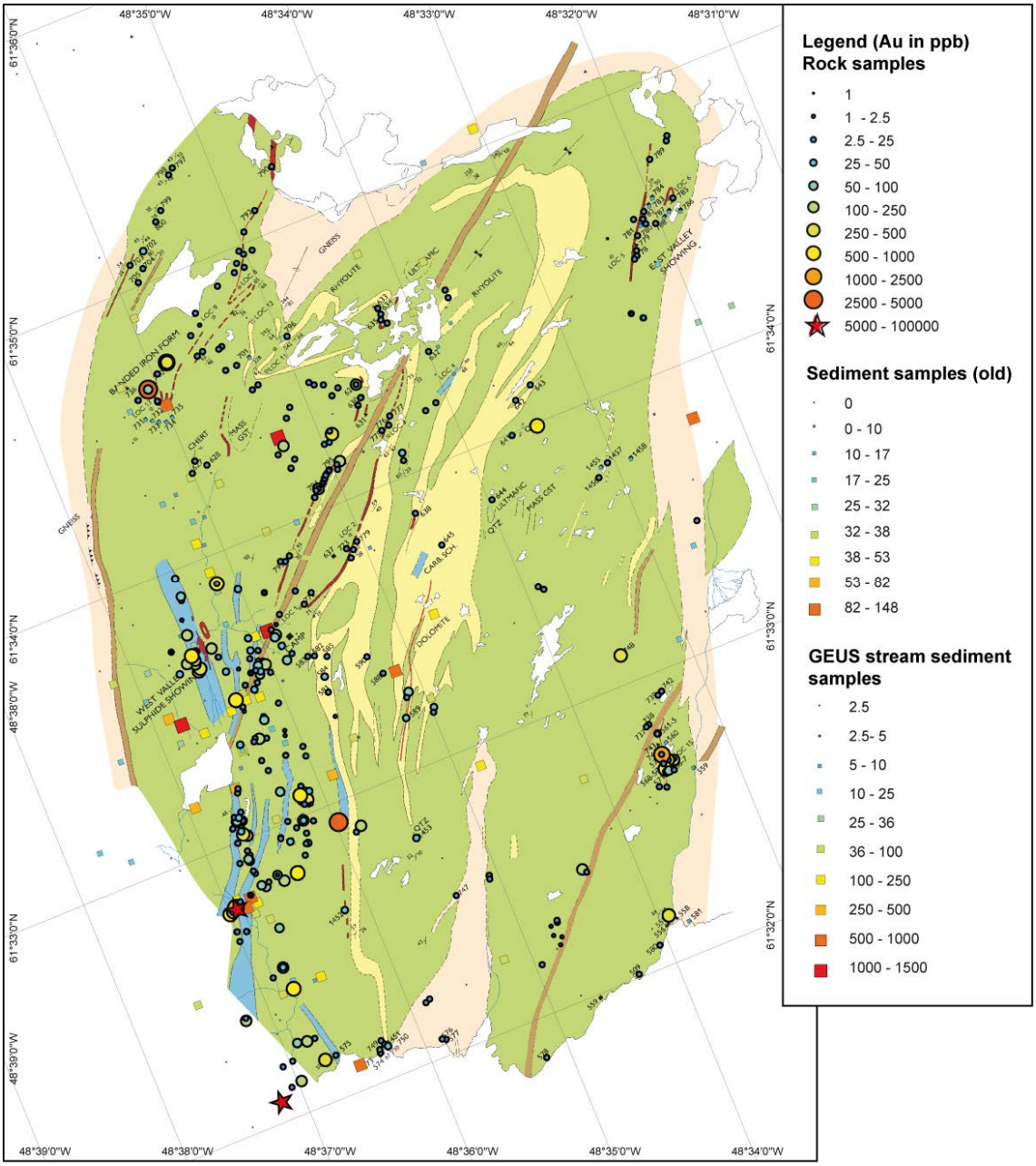

Figure 5. *Gold analyses plotted on the map from Figure 4 using data from various internal reports and the GEUS data base (Anonymous 1985; Edsen & Halkjær 1992; Geisler 1972, 1973, 1974, 1975; Gowen 1992, 1993; King 1983, 1985; Petersen 1991, 1992; Steenfelt 2001).*

Amitsuarsua gold occurrence

The Amitsuarsua area (also Midternæs North) to the north of the Sermiligaarsuk Fjord and glacier comprises greenschist, magnetite greenschist, greenstone, serpentinite and talc schist (Fig. 6). The rocks are overprinted by peak metamorphism in the epidote-amphibolite facies and later hydrothermal alteration in the greenschist facies (van Hinsberg *et al.* 2010). The map pattern shows a type 2 mushroom-like fold interference pattern (Fig. 6). An inclined isoclinal F_{1a} is overprinted by an isoclinal F_{1b} with NE-SW trending axial traces and NE plunging fold axis. The near vertical, NE-SW trending foliation is axial planar to the F_{1b}

folds. The F_{1b} folds and the foliation probably correlate with D_{1b} structures in the other locations (Kisters et al., this volume; Polat & Dziggel, this volume).

The hydrothermal alteration is similar to the Nuuluk area, comprising a distal carbonate alteration with local silification and a proximal ankerite-muscovite-quartz-sulphide alteration (Figs. 6 and 7). Foliation-parallel quartz veins are approximately 20 cm wide and form pinch-and-swell structures parallel to the regional foliation. The gold mineralisation is hosted in the quartz veins and hydrothermal alteration zones.

On a regional scale, the relationship between gold mineralisation, hydrothermal alteration and structures is only poorly understood. Higher gold values up to 1 ppm are generally associated with carbonate alteration (Fig. 8). A stronger gold enrichment to up to 5.6 ppm is spatially associated with F_{1b} hinge zones, where possibly saddle reefs are developed (Fig. 8). A more detailed structural understanding and sampling is, however, required in order to evaluate the potential for gold mineralisation in Amitsuarsua.

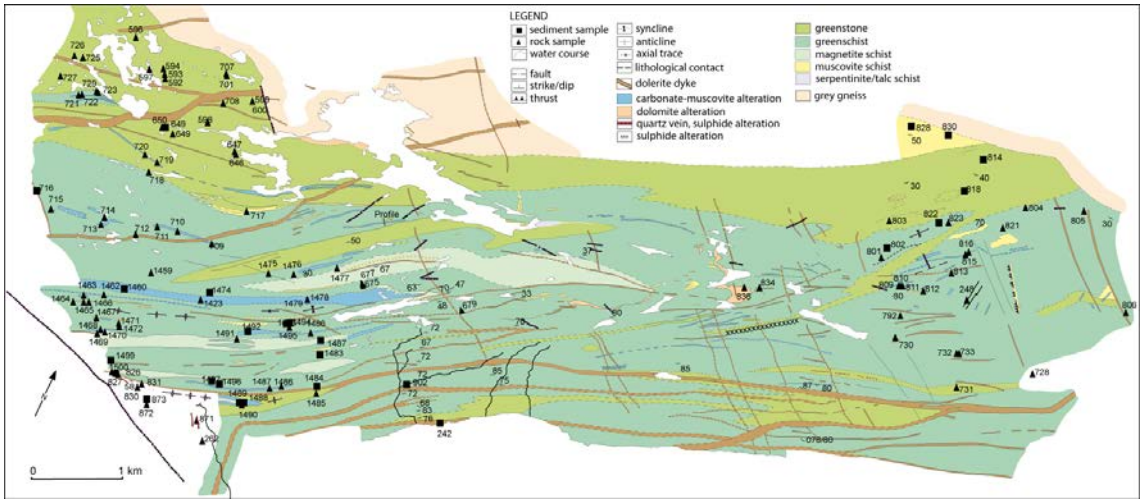

Figure 6. *Geological map of the Amitsuarsua area showing the distribution of hydrothermal alteration zones and the location of samples (modified after, King 1985).*

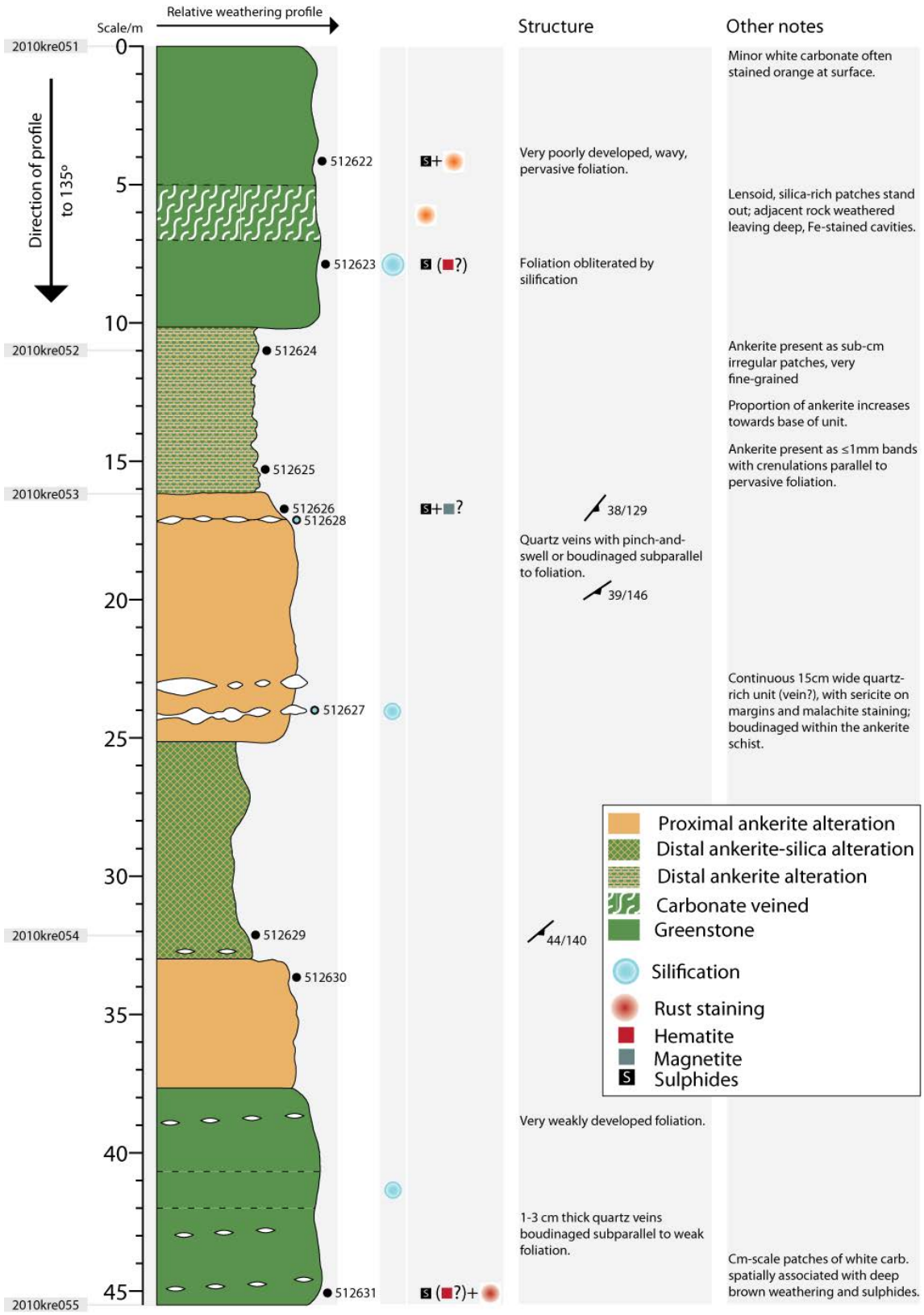

Figure 7. *Schematic profile through a representative hydrothermal alteration zone (see Figure 6 for location).*

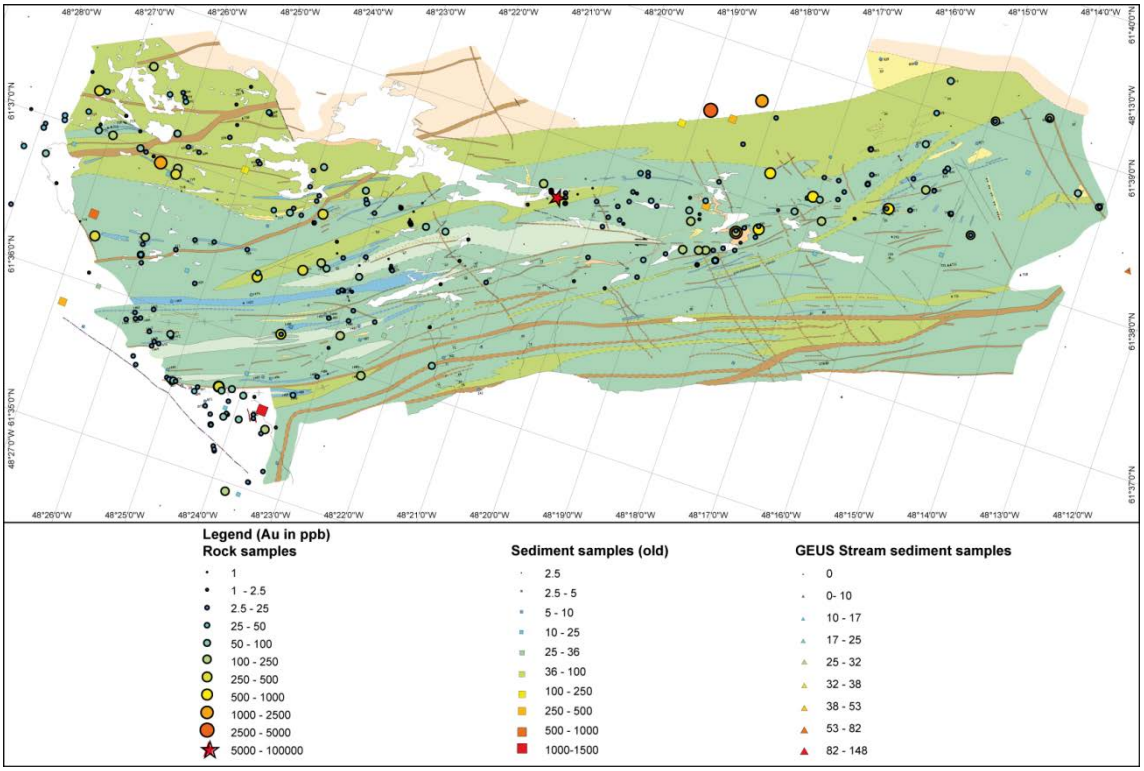

Figure 8. *Gold analyses plotted on the map from Figure 6 using data from various internal reports and the GEUS data base (Anonymous 1985; Edsen & Halkjær 1992; Geisler 1972, 1973, 1974, 1975; Gowen 1992, 1993; King 1983, 1985; Steenfelt 2001).*

Naalagaaffik and Akuliarusaq gold occurrences

The Naalagaaffik (also Midternæs East) and Akuliarusaq (also Midternæs West) areas are characterised by small, approximately 1 km wide and 3 km long belts of Tartoq Group rocks on a peninsula separating two branches of the Sermiligaarsuk fjord (Fig. 1). The Tartoq Group in these belts comprises greenschist, greenstone, serpentinite, talc schist and muscovite schist (Fig. 9). The peak metamorphic grade is in the epidote-amphibolite facies with widespread retrogression and hydrothermal alteration in the greenschist facies (van Hinsberg *et al.* 2010). In both areas, the foliation is near vertical and trends NE-SW. The foliation is interpreted to be related to strike-slip deformation in up to 100 m wide D_{1b} shear zones (Kisters et al., this volume).

The regional-scale hydrothermal alteration of greenschists is characterised by a carbonate-chlorite-pyrite assemblage as is typical for the Tartoq Group (Figs. 9 and 10). The proximal alteration comprises quartz, carbonate and sulphides in the greenschist, and muscovite, quartz and sulphides in the muscovite schist. The hydrothermally altered muscovite schist is distinguished from the non-altered rock by its rusty staining. Gold mineralisation of up to 1 ppm Au occurs disseminated in the proximal alteration zones and in quartz veins and pods surrounded by hydrothermal alteration zones (Fig. 11). A conjugate set of barren quartz veins is developed in the greenschist and greenstone cross cutting the foliation and lacking hydrothermal alteration halos.

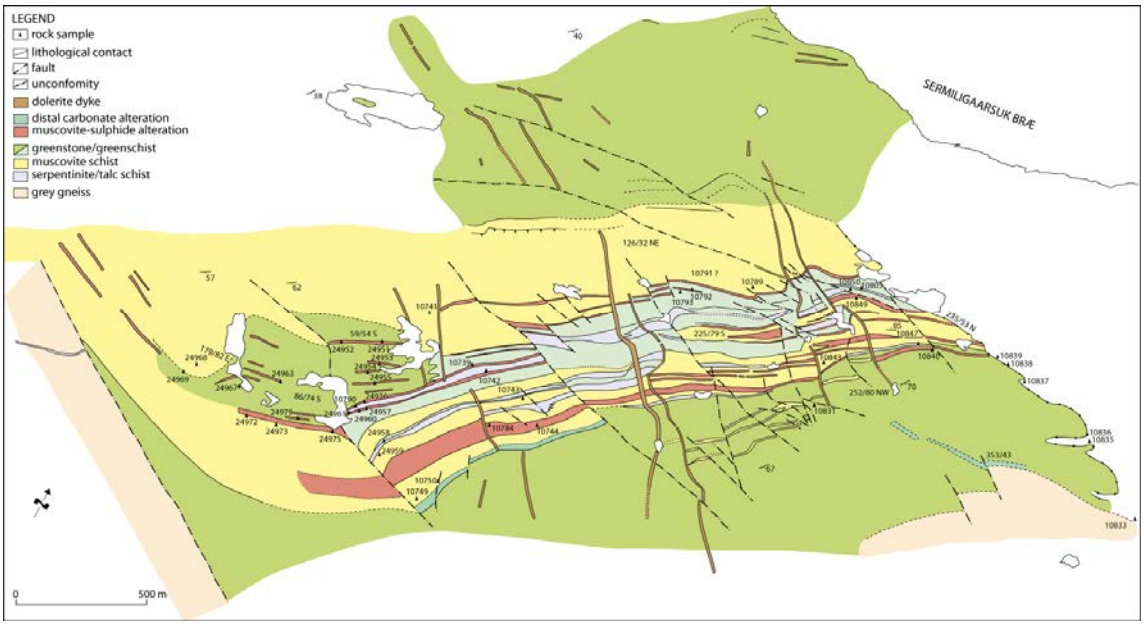

Figure 9. *Geological map of the Naalagaafik area showing the distribution of hydrothermal alteration zones and the location of samples (modified after, King 1985).*

The relationship between gold mineralisation, hydrothermal alteration and structures is only poorly understood. Compared to the better known areas, the hydrothermal alteration and structural control by D_{1b} shear zones are similar and suggest a potential for gold mineralisation in these two areas. No F_{1b} fold structures are, however, apparent from the map, which appear to host higher-grade gold mineralisation in the Amitsuarsua gold prospect across the Sermiligaarsuk fjord to the north.

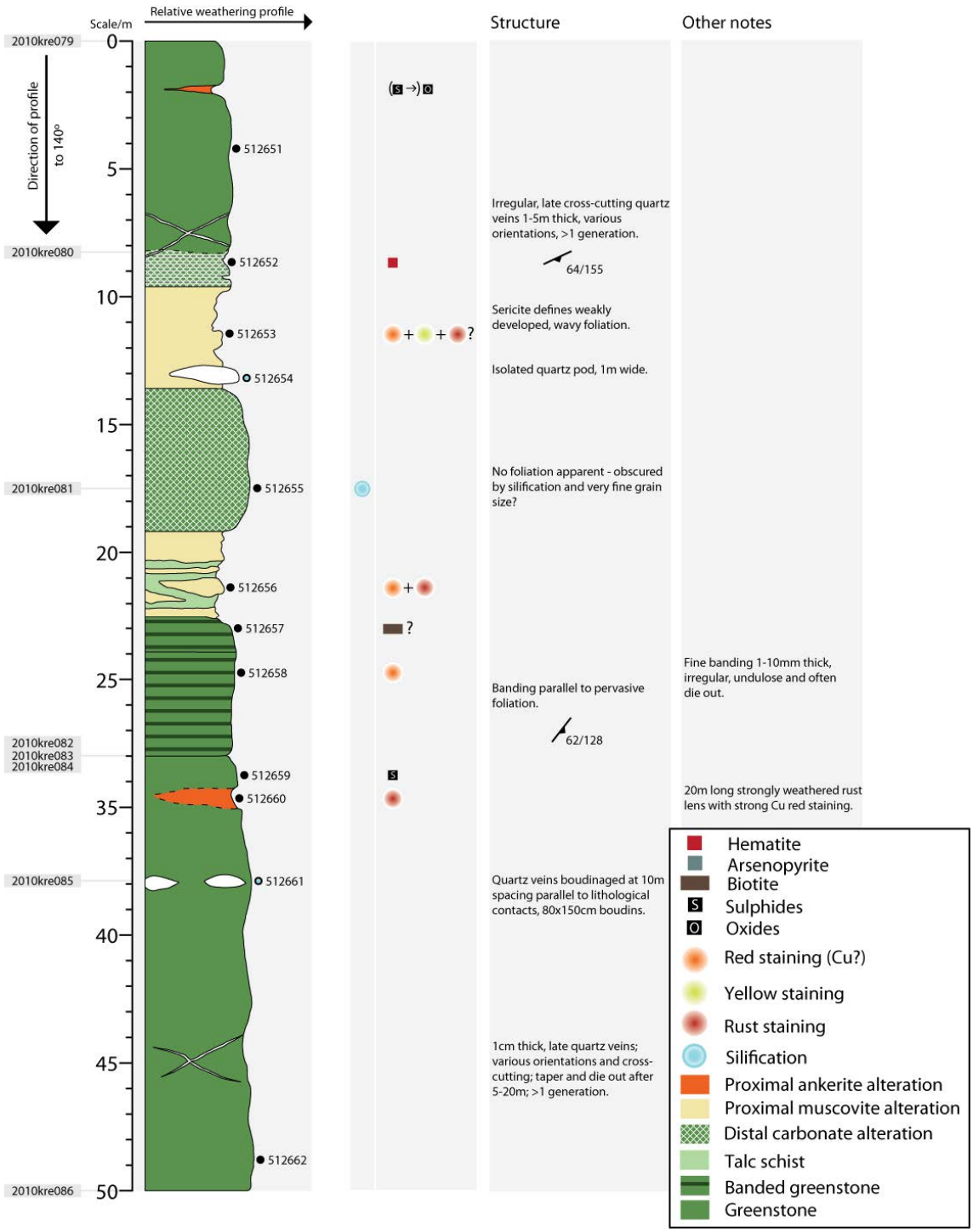

Figure 10. *Schematic profile through a representative hydrothermal alteration zone (see Figure 9, location east of the horseshoe-shaped lake).*

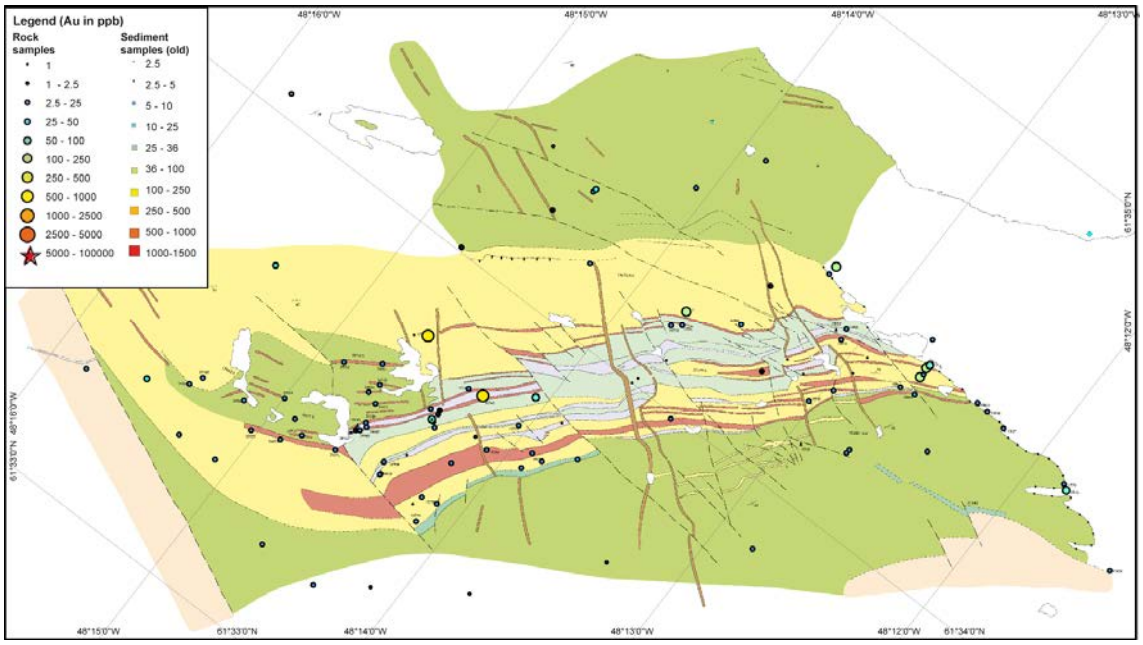

Figure 11. *Gold analyses plotted on the map from Figure 9 using data from various internal reports and the GEUS data base (Anonymous 1985; Edsen & Halkjær 1992; Geisler 1972, 1973, 1974, 1975; Gowen 1992, 1993; King 1983, 1985; Steenfelt 2001).*

Bikuben gold occurrence

The Bikuben (also Sioralik) area is located south of the Sermiligaarsuk Fjord, measuring approximately 4 km by 4 km (Fig. 1). The Tartoq Group lithology is characterised by banded amphibolite, ultramafic rocks, quartzo-feldspathic-mica schist and pegmatite (Fig. 12, see also Kisters et al., this volume; Polat & Dziggel, this volume). The metamorphic grade increases from mid-amphibolite facies conditions in the western and central parts to upper amphibolite facies and local migmatisation in the east. Van Hinsberg et al. (2010) determined peak P-T conditions of P > 6-7 kbar and T approximately 850°C. The dominant fabric is a variably dipping S_{1a} foliation that is parallel to bedding (Kisters et al., this volume). This foliation has been refolded by NE-trending and plunging F_{1a} folds. Shear sense indicators indicate top-to-the-SE kinematics. Brittle and brittle-ductile D_{1b} structures overprint earlier parallel fabrics and are commonly defined by foliated chlorite schist and/or cataclasite. The regional structure is interpreted to form a NNE trending, doubly-plunging F_2 synform, resulting in the overall keel-like structure.

A hydrothermal alteration zone is developed for several hundred metres along strike parallel to the penetrative foliation in gneiss and amphibolite wall rocks (Fig. 12). It is easily recognised in the field due to its rusty staining. The alteration assemblage surrounding foliation-parallel laminated quartz veins is probably garnet, muscovite, biotite, feldspar, tourmaline and sulphides. This assemblage is largely retrogressed to chlorite, which possibly could also be related to hydrothermal mineralisation and alteration.

The hydrothermal alteration and mineralisation are only poorly understood, and hypozonal as well as mesozonal hydrothermal overprint are possible. The mineralised structures are, however, similar to those found in the other prospects in the Sermiligaarsuk Fjord.

References

Anonymous 1985: Efterforskningskoncession til Greenex A/S Uummannaq i området mellem Ivigtut og Frederikshåb. Koncession nr. 61. 1985, 24, Greenex A/S. Internal report.

Appel, P.W.U. & Secher, K. 1984: On a gold mineralization in the Precambrian Tartoq Group, SW Greenland. Journal of the Geological Society London 141, 273–278.

Edsen, N.A. & Halkjær, M. 1992: Kujataa 1992. Results of geophysical fieldwork, 9, Nunaoil A/S. Internal report.

Escher, J.C. & Jensen, S.B. 1974: Geological map of Greenland, 1:100,000, 61 V.2 Nord, Midternæs. Copenhagen: Geological Survey of Greenland.

Evans, D.M. & King, A.R. 1993: Sediment and shear-hosted gold mineralization of the Tartoq Group supracrustals, southwest Greenland. Precambrian Research 62, 61-66.

Geisler, R.A. 1972: Investigations on the Renzy Mines Limited Frederikshåb concession, Greenland, to June 15, 1972, 6, Renzy Mines Ltd. Internal report.

Geisler, R.A. 1973: Investigations on the Renzy Mines Limited Frederikshåb concession, Greenland, during the year ended June 18, 1973, 3, Renzy Mines Ltd. Internal report.

Geisler, R.A. 1974: Investigations on the Renzy Mines Limited Frederikshåb concession, Greenland, for the year ending June 15, 1974. , 8, Renzy Mines Ltd. Internal report.

Geisler, R.A. 1975: Investigations on the Frederikshåb exploration concession of Renzy Mines Ltd. During the year ended June 15, 1975, 19, Renzy Mines Ltd. Internal report.

Gowen, J. 1992: Kujata 1992. Re-analysis of Nuuluk drill core, Taartoq greenstone belt, Sermiligaarsuk, SW Greenland, May 1992, 18, NunaOil A/S. Internal Report.

Gowen, J. 1993: 05/92-drilling and prospecting at the Taartoq Archean greenstone belt, SW Greenland July-August 1993, 16, NunaOil A/S. Internal Report.

Henriksen, N. 1968: Geological map of Greenland, 1:100,000, 61 V.1 South, Ivigtut. Copenhagen: Geological Survey of Greenland.

Hoffritz, S.E. 2011: Modellering af hydrotermale omdannelser og Au mineraliseringer i Nuuluk området, Tartoq guldprovins, 54. Unpublished thesis, Copenhagen University.

Jensen, S.B. 1975: Geological map of Greenland, 1:100,000, 61 V.1 Nord, Neria. Copenhagen: Geological Survey of Greenland.

King, A.R. 1983: Report on sampling and prospecting in Sermiligarssuk Fjord area, South-West Greenland, 16, Greenex A/S. Internal Report.

King, A.R. 1985: Sermiligarssuk exploration concession. Report on geological field work carried out in the Sermiligarssuk Fjord, South West Greenland, 18, Greenex A/S. Internal report.

Petersen, J.S. 1991: Kujataa project 1991. Gold mineralization in the Taartoq group greenstones, SW Greenland, results of structural, geochemical and geophysical studies, 44, NunaOil A/S. Internal Report.

Petersen, J.S. 1992: Kujataa: field report - 1992. Nuuluk-Iterlak gold and massive sulfide project, Taartoq Archaean greenstone belt, SW Greenland, 55, NunaOil A/S. Internal Report.

Petersen, J.S. & Madsen, A.L. 1995: Shear-zone hosted gold in the Archaean Taartoq greenstone belt, South-West Greenland. In: Ihlen, P.M., Pedersen, M. & Stendal, H. (eds): Gold mineralization in the Nordic countries and Greenland Extended abstracts and field trip guide Open File Series Grønlands Geologiske Undersøgelse 95/10, 65-68.

Reynolds, K. 2011: Chemical mass transfer during alteration and gold mineralization of the Tartoq Group greenstones, Sermiligaarsuk Fjord, SW Greenland, 48. Unpublished thesis, Imperial College.

Steenfelt, A. 2001: Geochemical atlas of Greenland – West and South Greenland, 39. København: Danmarks og Grønlands Geologiske Undersøgelse Rapport.

Szilas, K., van Hinsberg, V.J., Kisters, A.F.M., Kokfelt, T., Scherstén, A. & Windley, B.F. 2011: Remnants of Mesoarchaean oceanic crust in the Tartoq Group, South-West Greenland. Geological Survey of Denmark and Greenland Bulletin 23, 57-60.

van Hinsberg, V.J., Szilas, K. & Kisters, A.F.M. 2010: The Tartoq group, SW Greenland: Mineralogy, textures and a preliminary metamorphic to hydrothermal history, 40. Copenhagen: Geological Survey of Denmark and Greenland.

Summary and conclusions

Field work in 2010 focused around the already known gold occurrences in the Paamiut and Sermiligaarsuk areas. It could be shown that hydrothermal gold mineralisation and alteration is more widespread than previously known. Gold is hosted in quartz veins and hydrothermal alteration zones in various lithologies, suggesting orogenic gold mineralisation.

In the area south of Frederikshåb Isblink to the Tartoq gold province several critical processes for orogenic gold mineralisation have been identified. The area is endowed in gold, is, however, with ages clustering around 2850 Ma ca. 150 m.y. older than the metallogenetic most favourable epoch for orogenic gold, although metamorphic zircon ages of ca. 2720 Ma are also recorded. The structural grain of the Paamiut and Tartoq gold provinces characterises east-vergent fold-and-thrust belts, suggesting a regional-scale contractional orogen setting. Such a setting is favourable for large orogenic gold systems. The thrust and strike-slip zones provide large-scale damage zones, which could have acted as active pathway. In the Paamiut and the Tartoq gold provinces, these structures are characterised by ductile, brittle-ductile and brittle fabrics, indicating that they are long-lived structural breaks, which could provide permeability for a long-lived hydrothermal mineralising system. Pegmatites and leuco-granites form syn- to late-tectonic intrusions into the shear zones.

The Paamiut gold province comprises supracrustal rocks, grey gneiss and leuco-granite metamorphosed to amphibolite facies grades and retrogressed in the greenschist facies. The fold-and-thrust belt forms a frontal and lateral ramp structure, which acted as fluid pathway. Gold occurrences are situated either in structurally complex zones of the lateral ramp or in frontal ramp settings at lithological contacts. Gold occurs in both, supracrustal rocks and grey gneiss, suggesting together with the structural setting physical changes in the auriferous fluid as a cause for gold precipitation. Hydrothermal alteration is characteristic for the lower amphibolite facies, comprising mainly quartz, hornblende or orthoamphibole, biotite, muscovite, tourmaline, pyrrhotite, arsenopyrite, chalcopyrite and pyrite. In west-vergent back thrusts, higher metamorphic grade rocks occur also containing gold mineralisation. Partial melt fabrics of wall rocks and mineralisation indicate prograde metamorphic overprint up to granulite facies grades, which possibly caused remobilisation of gold and sulphides.

The Tartoq gold province comprises supracrustal rocks of the Tartoq Group that are thrust on top of a gneiss basement. The thrust system forms a frontal and lateral ramp with strike-slip shear zones linking various thrust segments, which served as the fluid pathway. Locally, pegmatites and leuco-granites intruded the structures syn- to late-tectonically. Gold mineralisation is restricted to Tartoq Group greenstone belts that are mainly metamorphosed at greenschist facies grades and are only preserved in regional-scale F_2 synclinoria. Regional-scale carbonate-chlorite-pyrite alteration indicates a large-scale hydrothermal mineralising system. The proximal alteration comprises ankerite-muscovite-quartz-pyrite assemblages. Strongest gold enrichment is recorded in rocks of favourable chemistry, such as graphite- and magnetite-bearing schists and banded iron formation. In the east, the Bikuben (Sioralik) belt is metamorphosed at upper amphibolite facies to granulite facies grades. Hydrothermal gold mineralisation probably also occurred at higher metamorphic grades. The structural model suggests that these rocks were partly subducted and pro-

gressively exhumed during contractional orogeny, similar to the situation further north in the Paamiut gold province.

We can show that many of the critical processes for orogenic gold mineralisation acted in the study area at various scales. This report and the attached information provides data that can be used as targeting criteria in predictor maps and the scientific background, which adds value in the exploration process in the Tartoq and Paamiut gold provinces. Exploration to date was not very successful using either direct detection technology (i.e., soil and stream sediment geochemistry) or the wrong exploration model (i.e., volcanic-hosted massive sulphide deposit). Here, we show that hydrothermal gold mineralisation is structurally controlled by the fold-and-thrust belt structures and formed in favourable structures as well as lithologies at greenschist to lower amphibolite facies grades. This regional interpretation provides new insight into the critical geological processes and their mappable expressions such as structures, favourable lithology, hydrothermal alteration assemblages and metamorphic grades, hopefully leading to more successful exploration in the area.